INELASTIC RESPONSE OF REINFORCED CONCRETE FRAMES TO SEISMIC GROUND MOTIONS HAVING DIFFERENT CHARACTERISTICS

by

TIAN-JIAN ZHU

A Thesis

Submitted to the School of Graduate Studies

in Partial Fulfillment of the Requirements

for the Degree

Doctor of Philosophy

McMaster University

INELASTIC RESPONSE OF REINFORCED CONCRETE FRAMES TO SEISMIC GROUND MOTIONS HAVING DIFFERENT CHARACTERISTICS

DOCTOR OF PHILOSOPHY (1989)
(Civil Engineering and
Engineering Mechanics)

McMASTER UNIVERSITY
Hamilton, Ontario

TITLE: Inelastic Response of Reinforced Concrete Frames to Seismic Ground Motions Having Different Characteristics

AUTHOR: Tian-Jian Zhu, B.Eng. (Zhejiang University)
M.Eng. (McMaster University)

SUPERVISOR: Dr. A. C. Heidebrecht
Dr. W. K. Tso

NUMBER OF PAGES: xxiv, 296

ABSTRACT

Observations of structural damage following recent major earthquakes have indicated that ground motion characteristics have a significant effect on the damage of building structures. An analytical study is undertaken to investigate the effect of ground motion characteristics on the inelastic response of multistorey reinforced concrete frame structures and to evaluate the seismic performance of reinforced concrete frame structures designed in conformance with current Canadian seismic provisions. In addition, the possibility of using simplified analysis procedures to estimate inelastic response is studied for regular building frames subjected to different types of earthquake ground motions.

An earthquake data set consisting of 45 horizontal components of strong motion records is selected and subdivided into three groups representative of seismic ground motions having low, intermediate, and high peak acceleration-to-velocity (A/V) ratios. This data set is analyzed to investigate the significance of the A/V ratio as a parameter to indicate the dynamic characteristics of earthquake ground motions resulting from different seismic environments. Four regular moment resisting reinforced concrete building frames having different fundamental periods are designed for combined gravity and seismic effects determined in accordance with the 1985 edition of the National Building Code of Canada (NBCC 1985). The structural members are proportioned and detailed to satisfy the requirements of the 1984 edition of the Canadian Concrete Code (CAN3-A23.3-M84). These four frames are used as structural

models having very short, short, moderate, and long fundamental periods.

To gain insight into the inelastic behaviour of the designed frames, the inelastic static responses of the frames to monotonically increased lateral loading are examined first. Following this inelastic static analysis, the inelastic dynamic responses of the frames to the three A/V groups of earthquake accelerograms are analyzed statistically. In addition, the elastic dynamic responses of the frames to the three A/V groups of earthquake records are obtained to provide a reference for the evaluation of the inelastic dynamic responses. In the course of the dynamic analyses, overall energy indices are defined for multistorey building frames, and their numerical computation is implemented in a computer program.

A simplified analysis procedure is proposed to estimate both overall and localized inelastic deformations for regular building frames. This simplified analysis procedure is evaluated based on a comparison of the inelastic deformational demands estimated from the procedure with the statistical results obtained from the inelastic dynamic analysis of the frames.

ACKNOWLEDGEMENTS

I wish to express my deep gratitude to Professors A. C. Heidebrecht and W. K. Tso, my research supervisors, for their constant encouragement and guidance throughout the course of my graduate studies. It has been a great privilege and pleasure for me to work under their supervision.

I am indebted to Professors J. N. Siddall and J. C. Wilson, members of my supervisory committee, for their valuable comments and suggestions.

Special thanks are due to Dr. N. Naumoski for his assistance with the selection of the earthquake records used in this study.

I am grateful for the scholarships granted by the Ontario Ministry of Education and McMaster University and the teaching assistantships provided by the Department of Civil Engineering.

Finally, I would like to dedicate this thesis to my parents for their encouragement and support throughout the years of my education.

TABLE OF CONTENTS

Table of Contents (cont'd)

Table of Contents (cont'd)

LIST OF TABLES

List of Tables (cont'd) PAGE

LIST OF FIGURES

List of Figures (cont'd) PAGE

List of Figures (cont'd) PAGE

List of Figures (cont'd)

List of Figures (cont'd) PAGE

LIST OF SYMBOLS

A	peak ground acceleration
A_g	area of column gross section
A_s	area of flexural reinforcement in beam
A_{st}	area of longitudinal steel bars in column
A/V	ratio of peak ground acceleration to velocity
b	beam section width
c	distance from extreme compressive fiber to neutral axis
c_1, c_2	proportional constants for damping matrix
C	damping coefficient for SDOF-1 model
C_1	first modal damping coefficient for SDOF-2 model
C_m	a factor relating actual moment diagram to an equivalent uniform moment diagram
COV	coefficient of variation
CRF	cumulative root-mean-square function
[C]	damping matrix
d	distance from extreme compressive fiber to centroid of tensile reinforcement
dt	time increment
{du(t)}	incremental relative displacement vector
D	dead load
D.L.	concentrated dead loads
D_s	dimension of a frame in direction parallel to lateral seismic loading
E_c, E_s	modulus of elasticity of concrete or reinforcing steel
E_I, E_K, E_D, E_H, E_S	input, kinetic, damping, hysteretic, and strain energy, respectively

List of Symbols (cont'd)

$E_I', E_K', E_D', E_H', E_S'$	input, kinetic, damping, hysteretic, and strain energy per unit mass, respectively
EI	flexural rigidity of structural member
EI_b, EI_c	flexural rigidity of beam or column
EI_c^T, EI_c^B	flexural rigidity of top or bottom column
f_c'	compressive strength of concrete
f_y	yield strength of reinforcing steel
F	foundation factor
F_e	equivalent force for SDOF-I model
$(F_e)_y$	equivalent force at incipient yield condition
F_n	lateral force at top level
F_t	portion of V concentrated at top level in addition to F_n
F_x	lateral force at level x
g,G	acceleration of gravity
h_b, h_c	section depth of beam or column
h_i, h_x	height above base to level i and x, respectively
h_n	total height of a frame above base
I	importance factor
I_g	moment of inertia of column gross section about centroidal axis
k	effective length factor
K	structural behaviour coefficient
K_c^T, K_c^B	stiffness of top or bottom column
$[K_G]$	geometric stiffness matrix for column
$[K_t]$	tangential stiffness matrix
l_b, l_c	clear length of beam or column

List of Symbols (cont'd)

l_b^L, l_b^M	clear length of left or middle span beam
l_c^T, l_c^B	clear height of top or bottom column
l_u	unsupported length of column
L	live load due to use and occupancy
L	length of structural member
L_e	equivalent height for SDOF-1 model
L.L.	concentrated live loads
m_i	lumped mass at storey level i
M	earthquake magnitude
M	bending moment
M_0	column yield moment at zero axial force
M_1	first modal mass for SDOF-2 model
M_b	beam design moment
M_b^+, M_b^-	positive or negative beam design moment
M_{b1}^+, M_{b2}^+, M_{b3}^+	positive beam moment capacity at section 1, 2, and 3, respectively
M_{b1}^-, M_{b2}^-, M_b^-3	negative beam moment capacity at section 1, 2, and 3, respectively
M_B	column yield moment at balanced condition
M_c^T, M_c^B	design moment for top or bottom column
M_e	equivalent mass for SDOF-1 model
M_i, M_j	bending moment at end i or j of a column
M_{JMA}	Japan Meterological Agency scale
M_L	local magnitude
M_{max}	maximum moment
MRF	moment reduction factor

List of Symbols (cont'd)

M_s	surface wave magnitude
M_t	total mass
M_y	yield moment
M_y^G, M_y^t	yield moment corresponding to initial gravity axial force and current axial force, respectively
[M]	mass matrix
N,n	total number of storeys
n_p	total number of yield excursions
p	ratio of strain-hardening to initial stiffness
P	column axial force
P_B	column axial force at balanced condition
P_c	critical axial load
P_c^T, P_c^B	axial force in top or bottom column
P_c^u	ultimate compressive axial force without bending
P_f	factored column axial force
P_G	column axial force under initial gravity loading
P_t	current column axial force
P_t^u	ultimate tensile axial force without bending
{P}	applied lateral load vector
Q	seismic load
R	epicentral distance
R	force reduction factor
R_S	ratio of elastic to inelastic dynamic base shears
R_1	first modal force for SDOF-2 model
$(R_1)_y$	first modal yield force

List of Symbols (cont'd)

$\{r\}$	a vector relating ground motion to structural degrees of freedom
$\{R\}$, $\{R(u(t))\}$	restoring force vector
S	seismic response factor
SI	spectrum intensity
S_v	pseudo spectral velocity
t	time
T	period
T_1, T_2	periods of first two vibrational modes
$\ddot{u}_g$, $\ddot{u}_g(t)$	ground acceleration
$\{u\}$, $\{u(t)\}$	relative displacement vector
$\{\dot{u}\}$, $\{\dot{u}(t)\}$	relative velocity vector
$\{\ddot{u}\}$, $\{\ddot{u}(t)\}$	relative acceleration vector
v	zonal velocity ratio
V	peak ground velocity
V	unfactored design base shear
V_{b1}, V_{b2}, V_{b3}	beam shear at section 1, 2, and 3, respectively
V_{b1}^G, V_{b2}^G, V_{b3}^G	beam shear due to gravity loading at section 1, 2, and 3, respectively
V_c^T, V_c^B	shear force for top or bottom column
w_c	unit weight of concrete
w_D	uniformly distributed dead loads
w_L	uniformly distributed live loads
W	weight of reactive masses
W_i, W_x	portion of W assigned to level i and x, respectively
X	equivalent displacement for SDOF-I model

List of Symbols (cont'd)

X_y	equivalent displacement at incipient yield condition
Y_1	first modal displacement for SDOF-2 model
$(Y_1)_y$	first modal yield displacement
Z_a	acceleration seismic zone
Z_v	velocity seismic zone
$Z_a<Z_v$, $Z_a=Z_v$, $Z_a>Z_v$	three different zonal combinations
β	ratio of top to bottom column stiffnesses
Γ_1	$\{\phi\}^T[M]\{r\}$
δ	roof displacement
δ_b	amplification factor due to slenderness effect
δ_{max}	maximum roof displacement
δ_y	roof displacement corresponding to first yielding
Δ	relative lateral displacement between two ends of a column
ΔE_I, ΔE_K, ΔE_D, ΔE_H, ΔE_S	incremental input, kinetic, damping, hysteretic, and strain energy, respectively
Δt	time increment
$\Delta\ddot{u}_g(t)$	incremental ground acceleration
$\{\Delta\dot{u}\}$	incremental relative velocity vector
η	column overstrength factor
θ	rotation
θ_{max}	maximum rotation
θ^p	plastic rotation
θ^p_{acc}	accumulative plastic rotation
θ^p_i	plastic rotation of each yield excursion
θ^p_{max}	maximum plastic rotation

List of Symbols (cont'd)

θ_y	yield rotation
λ	scaling factor for the intensity of input ground motion
μ_δ	global displacement ductility
μ_θ	rotation ductility
μ_θ^G, μ_θ^t	rotation ductility corresponding to initial gravity axial force and current axial force, respectively
μ_ϕ	curvature ductility
μ_ϕ^G, μ_ϕ^t	curvature ductility corresponding to initial gravity axial force and current axial force, respectively
ξ	damping ratio
ξ_1, ξ_2	damping ratios of first and second modes
ρ	percentage of flexural reinforcement
σ	one standard deviation
ϕ	curvature
ϕ_c	resistance factor for concrete
ϕ_m	member resistance factor
ϕ_{max}	maximum curvature
ϕ_s	resistance factor for reinforcing steel
ϕ_y	yield curvature
ϕ_y^G	yield curvature corresponding to initial gravity axial force
$\{\psi\}$	first modal vector
ψ	ratio of sum of column stiffnesses to sum of beam stiffnesses at a joint
ψ_{ave}	average of two ψ values at two ends of a column
ψ_e, ψ_i, ψ_n	ordinate of $\{\psi\}$ at equivalent height L_e, level i, and top level, respectively
$\{\psi\}$	first Ritz vector

CHAPTER 1

INTRODUCTION

1.1 Background and Motivation

Because of economic considerations, conventional building structures are usually designed to undergo inelastic deformations under strong earthquake ground shaking. Hysteretic energy dissipation through inelastic deformations enables seismic design forces to be significantly reduced from those that would be required if the buildings were to remain elastic. This is the basic premise in current seismic design practice for building structures. However, these inelastic deformations must be kept within permissible limits to prevent collapse due to excessive lateral displacements or substantial deterioration of energy dissipation capacities. Also, the potential costs of nonstructural and structural damage should be weighed against the savings made possible by allowing inelastic response.

During the past decade, many analytical models have been suggested to simulate the inelastic behaviour of structural elements or subassemblages, and sophisticated computer programs have been developed to predict the nonlinear seismic response of building structures (52). As a result, our ability to analyze the inelastic dynamic response of building structures has increased dramatically. However, there has not been a comparable progress in the development of reliable methods for the seismic design of structures that are allowed to tolerate limited amount of inelastic deformations. The specification of seismic design forces

accounting for the expected intensity of earthquake ground shaking and acceptable level of inelastic response remains a very difficult task.

In current practice, three methods may be employed to estimate seismic design forces and their distributions for building structures. They are (a) the time history analysis method; (b) the modal analysis-design spectrum method; and (c) the equivalent static code method. The time history analysis method involves step-by-step numerical integration of the equations of motion. Elastic dynamic analysis can be performed to estimate the elastic strength demands for structural members in a building structure. Actual design strengths for the structural members can be obtained from the elastic strength demands using appropriate strength reduction factors (40,41). Parametric studies based on inelastic dynamic analysis can be used to directly estimate the design strengths for structural members that are required to limit their inelastic deformations to the specified values. However, in order to encompass the possible range of structure-related parameters and the variabilities of earthquake ground motions, a number of time history analyses are usually required in this method. Because of the high cost of time history analyses, especially inelastic dynamic analysis, this method may not be practical for most building structures, particularly in the preliminary design stage.

The modal analysis-design spectrum method is attractive as a practical design tool for its relative simplicity. Although strictly applicable to linearly elastic structures, this method has often been used in the design of inelastic structures. There are two different approaches involved in the modal analysis-design spectrum method for

inelastic structures. One approach is to replace the inelastic structure by an equivalent linear elastic structure. This replacement enables the direct use of an elastic design response spectrum for estimating seismic design forces. Gulkan and Sozen (28), Iwan and Gates (42,43) have proposed procedures for estimating effective stiffness and viscous damping for linearized single degree of freedom (SDOF) systems. An extension to multi-degree of freedom (MDOF) systems, the "substitute-structure" technique, has been suggested by Shibata and Sozen (80). In their technique, the member stiffness of the linear elastic substitute structure is reduced, and its modal damping is increased to account for inelastic deformation in tne original structure. The seismic design forces and their distributions are estimated from an elastic modal analysis of the substitute structure coupled with an elastic design spectrum. The other approach involves the use of an inelastic design spectrum in conjunction with an elastic modal analysis based on the initial elastic properties of a building structure (3,4,60,62). This modal analysis-inelastic design spectrum approach has been commonly used in current practice. The inelastic design spectrum is usually derived from an elastic design spectrum using appropriate reduction factors. Simplified rules for obtaining inelastic design spectra from elastic design spectra were first proposed by Newmark and Hall (60). In their procedure, the reduction factors are expressed as a function of both the specified displacement ductility and period. Over the years, many studies (50,73,79) have been performed to investigate the effects of viscous damping, ductility level, and hysteretic behaviour on inelastic response spectra, and refined modification factors which can explicitly account

for these effects have been suggested.

The equivalent static code method has been widely used for the seismic design of regular building structures in many seismic codes. This method is closely related to the modal analysis-inelastic design spectrum approach. In this method, the total lateral seismic design force for a building structure is specified from a base shear formula. While the actual form of the base shear formula differs among seismic codes, it is essentially based on an inelastic design spectrum with some modifications. This inelastic design spectrum is usually obtained from an elastic design spectrum using a force reduction factor. The force reduction factor is intended to account for the energy dissipation capacities of different types of structural systems due to inelastic deformation and damping, and its value is qualitatively related to the expected overall seismic performance of the structural systems (72). In many seismic codes, the force reduction factor is specified independently of structural period. After the total design base shear is determined, it is distributed along the height of a building according to a distribution formula. The distribution formula is essentially based on the fundamental mode shape of the building with some modifications to approximately account for higher mode effects. It has been well recognized that the distributions of seismic design forces obtained from the equivalent static formulation are close to those computed from the modal analysis-inelastic design spectrum approach for regular buildings with relatively uniform distributions of mass, stiffness, and strength in both plan and elevation. For irregular buildings, the modal analysis-inelastic design spectrum approach would provide more accurate distributions of seismic

design forces throughout the buildings. However, Heidebrecht and Tso (32) have indicated that the total design base shears determined from the modal analysis-inelastic design spectrum approach bear little or no relation to those obtained from the static code provisions, and the assumptions made in the modal analysis-inelastic design spectrum calculations have at least as much, or more, uncertainties than those of the static calculations. For this reason, the 1985 edition of the National Building Code of Canada (NBCC 1985) (8) has suggested that the total design base shear be computed solely based on the static approach, and the modal analysis-inelastic design spectrum approach be used for distribution purposes for irregular buildings.

After the seismic design forces and their distributions are determined for a building, its structural components need to be proportioned along with design gravity loads. While it is possible to employ an optimum design procedure for this purpose (13,95), the proportioning of structural members in many seismic codes is based on elastic static analyses of the building under different combinations of gravity and seismic loads, coupled with load factors. In order to achieve a desirable hierarchy in the energy dissipation mechanism of a building, the weak beam-strong column concept can be incorporated into this proportioning process. One typical example of this consideration is the capacity design procedure developed by Paulay (69,70).

It is apparent from the preceding review of current seismic design practice that the modal analysis-design spectrum method and the closely related equivalent static code method have been and will continue to be viable techniques in earthquake-resistent design. In these methods, the

design response spectrum represents the statistical summary of the earthquake environment at a given building site, and it is the only linkage that relates ground motion information to the specification of seismic design forces. Ideally, the design response spectrum should be constructed based on an ensemble of seismic ground motions resulting from earthquakes with magnitudes and epicentral distances appropriate for the site and having soil conditions similar to the site. However, in most cases, the necessary seismological and geological information required to establish such an appropriate ensemble of earthquake ground motions is not readily available. Even if some of the information is available, the efforts needed to obtain this appropriate ensemble of earthquake accelerograms are usually excessive for most design projects. As a result, in many seismic codes, the standard design spectral shape suggested by Newmark and Hall (60,62) has been employed to describe the frequency characteristics of design ground shaking at a building site, and peak ground acceleration has been used as a single measure of the expected severity of the design ground shaking for scaling purposes. The wide use of peak ground acceleration as a measure of ground motion intensity may be due to the following reasons. First, it is a directly measured quantity related to inertia forces induced in building structures. Second, it is a convenient ground motion parameter to be used to scale acceleration response spectra at zero period.

However, as more earthquake records were obtained, especially after the 1971 San Fernando earthquake, it became apparent that the use of a single design spectral shape scaled by a peak site acceleration is inadequate. It has been shown that some of the recorded earthquake ground

motions have response spectra dramatically different from the standard design spectrum suggested by Newmark and Hall. Newmark et al. (58,59,61) and Page et al. (66) observed that structures near an earthquake source may experience large-amplitude, high-frequency, and short-duration acceleration motions. Observations of structural damage in areas where such ground motions were recorded have suggested that the levels of damage are not as great as might be inferred from the recorded peak ground accelerations (22,38). Based on several near-fault records obtained from the 1971 San Fernando earthquake, Bertero et al. (12,14,15) and Mahin et al. (53) indicated that earthquake ground motions near the fault rupture may contain severe, long-duration acceleration pulses. The use of the standard design spectrum would underestimate peak ground velocities for such ground motions, resulting in undesirably high displacement ductility demands for certain inelastic systems. Recently, Hall et al. (29,30) noted the need to use another design spectrum for a distant earthquake source on the basis that ground motions distant from the source of seismic energy release would usually be of long-period sustained type due to the filtering effect through ground media. This review of previous studies clearly indicates that while the standard design spectrum may be representative of strong seismic ground motions at moderate distances from the causative fault, additional design spectra need to be developed on the basis of recorded near-field and far-field earthquake accelerograms to account for ground motions close to or distant from the energy source.

Seismological studies have indicated that peak ground acceleration and velocity are usually caused by seismic waves of different

frequencies. Peak ground acceleration is associated with high frequency waves whereas peak ground velocity is related to moderate or low frequency waves. Because of the frequency-dependent attenuation of seismic waves, peak ground acceleration attenuates more rapidly with distance than peak ground velocity. As a result, one would expect that ground motions experienced near an earthquake source have higher peak ground acceleration-to-velocity (A/V) ratios than those at a large distance from the source of seismic energy release. Ground motions in the former case are usually of short-duration, high-frequency, and impulsive type whereas those in the latter case are normally of longer-duration and more periodic type. Therefore, even though it is a relatively simple parameter, the A/V ratio provides information on the relative frequency content and duration of strong shaking for ground motions resulting from different seismic environments.

A study by Basham et al. (10) has shown that the relative levels of peak ground acceleration and velocity vary considerably across Canada. The A/V ratio varies from about 0.5 g/m/s to 2.5 g/m/s. This ratio is low at sites that are influenced by large distant earthquakes (e.g. Prince George); it is high at sites that are influenced by moderate nearby earthquakes (e.g. Montreal). In recognition of this, both acceleration and velocity zoning maps have been developed to define expected ground motions for different locations in Canada (10). Accordingly, NBCC 1985 utilizes both zonal peak ground acceleration and velocity in the specification of seismic design base shears (31,32). The base shear formula in NBCC 1985 is directly tied to zonal peak ground velocity. However, three different levels of seismic response factor are used in

the short period range (up to 0.5 sec) for three different combinations of acceleration and velocity seismic zones in an attempt to accommodate the effect of zonal peak ground acceleration on short period structures (31,32). The three different zonal combinations correspond to low, intermediate, and high A/V ratios.

The effect of ground motions with different A/V ratios on the inelastic responses of SDOF systems was investigated by Zhu et al (98,99,100,101). The SDOF systems were designed in accordance with the base shear provisions in NBCC 1980 (7) and those in NBCC 1985 respectively. The NBCC 1980 base shear provisions were included to represent the common practice of specifying seismic design forces based on a single design spectral shape scaled by a peak site acceleration. Three sets of real earthquake accelerograms, recorded from past events, were selected to represent ground motions having low, intermediate, and high A/V ratios. It was found that if the specification of design yield strength is directly related to peak ground acceleration, the use of a single design spectral shape leads to substantially different displacement ductility demands for medium and long period systems when subjected to ground motions with their A/V ratios in the three different ranges. The consistency of the ductility demands for medium and long period systems is remarkably improved when the specification of design yield strength is directly tied to peak ground velocity. However, there exist marked differences in the ductility demands for short period systems. The use of three different levels of seismic response factor over the short period range, as suggested in NBCC 1985, reduces these differences significantly. Tso and Naumoski (87) studied both

acceleration and velocity based inelastic design spectra. It was found that if inelastic design spectra are based on peak ground acceleration, the mean plus one standard deviation ductility demands for moderate and long period systems are much higher than the specified values even when three different design spectral shapes are used for excitations having low, intermediate, and high A/V ratios. This is particularly true for low A/V excitations. The use of velocity based inelastic design spectra together with a period-dependent strength reduction factor in the short period range provides good control over ductility demands for systems having different periods.

In view of the foregoing discussion, it is apparent that the inadequacy in the specification of design ground shaking is the major source of the unreliability associated with current seismic design practice for building structures. This inadequacy is reflected in two aspects. First, peak ground acceleration is not a reliable parameter to represent the severity of design ground shaking at a building site. Second, the use of the Newmark-Hall design spectral shape alone is insufficient to describe the frequency content of design ground motions which may result from different seismic environments. The A/V ratio is a relatively simple, yet seismologically meaningful, parameter to distinguish the relative frequency characteristics of earthquake ground motions associated with different seismic environments. Studies based on SDOF systems have indicated that ground motion A/V ratio has a significant effect on the inelastic responses of the systems, and the specification of seismic design forces based on peak ground velocity along with the A/V ratio, as recommended in NBCC 1985, results in

consistent inelastic responses when the systems are subjected to ground motions having different A/V ratios. However, these observations and conclusions obtained from the studies of SDOF systems may not be directly generalized to real building structures. This is because the oversimplification of SDOF systems cannot account for many of the factors affecting the nonlinear seismic response of actual buildings. Also, design of actual buildings requires information on both overall inelastic deformations at storey levels and localized inelastic deformations in structural members. In the present study, realistic multistorey reinforced concrete building frames are considered, and they are designed and detailed in accordance with the 1985 NBCC and the 1984 Canadian Concrete Code (CAN3-A23.3-M84) (20). The primary purposes of this study are to investigate the effect of ground motions having different A/V ratios on the inelastic responses of multistorey reinforced concrete building frames and to evaluate the seismic performance of reinforced concrete building frames designed in compliance with current Canadian seismic provisions.

In the preliminary design stage, it may be necessary to evaluate the relative merits of different structural framing and/or proportioning schemes and the relative effects of different earthquake ground motions. Because of the various parameters involved, such an evaluation usually requires a large number of inelastic dynamic analyses. The cost of these analyses using sophisticated computer programs is usually prohibitive for most design projects. Therefore, it is desirable to employ simplified analysis procedures that are able to provide reasonably accurate estimates of both overall and local inelastic deformational demands at

relatively low cost. The suitability and accuracy of a simplified analysis procedure generally depend on both the dynamic properties of the building structure concerned and the dynamic characteristics of the input ground motion to which the structure is subjected. An additional purpose of this study is to investigate the possibilities of using simplified analysis procedures to estimate overall and local inelastic responses for multistorey building frames when they are subjected to ground motions having different A/V ratios.

1.2 Objectives and Scope

The objectives of this study are:

(a) to investigate the effect of earthquake ground motions having different A/V ratios on the inelastic responses of multistorey reinforced concrete frame structures;

(b) to evaluate the seismic performance of reinforced concrete frame structures designed in conformance with the 1985 NBCC and the 1984 Canadian Concrete Code when subjected to ground motions with different A/V ratios; and

(c) to study the possibilities of using simplified analysis procedures to estimate both overall and local inelastic deformations for frame structures when exposed to different types of earthquake ground motions.

To accomplish the objectives outlined above, five different phases are involved in this study. These five phases are (a) selection and analysis of an earthquake data set; (b) design of typical reinforced concrete moment-resisting frames; (c) static analysis of the designed reinforced concrete frames subjected to monotonically increased lateral

loading; (d) dynamic analysis of the reinforced concrete frames subjected to earthquake excitations; and (e) development and evaluation of simplified analysis procedures based on the dynamic analysis results. These five different phases are treated in five separate chapters. The organization of the present study is described in the following section.

1.3 Organization

This introductory chapter provides a brief review of the current seismic design practice for building structures. The problems associated with the specification of design ground motion were outlined in the light of recent research and observations of structural damage following recent major earthquakes. The significance of the A/V ratio in establishing design ground motion was identified from seismological considerations. These presentations provided the background and enabled the formulation of the objectives for the present study.

In Chapter 2, an earthquake data set selected for this study is described. The ground motion data are analyzed to investigate the significance of the A/V ratio as a parameter to indicate the dynamic characteristics of earthquake ground motions resulting from different seismic environments. The data set is subdivided into three groups representative of ground motions having low, intermediate, and high A/V ratios. These three groups of earthquake records are used as input ground motions for the dynamic analysis in Chapter 6.

Chapter 3 contains a detailed description of the multistorey reinforced concrete frames considered in this study. Two four storey frames with different fundamental periods, one ten storey frame, and one

eighteen storey frame are designed for combined gravity and seismic effects in accordance with NBCC 1985. The structural members are proportioned and detailed in compliance with CAN3-A23.3-M84. The elastic dynamic properties of the frames are presented, and the frames are checked for the serviceability requirements. These four frames are taken to represent regular buildings having very short, short, moderate, and long fundamental periods.

Chapter 4 begins with a description of the static and dynamic analysis procedures employed in this study. The basic assumptions made in the static and dynamic analyses are outlined. The analytical models used for beam and column elements are described. The consideration of the P-delta effect in the analyses is discussed. In the dynamic analysis, different energy indices are defined for inelastic MDOF systems, and their numerical implementation in computer programs is presented. Also included in this chapter is a definition of the various response parameters used to characterize inelastic response for the present study.

In Chapter 5, the inelastic behaviour of the reinforced concrete frames designed in Chapter 3, as subjected to monotonically increased lateral loading, is studied. This study focuses on the sequence of plastic hinge formation in structural members, the relationship between base shear and roof deflection, and the distribution of various response parameters over frame height. In addition, the significance of the P-delta effect on the computed results is examined. This inelastic static analysis provides background information for the evaluation of the inelastic dynamic responses of the frames to earthquake ground excitations to be described in Chapter 6.

In Chapter 6, the inelastic dynamic responses of the designed frames to the three A/V groups of earthquake ground motions are analyzed statistically. This statistical analysis is performed to investigate the effect of ground motion A/V ratio on the inelastic response of reinforced concrete frame structures and to evaluate the seismic performance of reinforced concrete frame structures designed in compliance with NBCC 1985 and CAN3-A23.3-M84. In addition, the effect of peak ground velocity level on the inelastic response of the designed frames is investigated. The statistical results of the inelastic responses of the frames are compared with those of the corresponding elastic responses for the three A/V groups of earthquake records. Finally, the distributions of overall response parameters are compared for four different analyses, namely: (a) elastic static; (b) elastic dynamic; (c) inelastic static; and (d) inelastic dynamic analyses.

Chapter 7 describes a simplified analysis procedure for estimating both overall and localized inelastic deformations for regular building frames. The applicability of the simplified analysis procedure is evaluated for frames having different number of storeys and for earthquake ground motions having different A/V ratios. This evaluation is based on a comparison of the inelastic deformational demands estimated from the simplified analysis procedure with the statistical results obtained from the inelastic dynamic analysis of the frames.

Finally, Chapter 8 presents a summary and the significant conclusions of this study. Also, the significant design implications of this study are reviewed, and future research needs are identified.

CHAPTER 2

INPUT GROUND MOTIONS

2.1 Introduction

This chapter contains a detailed description of the earthquake records selected as input ground motions for this study. Also included in this chapter is an analysis of the selected ground motion data. This analysis is performed to investigate the significance of the A/V ratio as a parameter to indicate the dynamic characteristics of earthquake ground motions resulting from different seismic environments. First, the correlation of the A/V ratio with the relationship between earthquake magnitude (M) and epicentral distance (R) is examined. In the light of this examination, the usefulness of the A/V ratio to reflect information on the relative frequency content and duration of strong shaking for earthquake ground motions associated with different seismic environments is investigated. Finally, the correlation of the A/V ratio with one of the more refined ground motion parameters is studied.

2.2 Earthquake Data Set

To form an earthquake data set for the present study, a total of 45 horizontal components of strong motion records were selected from the McMaster University Seismological Executive (MUSE) Database System which contains several thousand actual accelerograms recorded from past earthquakes around the world. All the chosen accelerograms were recorded in "free-field" conditions or building basements. Previous studies

(77,78) have indicated that local soil condition at a recording site has a significant effect on the dynamic characteristics of seismic ground motions. To minimize this effect, only those accelerograms recorded on rock or stiff soil sites are selected in this study. Several sources are used in determining the local site information for the chosen accelerograms. While a large portion of the data is obtained from past earthquakes in the western part of the United States, data from other parts of the world are also included to cover a broader range of geological and seismological conditions. The data set is obtained from 23 different earthquake events with magnitude ranging from 5.25 to 8.1. A list of the earthquake events included in this data set is presented in Table 2.1. The epicentral distance for the 45 records varies from 4 to 379 km. Therefore, both "near-field" and "far-field" earthquake ground motions are included in this data set.

All the selected records have been corrected. The adjustments involve base line correction of long period errors (83) and instrument corrections of high frequency errors (85). The peak acceleration of these corrected records ranges from 0.040 to 1.101g, and the peak velocity varies between 0.016 to 0.577 m/s.

The 45 records are subdivided into three groups in accordance with their A/V ratios, with 15 records in each group. The records having $A/V < 0.8$ g/m/s are classified into low A/V range whereas those having $A/V > 1.2$ g/m/s are categorized into high A/V range. The records with $0.8 \text{ g/m/s} \leq A/V \leq 1.2$ g/m/s are classified into intermediate A/V range. These three A/V ranges correspond to the three different combinations of acceleration and velocity seismic zones in NBCC 1985. Pertinent

information regarding the earthquake records in each of the three A/V ranges is tabulated in Tables 2.2, 2.3, and 2.4, respectively. The relative distributions of peak accelerations and velocities for the three groups of ground motions are shown in Fig. 2.1. A statistical summary of the A/V ratios for the three groups of records is included in Table 2.5.

Shown in Fig. 2.2 are the relationships between earthquake magnitude (M) and epicentral distance (R) for the three groups of earthquake records used in this study. It can be seen that the accelerograms having high A/V ratios were obtained in the vicinity of small or moderate earthquakes whereas those having low or intermediate A/V ratios were recorded at large distances from large or moderate earthquakes. Therefore, the A/V ratio is well correlated with the M-R relationship for this set of earthquake data, and this correlation is consistent with seismological considerations as discussed in Chapter 1.

2.3 Frequency Content

One of the most important characteristics of ground shaking as regards its effect on structural response is its frequency content. The frequency content of ground motion directly affects the elastic responses of structures. For structures excited into the inelastic range, the shaking intensity of ground motion both at and beyond the initial periods of the structures has effects on the inelastic responses because of the "effective period" elongation as damage progresses.

In order to indicate their frequency content, acceleration response spectra for 5% damping are computed for the three groups of earthquake records. Two normalization schemes are considered for the records. One is

to scale them to the same peak acceleration and the other to the same peak velocity. For each of the two normalization schemes, the mean values of the spectral accelerations are calculated for the three groups of records, and the coefficients of variation are obtained to indicate their dispersion characteristics. In addition, the mean values and the corresponding coefficients of variation are obtained for the whole ensemble of 45 records, irrespective of their A/V ratios, to serve as a reference.

Shown in Fig. 2.3 are the mean acceleration response spectra for the three separate groups and the whole ensemble of earthquake records normalized to a common peak acceleration of 1g. The mean spectral accelerations for the three groups of records are similar in the very short period range (up to 0.2 sec). For periods beyond 0.2 sec, the spectral accelerations for the high A/V group of records drop very rapidly with period as compared to those for the low A/V group. The mean spectral accelerations for the low A/V group of records can be more than twice as large as those for the high A/V group for periods longer than about 0.5 sec. Fig. 2.4 shows the coefficients of variation of the spectral accelerations for the three separate groups and the whole ensemble of earthquake records. It can be seen that the coefficients of variation generally increase with increases in period. Even though the number of earthquake records included in the statistical analysis for the whole ensemble is three times that for the three separate groups, the coefficients of variation for the whole ensemble are significantly higher than those for the three separate groups for periods longer than about 0.5 sec.

Fig. 2.5 shows the mean acceleration response spectra for the three separate groups and the whole ensemble of earthquake records scaled to a common peak velocity of 1 m/s. The mean acceleration response spectrum curves for the three groups of records agree fairly well for periods longer than about 0.7 sec. However, the mean spectral accelerations for the three groups of records are remarkably different in the short period range. Over this short period range, the high A/V group of records has the highest mean spectral accelerations whereas the low A/V group has the lowest. Shown in Fig. 2.6 are the coefficients of variation of the acceleration response spectra for the three separate groups and the whole ensemble of records. The coefficient of variation for the whole ensemble of records has a minimum at the period of about 1 sec, and it increases with decreasing or increasing period. However, the coefficients of variation for the three separate groups of records are relatively uniform over the period range considered.

The spectral analysis of the data set clearly indicates that there are differences in the frequency content for earthquake records having different A/V ratios, and these differences are statistically significant, as indicated by the coefficient of variation. The scaling of earthquake ground motions to a common peak acceleration will lead to different energy contents over the moderate and long period ranges for ground motions having different A/V ratios. On the other hand, different energy contents will result over the short period range for ground motions with different A/V ratios if they are scaled to a common peak velocity. Therefore, it is unlikely that the use of a single design spectral shape can accommodate the difference in spectral shape

associated with ground motions having vastly different A/V ratios, irrespective of whether peak ground acceleration or velocity is used as a measure of the intensity of ground shaking.

2.4 Strong-Motion Duration

In addition to its amplitude and frequency characteristics, the duration of strong shaking is also important in assessing the damage potential of an earthquake ground motion. The duration of strong shaking plays an important role in low-cycle fatigue-type damage to nonlinear degrading structures caused by sustained reversals of inelastic deformations. Also, the energy imparted to a structure and the hysteretic energy dissipated by inelastic deformations depend strongly on the strong-motion duration of the input ground motion (97,100). In this section, the significance of the A/V ratio as a simple parameter to indicate the relative duration of strong shaking for earthquake ground motions resulting from different seismic environments is presented.

Several definitions of strong-motion duration have been proposed in previous studies (18,54,84,89). The Vanmarcke-Lai and the McCann-Shah definitions are employed for the present study. In the Vanmarcke-Lai method (89), a real earthquake record is transformed into a segment of a fictitious stationary stochastic process. The duration of this segment of stationary motion is defined as the strong-motion duration of the original record. The transformation is made in such a way that the total energy of the original record, as expressed by the Arias intensity (i.e. the integral of the squared accelerations) (6), is preserved, and the peak acceleration of the original record is expected to be exceeded once

in the transformed motion. The cumulative root-mean-square function (CRF) for acceleration is used in the McCann-Shah procedure (54). The CRF can be interpreted as the square root of the average rate of seismic energy input as a function of time. The strong-motion duration is defined as the time interval during which the rate of seismic energy arrival keeps on increasing.

The duration of strong shaking is estimated for each of the 45 earthquake records based on the Vanmarcke-Lai and McCann-Shah definitions as described above. The results are compared graphically in Fig. 2.7. It can be noted that for a particular record, the durations calculated using these two approaches can be quite different. However, for the whole ensemble of records, the trends for the two definitions are consistent. In general, the high A/V records have shorter durations of strong shaking than the intermediate A/V records whereas the low A/V records have longer durations. Therefore, the A/V ratio of earthquake records is well correlated to the strong-motion duration of the records. A statistical summary of the durations of strong shaking for the three groups of records is presented in Table 2.5.

Previous studies (18,25,36,84,89) have indicated that in general, the larger the magnitude of an earthquake, the longer the duration of strong ground motion if the distance from the epicenter remains constant. If the magnitude of the earthquake is kept constant, duration increases with an increase in epicentral distance. Since the records with high A/V ratios were generated in the proximity of small or moderate earthquakes whereas those with low A/V ratios were obtained at large distances from large or moderate earthquakes, as shown in Fig. 2.2, the correlation of

the A/V ratio with the duration of strong shaking is to be expected.

2.5 Spectrum Intensity

In addition to the peak ground motions (peak acceleration, velocity, and displacement), many other parameters have been proposed to measure the intensity of earthquake ground shaking (37,39,92). Some of these parameters are directly based on the ground motion data and others on the response quantities of linearly elastic oscillators. In this section, the correlation of the A/V ratio with one of these more refined parameters is investigated.

A parameter derived directly from the response of linearly elastic oscillators is the spectrum intensity. Housner (35,37,39) defined the spectrum intensity as the area under a pseudo-velocity spectrum curve between the periods 0.1 and 2.5 sec, i.e.

$$SI(\xi) = \int_{0.1}^{2.5} S_v(T,\xi)\, dT \qquad (2.1)$$

in which S_v is the pseudo spectral velocity and ξ the fraction of critical damping. The spectrum intensity can be interpreted as an average measure of the severity of ground shaking as regards its effect on the elastic responses of structures in the sense that it is related to elastic vibrational energy and covers a period range of engineering interest (39). The use of the spectrum intensity as a scaling factor for response spectra has been investigated in a previous study (56). In this study, ξ is taken as 5% which is considered to be representative of the damping values for most structures.

Plotted in Fig. 2.8 are the spectrum intensities versus peak ground accelerations for the three groups of original records. It can be seen that if the spectrum intensities are plotted against peak accelerations, three distinctive regions may be identified in which the data points for the three groups of records are located. The boundaries separating these three regions may be taken empirically as

$$SI = 5\ A \tag{2.2a}$$

and

$$SI = 2.5\ A \tag{2.2b}$$

in which SI is expressed in meters and A in gravitational acceleration g. For a specified level of peak ground acceleration, ground motions having low A/V ratios would have higher spectrum intensities than those having high A/V ratios. To further illustrate this, the mean values of the spectrum intensity are computed for the three groups of records when scaled to a common peak acceleration of 1g. The results are shown in Table 2.5. It can be seen that the mean spectrum intensity for the low A/V group of records is over four times as high as that for the high A/V group. As shown in Fig. 2.3, the scaling of earthquake records to a common peak acceleration results in significantly different energy contents over moderate and long periods for records having different A/V ratios. This difference in the energy content directly leads to the difference in the spectrum intensity because the calculation of the spectrum intensity is related to the energy between the periods 0.1 and 2.5 sec.

The spectrum intensities are plotted against peak ground velocities in Fig. 2.9. In this case, the data points for the three sets of records

lie approximately along a straight line, irrespective of their A/V ratios. For the data set used, the correlation between the spectrum intensity and peak ground velocity may be given empirically by

$$SI = 3.3\ V \tag{2.3}$$

where SI is expressed in meters and V in meters per second. In addition, the mean values of the spectrum intensity are obtained for the three groups of records when normalized to a common peak velocity of 1m/s, and the results are presented in Table 2.5. The remarkable improvement in the consistency of the mean values among the three groups of records is evident when comparison is made with the case in which all the records are scaled to the same peak acceleration.

2.6 Summary

In this chapter, an earthquake data set selected as input ground motions for this study is described. The data set is analyzed to investigate the significance of the A/V ratio as a parameter to indicate the dynamic characteristics of earthquake ground motions resulting from different seismic environments. In the light of this investigation, the following conclusions can be drawn:

(1) The A/V ratio of ground motions is a viable indicator of the M-R relationship associated with the motions. Ground motions in the vicinity of small or moderate earthquakes usually have high A/V ratios whereas those distant from large earthquakes usually have low A/V ratios.

(2) As implied by its correlation with the M-R relationship, the A/V ratio is a useful, yet simple, parameter to indicate the relative frequency content and duration of strong shaking for earthquake ground

motions resulting from different seismic environments. Ground motions having high A/V ratios are usually of short duration with seismic energy in the high frequency range whereas those with low A/V ratios usually have long duration with energy in the low frequency range.

(3) Peak ground velocity correlates well with the spectrum intensity over earthquake records having drastically different A/V ratios, whereas the relationship between peak ground acceleration and the spectrum intensity strongly depends on the A/V ratio. Therefore, peak ground velocity is a superior parameter to describe the intensity of ground shaking at a site for building design, as compared to peak ground acceleration.

Table 2.1 List of Earthquake Events Considered in This Study

Earthquake	Magnitude	Date
Long Beach, Calif.	M_L: 6.3	Mar. 10, 1933
Lower California	M_L: 6.5	Dec. 30, 1934
Imperial Valley, Calif.	M_L: 6.6	May 18, 1940
Kern County, Calif.	M_L: 7.6	July 21, 1952
San Francisco, Calif.	M_L: 5.25	Mar. 22, 1957
Parkfield, Calif.	M_L: 5.6	June 27, 1966
Borrego Mtn., Calif.	M_L: 6.5	Apr. 8, 1968
Lytle Creek, Calif.	M_L: 5.4	Sept. 12, 1970
San Fernando, Calif.	M_L: 6.6	Feb. 9, 1971
Oroville, Calif.	M_L: 5.7	Aug. 1, 1975
Helena, Montana	M_L: 6.0	Oct. 31, 1935
Honshu, Japan	M_{JMA}: 5.4	Apr. 5, 1966
Near E. Coast of Honshu, Japan	M_{JMA}: 7.9	May 16, 1968
Central Honshu, Japan	M_{JMA}: 5.5	Feb. 26, 1971
Near S. Coast of Honshu, Japan	M_{JMA}: 7.0	Aug. 2, 1971
Near E. Coast of Honshu, Japan	M_{JMA}: 5.8	May 11, 1972
Near E. Coast of Honshu, Japan	M_{JMA}: 7.4	June 17, 1973
Near E. Coast of Honshu, Japan	M_{JMA}: 6.1	Nov. 16, 1974
Monte Negro, Yugoslavia	M_L: 5.4	Apr. 9, 1979
Monte Negro, Yugoslavia	M_L: 7.0	Apr. 15, 1979
Banja Luka, Yugoslavia	M_L: 6.1	Aug. 13, 1981
Nahanni, N.W.T., Canada	M_s: 6.9	Dec. 23, 1985
Michoacan, Mexico	M_s: 8.1	Sept. 19, 1985

M_L: Local Magnitude
M_{JMA}: Japan Meterological Agency Scale
M_s: Surface Wave Magnitude

Table 2.2 List of Low A/V Records (A/V < 0.8 g/m/s)

Earthquake	Date	Mag.	Site	Source Dist. (km)	Comp. Dir.	Max. Acc.(A) (g)	Max. Vel.(V) (m/s)	A/V Ratio (g/m/s)	Soil Cond.
Long Beach, Calif.	03/10/33	6.3	Subway Terminal, L.A.	59	N51W	0.097	0.237	0.41	Rock
Long Beach, Calif.	03/10/33	6.3	Subway Terminal, L.A.	59	N39E	0.064	0.173	0.37	Rock
Lower Calif.	12/30/34	6.5	El Centro	58	S00W	0.160	0.209	0.77	Stiff Soil
San Fernando, Calif.	02/09/71	6.6	2500 Wilshire Blvd., L.A.	40	N61W	0.101	0.193	0.52	Stiff Soil
San Fernando, Calif.	02/09/71	6.6	3550 Wilshire Blvd., L.A.	39	S00W	0.132	0.216	0.61	Stiff Soil
San Fernando, Calif.	02/09/71	6.6	222 Figueroa St., L.A.	41	S37W	0.129	0.186	0.69	Stiff Soil
San Fernando, Calif.	02/09/71	6.6	3470 Wilshire Blvd., L.A.	39	S90W	0.114	0.186	0.61	Stiff Soil
San Fernando, Calif.	02/09/71	6.6	4680 Wilshire Blvd., L.A.	38	N15E	0.117	0.215	0.54	Stiff Soil
San Fernando, Calif.	02/09/71	6.6	445 Figueroa St., L.A.	41	S38W	0.119	0.173	0.69	Rock
San Fernando, Calif.	02/09/71	6.6	Hollywood Storage L.A.	32	S00W	0.106	0.170	0.62	Stiff Soil
Near E. Coast of Honshu,Japan	05/16/68	7.9	Muroran Harbor	290	N00E	0.226	0.334	0.68	Stiff Soil
Near E. Coast of Honshu,Japan	06/17/73	7.4	Kushiro Central Wharf	112	N00E	0.205	0.275	0.75	Stiff Soil
Michoacan, Mexico	09/19/85	8.1	Zihuatenejo, Guerrero Array	135	S00E	0.103	0.159	0.65	Rock
Michoacan, Mexico	09/19/85	8.1	Teacalco, Guerrero Array	333	N00E	0.052	0.074	0.70	Rock
Michoacan, Mexico	09/19/85	8.1	Mesa Vibradora C.U.,Mexico City	379	N90W	0.040	0.110	0.36	Rock

Table 2.3 List of Intermediate A/V Records (0.8 < A/V < 1.2 g/m/s)

Earthquake	Date	Mag.	Site	Source Dist. (km)	Comp. Dir.	Max. Acc.(A) (g)	Max. Vel.(V) (m/s)	A/V Ratio (g/m/s)	Soil Cond.
Imperial Valley, Calif.	05/18/40	6.6	El Centro	8	S00E	0.348	0.334	1.04	Stiff Soil
Kern County, Calif.	07/21/52	7.6	Taft Lincoln School Tunnel	56	S69E	0.179	0.177	1.01	Rock
Kern County, Calif.	07/21/52	7.6	Taft Lincoln School Tunnel	56	N21E	0.156	0.157	0.99	Rock
Borrego Mtn., Calif.	04/08/68	6.5	SCE Power Plant, San Onofre	122	N57W	0.046	0.042	1.10	Stiff Soil
Borrego Mtn., Calif.	04/08/68	6.5	SCE Power Plant, San Onofre	122	N33E	0.041	0.037	1.11	Stiff Soil
San Fernando, Calif.	02/09/71	6.6	3838 Lankershim Blvd., L.A.	24	S90W	0.150	0.149	1.01	Rock
San Fernando, Calif.	02/09/71	6.6	Hollywood Storage P.E. Lot, L.A.	35	N90E	0.211	0.211	1.00	Stiff Soil
San Fernando, Calif.	02/09/71	6.6	3407 6th St., L.A.	39	N90E	0.165	0.166	0.99	Stiff Soil
San Fernando, Calif.	02/09/71	6.6	Griffith Park Observatory, L.A.	31	S00W	0.180	0.205	0.88	Rock
San Fernando, Calif.	02/09/71	6.6	234 Figueroa St., L.A.	41	N37E	0.199	0.167	1.19	Stiff Soil
Near E. Coast of Honshu,Japan	11/16/74	6.1	Kashima Harbor Works	38	N00E	0.070	0.072	0.97	Stiff Soil
Near S. Coast of Honshu,Japan	08/02/71	7.0	Kushiro Central Wharf	196	N90E	0.078	0.068	1.15	Stiff Soil
Monte Negro, Yugoslavia	04/15/79	7.0	Albatros Hotel, Ulcinj	17	N00E	0.171	0.194	0.88	Rock
Michoacan, Mexico	09/19/85	8.1	El Suchil, Guerrero Array	230	S00E	0.105	0.116	0.91	Rock
Michoacan, Mexico	09/19/85	8.1	La Villita, Guerrero Array	44	N90E	0.123	0.105	1.17	Rock

Table 2.4 List of High A/V Records (A/V > 1.2 g/m/s)

Earthquake	Date	Mag.	Site	Source Dist. (km)	Comp. Dir.	Max. Acc.(A) (g)	Max. Vel.(V) (m/s)	A/V Ratio (g/m/s)	Soil Cond.
Parkfield, Calif.	06/27/66	5.6	Temblor No. 2	7	N65W	0.269	0.145	1.86	Rock
Parkfield, Calif.	06/27/66	5.6	Cholame Shandon No. 5	5	N85E	0.434	0.255	1.70	Rock
San Francisco, Calif.	03/22/57	5.25	Golden Gate Park, S.F.	11	S80E	0.105	0.046	2.28	Rock
San Francisco, Calif.	03/22/57	5.25	State Bldg., S.F.	17	S09E	0.085	0.051	1.67	Stiff Soil
Helena, Montana	10/31/35	6.0	Carroll College	8	N00E	0.146	0.072	2.03	Rock
Lytle Creek, Calif.	09/12/70	5.4	Wrightwood	15	S25W	0.198	0.096	2.06	Rock
Oroville, Calif.	08/01/75	5.7	Seism. Station, Oroville	13	N53W	0.084	0.044	1.91	Rock
San Fernando, Calif.	02/09/71	6.6	Pacoima Dam	4	S74W	1.075	0.577	1.86	Rock
San Fernando, Calif.	02/09/71	6.6	Lake Hughes, Station 4	26	S21W	0.146	0.085	1.72	Rock
Nahanni, N.W.T., Canada	12/23/85	6.9	Site 1, Iverson	7.5	LONG	1.101	0.462	2.38	Rock
Central Honshu, Japan	02/26/71	5.5	Yoneyama Bridge	27	TRAN	0.151	0.059	2.56	Stiff Soil
Near E. Coast of Honshu,Japan	05/11/72	5.8	Kushiro Central Wharf	33	N00E	0.146	0.060	2.43	Stiff Soil
Honshu, Japan	04/05/66	5.4	Hoshina-A	4	N00E	0.270	0.111	2.43	Stiff Soil
Monte Negro, Yugoslavia	04/09/79	5.4	Albatros Hotel, Ulcinj	12.5	N00E	0.042	0.016	2.63	Rock
Banja Luka, Yugoslavia	08/13/81	6.1	Seism. Station, Banja Luka	8.5	N90W	0.074	0.032	2.31	Rock

Table 2.5 Statistical Summary of Ground Motion Parameters

	A/V Ratio (g/m/s)	Strong-Motion Duration (sec)		Spectral Intensity (m)	
		McCann-Shah Method	Vanmarcke-Lai Method	Scaled to 1g	Scaled to 1m/s
Low A/V Records	0.60* (0.213)+	12.58 (0.452)	12.49 (0.353)	5.787 (0.292)	3.301 (0.214)
Intermediate A/V Records	1.03 (0.094)	7.41 (0.290)	8.50 (0.282)	3.560 (0.119)	3.639 (0.106)
High A/V Records	2.12 (0.149)	2.71 (0.558)	1.73 (0.471)	1.401 (0.292)	2.883 (0.216)

* Mean
+ Coefficient of Variation

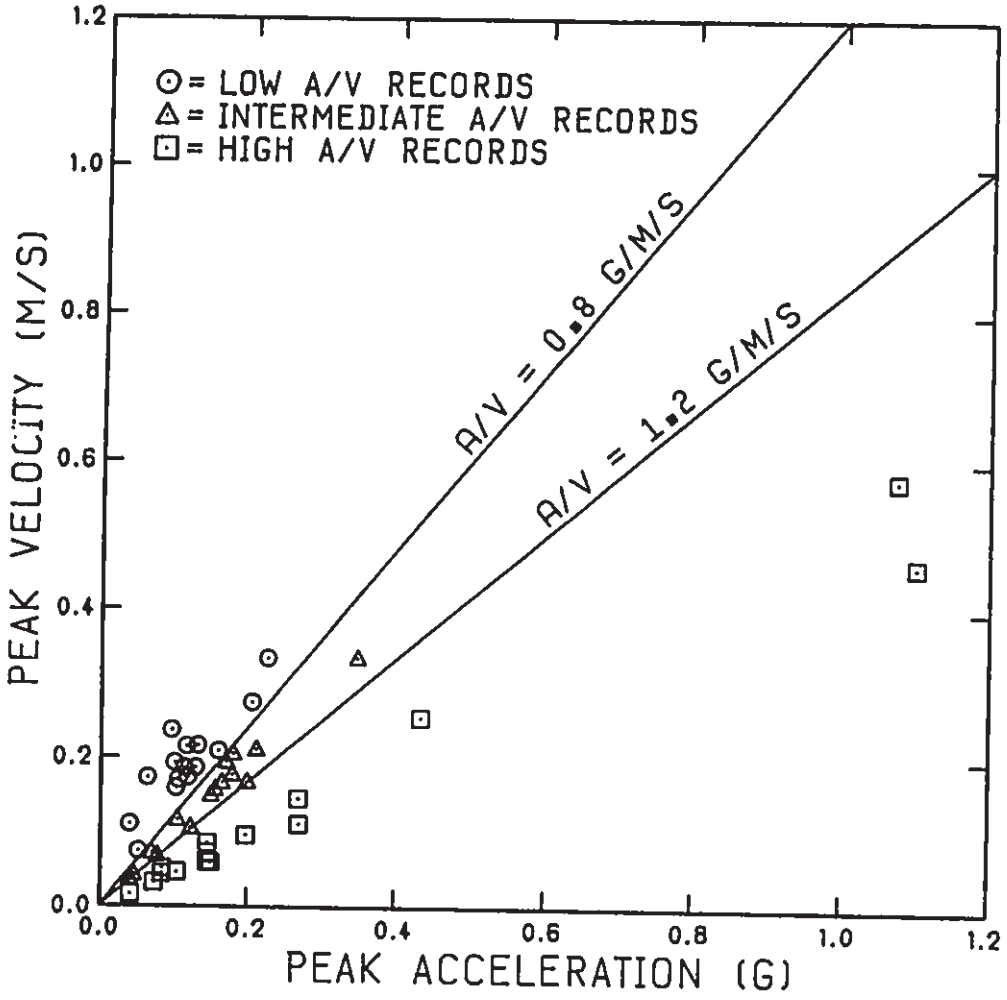

Fig. 2.1 Peak Acceleration vs. Peak Velocity for Three Groups of Records Having Low, Intermediate, and High A/V Ratios

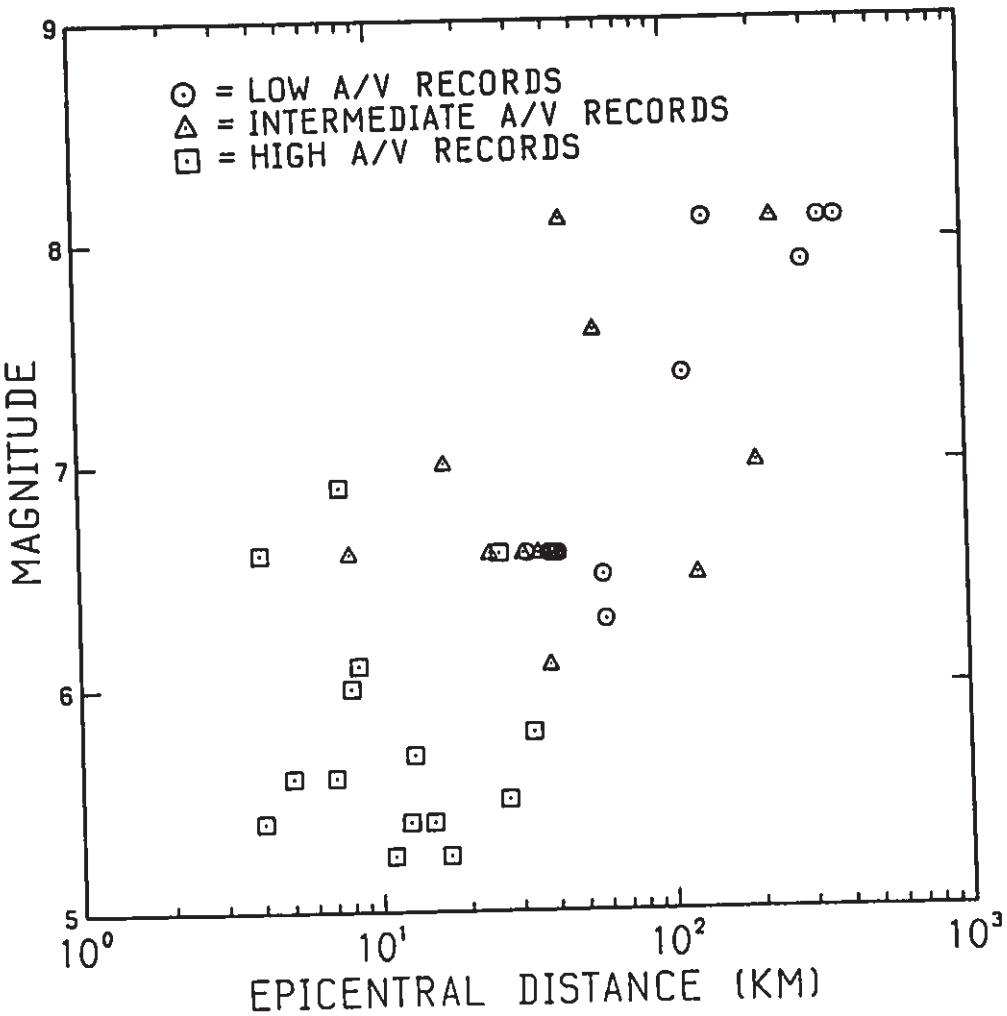

Fig. 2.2 Relationship between Earthquake Magnitude (M) and Epicentral Distance (R) for Three Groups of Records Having Low, Intermediate, and High A/V Ratios

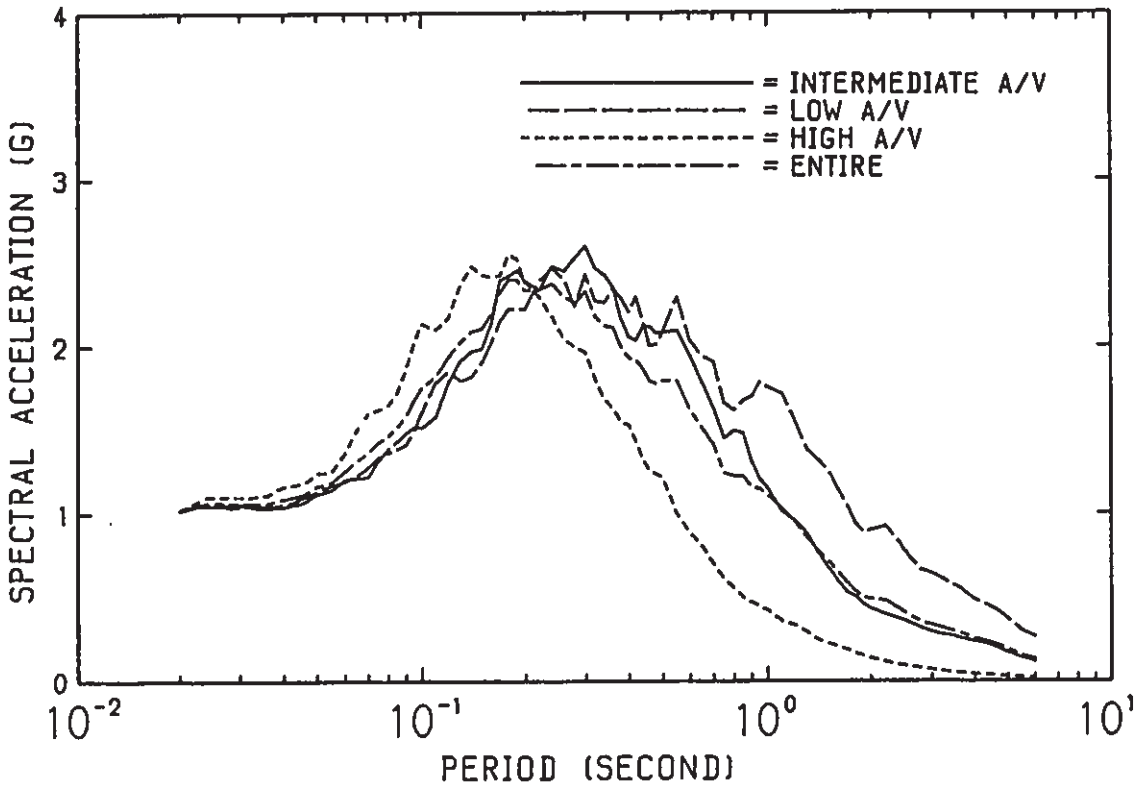

Fig. 2.3 Mean 5% Damped Elastic Acceleration Response Spectra for Three Separate Groups and Whole Ensemble of Records Scaled to a Common Peak Acceleration of 1g

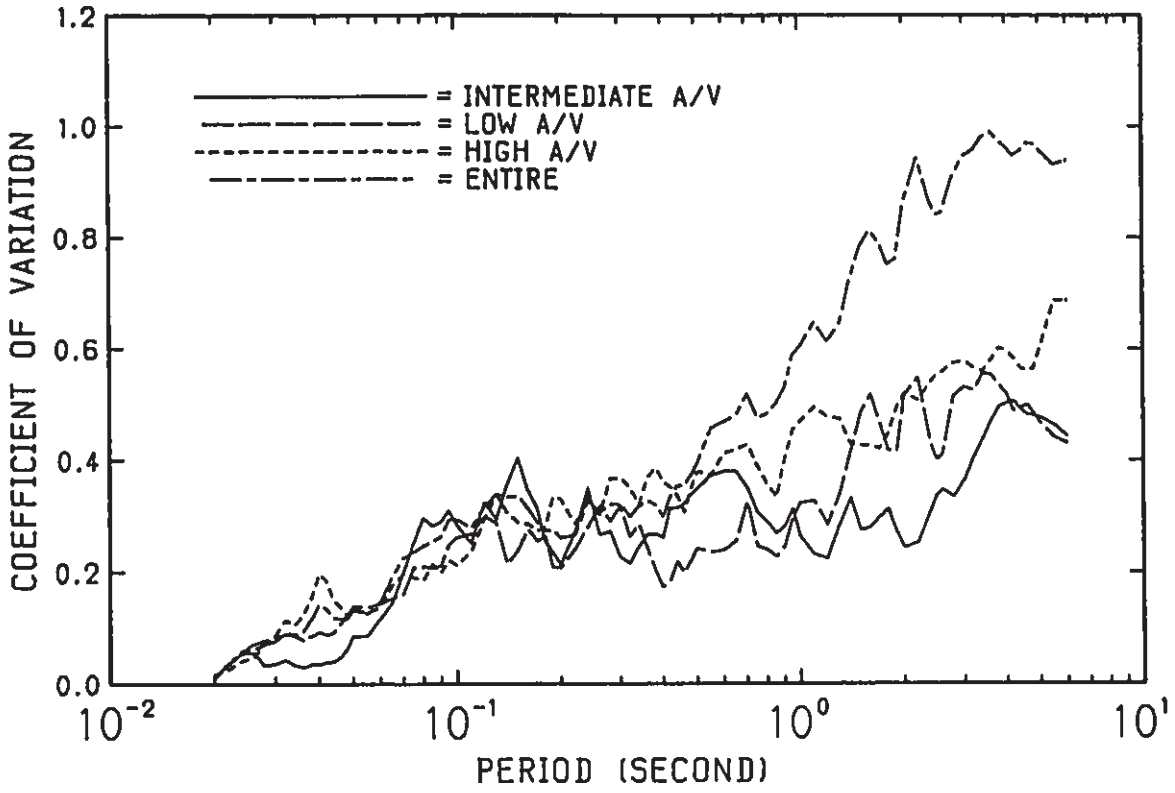

Fig. 2.4 Coefficients of Variation of Elastic Acceleration Response Spectra for Three Separate Groups and Whole Ensemble of Records Scaled to a Common Peak Acceleration of 1g

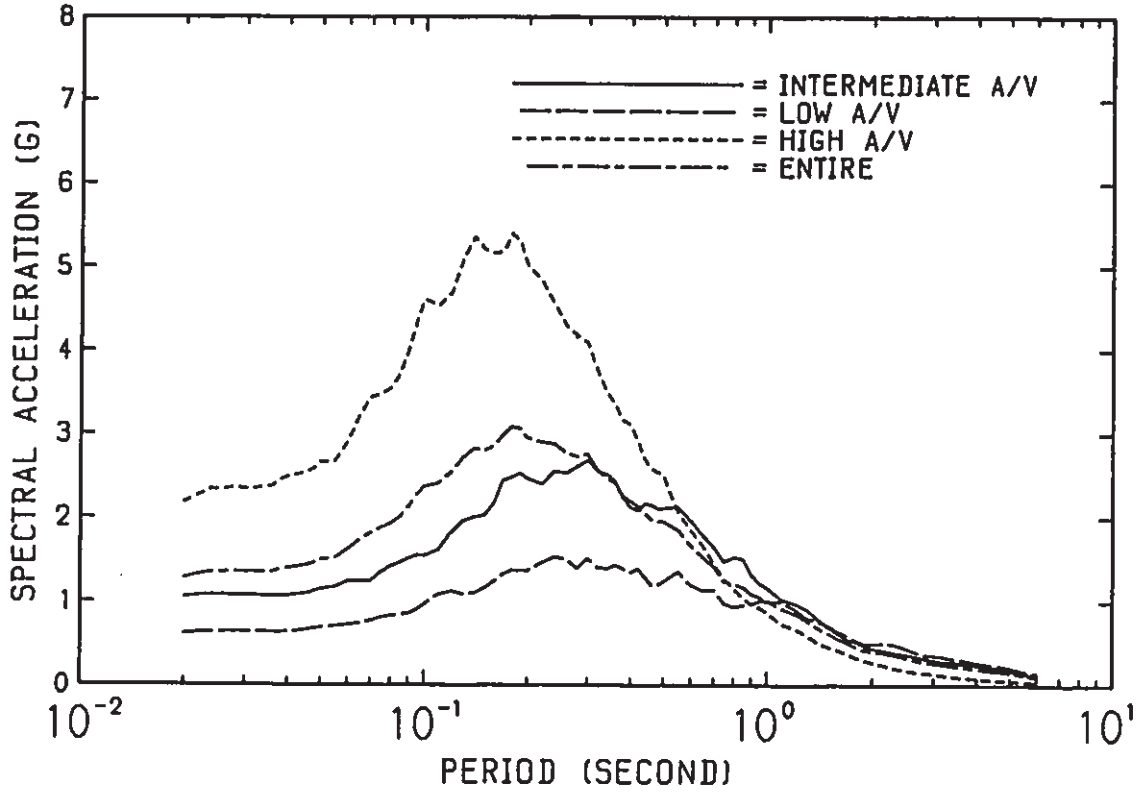

Fig. 2.5 Mean 5% Damped Elastic Acceleration Response Spectra for Three Separate Groups and Whole Ensemble of Records Scaled to a Common Peak Velocity of 1m/s

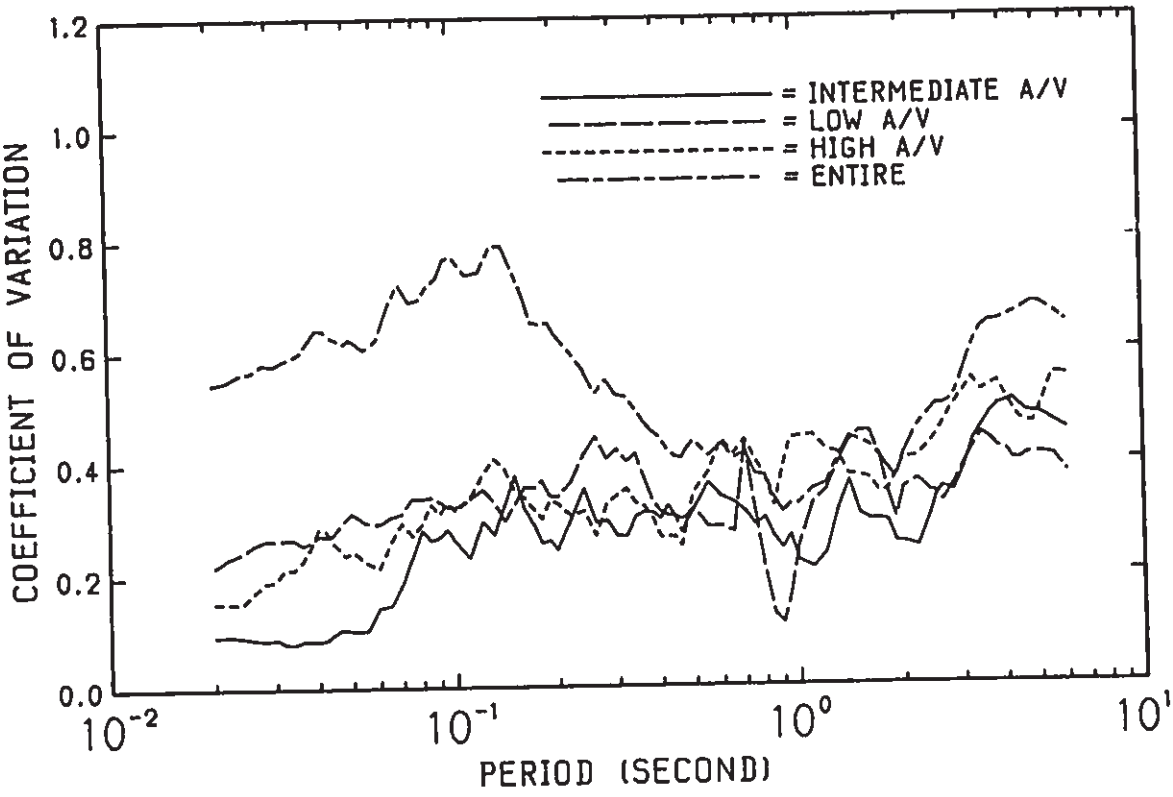

Fig. 2.6 Coefficients of Variation of Elastic Acceleration Response Spectra for Three Separate Groups and Whole Ensemble of Records Scaled to a Common Peak Velocity of 1m/s

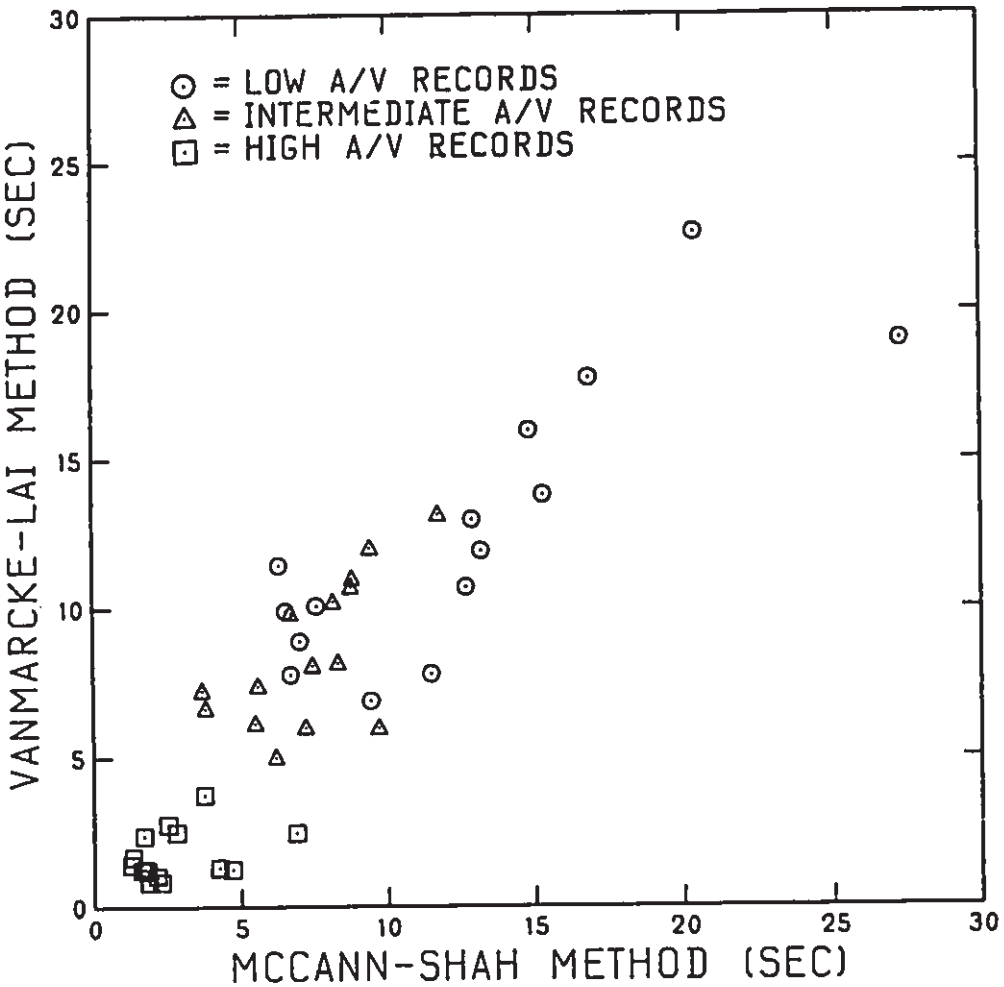

Fig. 2.7 Comparison of Strong-Motion Durations Calculated from Vanmarcke-Lai and McCann-Shah Definitions for Three Groups of Records Having Low, Intermediate, and High A/V Ratios

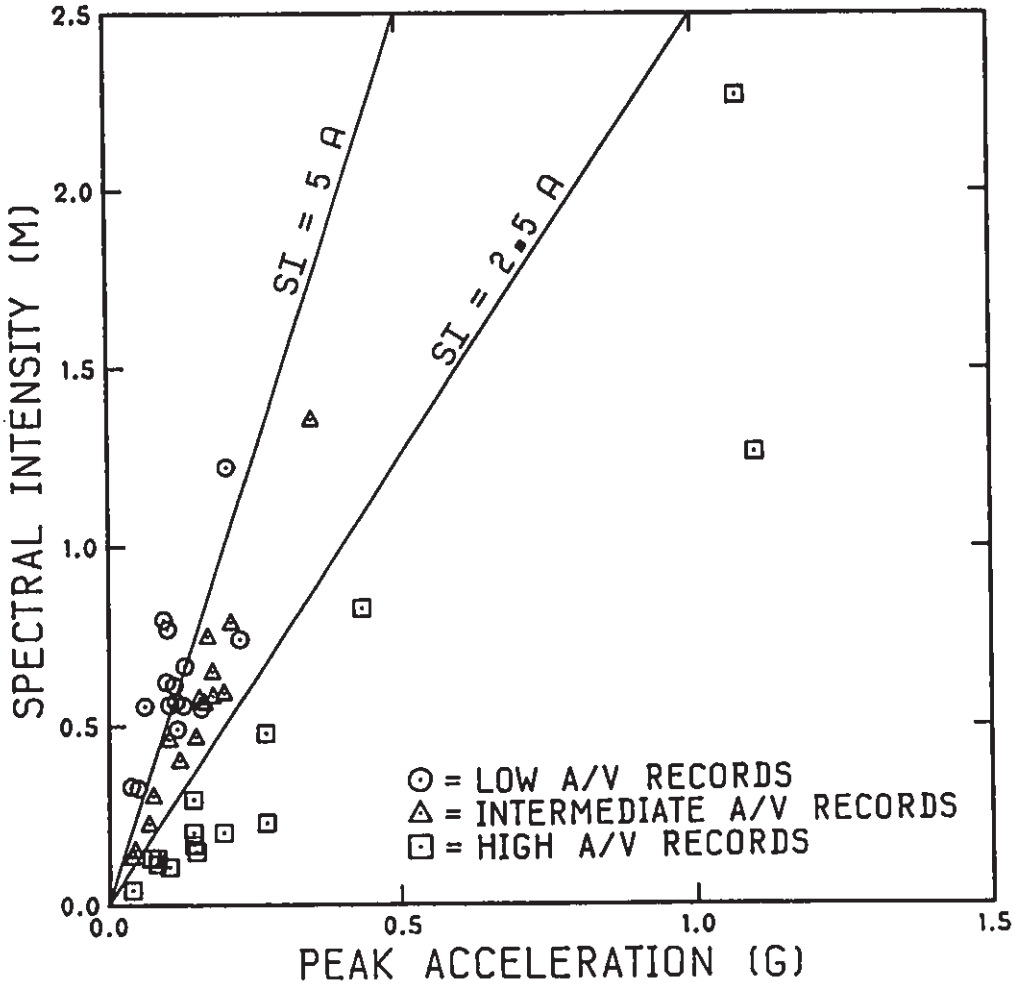

Fig. 2.8 Correlation between Spectrum Intensity and Peak Acceleration for Three Groups of Records Having Low, Intermediate, and High A/V Ratios

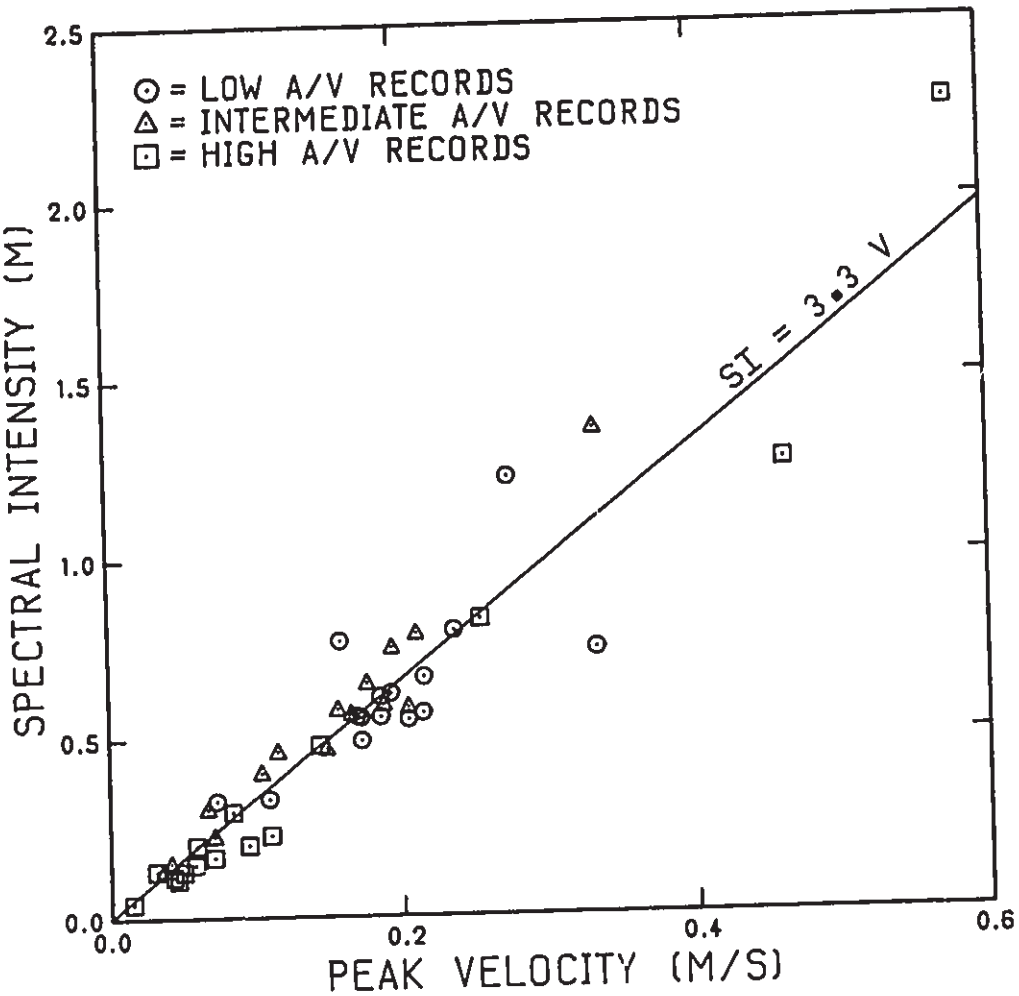

Fig. 2.9 Correlation between Spectrum Intensity and Peak Velocity for Three Groups of Records Having Low, Intermediate, and High A/V Ratios

CHAPTER 3

STRUCTURAL MODELS

3.1 Introduction

The most commonly used structural framing system for reinforced concrete buildings is ductile moment-resisting frame. Previous integrated experimental and analytical studies (34,63,65) have indicated that for regular reinforced concrete moment-resisting frames, their inelastic dynamic responses under strong earthquake excitation can be reasonably well predicted by current analytical models. Therefore, only reguiar reinforced concrete frame structures are used as structural models in this study.

To cover a wide range of structural period, four reinforced concrete frames with different fundamental periods are considered. Three basic frames with four, ten, and eighteen storeys are designed based on typical material properties. These three basic frames are designated as 4S2, 10S, and 18S, respectively, and they are used as structural models having short, moderate, and long fundamental periods. A special four-storey frame is created from the basic four-storey frame (4S2) by increasing the stiffness of its members. This special frame is denoted as 4S1 and represents a structural model having a very short fundamental period. Typical design gravity loads are assumed for the four frames. The seismic design forces for the four frames are determined in accordance with the seismic loading provisions in NBCC 1985. The structural members are proportioned and detailed to satisfy the requirements of CAN3-A23.3-M84.

This chapter provides a detailed description of the design procedure used to design the frames. The final designs are expressed in terms of reinforcement ratios for beams and columns. The elastic dynamic properties of the designed frames are presented. Also, the designed frames are checked for the serviceability requirements under service level wind loading.

3.2 Structural Configuration and Member Size

In terms of configuration, three basic frame structures with four, ten, and eighteen storeys are considered in this study. The three frame structures have the same floor plan, as shown in Fig. 3.1. There are three equal bays in the East-West direction and seven equal bays in the North-South direction. The bay widths are 8000 mm in both directions. The effect of seismic action is considered in the E-W direction, and typical interior frames of the three frame structures in the E-W direction are designed and analyzed in this study. The elevations of the three interior frames are shown in Fig. 3.2. The frames have equal storey heights of 3500 mm throughout.

The sizes of beams and columns for the three frames are also shown in Fig. 3.2. It should be noted that the determination of member size is an iterative process. The member sizes shown in Fig. 3.2 are the final values after preliminary design calculations. To achieve an optimum design, the sizes of beams and columns are varied along the height of each frame. However, the variation occurs every two or three storeys, and the change between two adjacent storeys is relatively small. This is done to ensure a smooth transition in member stiffness throughout the height

of each frame. The slabs in the buildings are two way slabs and assumed to have a thickness of 150 mm. This value of slab thickness will be used in the calculation of the dead load and effective beam stiffness.

3.3 Material Properties

For the purpose of design, nominal values are taken for the properties of concrete and reinforcing steel bars. The assumed properties are summarized in Table 3.1.

3.4 Design Loading

The frames are designed for the critical combinations of gravity and seismic loading based on the limit state approach suggested in NBCC 1985. In this section, the specification of gravity and seismic loads and their combinations is described.

3.4.1 Gravity Loading

The design gravity loading consists of dead load and live load. The design dead loads for each frame are estimated based on the weight of (a) structural components (slabs, beams, and columns); (b) partition walls; and (c) mechanical equipment. The design live loads are taken as those suggested by NBCC 1985 for ordinary office buildings. A summary of the design gravity loads used in this study is presented in Table 3.2.

The distributions of the gravity loading on the frames are obtained using the tributary area method. Fig. 3.3 shows the tributary areas and the resulting gravity loads on the beams at a typical floor level and the roof. Note that the live loads have been reduced as allowed by NBCC 1985.

Also, the distributed loads which are triangular or trapezoidal in shape are simplified as uniformly distributed loads. This simplification has only minor effect on the fixed end moments of beams and columns.

3.4.2 Storey Mass and Seismic Loading

The reactive mass at each storey level is estimated from the design dead load acting on that storey. Snow load is not included in the reactive mass for the roof. The estimated masses for a typical floor and the roof are given in Table 3.3. These estimated masses are lumped at the storey levels and used in the determination of lateral seismic design forces and the calculation of eigenvalue solutions as described below.

The total lateral seismic design force V for each frame is calculated from the following base shear formula:

$$V = v\ S\ K\ I\ F\ W \qquad (3.1)$$

in which

v = zonal velocity ratio;

S = seismic response factor;

K = structural behaviour coefficient;

I = importance factor;

F = foundation factor;

W = weight of the reactive masses in the frame.

The zonal velocity ratio v is defined as the ratio of zonal peak ground velocity to a velocity of 1 m/s and specified with an exceedance probability of 10 % in 50 [illegible]. This probability level is appropriate to the seismic design forces [illegible]ed by the base shear formula (31). The structural behaviour K is intended to account for the energy dissipation

capacities of different types of structural systems due to inelastic deformation and damping. The period dependence of the seismic response factor S is described graphically in Fig. 3.4. It can be noted that the design base shear is directly proportional to zonal peak ground velocity for structural periods beyond 0.5 sec. For periods shorter than 0.5 sec, three different levels of seismic response factor are used for three different combinations of acceleration and velocity seismic zones to accommodate the effect of zonal peak ground acceleration on short period structures. The three zonal combinations signify low, intermediate, and high A/V ratios and are symbolically referred to as $Z_a<Z_v$, $Z_a=Z_v$, and $Z_a>Z_v$, respectively.

Two different types of frames should be distinguished in terms of the relative significance between seismic and gravity loading (70). For earthquake load dominated frames, their design is controlled by seismic loading. Because of the predominant bending moments induced by earthquake excitation, plastic hinges in the beams are normally formed close to their ends. The design of gravity load dominated frames is controlled by gravity loading. Plastic hinges in the beams of these frames may form within their spans. In this study, only earthquake load dominated frames are considered. Therefore, the frames are assumed to be located in regions with high seismicity, namely $Z_v = 6$. Accordingly, v is taken as 0.4 in Eq. (3.1). The use of earthquake load dominated frames is consistent with the dynamic analysis procedure to be used in this study in which plasticity in structural members is assumed to be concentrated at their two ends.

For ordinary office buildings, the importance factor I is taken as 1.0. The frames are assumed to be situated on rock or stiff soil sites, which are consistent with the local soil conditions for the selected earthquake accelerograms to be used as input ground motions for the frames. Accordingly, the foundation factor F is assigned a value of 1.0.

In order to determine the seismic response factor S, the fundamental period T must be known. NBCC 1985 gives the following formula to estimate the fundamental period for regular moment-resisting frames:

$$T = 0.1\ N \tag{3.2}$$

in which N is the total number of storeys. This formula only depends on the number of storeys. The fundamental periods of the three basic frames (4S2, 10S, 18S) are estimated from Eq. (3.2) in the calculation of their seismic response factors. The computed design base shears for these three frames are summarized in Table 3.4. It should be noted that the design base shear for the 4S2 frame is different for the three different zonal combinations. The use of three different seismic design forces will result in three frames with different amounts of reinforcement steel for beams and columns. These three frames have the same initial elastic properties but different inelastic characteristics. The three frames will be denoted as 4S2L, 4S2I, and 4S2H, where L, I, and H refer to low, intermediate, and high A/V ratio corresponding to $Z_a<Z_v$, $Z_a=Z_v$, and $Z_a>Z_v$ in Fig. 3.4.

The elastic dynamic properties of the three frames are determined from their eigenvalue solutions. The storey masses shown in Table 3.3 are used for the eigenvalue solutions. The slab effect is accounted for in the calculation of beam stiffness. The effective flange width for the

beams is found to be 2000 mm based on CAN3-A23.2-M84 (Clause 8.10.2). To account for cracking, the flexural rigidity of the beams is assumed to be 0.5 of their gross section value. The flexural rigidity of the columns is not reduced because they are expected to remain uncracked in the service load range (68). The periods of the first three vibration modes are computed for the three frames, and they are given in Table 3.5 and shown on Fig. 3.4. It can be seen that the computed fundamental periods of the three frames are about 10% to 20% higher than the values estimated from Eq.(3.2). Had the fundamental periods obtained from the eigenvalue solutions been used to estimate the seismic response factors, the seismic design forces for the three frames would have been slightly lower than those used in this study.

To evaluate the suitability of using three different levels of seismic response factor over the short period range, as suggested in NBCC 1985, a special frame with a fundamental period shorter than 0.25 sec is created from the 4S2 frame. This special frame (4S1) is identical to the 4S2 frame in structural configuration and member sizes with the exception that the modulus of elasticity is increased to give a fundamental period of 0.23 sec. The first three vibrational periods for the 4S1 frame are shown in Table 3.5. This modification places the frame in the three constant regions of the seismic response factor for the three different zonal combinations, as shown in Fig.3.4. The computed design base shears for the three zonal combinations are also given in Table 3.4. The three frames corresponding to the three zonal combinations will be referred to as 4S1L, 4S1I, and 4S1H, respectively.

The computed design base shear for each of the eight frames (4S1L, 4S1I, 4S1H, 4S2L, 4S2I, 4S2H, 10S, 18S) is distributed through the height of the frame based on the following distribution formula suggested by NBCC 1985:

$$F_x = \frac{(V-F_t)W_x h_x}{\sum_{i=1}^{n} W_i h_i} \qquad (3.3a)$$

in which

W_i, W_x = that portion of W assigned to level i or x, respectively;

h_i, h_x = the height above the base to level i or x, respectively;

n = total number of storeys;

F_x = lateral force at level x;

F_t = that portion of V concentrated at the top of the frame in addition to F_n defined by Eq.(3.3a).

F_t is given by

$$F_t \begin{cases} = 0.004\ V\ (h_n/D_s) \leq 0.15\ V \\ = 0.0 \qquad \text{if } h_n/D_s \leq 3 \end{cases} \qquad (3.3b)$$

in which

h_n = the total height of the frame above the base;

D_s = the dimension of the frame in the direction parallel to the lateral seismic loading.

It can be seen from Eqs. (3.3) that if $h_n/D_s > 3$, a portion of the design base shear is concentrated at the top of the frame in an attempt to accommodate higher mode effects on the force distribution. For the frames considered in this study, only the eighteen-storey frame has a value of h_n/D_s higher than 3. Accordingly, an F_t is applied at the top of the eighteen-storey frame. The distributions of the lateral seismic design

forces for the eight frames are shown in Table 3.6.

3.4.3 Load Combinations

In conformance with NBCC 1985, three critical load combinations are considered in the design of the eight frames. These three load combinations are given as follows:

$$\begin{cases} 1.25\ D + 1.5\ L \\ 1.25\ D + 1.5\ Q \\ 1.25\ D + 0.7\ (\ 1.5\ L + 1.5\ Q\ ) \end{cases} \tag{3.4}$$

where

D = dead load;

L = live load due to use and occupancy;

Q = seismic load.

The magnitudes and distributions of D, L, and Q are shown in Fig. 3.3 and Table 3.6. Loading patterns for live loads are not considered, but live load reduction, as allowed in NBCC 1985, is incorporated in the design process.

3.5 Effects of Geometric Nonlinearity

The effects of geometric nonlinearity should be considered in the design of moment-resisting frames. The geometric effects can be decomposed into two types (49). One is lateral drift effect (also called P-delta effect) and the other is member slenderness effect. CAN3-A23.3-M84 has separate provisions to account for these two types of geometric effects in design (Clauses 10.11.6 and 10.11.7).

The P-delta effect increases design moments for both beams and columns. CAN3-A23.3-M84 allows the use of a second-order analysis to evaluate the P-delta effect. Several iterative solution techniques are available for this purpose (49,74). However, these iterative methods are not appropriate for dynamic analysis (93). In the dynamic analysis of this study, a linearized solution (93) will be employed to account for the P-delta effect. To be consistent with the dynamic analysis, the same procedure is used herein for the design of the frames. In this procedure, a geometric stiffness matrix is evaluated from the column axial force due to gravity loading, and the solution to the P-delta effect is obtained directly without iteration. A detailed description of this procedure will be given in Chapter 4. The member slenderness effect is considered only for compression members and will be described in column design.

3.6 Member Design

In this study, only flexural reinforcement is designed for the structural members in the eight frames. The design of transverse reinforcement is not considered. The factored beam design moments are obtained from elastic static analyses of the frames under the three different load combinations described previously. The same beam and column stiffnesses as those for the eigenvalue solutions are used in the elastic static analyses. Rigid end zones are considered for the beams and columns, and the beam design moments are obtained at column faces. The factored column design moments are determined based on the weak beam-strong column criterion. The column design moments are related to the beam moment capacities by considering the equilibrium of each beam-column

joint, coupled with a column overstrength factor. The obtained column design moments are further amplified to account for slenderness effect. The detailed considerations for the design of beams and columns are given as follows.

3.6.1 Beam Design

The factored beam moments obtained from the three load combinations as described above are used as design moments for the beams. At each storey level, the computed moments at the two ends of the two exterior bay beams are very close to those at the two ends of the interior bay beam. Therefore, the maximum moment at each storey level is used in the design of all three beams. The use of the same design moment at either side of interior columns avoids termination and anchorage of beam bars at interior beam-column joints in which a congestion of reinforcement may create construction difficulties.

CAN3-A23.3-M84 allows moment redistribution for continuous beams (Clause 8.4). The magnitude of moment redistribution is controlled by

$$\text{MRF} \begin{cases} \leq 30 - 50\ c/d \\ \leq 20\% \end{cases} \quad \text{whichever is smaller} \qquad (3.5)$$

where

MRF = moment redistribution factor;

c = distance from extreme compression fiber to neutral axis;

d = distance from extreme compression fiber to centroid of tension reinforcement.

While it is acceptable to redistribute the seismic load moments in the case of weak beam-strong column design, only the dead and live load moments are redistributed in this study. For simplicity, the dead and

live load moments at the two beam ends are reduced by 20%. This redistribution has minor effect on the final design moments for the beams because the beam design in this study is controlled by seismic loading. This is particularly true for the beams at lower storey levels.

A lower bound is imposed in determining the positive design moments at the beam ends. This lower bound is recommended by CAN3-A23.3-M84 and given as follows:

$$M_b^+ \geq 0.5\ |M_b^-| \tag{3.6}$$

where M_b^+, M_b^- = positive or negative beam design moment at a support section. This lower bound intends not only to recognize the cyclic nature of seismic response but also to include the beneficial effect of compressive reinforcement on the inelastic deformation capacity of the beam under large negative moment.

In the determination of the flexural reinforcement for the beams, the contribution of reinforcing bars in the slab to the negative moment capacity is neglected. The flexural reinforcement for the beams is determined from the following equation:

$$M_b = bd^2\rho(\phi_s f_y)\left(1 - 0.59\rho\ \frac{\phi_s f_y}{\phi_c f_c'}\right) \tag{3.7}$$

in which

M_b = design beam moment

b = section width;

f_y = yield strength of reinforcing steel;

f_c' = compressive strength of concrete;

ϕ_s = resistance factor for reinforcing steel (0.85);

ϕ_c = resistance factor for concrete (0.60);

ρ = percentage of flexural reinforcement (A_s/bd);

A_s = area of flexural reinforcement.

The computed reinforcement ratio is bounded by the following lower and upper limits prescribed by CAN3-A23.3-M84:

$$\text{lower bound} \quad \rho \geq \frac{1.4}{f_y} \tag{3.8a}$$

$$\text{upper bound} \begin{cases} \dfrac{c}{d} \leq \dfrac{600}{600 + f_y} \\ \rho \leq 0.025 \end{cases} \quad \text{whichever is smaller} \tag{3.8b}$$

The first upper limit is recommended for the design of flexural members. The upper limit of 0.025 is suggested for ductile moment-resisting frames in the special provisions for seismic design.

3.6.2 Column Design

As shown in Fig. 3.5, the relationships between the column design moments and the beam moment capacities are derived from the equilibrium of each beam-column joint, coupled with a column overstrength factor. For an exterior joint, only one load condition controls the column design. In the case of an interior joint, two possible load conditions should be considered. The expressions relating the column design moments to the beam moment capacities for a typical exterior or interior joint are given as follows. In these expressions, all variables are assumed to be in absolute values.

(a) Exterior columns:

$$M_c^T + M_c^B + \frac{h_b}{2}(V_c^T + V_c^B) = [\, M_{b1}^- + \frac{h_c}{2}\left(\frac{M_{b1}^- + M_{b2}^+}{l_b^L} + V_{b1}^G\right)\,]\,\eta \qquad (3.9a)$$

(b) Interior columns:

Load condition 1:

$$M_c^T + M_c^B + \frac{h_b}{2}(V_c^T + V_c^B) = [\,\left(M_{b2}^- + M_{b3}^+\right) + \frac{h_c}{2}\left(\frac{M_{b1}^+ + M_{b2}^-}{l_b^L} + \frac{M_{b3}^+ + M_{b3}^-}{l_b^M}\right) + \frac{h_c}{2}\left(V_{b2}^G - V_{b3}^G\right)\,]\,\eta \qquad (3.9b)$$

Load condition 2:

$$M_c^T + M_c^B + \frac{h_b}{2}(V_c^T + V_c^B) = [\,\left(M_{b2}^+ + M_{b3}^-\right) + \frac{h_c}{2}\left(\frac{M_{b1}^- + M_{b2}^+}{l_b^L} + \frac{M_{b3}^- + M_{b3}^+}{l_b^M}\right) + \frac{h_c}{2}\left(V_{b3}^G - V_{b2}^G\right)\,]\,\eta \qquad (3.9c)$$

where

M_c^T, M_c^B = design moment for top or bottom column;

V_c^T, V_c^B = shear force for top or bottom column;

M_{b1}^+, M_{b2}^+, M_{b3}^+ = positive beam moment capacity at section 1, 2, and 3, respectively (ϕ_s=1.0; ϕ_c=1.0);

M_{b1}^-, M_{b2}^-, M_{b3}^- = negative beam moment capacity at section 1, 2, and 3, respectively (ϕ_s=1.0; ϕ_c=1.0);

V_{b1}^G, V_{b2}^G, V_{b3}^G = beam shear due to gravity loading at section 1, 2, and 3, respectively;

h_b, h_c = cross section depth of beam or column;

l_b^L, l_b^M = clear beam length in left or middle span;

η = column overstrength factor.

For the intermediate storeys, column inflection points are assumed to be at mid-height. Therefore, the column shears can be expressed in terms of the column end moments as follows:

$$V_c^T = \frac{2\ M_c^T}{l_c^T} \tag{3.10a}$$

$$V_c^B = \frac{2\ M_c^B}{l_c^B} \tag{3.10b}$$

where l_c^T, l_c^B = clear height of top or bottom column. Some adjustments are made for the upper and lower storeys based on Muto's procedure (55). The column overstrength factor η is taken as 1.2 in this study. This value is slightly higher than the value of 1.1 suggested by CAN3-A23.3-M84.

The relationship between M_c^T and M_c^B is based on the relative stiffness distribution between the top and bottom columns and given by

$$M_c^T = \beta\ M_c^B \tag{3.11}$$

where

$$\beta = \frac{K_c^T}{K_c^B};$$

$$K_c^T \sim \frac{EI_c^T}{(l_c^T)^2};$$

$$K_c^B \sim \frac{EI_c^B}{(l_c^B)^2};$$

where EI_c^T, EI_c^B = flexural rigidity of top or bottom column.

The column design moments obtained from the combination of Eqs. (3.9), (3.10), and (3.11) are further amplified to account for slenderness effect. This is in conformance with Clause 10.11.6 of CAN3-A23.3-M84. The amplification factor is given by

$$\delta_b = \frac{C_m}{1 - \dfrac{P_f}{\phi_m P_c}} \geq 1.0 \qquad (3.12)$$

where

$$P_c = \frac{\pi^2 EI}{(kl_u)^2};$$

P_f = factored axial load;

C_m = a factor relating actual moment diagram to an equivalent uniform moment diagram (1.0);

ϕ_m = member resistance factor (0.65);

$EI = 0.25 E_c I_g$;

E_c = modulus of elasticity of concrete;

I_g = moment of inertia of gross concrete section about centroidal axis;

l_u = unsupported length of column;

k = effective length factor.

The effective length factor k depends on the rotation restraint of a beam-column joint. A measure of this restraint is given by

$$\psi = \frac{\Sigma (EI_c/l_c)}{\Sigma (EI_b/l_b)} \qquad (3.13)$$

The summation is carried out for all beams or columns at the joint. The effective length factor k is determined based on the following relationships suggested by Furlong (26).

$$k = \begin{cases} \dfrac{20 - \psi_{ave}}{20}\sqrt{1 + \psi_{ave}} & \psi_{ave} < 2 \\ 0.9\sqrt{1 + \psi_{ave}} & \psi_{ave} > 2 \end{cases} \qquad (3.14)$$

where ψ_{ave} is the average value of the two ψ values obtained at the

two ends of a column.

The amplification factors are computed for the eight frames based on the procedure described above, and they are shown in Table 3.7.

The maximum and minimum design axial forces for the columns are determined from the elastic static analyses of the frames under the three load combinations. The columns are designed based on the most critical combination of design bending moment and axial force. The column design charts suggested by Canadian Portland Cement Association (19) are used to determine the reinforcement ratio on the basis of the critical combination.

The computed column reinforcement ratios are bounded by the following lower and upper limits:

$$0.01 \leq \rho \leq 0.06 \qquad (3.15)$$

where

$$\rho = \frac{A_{st}}{A_g};$$

A_{st} = area of longitudinal steel bars in a column;

A_g = gross area of column cross section.

The upper bound of 0.06 is controlled by the special provisions for seismic design.

At each joint, the column section immediately above or below the joint is designed for its own critical combination of design bending moment and axial force, and the larger amount of reinforcement obtained is used for both columns. The use of the same reinforcement above and below a joint avoids the termination and anchorage of column longitudinal steel bars within the joint. All column steel bar splices occur near

mid-column height where bending moment is relatively small.

3.7 Final Design Results

The ETABS program (94) is used to carry out elastic static analysis of each frame in the design. The design procedure for structural members described in the previous section has been programmed as separate subroutines, and these subroutines are combined with the ETABS program. Therefore, the whole design procedure can be formulated automatically. The final design results for the eight frames are presented in terms of flexural reinforcement ratios for beams and columns, and they are summarized in Fig. 3.6.

3.8 Check for Serviceability Requirement

Generally speaking, two limit states should be considered in the design of building structures. One is the ultimate limit state which concerns the safety of the buildings against collapse, and the other is the serviceability limit state which restricts the intended use and occupancy of the buildings. The design of the frames considered in this study is based on the ultimate limit state, as described above. In this section, the serviceability of the designed frames is checked for service level wind loading. The calculation and distribution of the wind loading are based on Clause 4.1.8.1 in NBCC 1985. The reference velocity pressure is assumed to be 0.6 kPa in the calculation of the wind loading. This level of reference velocity pressure corresponds to severe wind loading.

The frames remain elastic under the service level wind loading. The interstorey drifts due to the wind loading are shown in Fig. 3.7. It can

be seen that the drift indices are well within the acceptable limit of 0.2% suggested by NBCC 1985 (Clause 4.1.1.5(5)). The drifts increase with an increase in the number of storeys. The interstorey drifts for the 4S1 frame are smaller than those for the 4S2 frame because of its higher member stiffness.

Table 3.1 Assumed Material Properties

Concrete:	
Compressive Strength:	f'_c = 30 MPa
Modulus of Elasticity:	E_c = 27000 MPa
Unit Weight:	w_c = 23.5 kN/m^3
Reinforcing Steel:	
Yield Strength:	f_y = 350 MPa
Modulus of Elasticity:	E_s = 200000 MPa

Table 3.2 Design Gravity Loads (kN/m^2)

	Dead Load		Live Load
Floor	Weight of Slabs	3.5	
	Weight of Beams and Columns	2.5	
	Partition Loading	0.5	
	Mechanical Service Loading	0.5	
	Total	7.0	2.4
Roof	Weight of Slabs	3.5	
	Weight of Beams and Columns	2.0	
	Roof Insulation	0.5	
	Mechanical Service Loading	0.5	
	Total	6.5	1.0

Table 3.3 Estimated Storey Masses ($\times 10^3$ kg)

Floor	137
Roof	127

Table 3.4 Design Base Shears (kN)

	4S1	4S2	10S	18S
$Z_a<Z_v$	4S1L: 461.7	4S2L: 461.7	821.8	1106.4
$Z_a=Z_v$	4S1I: 650.2	4S2I: 539.7	821.8	1106.4
$Z_a>Z_v$	4S1H: 916.8	4S2H: 643.7	821.8	1106.4

Table 3.5 Vibrational Periods of First Three Modes (sec)

	4S1	4S2	10S	18S
First Mode	0.23	0.47	1.20	2.01
Second Mode	0.07	0.15	0.43	0.73
Third Mode	0.04	0.08	0.24	0.43

Table 3.6 Distributions of Seismic Design Forces (kN)

Storey Level	4S1			4S2			10S	18S
	4S1L ($Z_a<Z_v$)	4S1I ($Z_a=Z_v$)	4S1H ($Z_a>Z_v$)	4S2L ($Z_a<Z_v$)	4S2I ($Z_a=Z_v$)	4S2H ($Z_a>Z_v$)		
18								108.8
17								110.8
16								104.3
15								97.8
14								91.3
13								84.8
12								78.3
11								71.7
10							140.4	65.2
9							136.3	58.7
8							121.1	52.2
7							106.0	45.6
6							90.9	39.1
5							75.7	32.6
4	176.3	248.3	350.2	176.3	206.1	245.9	60.6	26.1
3	142.7	200.9	283.3	142.7	166.8	198.9	45.4	19.6
2	95.1	134.0	188.9	95.1	111.2	132.6	30.3	13.0
1	47.6	67.0	94.4	47.6	55.6	66.3	15.1	6.5

Table 3.7(a) Amplification Factors due to Slenderness Effect for 4SI Frames

Storey Level	Exterior Column	Interior Column
	4SIL ($Z_a<Z_v$)	
4	1.004	1.005
3	1.013	1.014
2	1.014	1.015
1	1.016	1.017
	4SII ($Z_a=Z_v$)	
4	1.005	1.005
3	1.013	1.014
2	1.015	1.015
1	1.017	1.017
	4SIH ($Z_a>Z_v$)	
4	1.005	1.005
3	1.014	1.014
2	1.016	1.015
1	1.018	1.017

Table 3.7(b) Amplification Factors due to Slenderness Effect for 4S2 Frames

Storey Level	Exterior Column	Interior Column
	4S2L ($Z_a<Z_v$)	
4	1.018	1.020
3	1.054	1.060
2	1.060	1.062
1	1.069	1.071
	4S2I ($Z_a=Z_v$)	
4	1.019	1.020
3	1.054	1.060
2	1.061	1.062
1	1.071	1.071
	4S2H ($Z_a>Z_v$)	
4	1.019	1.020
3	1.055	1.060
2	1.063	1.062
1	1.073	1.071

Table 3.7(c) Amplification Factors due to Slenderness Effect for 10S Frame

Storey Level	Exterior Column	Interior Column
10	1.030	1.031
9	1.090	1.098
8	1.104	1.104
7	1.153	1.167
6	1.139	1.132
5	1.192	1.175
4	1.231	1.225
3	1.198	1.177
2	1.242	1.210
1	1.197	1.174

Table 3.7(d) Amplification Factors due to Slenderness Effect for 18S Frame

Storey Level	Exterior Column	Interior Column
18	1.031	1.030
17	1.096	1.089
16	1.156	1.157
15	1.153	1.143
14	1.225	1.201
13	1.272	1.271
12	1.223	1.193
11	1.294	1.243
10	1.342	1.301
9	1.279	1.225
8	1.350	1.271
7	1.373	1.322
6	1.287	1.221
5	1.347	1.258
4	1.373	1.297
3	1.298	1.222
2	1.335	1.244
1	1.257	1.195

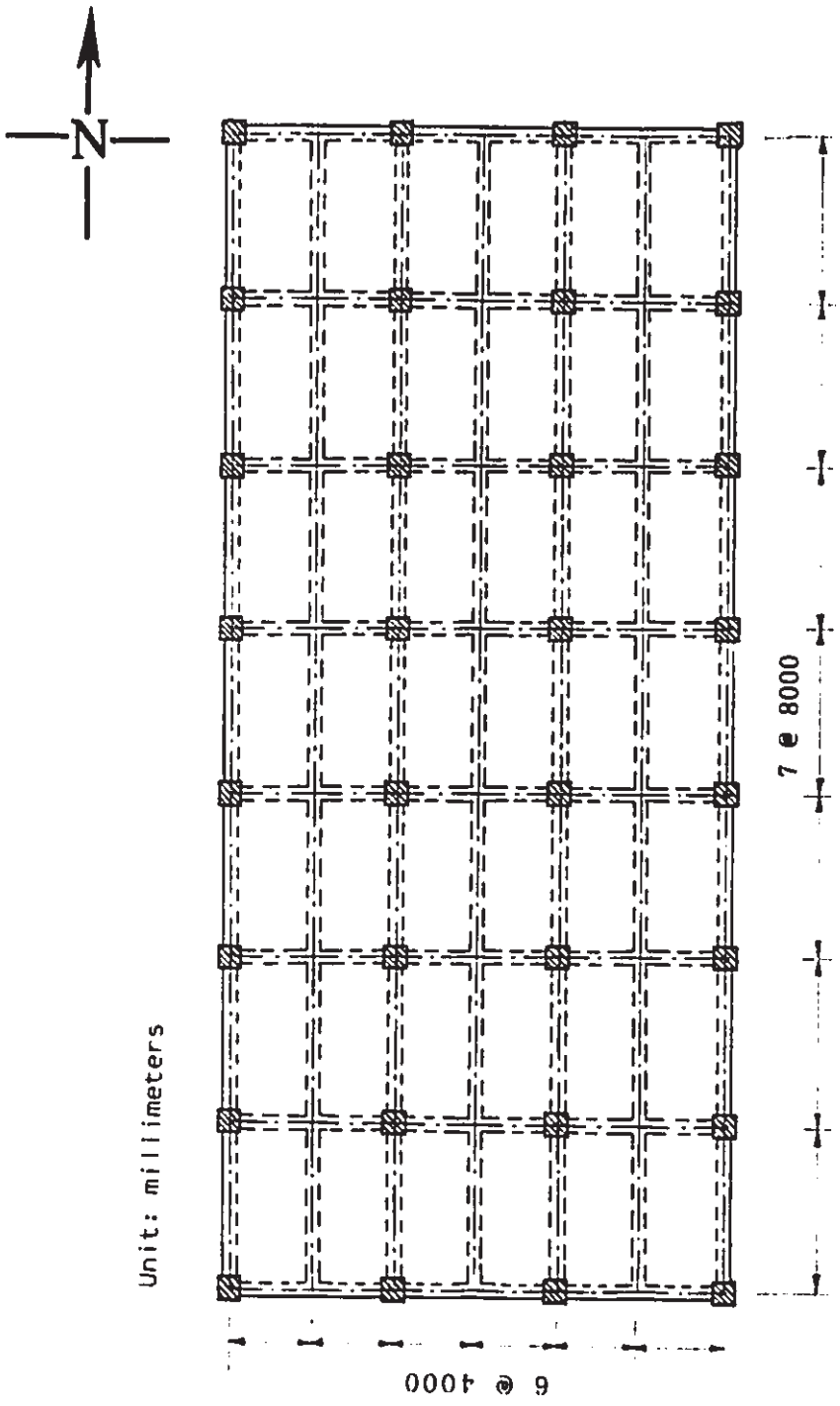

Fig. 3.1 Typical Floor Plan

Unit: millimeters

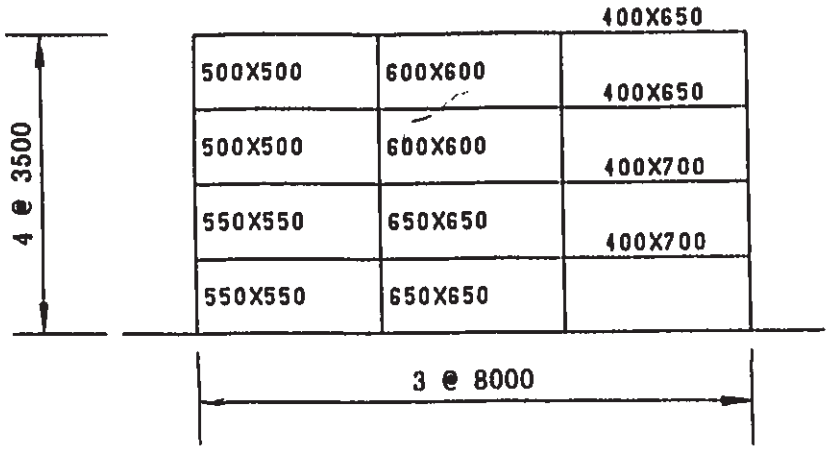

(a) Four Storey Frame

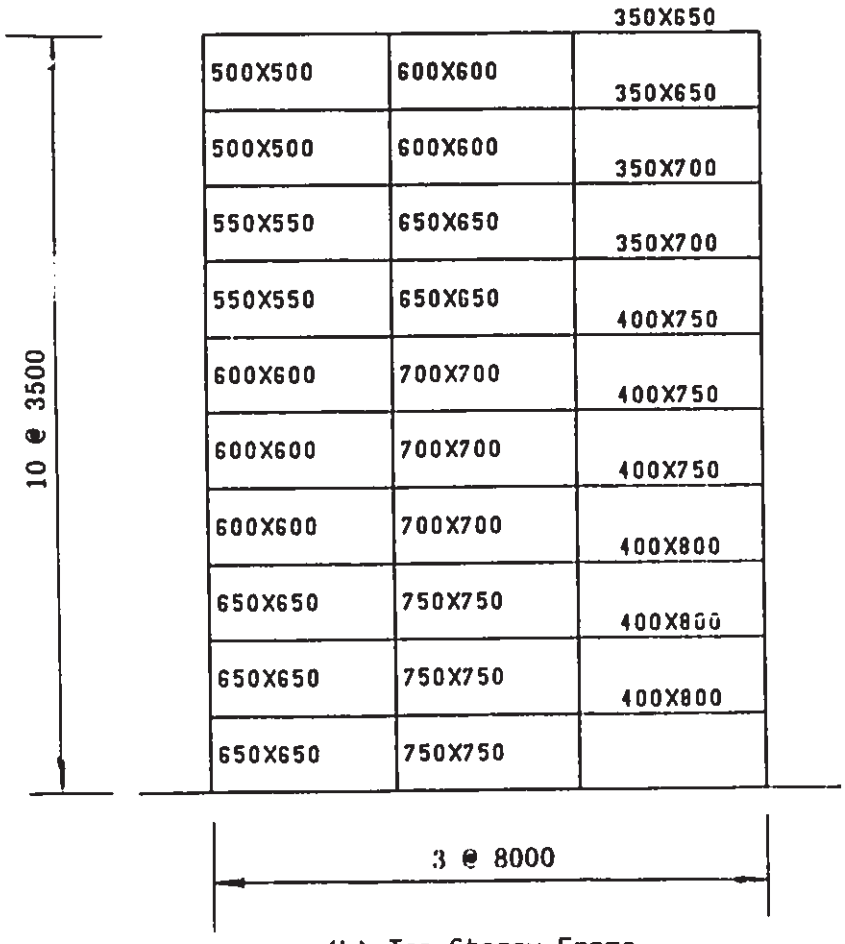

(b) Ten Storey Frame

Fig. 3.2 Frame Elevations

Unit: millimeters

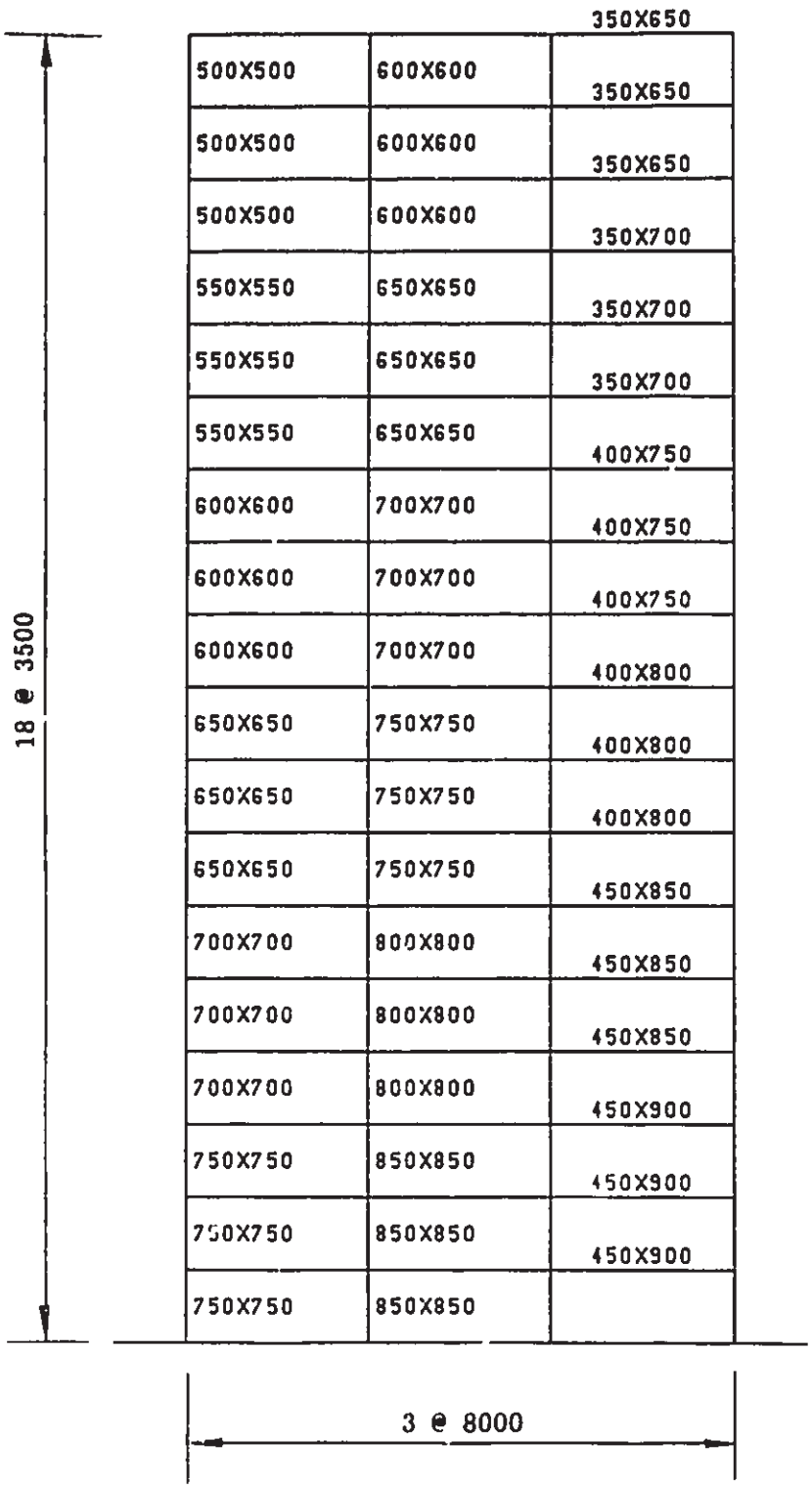

(c) Eighteen Storey Frame

Fig. 3.2 (cont'd) Frame Evaluations

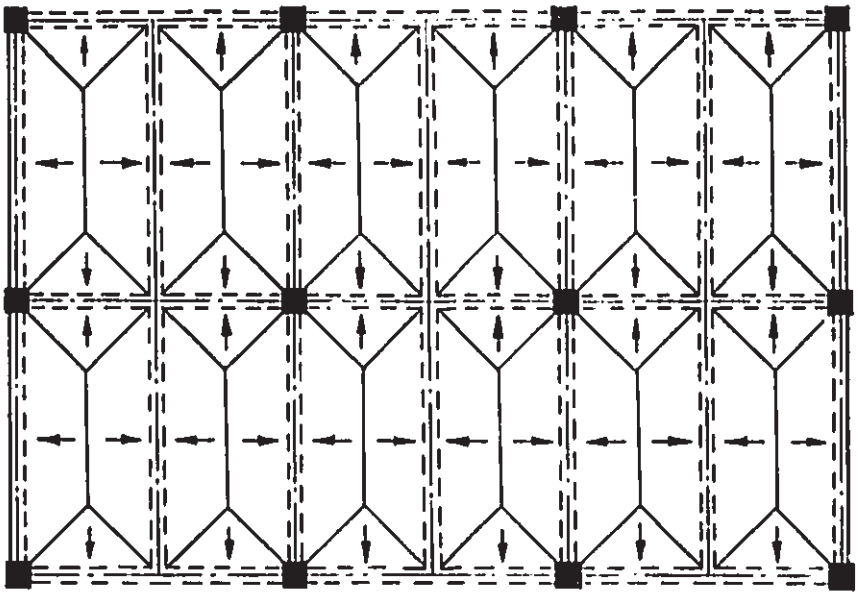

(a) Tributary Areas

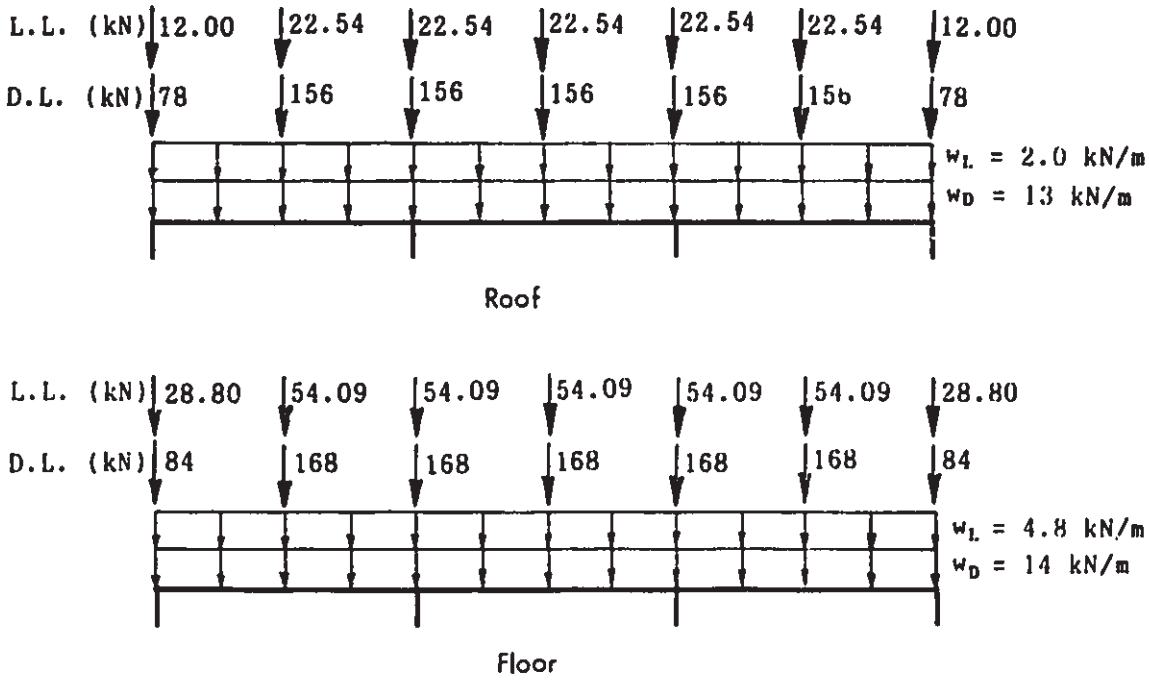

(b) Gravity Load Distributions

Fig. 3.3 Distributions of Gravity Loads

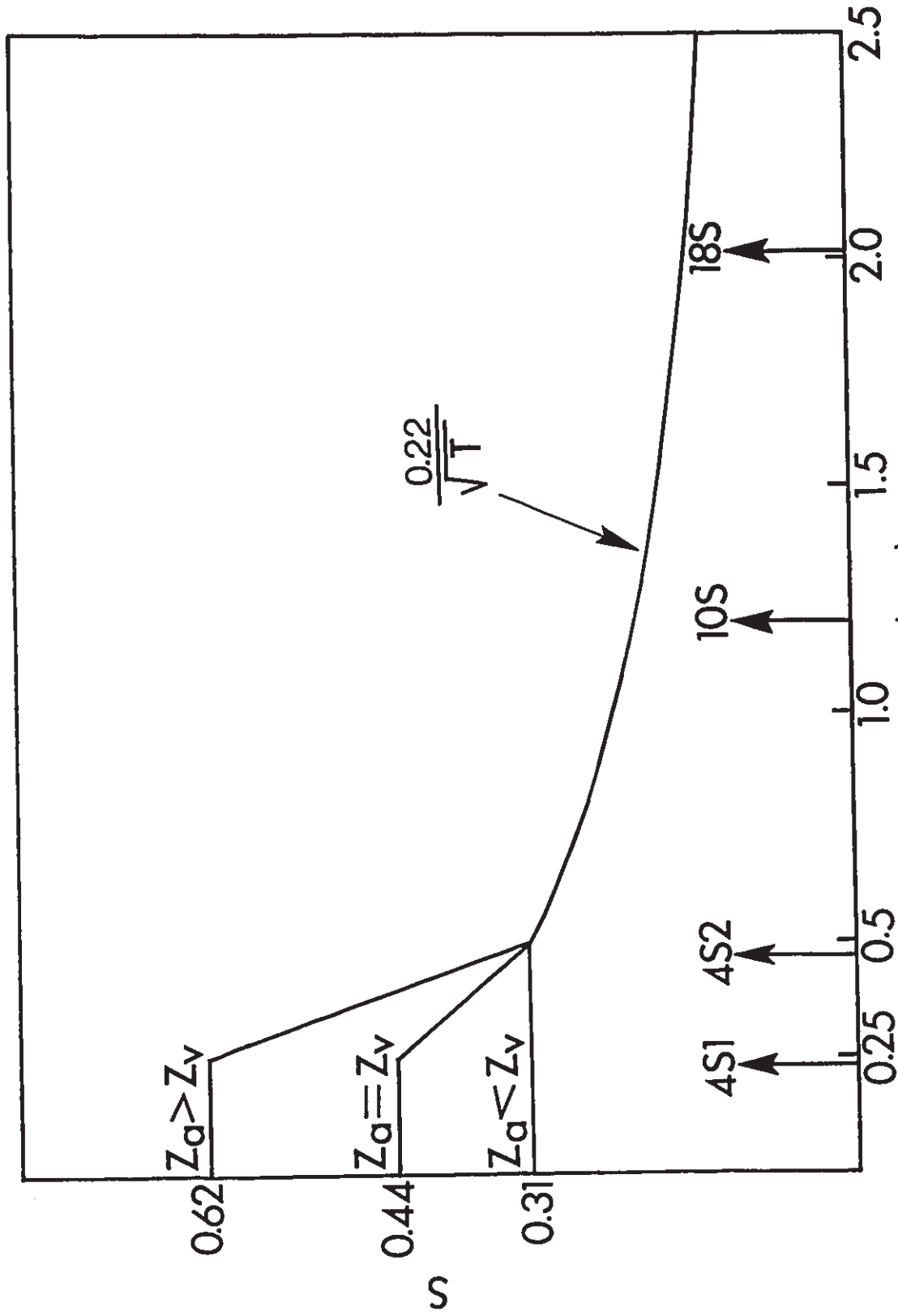

Fig. 3.4 Seismic Response Factor S in NBCC 1985

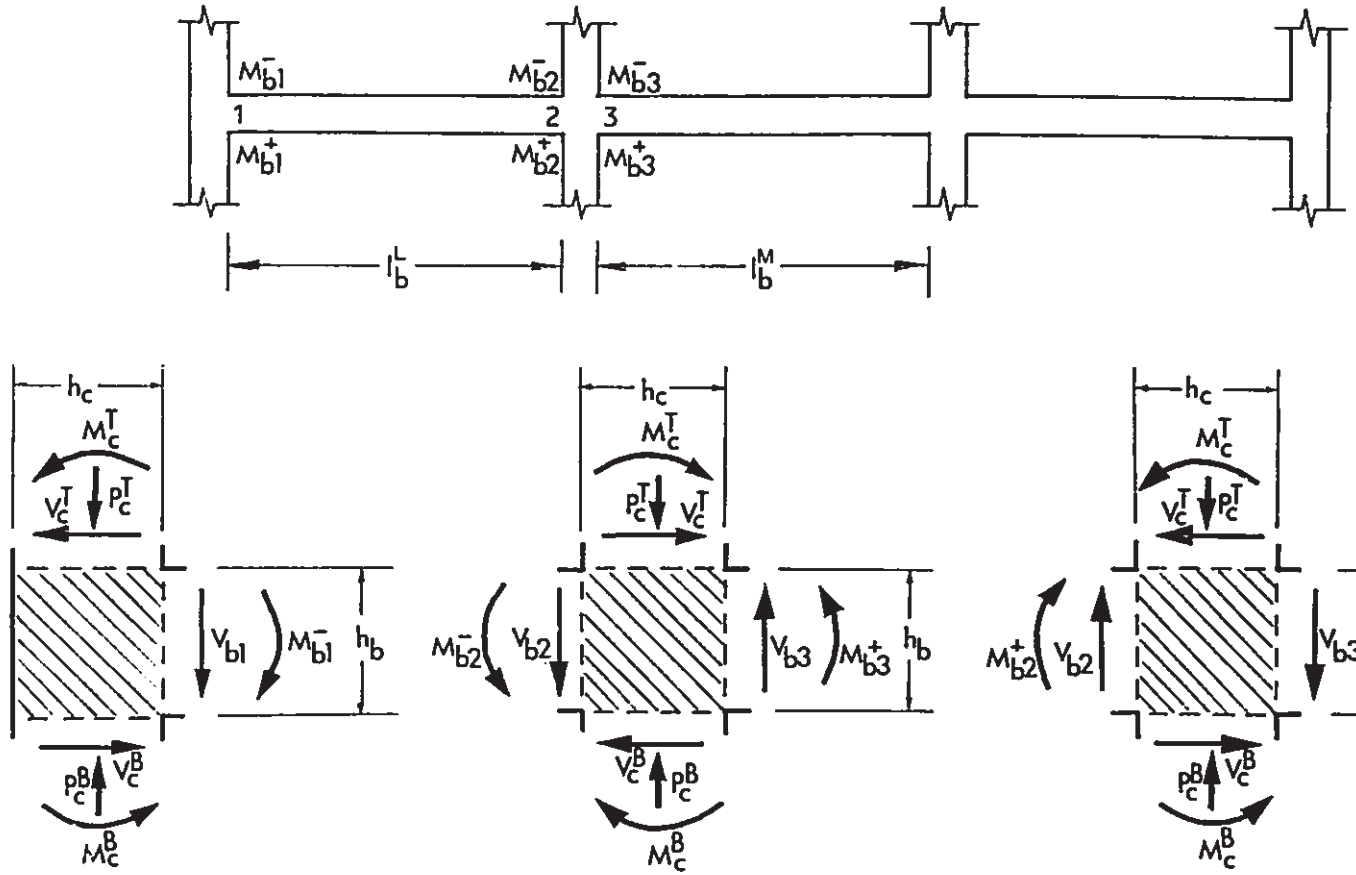

$$V_{b1} = \frac{M_{b1}^{-} + M_{b2}^{+}}{l_b^L} + V_{b1}^G$$

$$V_{b2} = \frac{M_{b1}^{+} + M_{b2}^{-}}{l_b^L} + V_{b2}^G$$

$$V_{b3} = \frac{M_{b3}^{+} + M_{b3}^{-}}{l_b^M} - V_{b3}^G$$

$$V_{b2} = \frac{M_{b1}^{-} + M_{b2}^{+}}{l_b^L} - V_{b2}^G$$

$$V_{b3} = \frac{M_{b3}^{-} + M_{b3}^{+}}{l_b^M} + V_{b3}^G$$

Fig. 3.5 Derivation of Column Design Moments

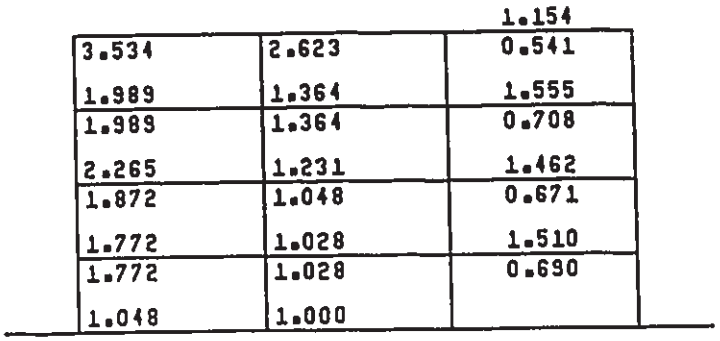

4S1L

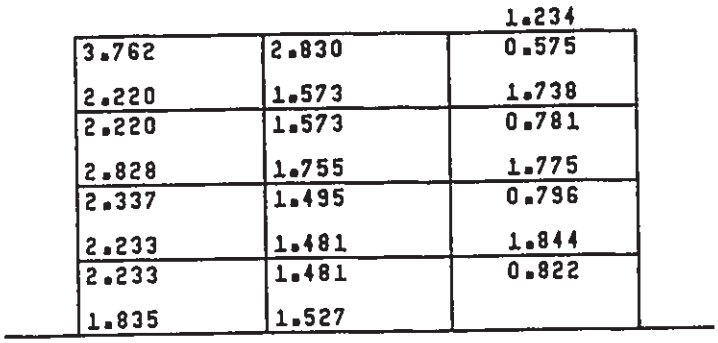

4S1I

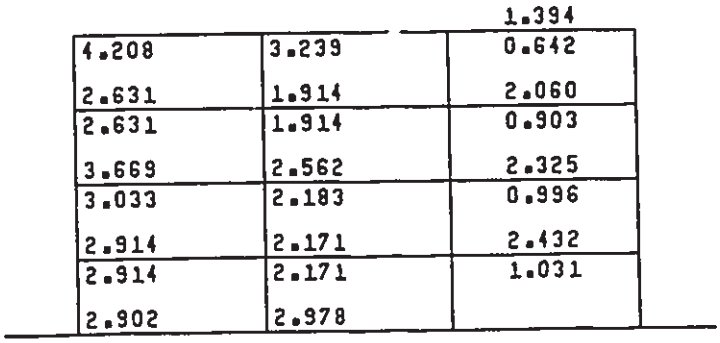

4S1H

(a) 4S1 Frames

Fig. 3.6 Reinforcement Ratios for the Designed Frames

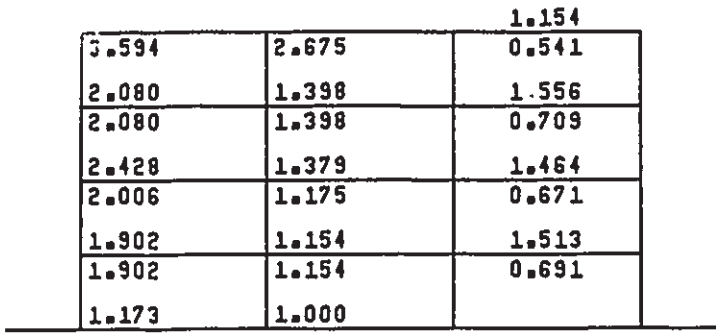

4S2L

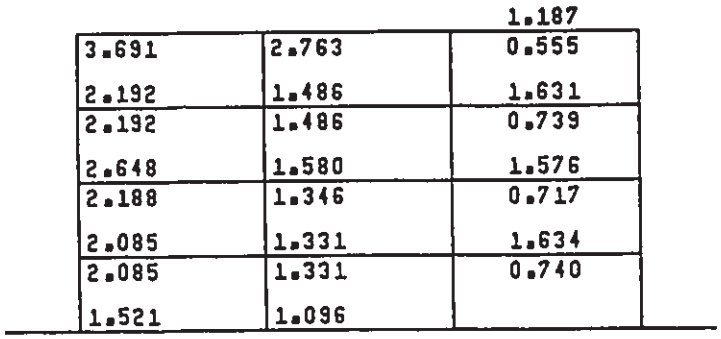

4S2I

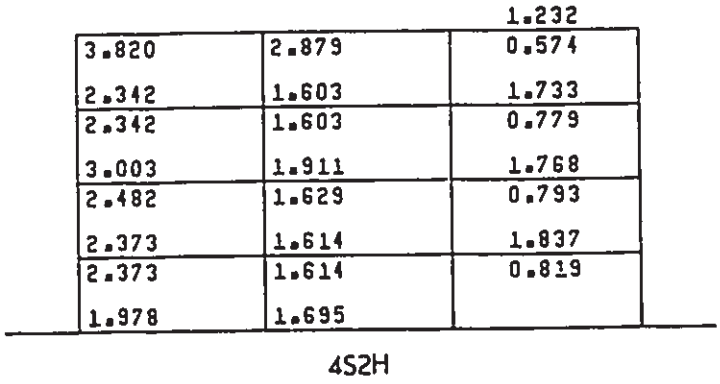

4S2H

(b) 4S2 Frames

Fig. 3.6 (cont'd) Reinforcement Ratios for the Designed Frames

		1.217
3.313	2.418	0.568
2.026	1.311	1.720
2.026	1.311	0.774
2.474	1.444	1.672
2.045	1.230	0.755
1.854	1.059	1.902
1.854	1.059	0.844
2.300	1.212	1.627
1.932	1.045	0.737
1.666	1.000	1.746
1.666	1.000	0.784
1.861	1.207	1.836
1.861	1.207	0.819
2.020	1.148	1.700
1.721	1.000	0.766
1.326	1.066	1.688
1.326	1.066	0.762
1.530	1.292	1.538
1.530	1.292	0.702
1.638	2.586	

10S

(c) 10S Frame

Fig. 3.6 (cont'd) Reinforcement Ratios for the Designed Frames

		1.213
3.304	2.410	0.566
2.097	1.416	1.798
2.097	1.416	0.804
2.357	1.445	1.923
2.357	1.445	0.852
2.882	1.691	1.888
2.382	1.441	0.839
2.170	1.228	2.127
2.170	1.228	0.926
2.532	1.832	2.336
2.532	1.832	0.999
2.951	2.051	1.928
2.480	1.769	0.854
2.145	2.006	2.035
2.145	2.006	0.894
2.769	3.021	2.130
2.769	3.021	0.928
2.659	2.925	1.998
2.265	2.548	0.880
2.282	2.660	2.043
2.282	2.660	0.896
2.897	3.476	2.052
2.897	3.476	0.900
2.602	3.139	1.670
2.243	2.759	0.755
2.168	2.753	1.653
2.168	2.753	0.748
2.667	3.375	1.629
2.667	3.375	0.738
2.167	2.938	1.480
1.887	2.603	0.700
1.739	2.476	1.420
1.739	2.476	0.653
1.938	2.668	1.251
1.938	2.668	0.582
3.014	4.381	

18S

(d) 18S Frame

Fig. 3.6 (cont'd) Reinforcement Ratios for the Designed Frames

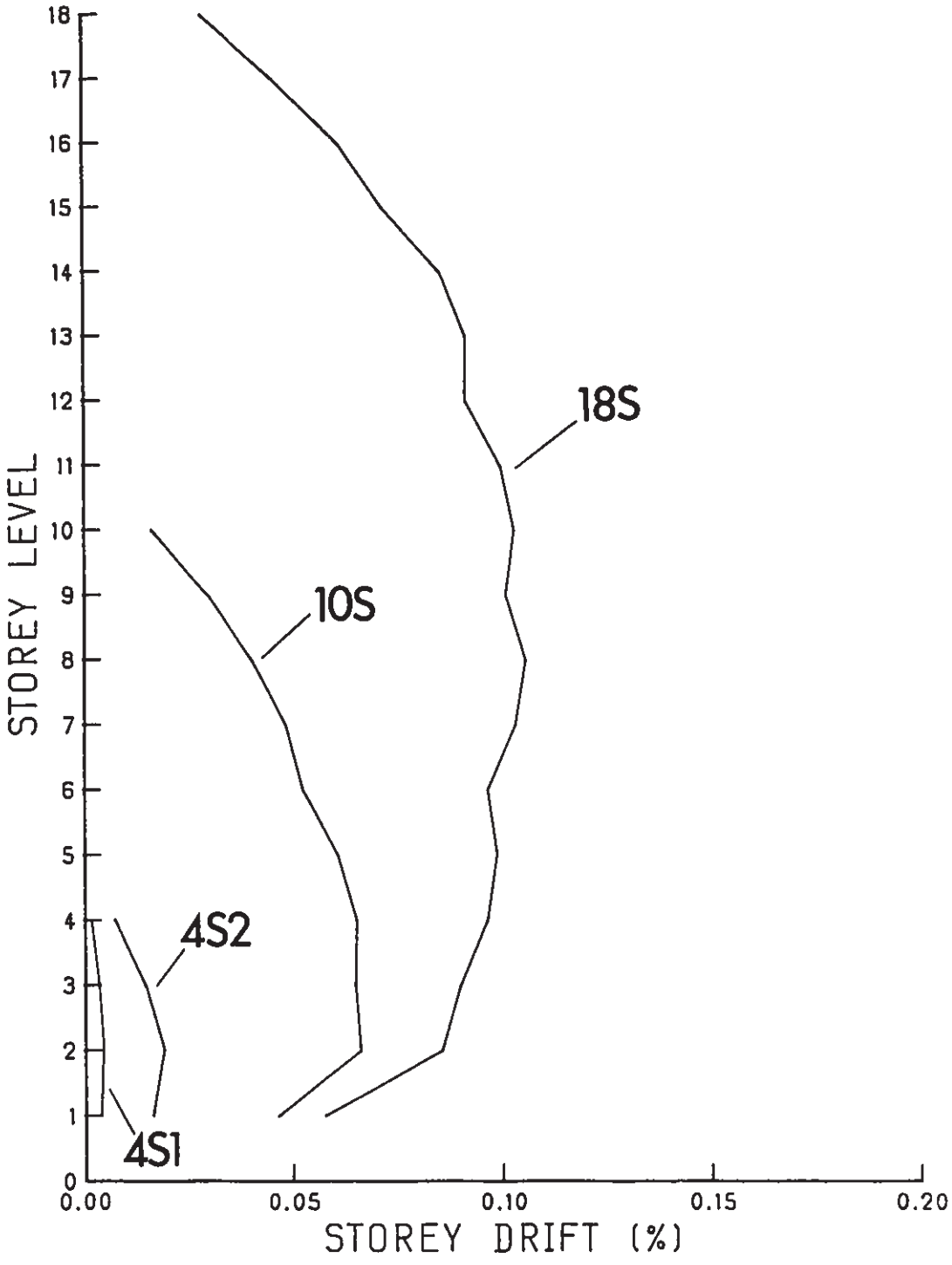

Fig. 3.7 Interstorey Drift due to Service Level Wind Loading

CHAPTER 4

STATIC AND DYNAMIC ANALYSIS PROCEDURES AND DEFINITION OF RESPONSE PARAMETERS

4.1 Introduction

In this chapter, the inelastic static and dynamic analysis procedures employed in this study are described. Also included in this chapter is a definition of the response parameters used to characterize inelastic response for the present study. The chapter begins with a description of the basic assumptions made for the inelastic static and dynamic analyses. Following this description, the available analytical modelling techniques for building structures are briefly reviewed, and the analytical models used for this study are described. The consideration of P-delta effect in the static and dynamic analyses is outlined. In the dynamic analysis, a definition of energy indices for inelastic MDOF systems is proposed, and their numerical implementation in computer programs is presented. The chapter closes with a definition of the various response parameters used to characterize inelastic response for this study.

4.2 Basic Assumptions

In order to simplify the analytical modelling of a building structure, some idealizations are considered to be necessary. Summarized in the following are the basic assumptions made in this study for the inelastic static and dynamic analyses.

(1) Only one horizontal component of ground motion is applied at the base of the frames in the E-W direction, and all supports are assumed to move in phase. Accordingly, only planar response of the frames in the E-W direction is considered, and each node possesses three independent displacement degrees of freedom (two translations and one rotation).

(2) Axial stiffness and strength in the plane of a diaphragm are assumed to be infinitely large. Therefore, the nodes at each storey level are constrained to have the same lateral displacement.

(3) The flexural coupling of the frames in the E-W direction through the transverse slab-beam system is neglected. Therefore, the deformation of a typical interior frame is representative of the behaviour of the complete building under seismic excitation.

(4) The frames are assumed to be perfectly fixed at their base.

(5) The mass of each frame is lumped at its storey levels. The storey mass possesses lateral inertia only. The vertical inertia forces and rotational inertia moments are neglected.

(6) The deflections of the frames are assumed to be small as compared to their dimensions, and the static or dynamic equilibrium is based on the initial configurations of the frames.

4.3 Analytical Models

In current practice, three different approaches corresponding to different levels of sophistication may be used in modelling the inelastic dynamic response of building structures. They are (a) macroscopic approach based on simplified overall nonlinear behaviour of structural subassemblages; (b) discrete member idealization based on inelastic

characteristics of individual structural members; and (c) microscopic approach based on finite element discretization of structural members. Fig. 4.1 shows a schematic illustration of the three approaches. A typical example of the macroscopic approach is to idealize an actual building as an inelastic shear building (2,21). The interstorey hysteretic behaviour of the shear building model represents the gross interstorey shear-deflection characteristics of the actual building. However, because of the problems involved in determining the required interstorey shear-deflection relationship, it is usually difficult to realistically model actual buildings as shear structures. Also, the inelastic shear beam representation of actual buildings only provides information on overall inelastic response at storey levels.

In the discrete member representation of a building structure, the distribution of inelastic deformation and the force-deformation relationship are assumed for each structural member (23,27). This modelling technique enables one to obtain information regarding both overall inelastic deformations at storey levels and local inelastic deformations in structural members with reasonable computational effort. Previous integrated experimental and analytical studies (34,63,65) have indicated that this discrete member idealization is capable of realistically simulating the nonlinear seismic response of moment-resisting frame structures.

In the microscopic modelling technique, a structural member is subdivided longitudinally into a number of segments and transversely into a number of layers or fibers (45). As a result, detailed information can be obtained regarding the local behaviour in the critical regions of a

structural member. However, because of the large amounts of computational efforts required, this technique is usually used for the analysis of individual structural members. The use of this technique for the analysis of an entire building is too costly and time consuming.

In this study, the discrete member idealization is used. Beams and columns are treated as fundamental elements, and the distribution of inelastic deformations and the hysteretic behaviour are assumed for each element. Also, the beam-column joints are assumed to be completely rigid, and finite rigid end zones are considered for the beams and columns. This assumption is the same as that used for the eigenvalue solution and elastic static analysis in Chapter 3.

4.3.1 Element Modelling

There are three analytical models which may be used to simulate the inelastic behaviour of a structural member in the discrete member idealization. They are (a) single component model; (b) dual component model; and (c) inelastic zone model. In the single component model (27,65), a structural member is represented by an elastic line element with inelastic springs attached at its two ends (Fig. 4.2a). Therefore, inelastic deformation in the member is assumed to be lumped at its two ends. Because of the use of two independent inelastic springs, the inelastic rotation at one end is independent of that at the other end. In order to determine the moment-rotation behaviour of the two inelastic springs, some assumptions have to be made regarding the deformed shape of the member. It is usually assumed that the member deforms in double curvature with its inflection point in the middle. However, this

assumption may not be appropriate for beams in gravity load dominated frames and for lower storey columns in earthquake load dominated frames. The main advantage of the single component model is its versatility to incorporate different hysteretic models for the moment-rotation relationship of the inelastic springs.

In the dual component model (23,27), a structural member is represented by an elastic component and an elasto-plastic component in parallel (Fig. 4.2b). Inelastic deformation is associated with the elasto-plastic component and assumed to be concentrated at the two ends of the member. The elastic component is included to account for the strain-hardening effect. One advantage of the dual component model is that the inelastic rotation at one end of the member depends on the end rotations at both ends, and no assumption needs to be made regarding the deformed shape of the member. However, the dual component model can only reproduce bilinear hysteretic behaviour.

In the inelastic zone model (48), the expansion of the inelastic zones at the two ends of a structural member is considered (Fig. 4.2c). The reduced flexural rigidity is assumed to be uniform within the inelastic zone at each end and depends on the moment-curvature relationship of the end section. Different hysteretic models may be used to describe the moment-curvature relationship. In order to determine the length of the two end inelastic zones, the distribution of bending moment along the member has to be assumed. It is usually assumed that the bending moment varies linearly along the member. However, this assumption may not be appropriate for beams in gravity load dominated frames.

The level of axial force in a column has a significant effect on its inelastic behaviour. In general, the variation of the axial force in a column affects both its flexural yield strength and stiffness. The effect of column axial force on its flexural yield strength can be described by a yield moment-axial force interaction diagram, as shown in Fig. 4.3. The interaction diagram can be divided into two regions corresponding to two different types of failure mode. If the axial force in a column is below the balanced axial force P_B, the column will fail in tension. In a tension failure, the tensile steel reaches its yield strength before the concrete in compression attains its ultimate strain. If the column axial force exceeds P_B, a compression failure will occur. In a compression failure, the concrete in compression crushes before the yielding of the tensile steel. To achieve high ductility level, it is desirable for a column to fail in tension. However, unlike a beam, a tension failure for a column cannot be achieved by limiting the steel area. It can only be achieved by increasing either the column size or the concrete strength. For a tall building subjected to severe earthquake excitation, the axial forces in lower storey columns are very high. Because of the practical limitation on the column size and the concrete strength, it may be unavoidable for the column axial forces to exceed their balanced axial forces. In order to attain certain amount of ductility for these columns, it is essential to provide sufficient transverse confinement by means of transverse reinforcement.

Previous studies have suggested procedures to account for the effect of varying axial forces in the three analytical models described above. In order to accommodate the effect of varying axial force on the

flexural yield strength and post-yield stiffness, Saatcioglu et al. (75) modified the moment-rotation hysteretic models of the inelastic springs in the single component model. Kannan and Powell (46) employed a yield moment-axial force interaction curve for the elasto-plastic component in the dual component model. Because the interaction curve is associated with the elasto-plastic component only, it remains stationary during the dynamic response. In this procedure, the effect of varying axial force on member stiffness is not considered. Keshavarzian and Schnobrich (48) modified the moment-curvature hysteretic model to account for the effect of axial force in the inelastic zone model. In their procedure, a moment increment is expressed as a sum of two terms. One is related to a change in curvature, and the other is associated with a change in axial force. The changing rate of bending moment with respect to axial force is based on the slope of the yield moment-axial force interaction curve. In this procedure, the variation of axial force has effects on flexural yield strength, initial elastic stiffness, and post-yield stiffness.

In addition to the bilinear model, many other hysteretic models have been proposed in the previous studies to simulate the inelastic cyclic behaviour of reinforced concrete structural members. A recent review of these hysteretic models was given by Otani (64). Some of these models are used to simulate the stiffness degradation phenomenon (24,82), whereas others intend to account for the pinching and strength decay effects due to significant shear deformation, bond deterioration, and anchorage slippage (81). Most of these models involve some empirical parameters which need to be determined based on experimental results. The effect of stiffness degradation on the analytical inelastic response has

been investigated in the previous studies for SDOF systems (24), shear beam models (21), and simple moment-resisting frames (41). It is found that stiffness degradation has minor effects on the displacement ductility demands for intermediate and long period systems. For short period systems, stiffness deterioration tends to increase the ductility demands.

In the analysis of a building structure, the choice of a particular hysteretic model for the structural members depends on the actual design and detailing of the members. If the members are well designed and detailed, the effects of stiffness and strength deterioration may not be significant, and the bilinear model may be used to simulate approximately the hysteretic behaviour of the members. In this study, it is assumed that sufficient transverse reinforcement has been provided for the structural members, and the stiffness and strength deterioration due to shear and bond loss is not significant. Accordingly, the dual component model is used to describe the inelastic behaviour of the structural members. The use of the dual component model also reduces computational cost because of its relative simplicity, particularly in the incorporation of axial force-flexural yield strength interaction for the columns. This is desirable because a large number of inelastic dynamic analyses are involved in this study, as will be described in Chapter 6.

The initial elastic stiffnesses for the beams and columns are the same as those used for the eigenvalue solution and elastic static analysis in Chapter 3. The yield moments for the beams and the yield moment-axial force interaction curves for the columns are determined from their reinforcement ratios. The yield moment-axial force interaction

curve for a column used in the static and dynamic analyses is idealized from the actual curve, as shown in Fig.4.3. The strain-hardening stiffness of the structural members is assumed to be 3% of their initial elastic stiffness. Axial deformation is not considered for the beams due to the assumption of rigid diaphragms in their own planes. For the columns, axial deformation is considered and assumed to remain in the elastic range. Shear deformation is not considered for both beams and columns.

4.3.2 P-Delta Effect

Axial force in a column produces secondary moments due to the relative displacement between its two ends. These second-order moments tend to increase inelastic deformations. Many techniques have been proposed for evaluating this second-order effect (49,74). In this study, a linearized solution (93) has been used. As shown in Fig. 4.4, the axial force in a column can be decomposed into two components. One is parallel to the line joining the two ends of the deformed column, and the other is horizontal. If the column deflection Δ is small as compared to its length L, the horizontal component is equal to $P\Delta/L$. Consequently, the total shear acting at each end of the column is the sum of the original shear V and the shear ($P\Delta/L$) resulting from the moment induced by P acting through the deflection Δ. Therefore, the shear terms in the element stiffness matrix are modified by the following geometric stiffness matrix:

$$[K_G] = \frac{P}{L} \begin{bmatrix} 1 & -1 \\ -1 & 1 \end{bmatrix} \qquad (4.1)$$

This linearized solution has been used for both the static and dynamic analyses. The axial force P in Eq.(4.1) is based on the unfactored gravity loading and is assumed to remain constant during the application of monotonically increased lateral loading or the dynamic response. A more complete analysis would be to allow the axial force to change, but this requires that the structural stiffness matrix be modified at each load or time step.

4.4 Static Analysis

The computer program DRAIN-2D developed by Kaanan and Powell (46) has been used in this study. The original version of the program can only perform dynamic analysis of an arbitrary planar structure subjected to earthquake ground motion. In this study, the program has been modified to be able to perform inelastic static analysis of a planar structure subjected to monotonically increased lateral loading. The use of the same program for both the static and dynamic analyses is desirable because of the consistency in their assumptions.

In the static analysis, gravity loading is applied as nodal forces prior to lateral loading. The lateral loading is distributed at storey levels based on the distribution formula in NBCC 1985, as described in Chapter 3. The load distribution shape remains unchanged during the loading process. The magnitude of the lateral loading is increased monotonically in small increments. The load increment is chosen to be small enough to avoid any significant computation errors due to overshooting in the hysteretic loops of the structural elements. The structural stiffness matrix is assumed to be constant during each small

load increment. The incremental nodal displacements corresponding to the degrees of freedom are calculated at the end of each load step. Based on the incremental nodal displacements, the incremental member deformations and forces can be obtained. If a plastic hinge has been formed in a member, the member stiffness is modified in accordance with the hysteresis rules, and the structural stiffness matrix is updated for the next load step. This analysis is continued until the maximum global displacement exceeds some specified value, or the number of iterations as specified by the user has been exceeded. The program assumes that all structural members have unlimited strength and deformation capacity.

4.5 Dynamic Analysis

In the dynamic analysis, gravity loading is applied as nodal forces prior to earthquake ground motion. The DRAIN-2D program is used to perform the dynamic analysis. The program carries out step-by-step numerical integration of the equation of motion. In this section, the evaluation of the mass matrix, the damping matrix, and the instantaneous stiffness matrix is described. The numerical integration scheme employed to solve the equation of motion is briefly outlined. Also included in this section is a definition of various energy indices based on the equation of motion.

4.5.1 Mass Matrix

In an actual structure, the mass at each storey level is distributed along structural members. In this study, only lateral inertia terms are considered, and rotational and vertical inertia are ignored.

Also, all the nodes at each storey level are constrained to have the same lateral displacement due to the assumption that a diaphragm is totally rigid in its own plane. Therefore, the mass at each storey level is lumped at the nodes. The mass matrix is a diagonal matrix with zero off-diagonal terms and given by

$$[M] = \begin{bmatrix} m_1 & & & \\ & m_2 & & \\ & & \ddots & \\ & & & m_n \end{bmatrix} \qquad (4.2)$$

where m_1, m_2, ..., m_n = lumped masses at storey levels, and n = total number of storeys.

4.5.2 Damping Matrix

Viscous type damping is adopted in this study. While damping in a structure is not necessarily of viscous form, this assumption has been widely used in previous analytical studies because of its mathematical simplicity. This simplification may be justified on the grounds that the actual damping phenomenon in a building structure is not fully understood with present knowledge.

The damping matrix for the viscous damping is assumed to be of Rayleigh type, and it is expressed as a linear combination of the mass matrix and the instantaneous stiffness matrix as follows:

$$[C] = c_1 [M] + c_2 [K_t] \qquad (4.3)$$

where $[K_t]$ is the tangential stiffness matrix, and c_1 and c_2 are the proportional constants. c_1 and c_2 are determined from the modal damping ratios of the first two modes based on the following expressions:

$$c_1 = \frac{4\pi \left(T_1\xi_1 - T_2\xi_2 \right)}{T_1^2 - T_2^2} \qquad (4.4a)$$

$$c_2 = \frac{T_1T_2 \left(T_1\xi_2 - T_2\xi_1 \right)}{\pi \left(T_1^2 - T_2^2 \right)} \qquad (4.4b)$$

in which

T_1, T_2 = undamped period of the first or second mode;

ξ_1, ξ_2 = damping ratio of the first or second mode.

In this study, both ξ_1 and ξ_2 are taken as 5%. This value is considered to be appropriate for reinforced concrete frame structures with cracked beams under service level loading (60). The values of c_1 and c_2 computed for the frames considered in this study are shown in Table 4.1.

4.5.3 Stiffness Matrix

The global structural stiffness matrix is obtained by assembling individual element stiffness matrices. The structural stiffness matrix for the current time step is evaluated at the end of the previous time step and assumed to remain constant during the small time increment. If the stiffness of one or more members has changed at the end of the current time step, the structural stiffness matrix is updated based on this change in element stiffness for the next time step.

4.5.4 Numerical Integration

The Newmark-beta method (57) with beta equal to 1/4 is used in the DRAIN-2D program for the numerical integration of the equation of motion. In this method, the acceleration is assumed to be constant within a small

time increment. As a result, the velocity varies linearly with respect to time, and the displacement varies quadratically. This constant average acceleration method is known to be unconditionally stable for linear problems (11). However, it may become conditionally stable for nonlinear problems (1). A time increment of 0.005 sec is used in this study for all the frames. This time increment is about 1/5 of the highest mode period for the 4S1 and 18S frames, 1/7 of the highest mode period for the 10S frame, and 1/10 of the highest mode period for the 4S2 frames. A sensitivity study using a reduced time increment of 0.002 sec is performed, and the results are very similar to those using a time increment of 0.005 sec.

In the numerical integration, the stiffness matrix at the beginning of a time step is used, and it is assumed to remain constant during the time step. However, one or more structural members may actually have yielded during the time step. The actual change of member stiffness results in unbalanced forces, and consequently, the dynamic equilibrium at the end of the time step is not exactly satisfied. This phenomenon is usually referred to as "overshooting". If these errors are not corrected, the computed response may diverge from the true response. In the DRAIN-2D program, a "corrective forces" procedure is used to approximately correct the equilibrium errors. In this procedure, corrective forces which are equal to the unbalanced forces in magnitude but opposite in direction are added to the load vector during the subsequent time step. These corrective forces are present only for the duration of the time step in which they are applied. This procedure is satisfactory if the time step is relatively small.

4.5.5 Energy Indices

During the inelastic seismic response of a building structure, one part of the imparted energy is stored temporarily in the building structure in the form of kinetic and strain energy, and the rest is dissipated by inelastic deformation and damping. By the end of the response, all the imparted energy will have been dissipated through inelastic deformation and damping. Jennings (44) and Zahrah and Hall (97) defined the various energy terms for inelastic SDOF systems. In this study, their definitions are extended to inelastic MDOF systems. In this section, the various energy indices are defined for inelastic MDOF systems, and their numerical implementation in the DRAIN-2D program is described.

The equation of motion for a MDOF system is given by

$$[M]\{\ddot{u}(t)\} + [C]\{\dot{u}(t)\} + \{R(u(t))\} = - [M]\{r\}\ddot{u}_g(t) \qquad (4.5)$$

where [M] = the mass matrix; [C] = the damping matrix; {R(u(t))} = the restoring force vector; $\{\ddot{u}(t)\}$, $\{\dot{u}(t)\}$, $\{u(t)\}$ = the relative acceleration, velocity, or displacement vector, respectively; $\ddot{u}_g(t)$ = the horizontal component of ground acceleration; and {r} = a vector relating the horizontal component of ground acceleration to the lateral degrees of freedom. The elements of {r} corresponding to the lateral degrees of freedom are unity, and the remaining elements are zero. Pre-multiplying Eq.(4.5) by the transpose of the incremental relative displacement vector $\{du(t)\}^T$ leads to

$$\{du(t)\}^T[M]\{\ddot{u}(t)\} + \{du(t)\}^T[C]\{\dot{u}(t)\} + \{du(t)\}^T\{R(u(t))\} =$$

$$- \{du(t)\}^T[M]\{r\}\ddot{u}_g(t) \qquad (4.6)$$

Eq.(4.6) can be written in terms of time increment dt using the

relationship $\{du(t)\} = \{\dot{u}(t)\}dt$.

$$\{\dot{u}(t)\}^T[M]\{\ddot{u}(t)\}\,dt + \{\dot{u}(t)\}^T[C]\{\dot{u}(t)\}\,dt + \{\dot{u}(t)\}^T\{R(u(t))\}\,dt = - \{\dot{u}(t)\}^T[M]\{r\}\ddot{u}_g(t)\,dt \tag{4.7}$$

Integration of Eq.(4.7) with respect to time yields

$$\int_0^t \{\dot{u}(t)\}^T[M]\{\ddot{u}(t)\}\,dt + \int_0^t \{\dot{u}(t)\}^T[C]\{\dot{u}(t)\}\,dt + \int_0^t \{\dot{u}(t)\}^T\{R(u(t))\}\,dt = - \int_0^t \{\dot{u}(t)\}^T[M]\{r\}\ddot{u}_g(t)\,dt \tag{4.8a}$$

Eq.(4.8a) defines the various energy terms as follows:

$$E_K + E_D + E_H + E_S = E_I \tag{4.8b}$$

in which

$$E_I = - \int_0^t \{\dot{u}(t)\}^T[M]\{r\}\ddot{u}_g(t)\,dt = \text{the input energy} \tag{4.9a}$$

$$E_K = \int_0^t \{\dot{u}(t)\}^T[M]\{\ddot{u}(t)\}\,dt = \text{the kinetic energy} \tag{4.9b}$$

$$E_D = \int_0^t \{\dot{u}(t)\}^T[C]\{\dot{u}(t)\}\,dt = \text{the damping energy} \tag{4.9c}$$

$$E_H + E_S = \int_0^t \{\dot{u}(t)\}^T\{R(u(t))\}\,dt = \text{the sum of the hysteretic energy and the strain energy} \tag{4.9d}$$

Eq.(4.8b) indicates that the energy imparted to a structure is equal to the sum of the energy dissipated by damping and inelastic deformation and the energy stored temporarily in the form of kinetic and strain energy. The energy indices defined by Eqs.(4.9) can be computed numerically in accordance with the numerical integration scheme used to solve the equation of motion. In this study, the Newmark constant average acceleration method is used. Accordingly, the incremental values of the energy indices between times t and t+Δt can be computed based on the following expressions:

$$\Delta E_I = - [\ \{\dot{u}(t)\}^T[M]\{r\}(\ddot{u}_g(t) + \Delta\ddot{u}_g(t)/2)\Delta t + \{\Delta\dot{u}\}^T[M]\{r\}(\ddot{u}_g(t)/2 + \Delta\ddot{u}_g(t)/3)\Delta t\ ] \tag{4.10a}$$

$$\Delta E_K = \{\dot{u}(t)\}^T[M]\{\Delta\dot{u}\} + 1/2\ \{\Delta\dot{u}\}^T[M]\{\Delta\dot{u}\} \tag{4.10b}$$

$$\Delta E_D = [\ (\dot{u}(t))^T[C](\dot{u}(t)) + (\dot{u}(t))^T[C](\Delta\dot{u}) + 1/3\ (\Delta\dot{u})^T[C](\Delta\dot{u})\ ]\ \Delta t \tag{4.10c}$$

$$\Delta E_H + \Delta E_S = [\ (\dot{u}(t))^T\{R(u(t))\} + 1/2\ \{\Delta\dot{u}\}^T\{R(u(t))\}\ ]\ \Delta t + [\ (\dot{u}(t))^T[K_t](\dot{u}(t)) + (\dot{u}(t))[K_t](\Delta\dot{u}) + 1/4\ (\Delta\dot{u})^T[K_t](\Delta\dot{u})\ ]\ \Delta t^2/2 \tag{4.10d}$$

The values of the energy terms at time t+Δt are obtained by adding the incremental energy quantities calculated from Eqs.(4.10) to the values at the beginning of the time step t.

$$E_I(t+\Delta t) = E_I(t) + \Delta E_I \tag{4.11a}$$

$$E_K(t+\Delta t) = E_K(t) + \Delta E_K \tag{4.11b}$$

$$E_D(t+\Delta t) = E_D(t) + \Delta E_D \tag{4.11c}$$

$$E_H(t+\Delta t) + E_S(t+\Delta t) = E_H(t) + E_S(t) + \Delta E_H + \Delta E_S \tag{4.11d}$$

For the purpose of comparison among different structures, the energy indices may be normalized with respect to the total mass. The values of the energy indices per unit mass are given by

$$E_I^* = E_I/M_t \tag{4.12a}$$

$$E_K^* = E_K/M_t \tag{4.12b}$$

$$E_D^* = E_D/M_t \tag{4.12c}$$

$$E_H^* + E_S^* = (E_H + E_S)/M_t \tag{4.12d}$$

in which $M_t = \sum_{i=1}^{n} m_i$ = the total mass.

It is possible to calculate the hysteretic energy of the structure E_H by summing up the hysteretic work from individual structural members during the dynamic response. At the end of the response, the strain energy E_S disappears, and Eq. (4.9d) represents the hysteretic energy dissipated by inelastic deformation during the total duration of the

response.

The numerical computations of the various energy terms as described by Eqs. (4.10) and (4.11) have been incorporated into the DRAIN-2D program. The calculation of these energy terms may be used (a) to evaluate the damage potential of different earthquake ground motions in terms of the total energy imparted to a structure and the hysteretic energy dissipated by inelastic deformations; (b) to evaluate the suitability of using a simplified structural model (e.g. inelastic shear beam model or equivalent inelastic SDOF system) to replace the actual building structure in terms of their similarity in energy absorption and dissipation; and (c) to check the accuracy of the numerical integration of the equation of motion. These three aspects of application will be described in detail in Chapters 6 and 7.

4.6 Definition of Response Parameters

In order to describe the amount of damage that a building structure sustains during its seismic response, damage parameters need to be defined. Damage parameters can be divided into two groups corresponding to different response levels. One is related to overall structural response, and the other is associated with localized member response. Damage parameters may also be classified into two categories corresponding to different types of damage. One is related to damage caused by sudden large inelastic deformation excursions, and the other is associated with low-cycle fatigue-type damage due to sustained reversals of inelastic deformations. In this section, the response parameters used in this study are defined.

4.6.1 Overall Response Parameters

The overall response parameters can be subdivided into two groups. One is related to the response of a frame at storey levels, and the other is associated with the response of a frame as a whole. The storey level response parameters include maximum storey displacement, interstorey drift, interstorey shear, and interstorey moment. The global response parameters comprise global displacement ductility and energy indices.

The interstorey drift is defined as the maximum interstorey displacement divided by the storey height. This is a very useful parameter to indicate nonstructural damage. The global displacement ductility is defined as

$$\mu_\delta = \frac{\delta_{max}}{\delta_y} \tag{4.13}$$

in which

δ_{max} = the maximum roof displacement;

δ_y = the roof displacement corresponding to first yielding.

The roof displacement corresponding to first yielding is obtained from an inelastic static analysis for a frame, as will be described in Chapter 5. In the inelastic static analysis, a frame is subjected to monotonically increased lateral loading which is distributed over height in accord with the NBCC 1985 distribution formula.

4.6.2 Local Member Response Parameters

The deformation response parameters for structural members include rotation ductility, curvature ductility, maximum plastic rotation, and accumulative plastic rotation. The definitions of these parameters are

given as follows.

The rotation ductility is defined as the ratio of the maximum total rotation at the end of a member to the yield rotation.

$$\mu_\theta = \frac{\theta_{max}}{\theta_y} \tag{4.14}$$

The maximum total rotation θ_{max} can be obtained from the static or dynamic analysis. In order to estimate the yield rotation θ_y, assumption needs to be made regarding the deformed shape of the member at first yielding. It is usually assumed that the member yields in antisymmetric bending. Therefore, the yield rotation is given by

$$\theta_y = \frac{M_y L}{6EI} \tag{4.15}$$

in which L = the member length; EI = the member stiffness; and M_y = the yield moment. For the beams, the effect of varying axial force on the flexural yield strength is not considered. Therefore, θ_y is a constant. For the columns, the yield moment M_y varies with axial force, as described by the yield moment-axial force interaction diagram in Fig. 4.3. Therefore, θ_y also varies with axial force. In this study, two definitions are considered for the columns. One corresponds to the initial axial force under gravity loading, and the other is associated with the current axial force.

$$\mu_\theta^G = \frac{\theta_{max}}{\frac{M_y^G L}{6EI}} \tag{4.16a}$$

$$\mu_\theta^t = \frac{\theta_{max}}{\frac{M_y^t L}{6EI}} \tag{4.16b}$$

in which M_y^G, M_y^t = the yield moment corresponding to the initial gravity axial force P_G or the instantaneous axial force P_t (Fig. 4.5).

The curvature ductility is defined as the ratio of the maximum curvature to the yield curvature.

$$\mu_\phi = \frac{\phi_{max}}{\phi_y} \tag{4.17}$$

In this definition, the need to assume antisymmetric bending for a member is eliminated. For a bilinear moment-curvature relationship, the curvature ductility may be written as (Fig. 4.6):

$$\mu_\phi = 1 + \frac{M_{max} - M_y}{pM_y} \tag{4.18}$$

in which M_{max} = the maximum moment; and p = the ratio of the strain-hardening stiffness to the initial elastic stiffness. Eq.(4.18) eliminates the need to compute maximum curvature which is not directly accessible in the computer program. It should be noted that Eq.(4.18) is valid only if M_{max} and M_y correspond to the same time instant. For the columns, the curvature ductility corresponding to the instantaneous axial force can be calculated from Eq.(4.18).

$$\mu_\phi^t = 1 + \frac{M_{max} - M_y^t}{pM_y^t} \tag{4.19}$$

The curvature ductility corresponding to the initial gravity axial force should be computed as follows:

$$\phi_y^G = \frac{M_y^G}{EI} \tag{4.20a}$$

$$\phi_{max} = \frac{M_y^t}{EI} + \frac{M_{max} - M_y^t}{pEI} \tag{4.20b}$$

$$\mu_\phi^G = \frac{\phi_{max}}{\phi_y^G} = \frac{M_y^t}{M_y^G} + \frac{M_{max} - M_y^t}{pM_y^G} \tag{4.20c}$$

In addition to the rotation and curvature ductility factors defined above, the maximum plastic rotation θ^p_{max} at the end of a member is also calculated.

All the damage parameters defined previously are associated with peak inelastic response values. Therefore, they reflect information on damage caused by large inelastic deformation excursions. In order to account for low-cycle fatigue-type damage due to sustained reversals of inelastic deformations, the accumulative plastic rotation θ^p_{acc} is computed. This damage parameter is defined as the sum of the absolute values of all the plastic rotations experienced at the end of a member during the total duration of the response

$$\theta^p_{acc} = \sum_{i=1}^{n_p} |\theta^p_i| \tag{4.21}$$

in which n_p = total number of yield excursions.

Table 4.1 Values of c_1 and c_2 for Frames Considered in This Study

	4S1	4S2	10S	18S
c_1	2.053329	1.021656	0.386182	0.234098
c_2	0.000893	0.001789	0.005005	0.008370

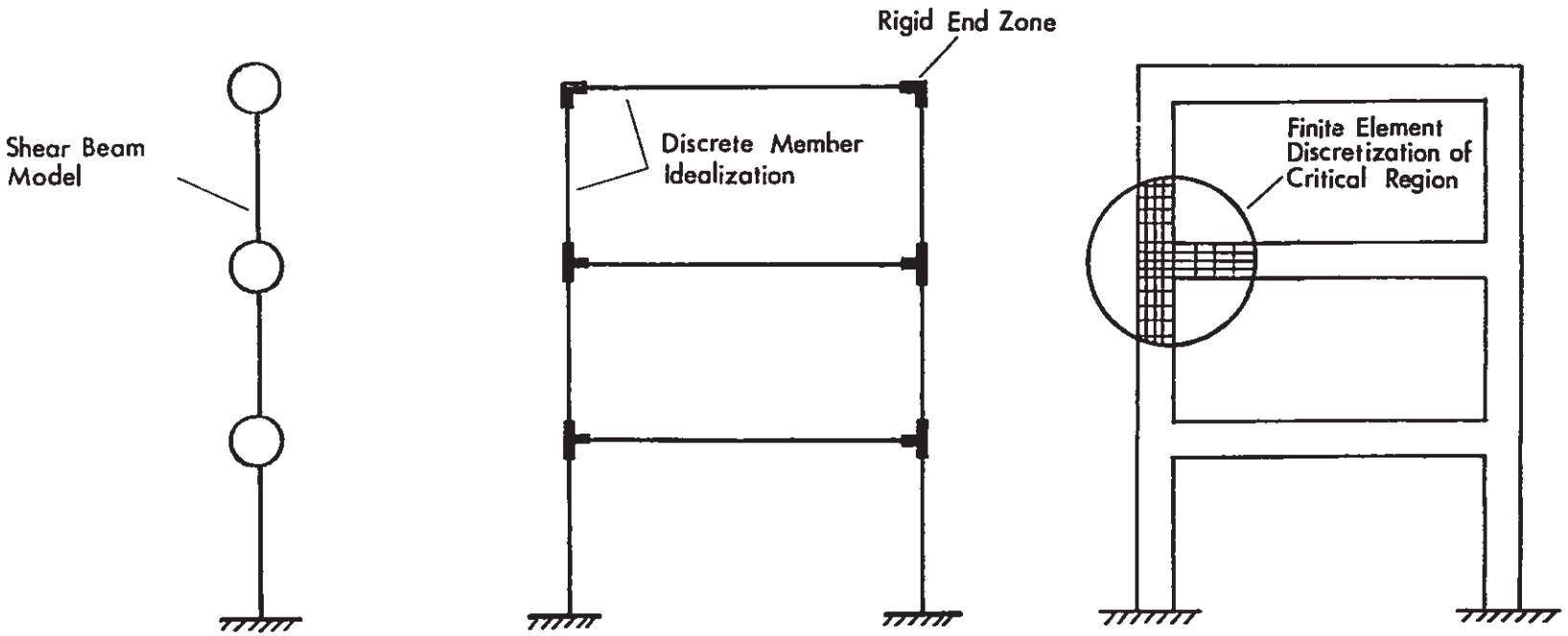

Fig. 4.1 Schematic Illustration of Three Modelling Approaches

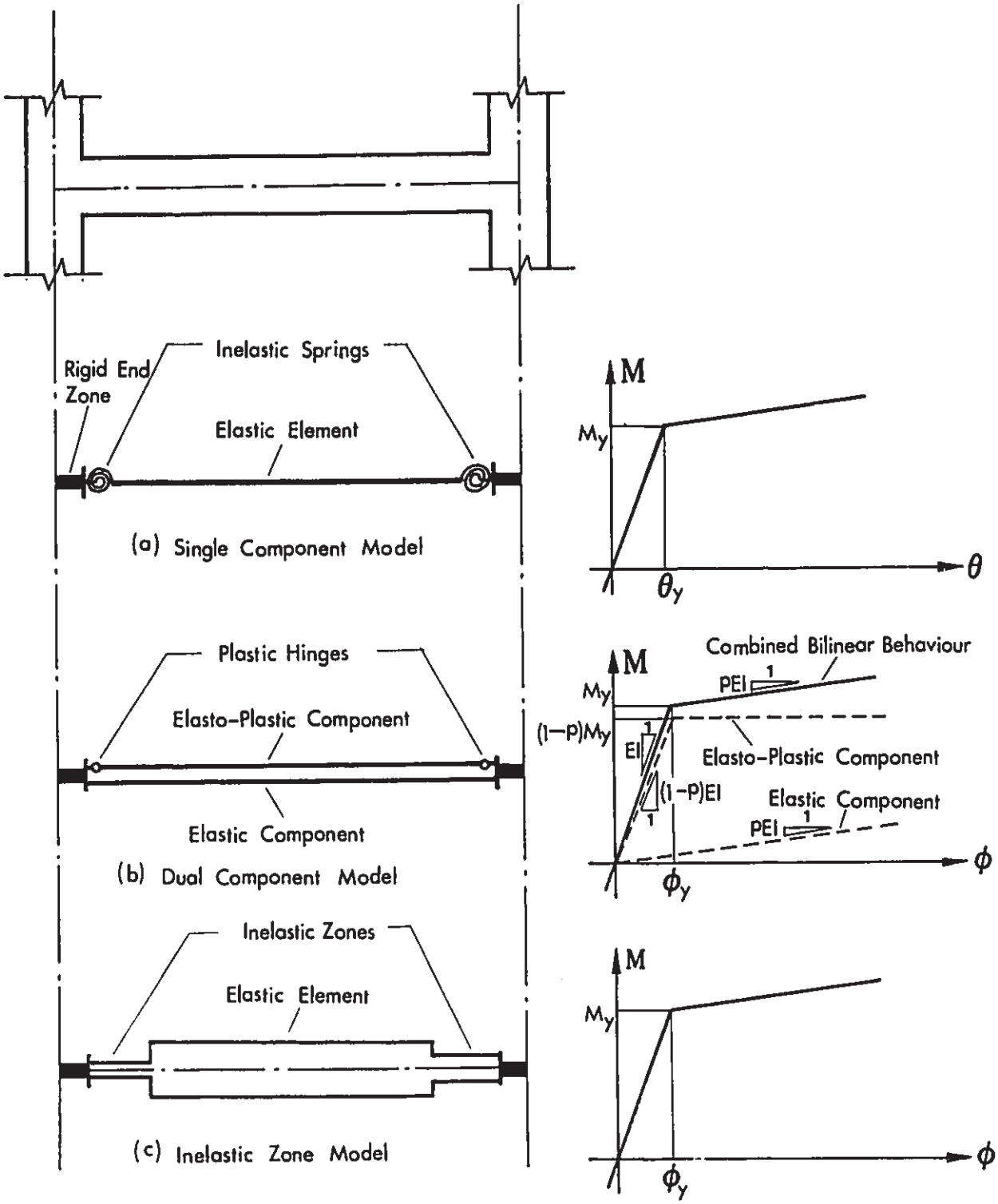

Fig. 4.2 Three Analytical Models for Discrete Member Idealization

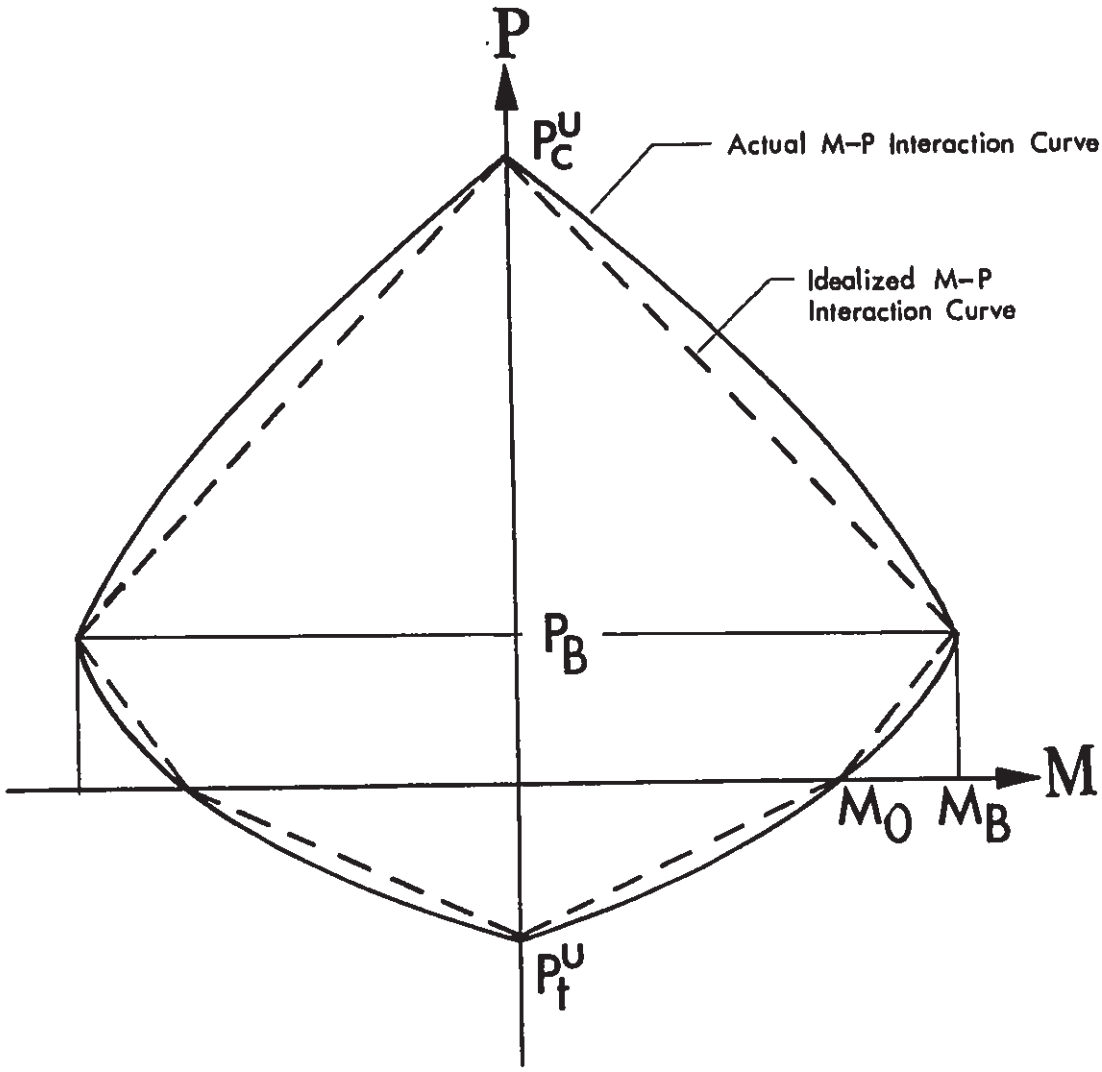

Fig. 4.3 Bending Moment-Axial Force Interaction Curves for Columns

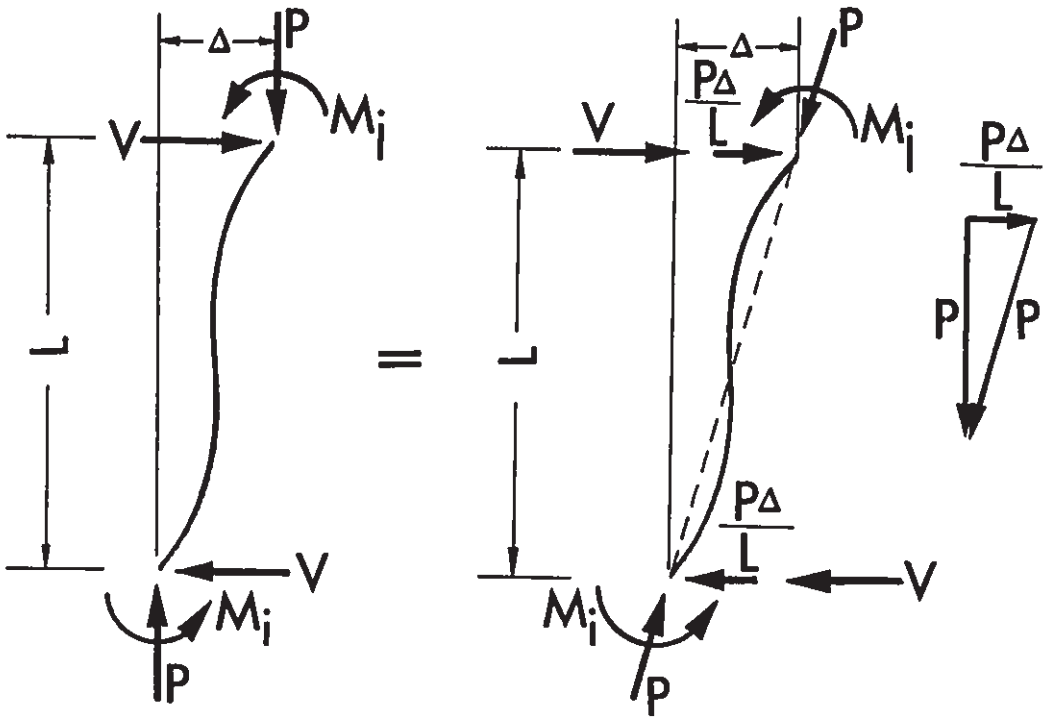

Fig. 4.4 P-Delta Effect

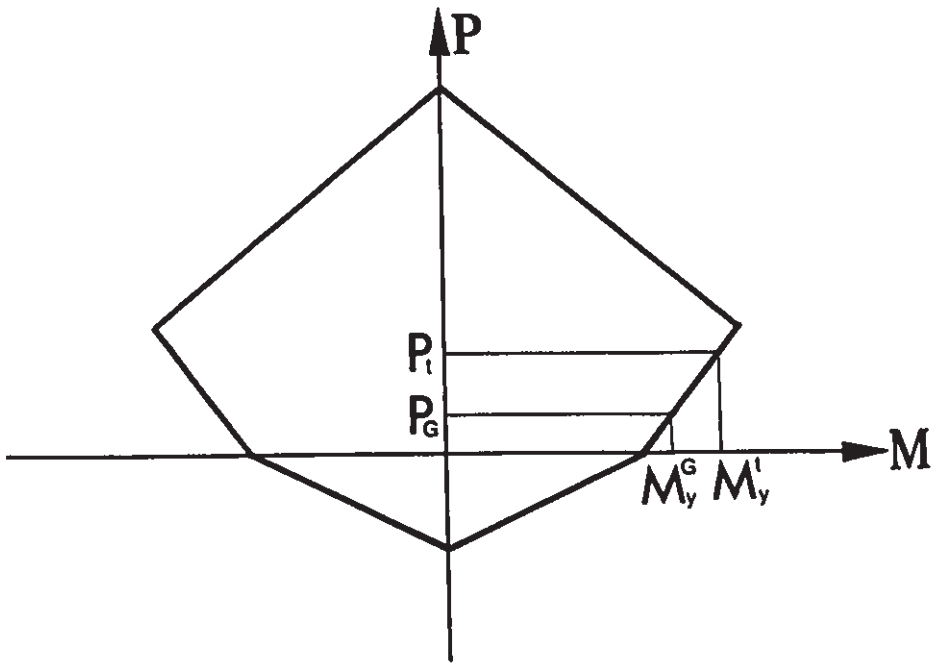

Fig. 4.5 Yield Moments Corresponding to Initial and Current Column Axial Forces for Definition of Ductility Factors

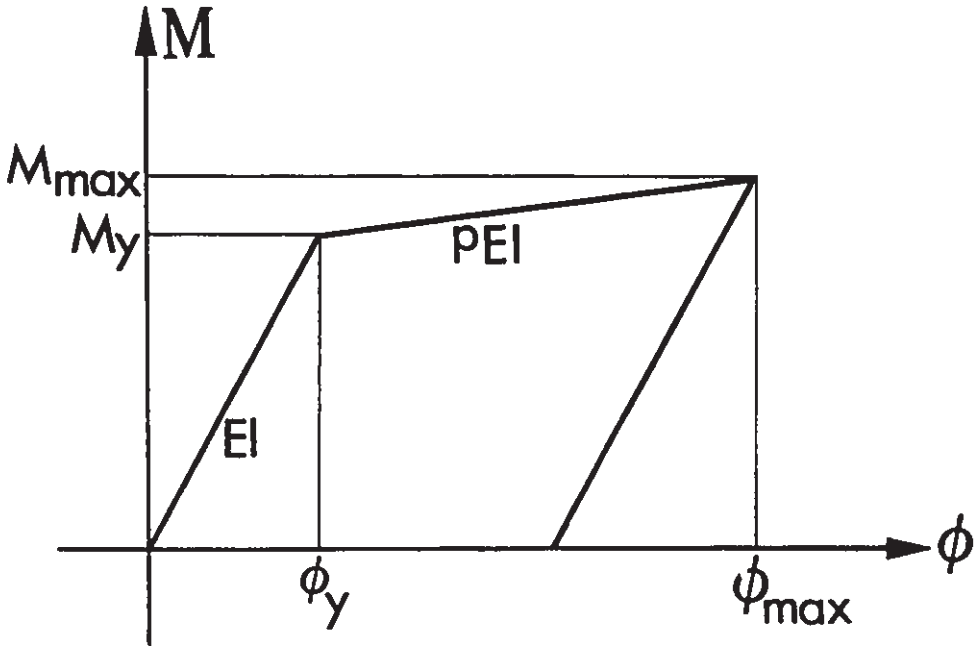

Fig. 4.6 Definition of Curvature Ductility

CHAPTER 5

RESULTS OF STATIC ANALYSIS

5.1 Introduction

In this chapter, the inelastic behaviour of the designed frames, as subjected to monotonically increased lateral loading, is studied. The lateral loading is distributed along the height of each frame in accordance with the NBCC 1985 distribution formula described in Chapter 3. This static load analysis is important for the following two reasons. First, in current practice of seismic design for regular building structures, earthquake loading is usually simplified as equivalent static lateral loading. Second, the inelastic static analysis provides background information for the evaluation of the inelastic dynamic responses of the frames to earthquake ground excitations to be described in Chapter 6.

The static analysis begins with a study of the P-Delta effect on the overall response of the frames. This study is useful to help understand the detailed inelastic behaviour of the frames. Following this study, the detailed inelastic behaviour of the frames under monotonically increased lateral loading is investigated from three different aspects. First, the sequence of plastic hinge formation in the beams and columns is traced. Second, the relationship between base shear and roof deflection is examined. Finally, the distribution of the various response parameters along the height of each frame for two different levels of overall drift is examined.

5.2 P-Delta Effect

In order to investigate the significance of the P-delta effect, two analyses are performed for each of the eight frames considered in this study. One includes and the other ignores the negative geometric stiffness matrix for each column. Shown in Fig. 5.1 are the comparisons of the base shear versus roof deflection curves between the two analyses for the 4S2 and 18S frames. It can be seen that the P-Delta effect is not noticeable when the frames are in the linear elastic range. When the frames are loaded into the inelastic range, the P-Delta effect becomes significant. In the inelastic range, the P-Delta effect for the 18S frame is much more significant than that for the 4S2 frames. In the case of the 4S2 frames, the base shear without P-Delta effect is about 4% higher than that with P-Delta effect for an overall drift of 1%, whereas this difference increases up to 15% for the 18S frame. The overall drift is defined as the roof displacement of a frame divided by its total height.

As described in Chapter 4, the P-Delta effect is accounted for by including a negative geometric stiffness matrix for each column based on the initial axial force due to gravity loading. The global geometric stiffness matrix is obtained by assembling the column geometric stiffness matrices, and it is assumed to remain constant during the application of lateral loading. In the elastic range, the initial elastic structural stiffness is much higher than the geometric stiffness. Therefore, the effect of including the negative geometric stiffness matrix is not significant. As more and more structural members are loaded into the inelastic range, the structural stiffness is reduced substantially, and the contribution of the geometric stiffness becomes more significant. The

column axial forces under gravity loading for the 18S frame are much higher than those for the 4S2 frames. Therefore, the softening effect due to the negative geometric stiffness matrix for the 18S frame is more significant than that for the 4S2 frames in the inelastic range.

5.3 Plastic Hinge Formation

Shown in Fig. 5.2 are the sequences of plastic hinge formations for the eight frames when subjected to monotonically increased lateral loading. The open circles denote the plastic hinges in the beams, whereas the solid circles represent the plastic hinges in the columns. The number beside each circle indicates the formation sequence. The hinge patterns for the 4S2, 10S, and 18S frames correspond to an overall drift of 1%, whereas those for the 4S1 frames are associated with an overall drift of 0.2%. The use of a smaller overall drift for the 4S1 frames is because the 4S1 frames are much stiffer than the 4S2 frames.

It can be seen in Fig. 5.2 that plastic hinges are formed first in the beams. Furthermore, the beam hinges initiate at their right ends. The beam ends are initially subjected to negative moments under gravity loading. The lateral loading produces negative moments at the right ends of the beams and positive moments at their left ends. Therefore, the lateral loading increases the initial negative moments at the right ends of the beams and causes the right ends to yield first. After a number of plastic hinges have formed in the beams, plastic hinges start to form at the base of the first storey columns. The earlier formation of column hinges at the base of the first storey columns is due to the large overturning moment caused by the lateral loading and the assumption of

total fixity at the frame base. After the yielding of the first storey columns at their base, further plastic hinges are formed in the beams, particularly at their left ends. Following this, column plastic hinges begin to form at upper or middle storeys.

In a moment-resisting frame, the columns and beams are the principal elements resisting the lateral seismic and vertical gravity loads. Unlike the beams, the columns are subjected not only to bending moments and shears but also to large axial forces. Therefore, large inelastic deformations in the columns may cause instability. A typical example of frame collapse due to column instability is a soft storey sway mechanism, as shown in Fig. 5.3a. In this column sidesway mechanism, inelastic deformations are concentrated at both ends of the columns within one storey. Because a column failure has more serious consequences than a beam failure, it is desirable for plastic hinging to occur in the beams instead of in the columns. The desired sway mechanism for a frame is shown in Fig. 5.3b. In this beam sidesway mechanism, plastic hinges are developed in all the beams, and column hinges are located only at the base of the first storey columns. It can be seen in Fig. 5.2 that for the frames considered in this study, some column yielding occurs in upper or middle storeys. However, because there is hinging at only one end of the columns, the column sidesway mechanism cannot form. Therefore, the sway mechanisms of the frames designed in accordance with NBCC 1985 and CAN3-A23.3-M84 are somewhat between the column sidesway mechanism and the beam sidesway mechanism. In order to attain the desired complete beam sidesway mechanism, the column moment capacities need to be increased.

5.4 Force-Displacement Response

The base shear vs. roof displacement response of a frame subjected to monotonically increased lateral loading provides information regarding the overall stiffness and strength of the frame. This response depends on the particular distribution of the lateral loading. In this study, the lateral loading is distributed in accordance with the NBCC 1985 distribution formula. For the 4S1, 4S2, and 10S frames, this is an inverted triangular distribution. For the 18S frame, the inverted triangular distribution is modified by an additional concentrated load at the roof level.

The base shear vs. roof displacement curves for the eight frames are depicted in Fig. 5.4. The points corresponding to the first beam hinge and the first column hinge are shown in the same figure to indicate the possible change in the behaviour of the frames after the formation of the first beam or column hinge. In order to indicate the overall strengths of the frames relative to their seismic design forces, the design base shears for the frames obtained directly from the NBCC 1985 base shear formula (Table 3.4) and the correponding factored design base shears are also shown in the figure. The factored design base shears are obtained by multiplying the design base shears by a load factor of 1.5. In addition, two points corresponding to the overall drifts of 0.5% and 1.0% are shown on the curves for the 4S2, 10S, and 18S frames. For the 4S1 frames, the two points are associated with the overall drifts of 0.1% and 0.2%. The distributions of the various response parameters along the height of each frame for its corresponding two levels of overall drift will be discussed in a later section.

It can be seen in Fig. 5.4 that the base shear-roof displacement response is nearly linear up to the formation of the first column hinge. After the formation of the first column hinge, the overall stiffness of the 10S and 18S frames decreases drastically. The average overall stiffness after the first column hinge is about 4% of the initial elastic stiffness. For the 4S1 and 4S2 frames, the overall stiffness decreases gradually after the first column hinge, and a drastic change occurs at a base shear higher than that corresponding to the first column hinge. The average overall stiffness after this drastic change is about 8% of the initial elastic stiffness. The higher overall stiffness of the 4S1 and 4S2 frames in the inelastic range as compared to the 10S and 18S frames is because the P-Delta effect for the 4S1 and 4S2 frames is less significant than that for the 10S and 18S frames, as discussed in the previous section.

It can be seen in Fig. 5.4 that the base shear corresponding to the first beam hinge is slightly lower than the factored design base shear for each of the eight frames. The earlier yielding of the beams before the base shear reaches the factored design base shear is due to the following two reasons. First, in the inelastic static analysis, full gravity loads without load factors are applied to the frame prior to the application of the lateral loading, whereas the beam design moments are obtained from the three combinations of gravity and seismic loads coupled with load factors, as described in Chapter 3. Therefore, the combination of gravity and seismic loads in the analysis is different from that in the design. Second, in the design of the beams, the moments due to gravity loading have been reduced by 20% to account for moment

redistribution.

As can be seen in Fig. 5.4, the 4S1L, 4S1I, and 4S1H frames have the same initial elastic stiffness but different overall strengths. This difference in the overall strength results from the use of three different lateral seismic design forces in the design of the frames as described in Chapter 3. At the specified overall drift of 0.1%, the overall strength of the 4S1L frame is about 14% lower than that of the 4S1I frame, and the overall strength of the 4S1H frame is about 22% higher than that of the 4S1I frame. The corresponding differences in the seismic response factor S shown in Fig. 3.4 are 30% and 41%. Therefore, the difference in the actual strengths of the three frames is about half of that in their seismic design forces. This is because the design of the three frames is not based on lateral seismic loading alone. Instead, it is based on the combinations of gravity and seismic loads coupled with load factors. Because the design gravity loading is the same for the three frames, the presence of the gravity loading in the design tends to reduce the effect of the difference in the seismic loads for the three frames. As a result, the difference in the overall strengths of the three frames is less than the corresponding difference in their seismic design loads. This observation can be further confirmed by the 4S2 frames. At the specified overall drift of 0.5%, the overall strength of the 4S2L frame is about 6% less than that of the 4S2I frame, and the overall strength of the 4S2H frame is about 9% higher than that of the 4S2I frame. However, the corresponding differences in the seismic response factor are 14% and 19%. It should be noted that the design of the frames considered in this study is dominated by seismic loading because of the

high level of seismicity, i.e. Z_v = 6. For gravity load dominated frames, i.e. in lower seismic zones, the difference in their overall strengths resulting from the use of different seismic design forces for different zonal combinations would be even less significant.

It can be observed in Fig. 5.4 that the actual strengths of the frames are higher than the factored design base shears. For example, the strength corresponding to an overall drift of 0.5% is about 80%, 62%, and 47% higher than the factored design base shear for the 4S2L, 4S2I, and 4S2H frames, respectively. This overstrength is about 29% and 13% for the 10S and 18S frames, respectively. The lower overstrength for the 10S and 18S frames is mainly because the P-Delta effects for these two frames are more significant.

The overstrength of the frames considered in this study can be attributed to the following factors. First, the column strengths are higher than those obtained directly from the elastic static analyses of the frames under the three load combinations because they are keyed to the beam strengths based on the weak beam-strong column criterion. Second, the formation of plastic hinges in the frames is a gradual process, as shown in Fig.5.2, whereas in the ultimate limit state design, it is implicitly assumed that a frame would be transformed into a mechanism instantaneously. Finaily, strain-hardening effect for the beams and columns has been included in the analysis.

It should be noted that the yield moments for the beams and the yield moment-axial force interaction curves for the columns used in the analysis are based on the dependable material strengths (ϕ_c=0.6; ϕ_s=0.8). This is because in the design of the frames, the determination

of flexural reinforcing steel for the structural members is also based on the dependable material strengths. Therefore, the use of the dependable strengths instead of the nominal values in the analysis is consistent with the design. Also, the dependable values may be considered as a lower bound for the material strengths. Had the nominal strengths (ϕ_c=1.0; ϕ_s=1.0) been used in determining the yield moments for the beams and the yield moment-axial force interaction curves for the columns, the overstrength of the frames as compared to their seismic design forces would have been more significant.

5.5 Distribution of Response Parameters

The inelastic behaviour of the frames is also studied by examining the distributions of the various response parameters along their height when the frames are loaded well into the inelastic range. The distributions for the 4S1 and 4S2 frames are very similar, and so are the distributions between the 10S and 18S frames. Therefore, only the distributions for the 4S2 and 10S frames are presented. The distributions of the response parameters correspond to two overall drift levels of 0.5% and 1%.

Shown in Fig. 5.5 are the interstorey drifts of the 4S2 and 10S frames for the two overall drifts of 0.5% and 1%. Plotted in the same figure are the interstorey drifts corresponding to the formation of the first beam hinge and the first column hinge. It can be seen that the interstorey drifts are relatively uniform across the frame height at the time the first beam hinge or the first column hinge is formed. As the frames are loaded well into the inelastic range, the interstorey drifts

in the lower storeys increase substantially, whereas those in the upper storeys remain relatively unchanged. For the specified overall drift of 1%, the maximum interstorey drift in the lower storeys becomes 1.37%, 1.47%, and 1.65% for the 4S2, 10S, and 18S frames, respectively. The tendency for the concentration of interstorey deflections in the lower storeys is more significant for taller frames.

Plotted in Fig. 5.6 are the curvature ductility, rotation ductility, and plastic rotation for the beams at each storey level of the 4S2 and 10S frames for the two overall drift levels of 0.5% and 1%. The value of each response parameter at a storey level is the largest of those computed at the ends of the three beams of that storey. As in the case of interstorey drift, the beam ductility demands and plastic hinge rotation tend to be concentrated in the lower storeys as the frames are loaded well into the inelastic range. When the overall drift of the frames is doubled from 0.5% to 1%, the beam ductility demands and plastic rotation in the lower storeys are also doubled, whereas those in the upper storeys remain nearly unchanged.

Shown in Fig. 5.7 are the curvature ductility, rotation ductility, and plastic rotation for the columns in the 4S2 and 10S frames for the two levels of overall drift. The results are presented separately for the exterior and interior columns. This is because the axial forces in the exterior columns vary considerably during the application of lateral loading, whereas those in the interior columns remain relatively unchanged. Therefore, the effect of varying axial forces on the response parameters can be examined. For the curvature or rotation ductility, two different definitions are used, as described in Chapter 4. One is based

on the initial axial force under gravity loading (μ_ϕ^G, μ_θ^G), and the other is based on the current axial force under combined gravity and lateral loading (μ_ϕ^t, μ_θ^t). It can be seen that the column inelastic deformations are concentrated at the base of the first-storey columns.

For the inverted triangular distributions of lateral loading, the beam and column moments in the lower storeys are far more sensitive to a change in the magnitude of the lateral loading than those in the upper storeys. This is particularly true for taller frames. Therefore, as the lateral loading is increased monotonically, the bending moments of the beams and columns in the lower storeys increase much more rapidly than those in the upper storeys. This rapid increase in the bending moments results in the concentration of large inelastic deformations in the lower storey beams and at the base of the first storey columns. These large inelastic deformations in turn leads to the concentration of interstorey displacements in the lower storeys. Therefore, for the frames designed in accordance with NBCC 1985 and CAN3-A23.3-M84, the interstorey deflections tend to be concentrated at the bottom of the frames if the actual distributions of the seismic loading can be simulated by those assumed in their design. This concentration of interstorey deflections is undesirable because the axial loads are the highest in the lower storeys, and therefore, the lower storeys are more vulnerable to the adverse second-order P-delta effects.

It can be seen in Fig. 5.7 that the two definitions of curvature or rotation ductility based on different axial forces provide somewhat different values for the exterior columns whereas they give nearly identical values for the interior columns. At the base of the first-

storey exterior columns where maximum ductilities occur, μ_ϕ^G and μ_θ^G tend to be lower than μ_ϕ^t and μ_θ^t. This difference increases with an increase in the number of storeys and the level of inelastic deformation. For the specified overall drift of 1%, μ_ϕ^G and μ_θ^G are about 9%, 16%, and 39% lower than μ_ϕ^t and μ_θ^t for the 4S2, 10S, and 18S frames, respectively. The lateral loading produces tensile axial forces in the left exterior columns and compressive axial forces in the right exterior columns. As a result, the axial forces due to combined gravity and lateral loads in the left exterior columns are lower than their initial axial forces under gravity loading, whereas the combined axial forces in the right exterior columns are higher than their initial gravity axial forces. This change in the axial forces of the exterior columns can be seen clearly in Fig. 5.8 in which the ratios of the column axial forces to their corresponding balanced axial forces are plotted for the case of combined gravity and lateral loads and that of initial gravity load. For the interior columns, the effect of the lateral loading on their axial forces is very small, and the axial forces under combined lateral and gravity loads are very similar to the initial axial forces due to gravity load. Therefore, the variation of the axial forces in the exterior columns due to lateral loading results in different values for the two definitions of curvature or rotation ductility. For taller frames, this difference can be significant, and therefore, the two definitions should be clearly distinguished.

It can be observed in Figs. 5.6 and 5.7 that the curvature ductility is similar to the rotation ductility for the beams. However, at the base of the first-storey columns, the rotation ductility is

significantly higher than the curvature ductility, and this is true for both definitions. For the overall drift of 1%, the rotation ductility is about 50%, 56%, and 57% higher than the curvature ductility for the 4S2, 10S, and 18S frames, respectively. As noted in Chapter 4, the yield rotation required for the definition of the rotation ductility is obtained from the assumption of antisymmetric bending for a structural member, whereas the dual-component model itself does not need this assumption. An examination of the bending moment distributions of the columns in the lower storeys reveals that the actual deformed shapes of the columns are far from the antisymmetric bending assumption. For the 10S and 4S2 frames, the contraflexure points of their first-storey columns are shifted well towards the top ends. For the 18S frame, the first-storey columns are actually in single curvature bending. Therefore, the definition of rotation ductility, as described in Chapter 4, may not be appropriate for the columns in the lower storeys, and the curvature ductility is more suitable because its definition does not involve any assumption regarding the deformed shape of the columns.

5.6 Summary

In this chapter, the inelastic behaviour of the frames designed in Chapter 3, as subjected to monotonically increased lateral loading, has been investigated. The lateral loading is distributed along the height of the frames in accordance with the NBCC 1985 distribution formula. Therefore, the distributions of the lateral loading in the analysis of the frames is the same as those used in their design. Based on this investigation, the following conclusions can be drawn:

(1) The P-Delta effect is negligible when the frames remain in the linear elastic range. It becomes significant as the frames are loaded well into the inelastic range. In the inelastic range, the P-Delta effect for high rise frames is much more significant than that for low rise frames.

(2) The sway mechanisms of the frames designed in accordance with NBCC 1985 and CAN3-A23.3-M84 are somewhat between the beam sidesway mechanism and the column sidesway mechanism, when they are subjected to monotonically increased lateral loading whose distributions are the same as those assumed for their design. In order to attain the desired complete beam sidesway mechanism, the column strengths would need to be increased over those suggested by CAN3-A23.3-M84.

(3) In the short period range (less than 0.5 sec), the differences in the actual overall strengths of the three frames corresponding to the three zonal combinations are smaller than the differences in their seismic design forces. This is because the design of the three frames is based on the combinations of gravity and seismic loads coupled with load factors, and the design gravity loading is the same for the three frames. This observation would be particularly true for gravity load dominated frames whose design is controlled by gravity loading.

(4) The actual overall strengths of the frames are higher than their factored design base shears. Therefore, there is seismic overstrength for the frames designed in conformance with NBCC 1985 and CAN3-A23.3-M84. This overstrength for low rise frames is more significant than that for high rise frames.

(5) The overall stiffnesses of the frames are reduced substantially after the formation of the first column hinge. This reduction in the overall stiffness is particularly pronounced for high rise frames because the softening effect due to the P-Delta phenomenon for high rise frames is more significant than that for low rise frames in the inelastic range.

(6) As the frames are loaded well into the inelastic range, inelastic deformations tend to be concentrated in the lower storey beams and at the base of the first storey columns. This concentration of inelastic deformations leads to very large interstorey displacements in the lower storeys, and the maximum interstorey drift in the lower storeys can be substantially higher than the corresponding specified overall drift.

(7) The large variations of the axial forces in the exterior columns due to lateral loading results in different values for the two different definitions of curvature or rotation ductility. This is particularly true for high rise frames. The definition based on the current column axial force tends to be larger than that based on the initial column axial force under gravity loading. Therefore, for the exterior columns in high rise frames, the level of axial force on which the definition of ductility factors is based should be clearly identified.

(8) For the dual-component model used in this study, the rotation ductility can be significantly larger than the curvature ductility for the columns in the lower storeys. In the definition of the rotation ductility, the yield rotation is obtained based on the assumption that a structural member deforms in double curvature with its inflection point

in the middle. However, the actual deformed shapes of the columns in the lower storeys are far from this assumption, and the lower storey columns in a high rise frame subjected to large lateral loading can be in single curvature bending. Therefore, the definition of rotation ductility described in Chapter 4 may not be applicable to columns in the lower storeys of high rise frames.

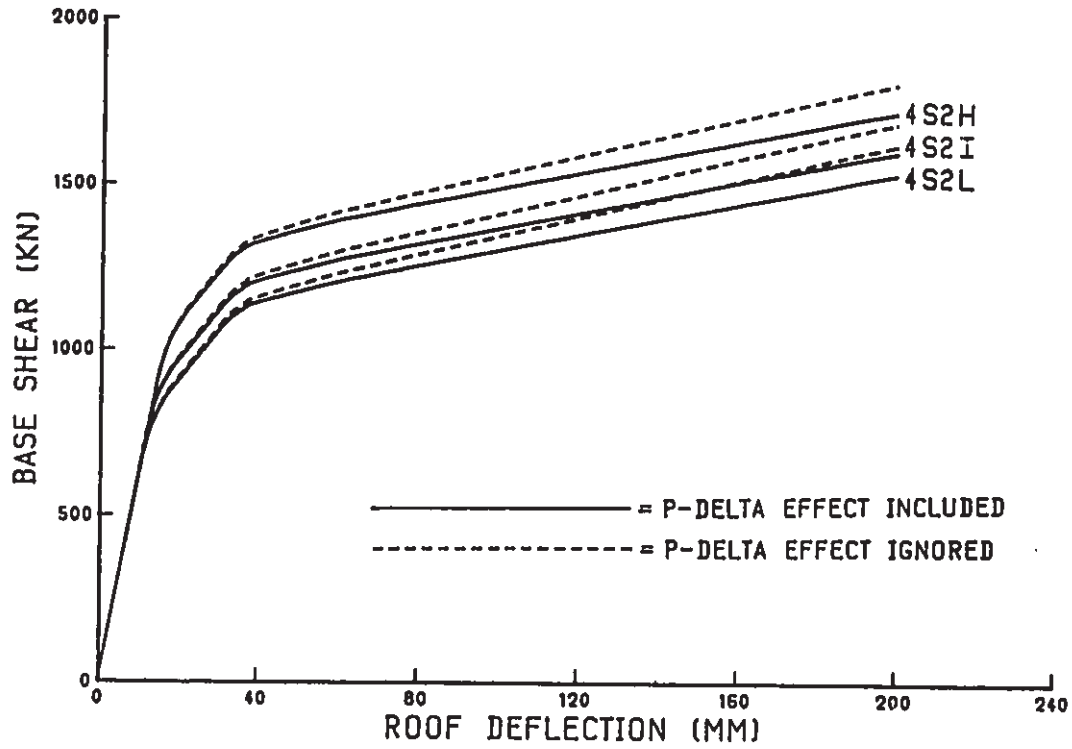

(a) 4S2 Frames

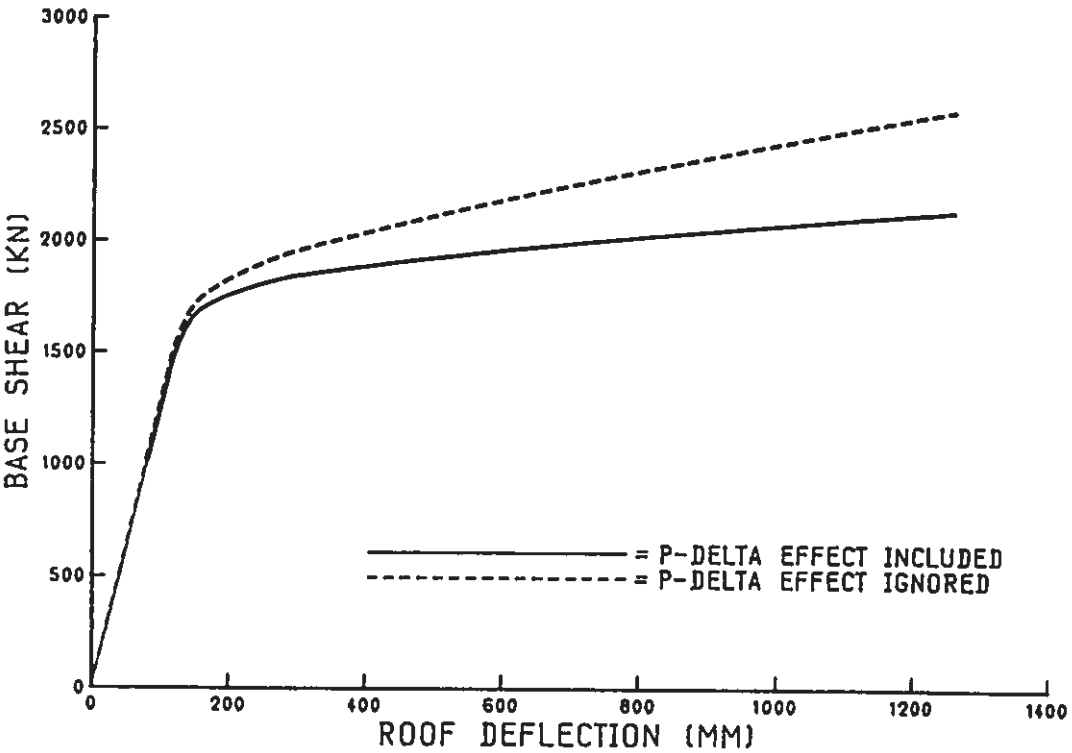

(b) 18S Frame

Fig. 5.1 P-Delta Effect on Static Base Shear vs. Roof Displacement Response

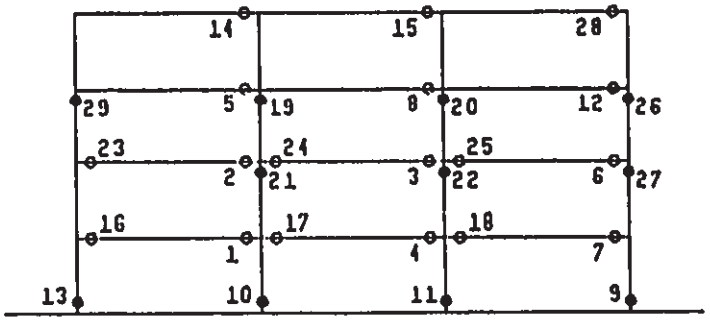

4S1L

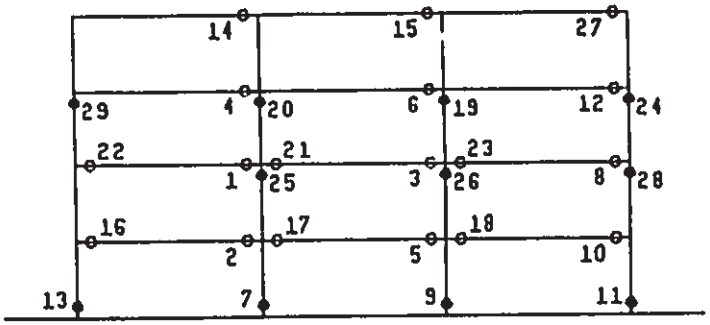

4S1I

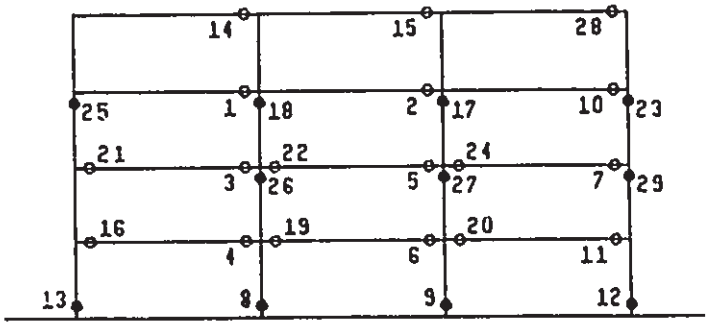

4S1H

(a) 4SI Frames

Fig. 5.2 Sequence of Plastic Hinge Formation under Monotonically Increased Lateral Loading

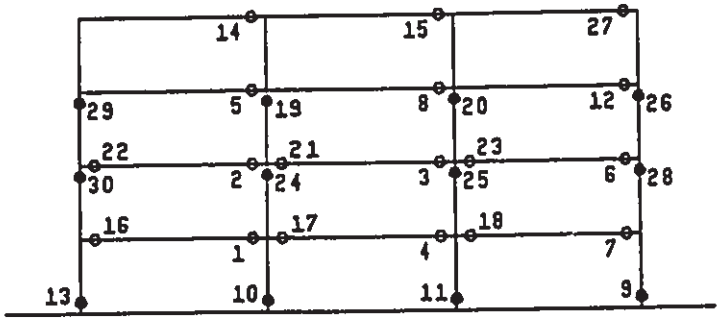

4S2L

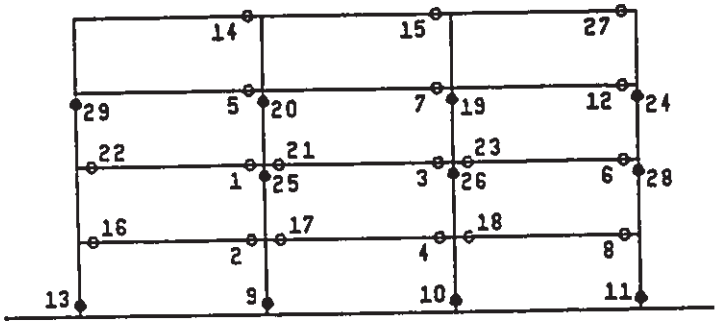

4S2I

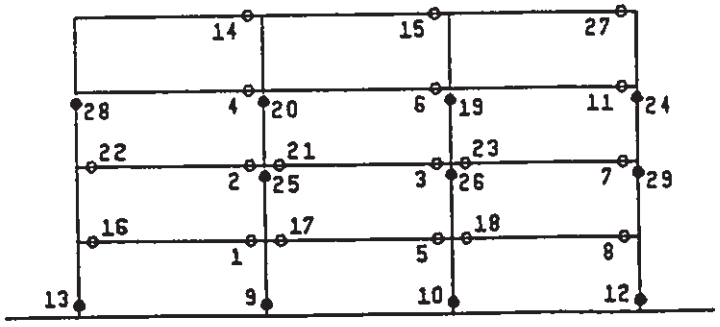

4S2H

(b) 4S2 Frames

Fig. 5.2 (cont'd) Sequence of Plastic Hinge Formation under Monotonically Increased Lateral Loading

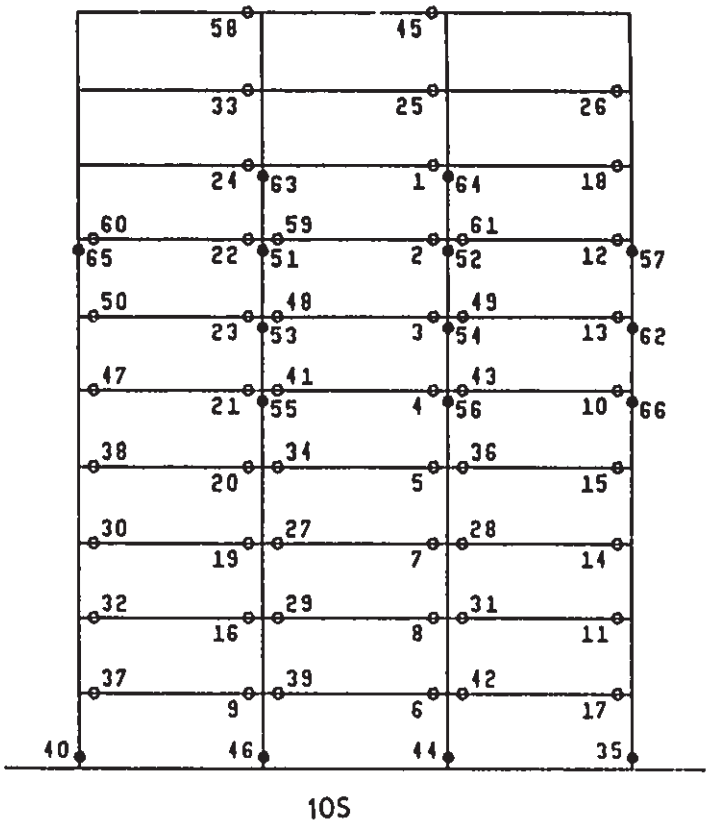

10S

(c) 10S Frame

Fig. 5.2 (cont'd) Sequence of Plastic Hinge Formation under Monotonically Increased Lateral Loading

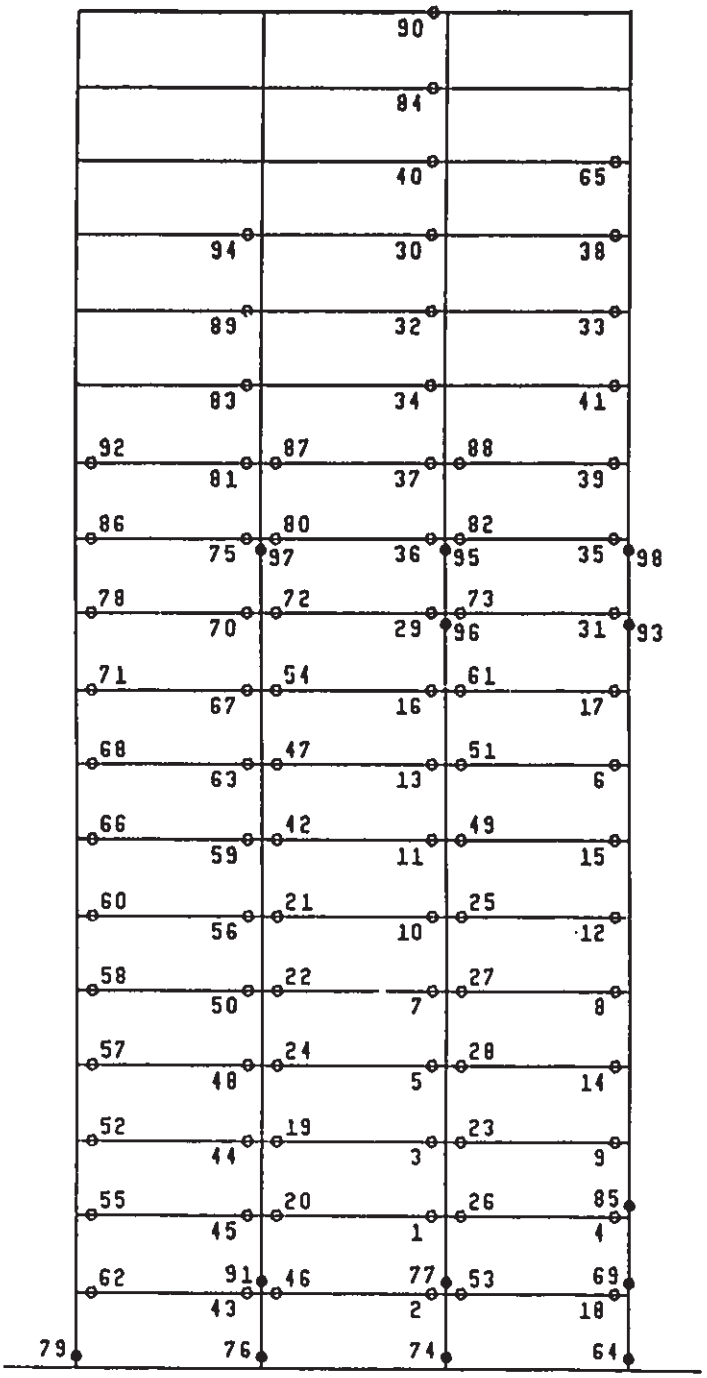

18S

(d) 18S Frame

Fig. 5.2 (cont'd) Sequence of Plastic Hinge Formation under Monotonically Increased Lateral Loading

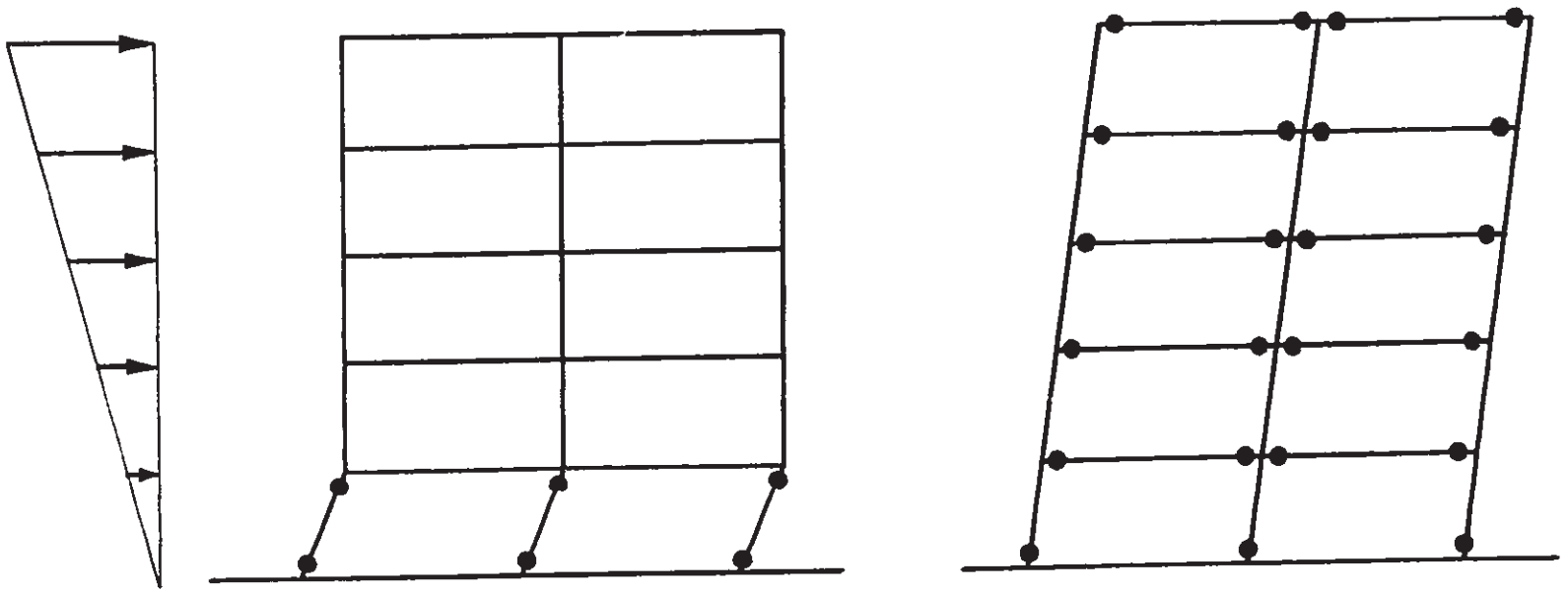

(a) Column Sidesway Mechanism

(b) Beam Sidesway Mechanism

Fig. 5.3 Possible Mechanisms for Building Frames under Seismic Lateral Loading

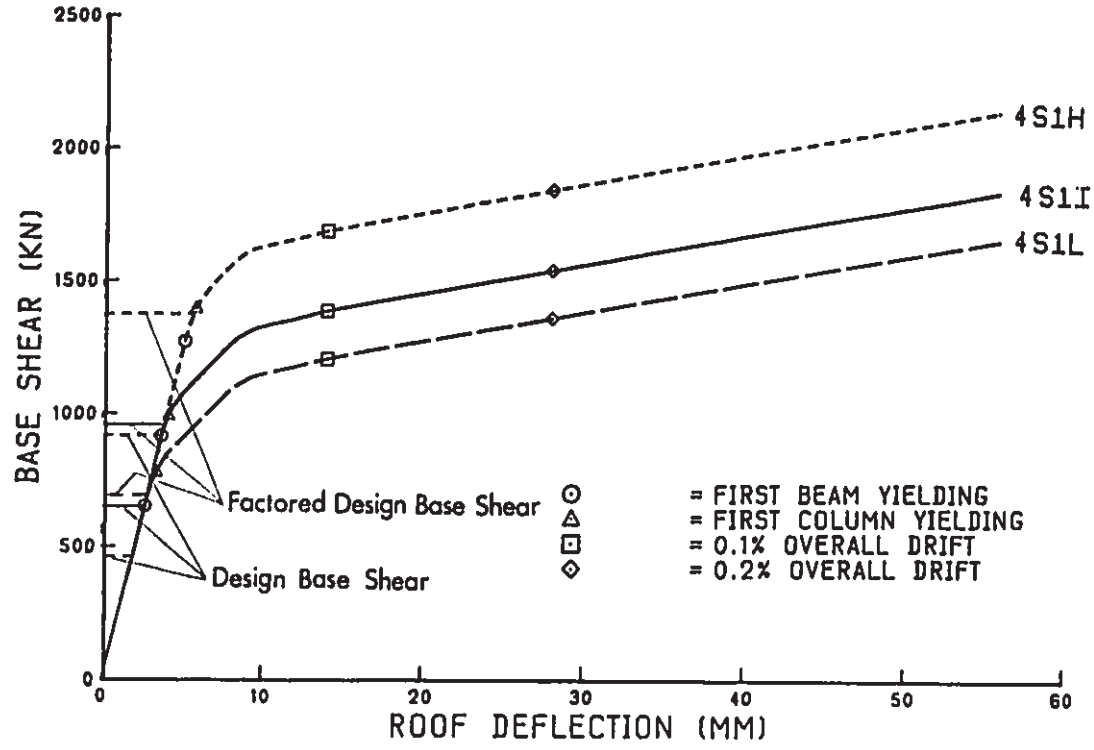

(a) 4S1 Frames

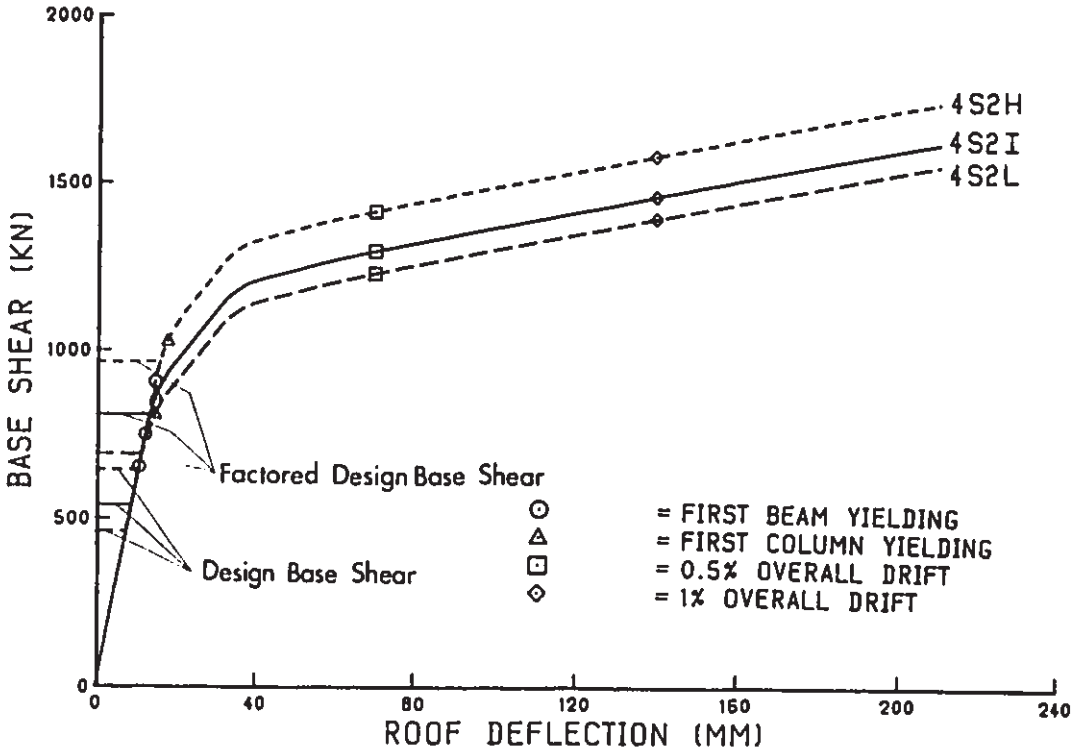

(b) 4S2 Frames

Fig. 5.4 Base Shear vs. Roof Displacement Response under Monotonically Increased Lateral Loading

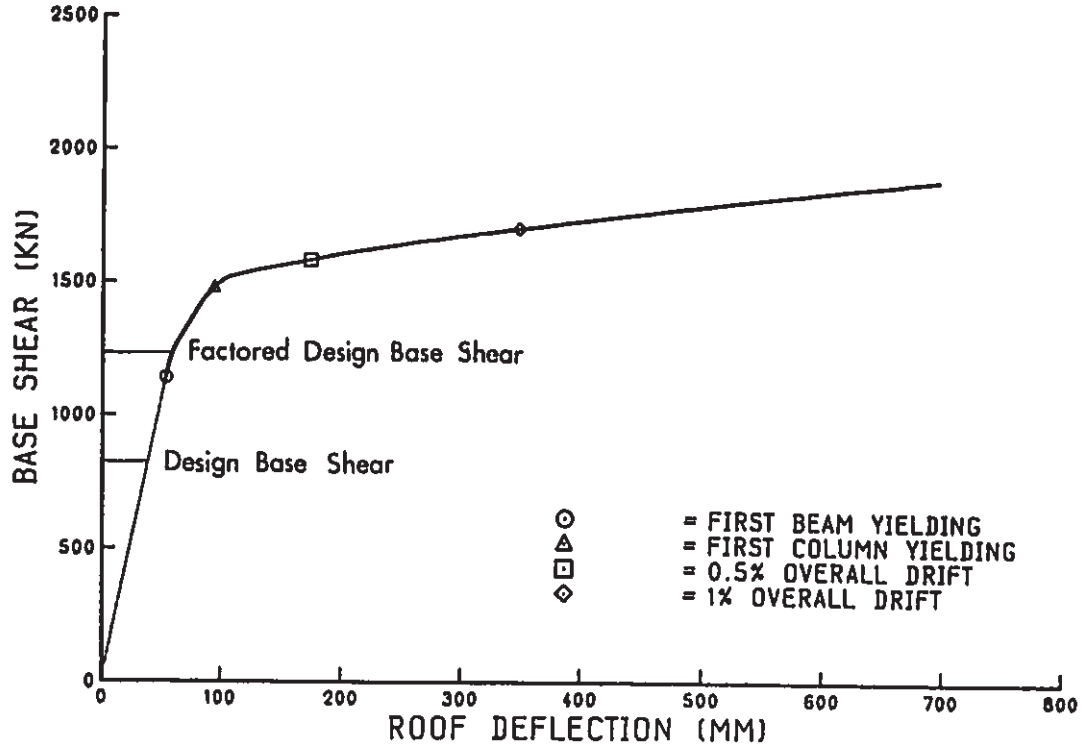

(c) 10S Frame

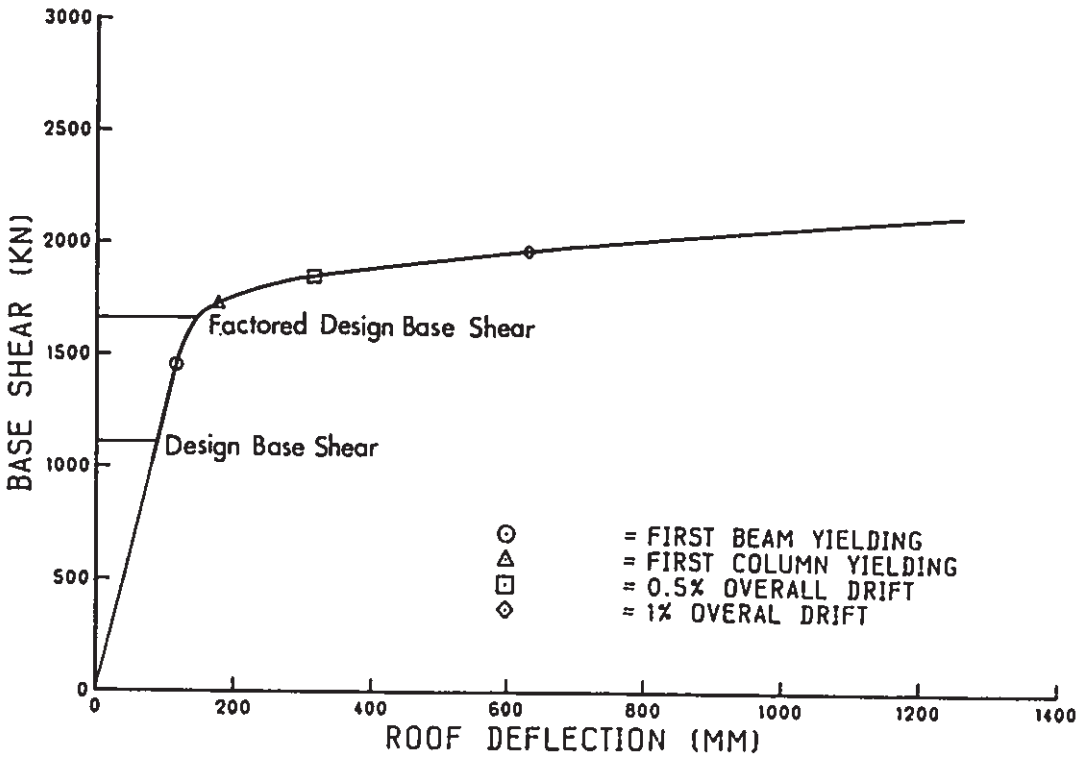

(d) 18S Frame

Fig. 5.4 (cont'd) Base Shear vs. Roof Displacement Response under Monotonically Increased Lateral Loading

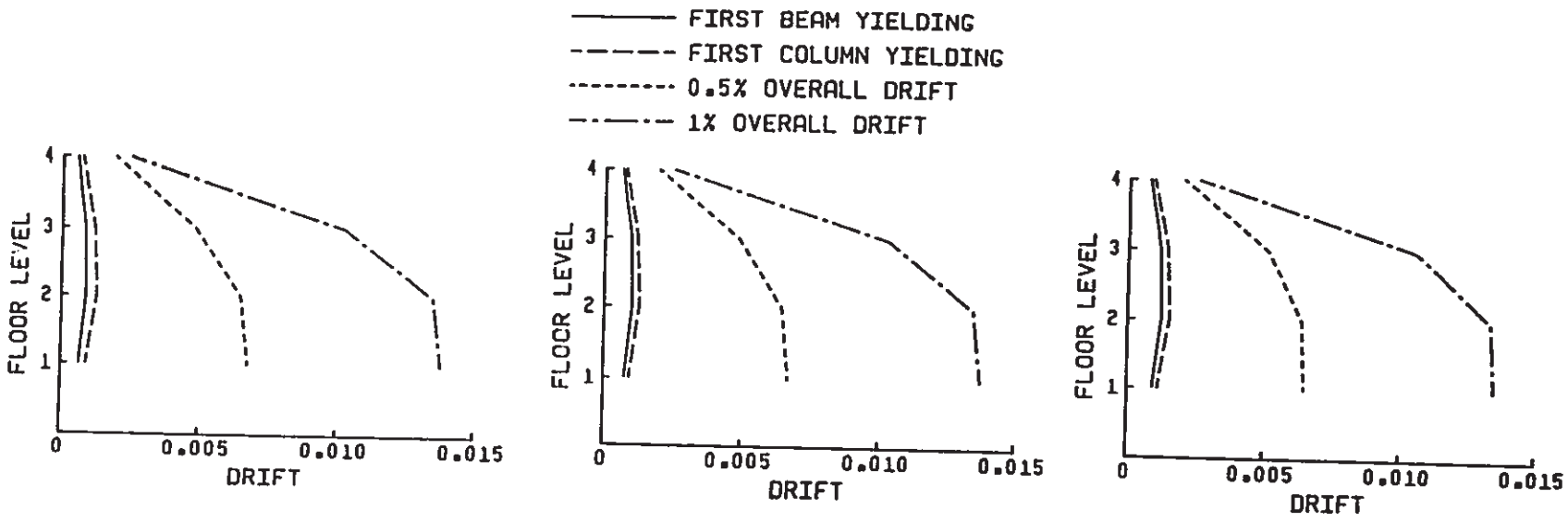

(a) 4S2 Frames

Fig. 5.5 Distribution of Interstorey Drift over Height under Lateral Loading

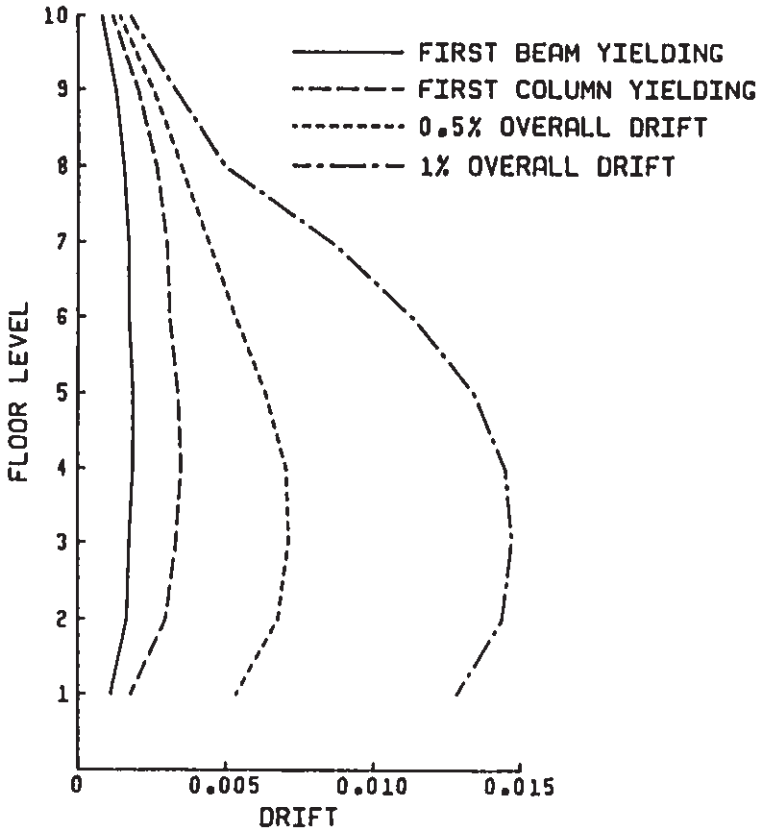

(b) 10S Frame

Fig. 5.5 (cont'd) Distribution of Interstorey Drift over Height under Lateral Loading

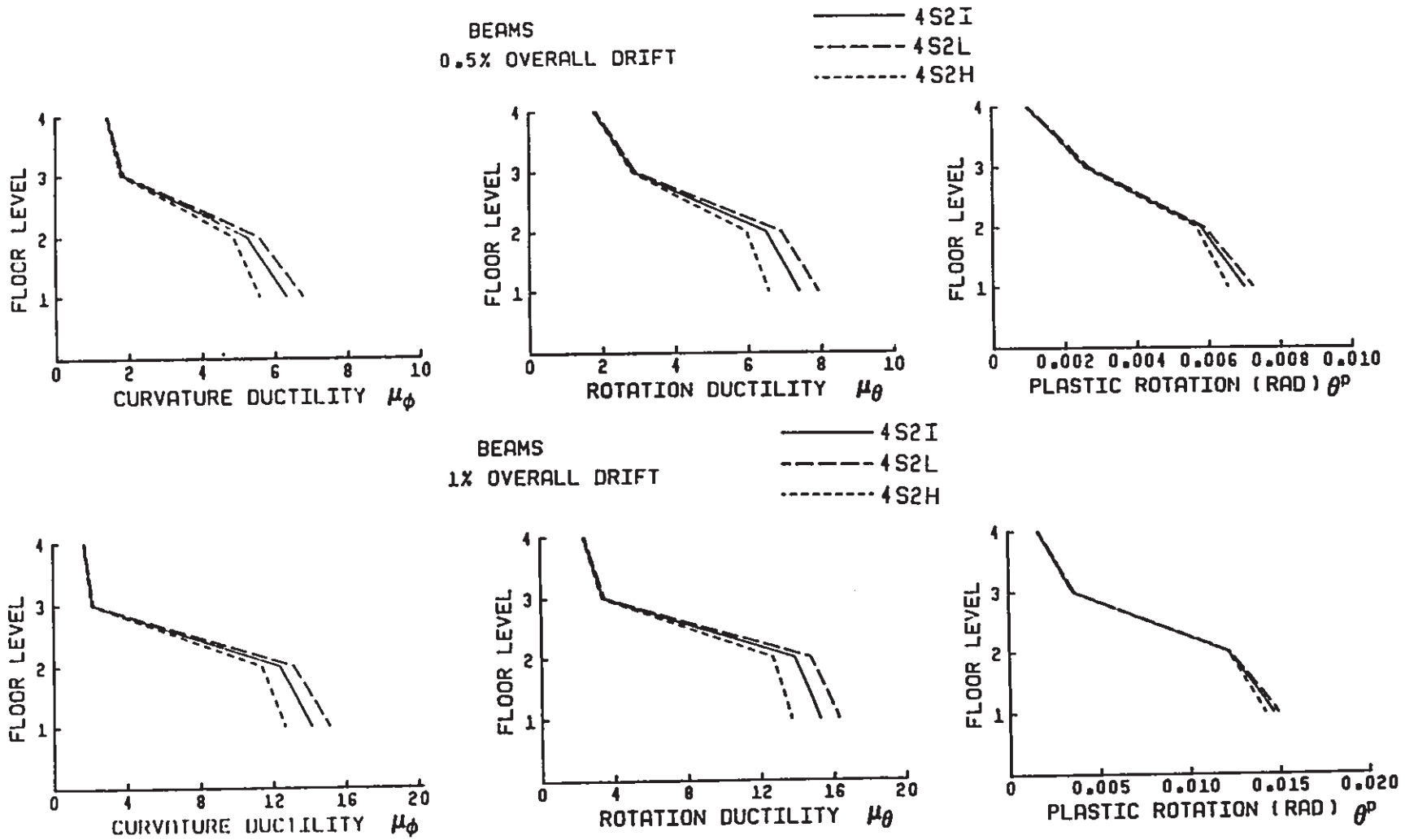

(a) 4S2 Frames

Fig. 5.6 Distribution of Beam Response Parameters over Height under Lateral Loading

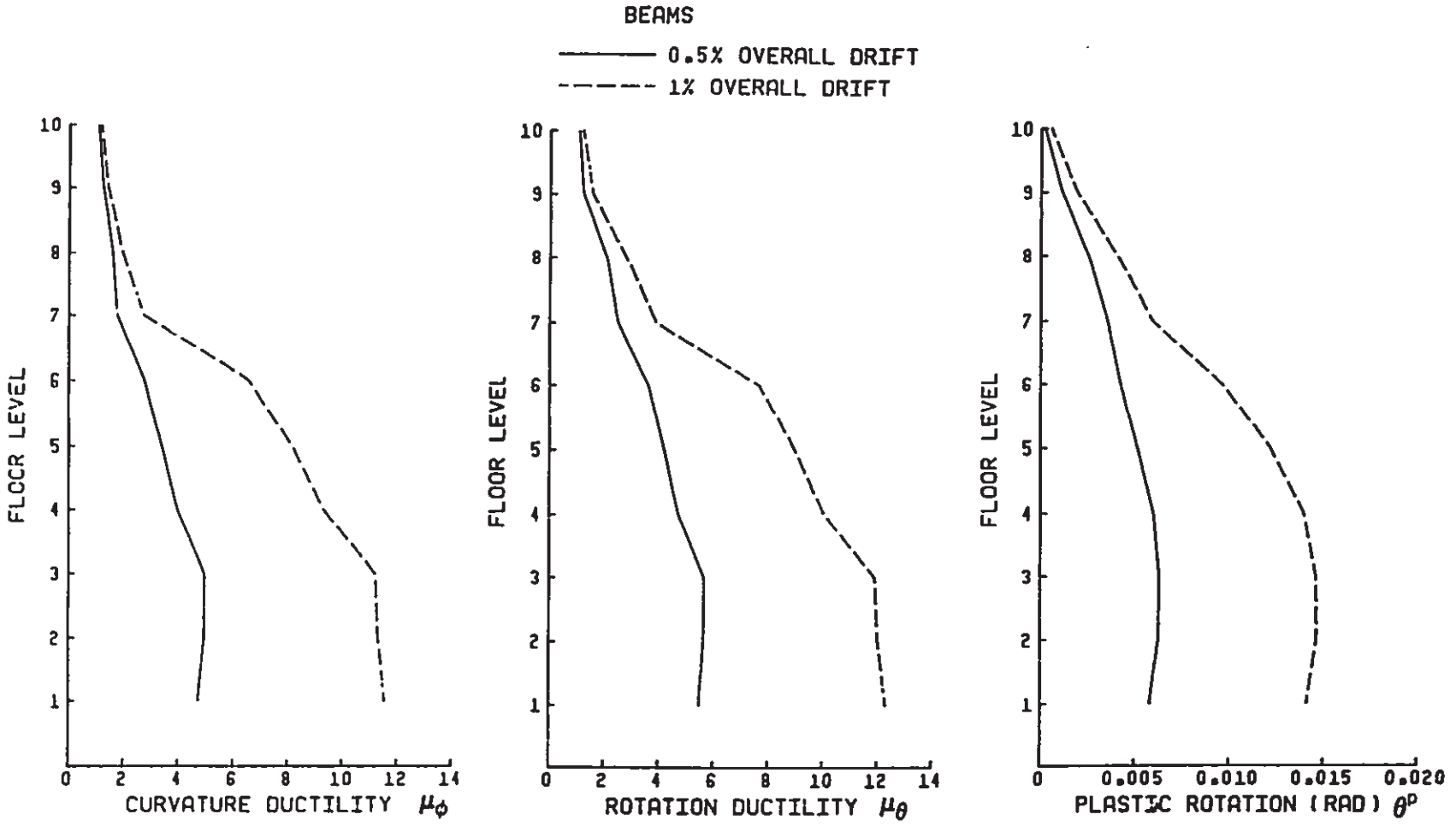

(b) 10S Frame

Fig. 5.6 (cont'd) Distribution of Beam Response Parameters over Height under Lateral Loading

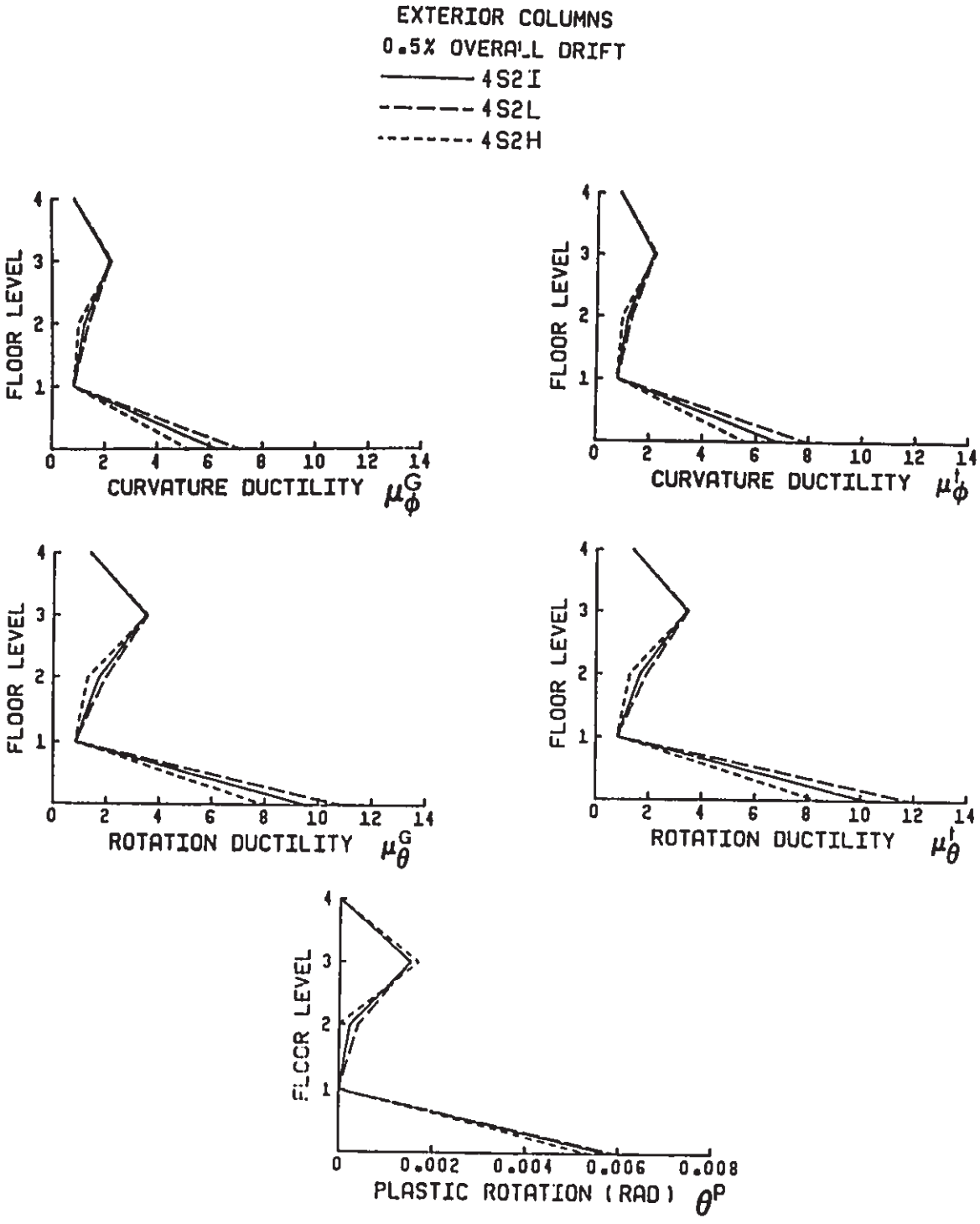

(a) 4S2 Frames

Fig. 5.7 Distribution of Column Response Parameters over Height under Lateral Loading

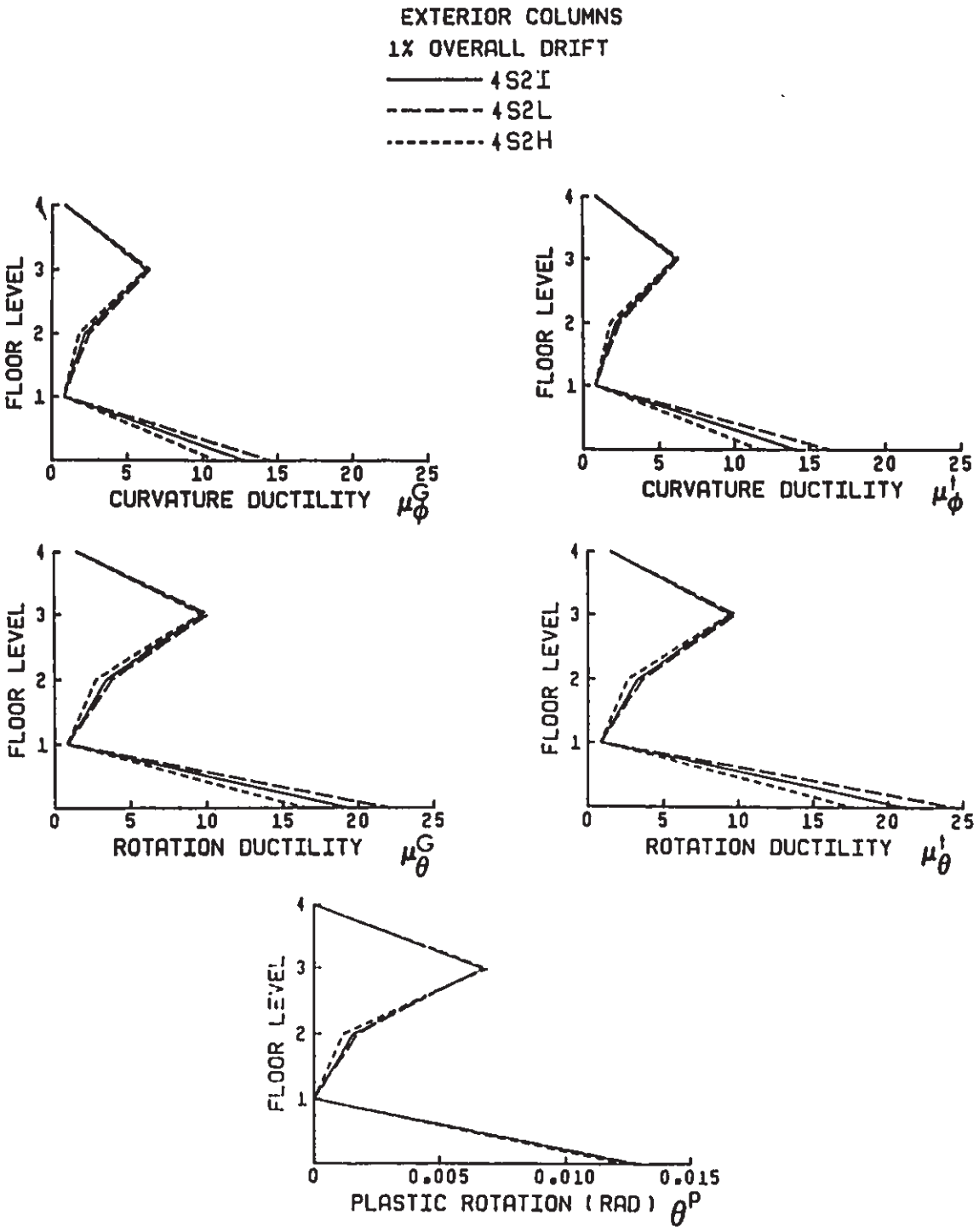

(a) 4S2 Frames

Fig. 5.7 (cont'd) Distribution of Column Response Parameters over Height under Lateral Loading

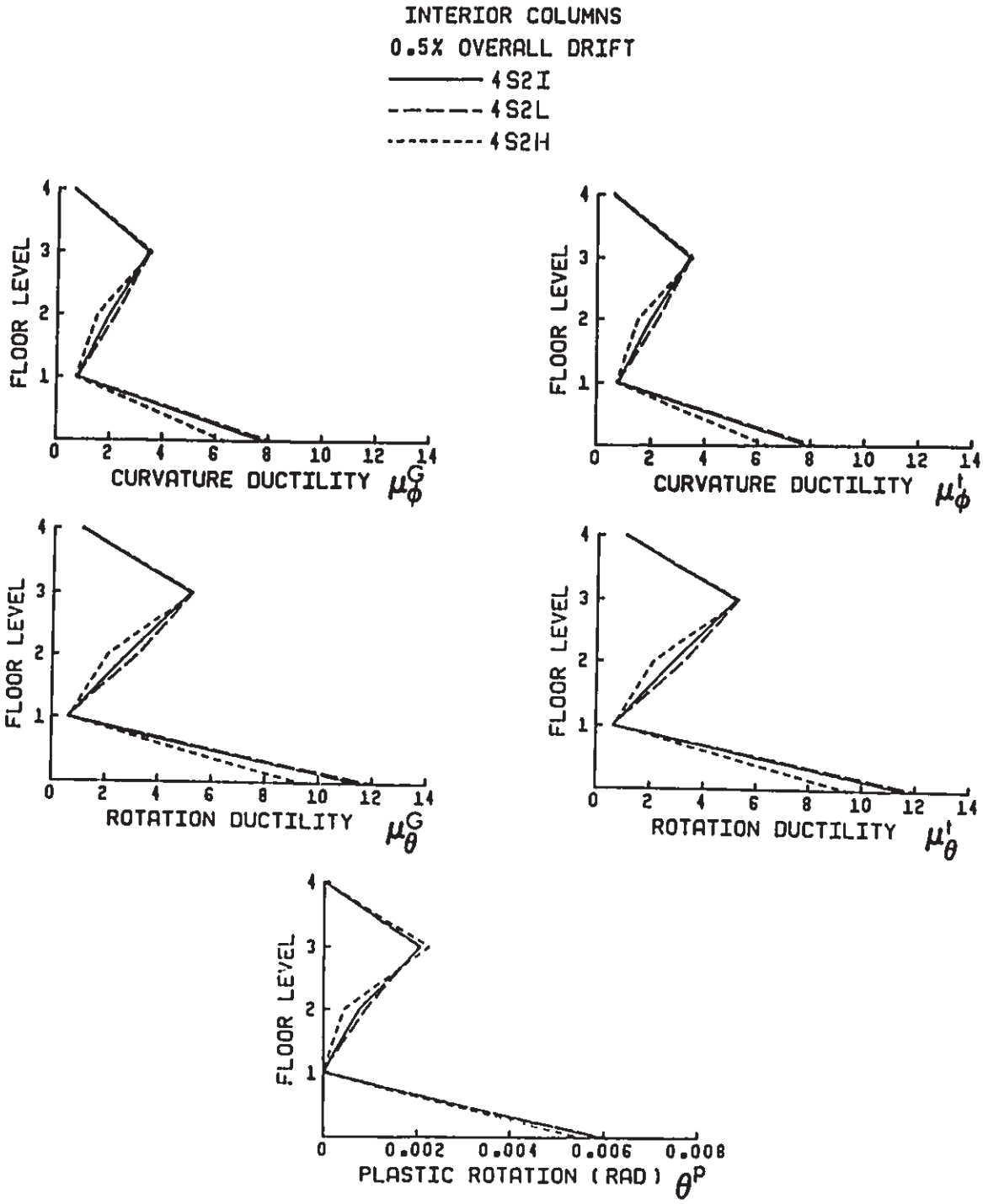

(a) 4S2 Frames

Fig. 5.7 (cont'd) Distribution of Column Response Parameters over Height under Lateral Loading

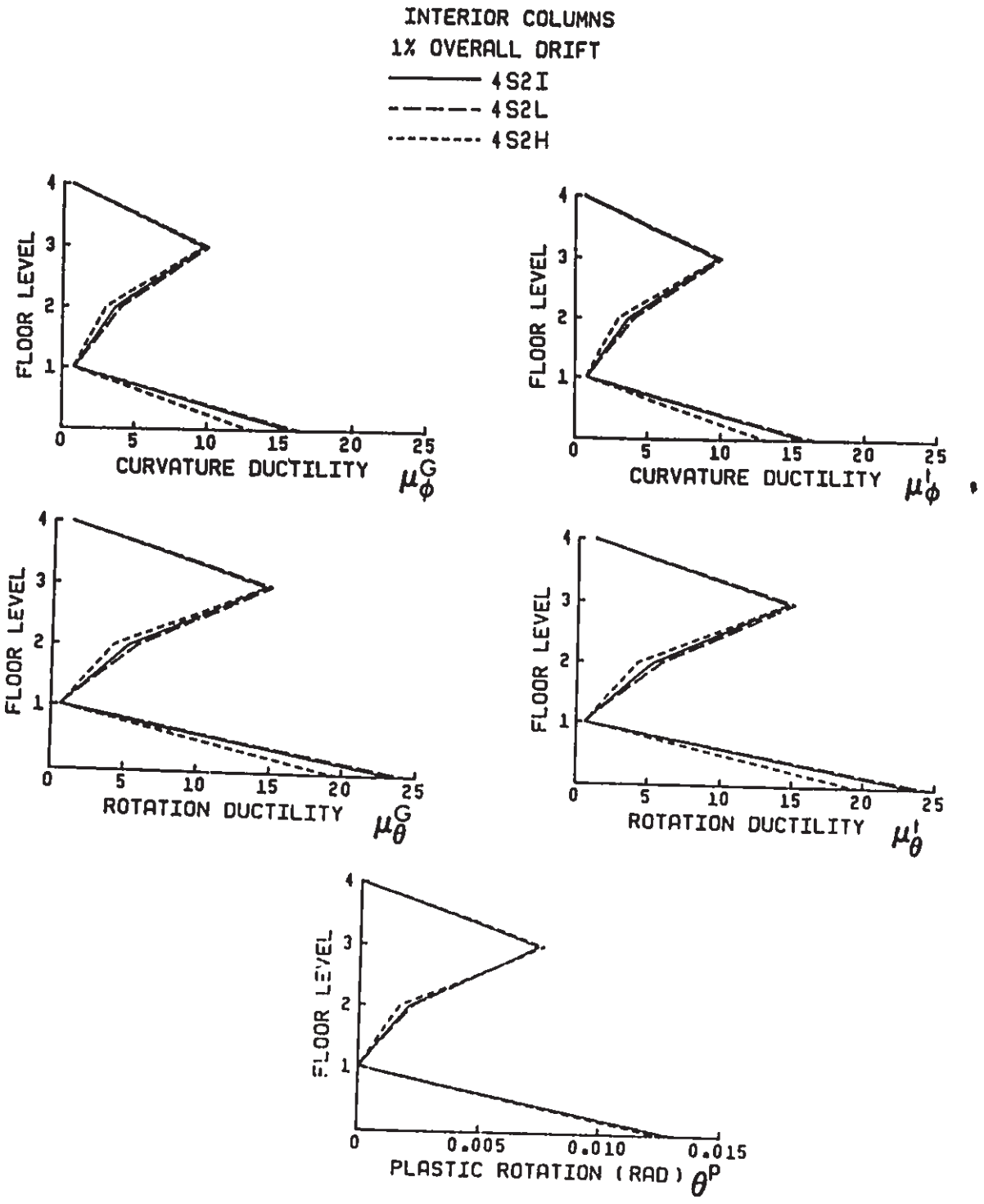

(a) 4S2 Frames

Fig. 5.7 (cont'd) Distribution of Column Response Parameters over Height under Lateral Loading

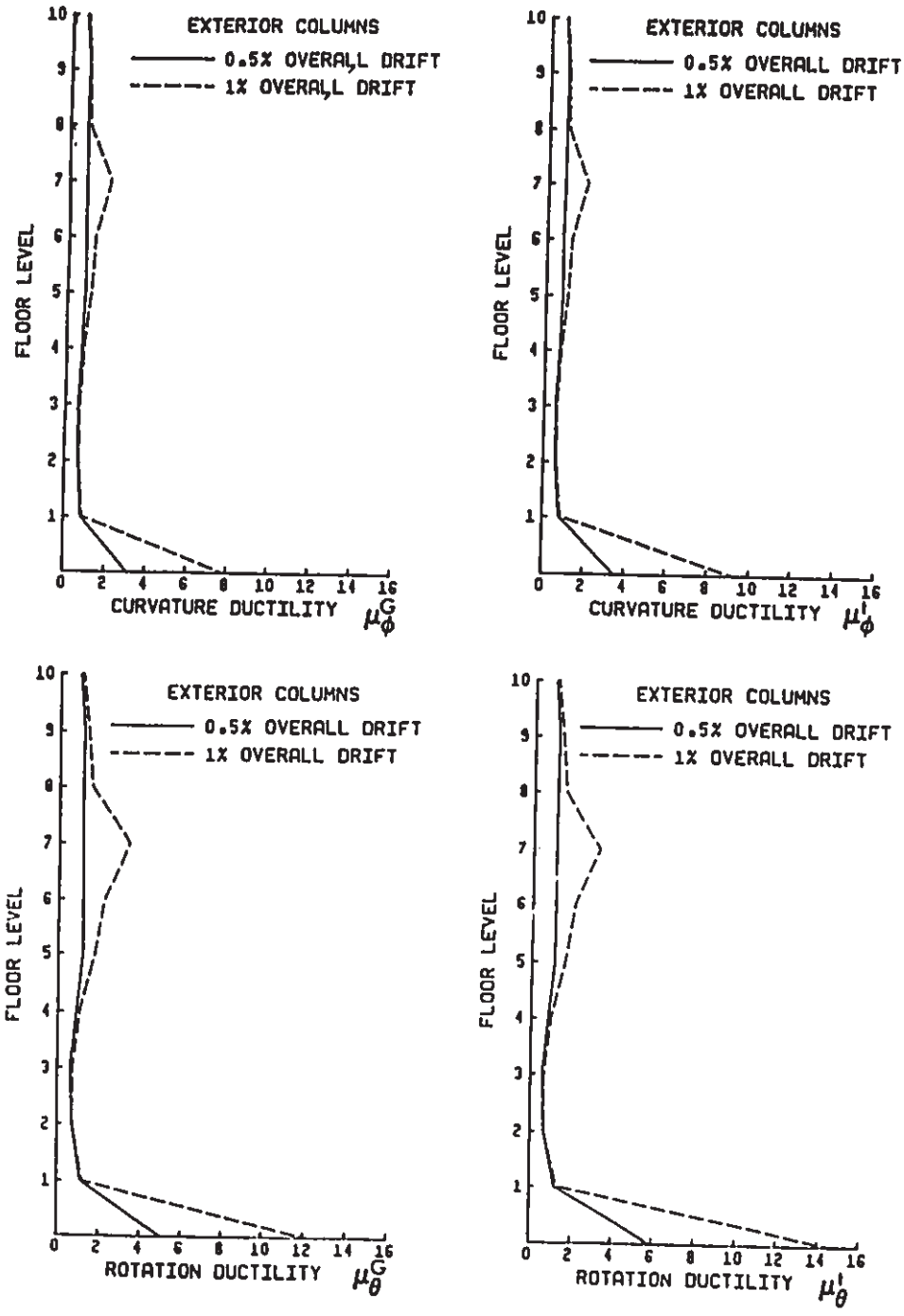

(b) 10S Frame

Fig. 5.7 (cont'd) Distribution of Column Response Parameters over Height under Lateral Loading

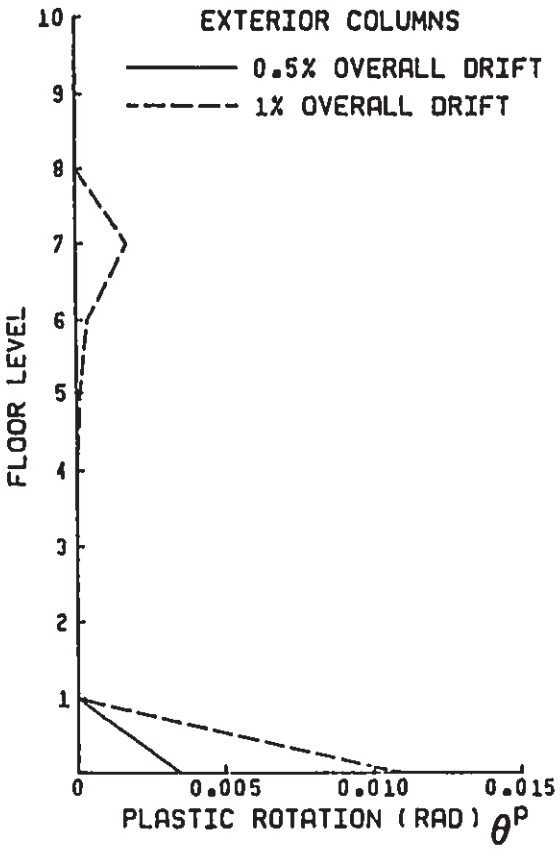

(b) 10S Frame

Fig. 5.7 (cont'd) Distribution of Column Response Parameters over Height under Lateral Loading

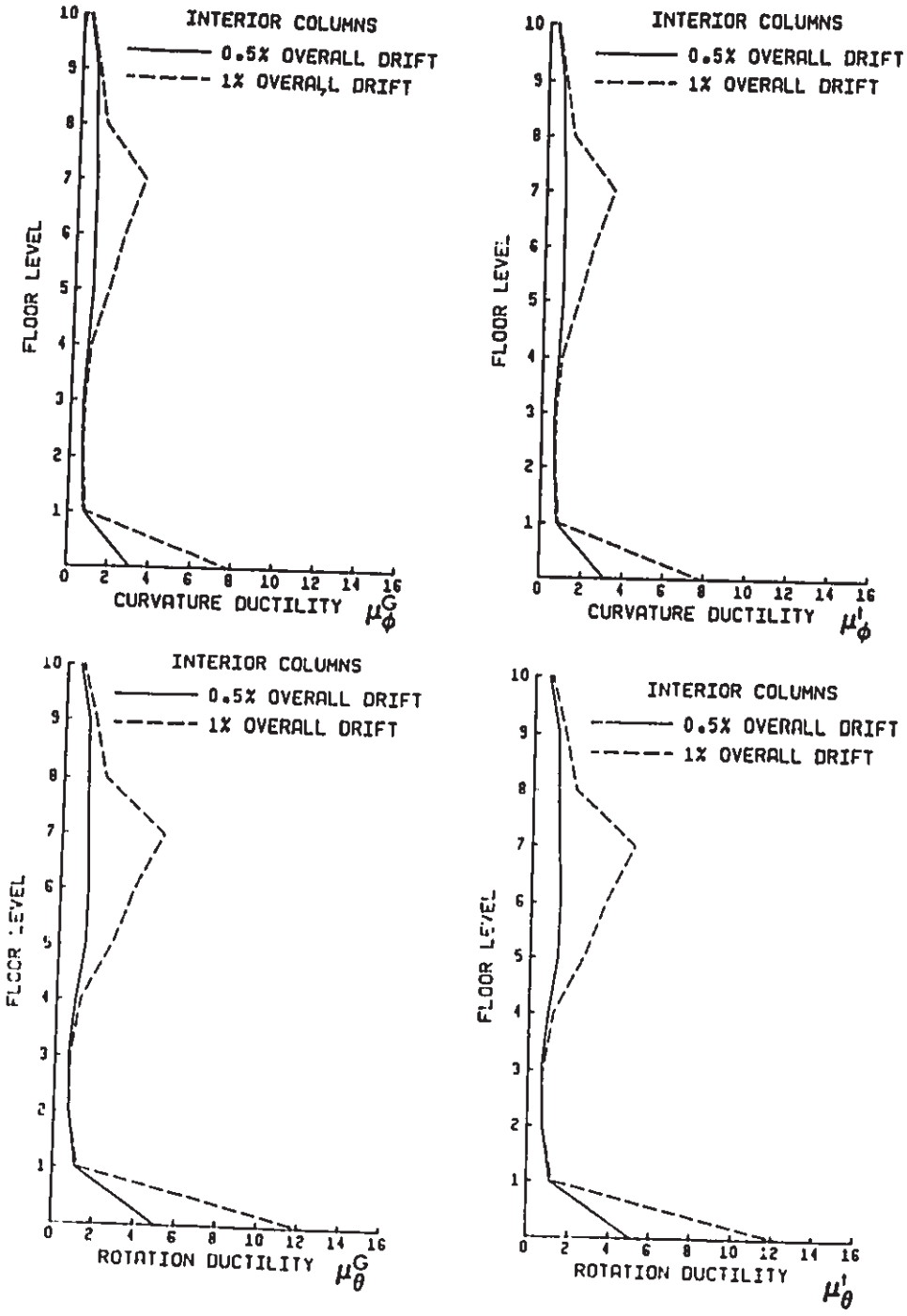

(b) IOS Frame

Fig. 5.7 (cont'd) Distribution of Column Response Parameters over Height under Lateral Loading

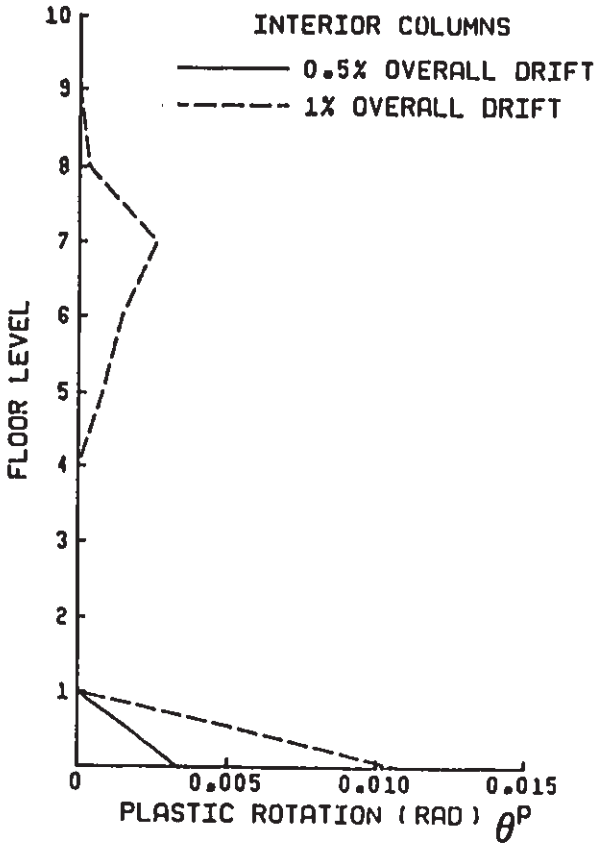

(b) 10S Frame

Fig. 5.7 (cont'd) Distribution of Column Response Parameters over Height under Lateral Loading

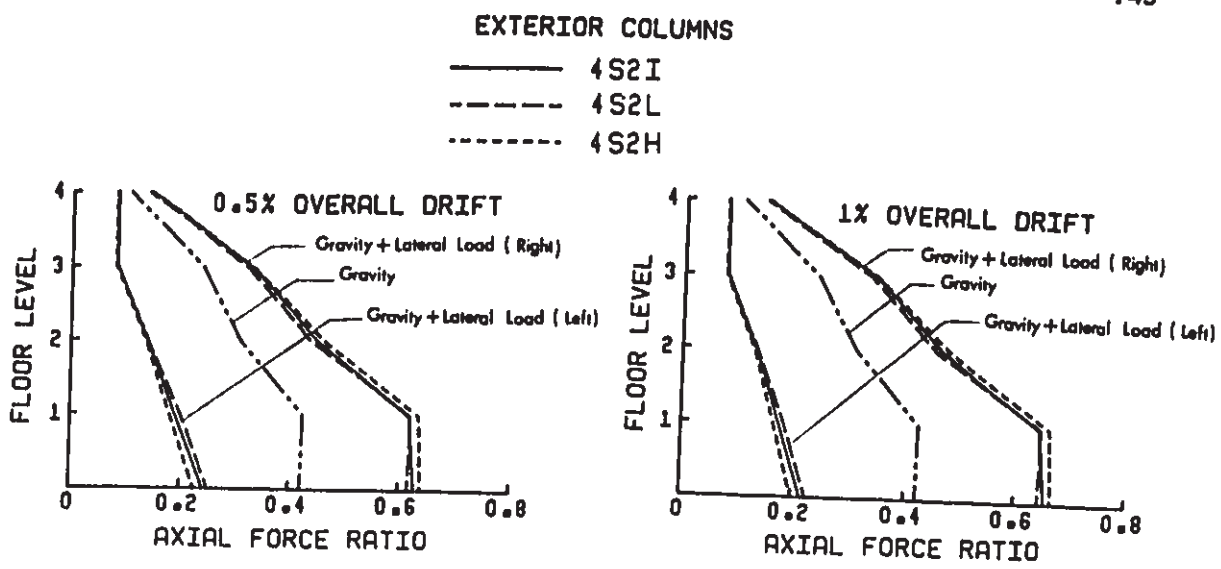

(a) 4S2 Frames

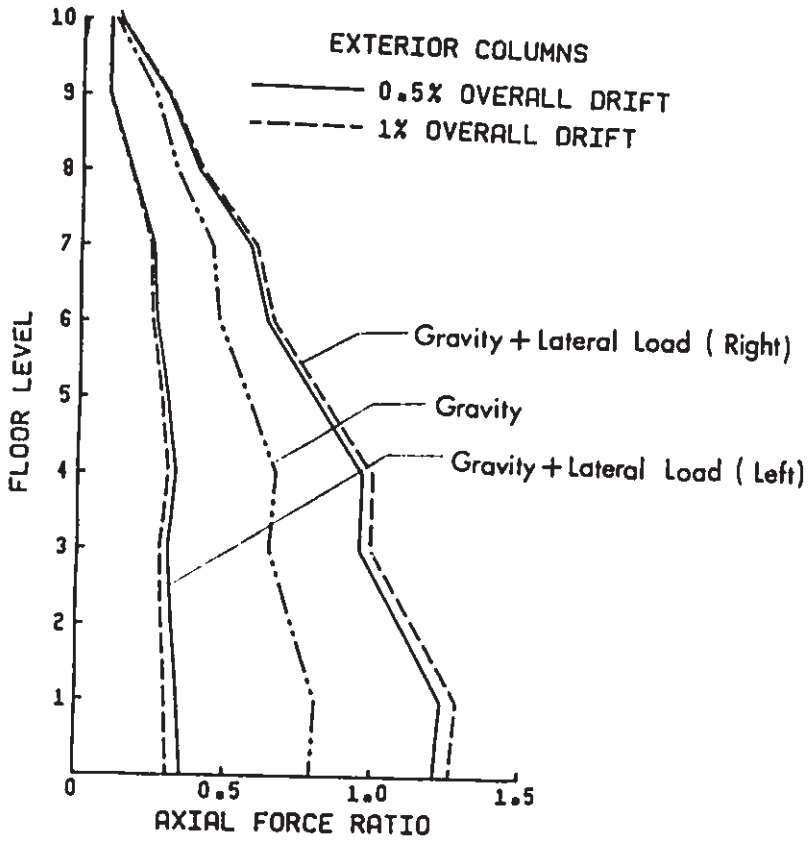

(b) 10S Frame

Fig. 5.8 Ratios of Column Axial Forces Resulting from Gravity and Lateral Loads to Balanced Axial Forces

CHAPTER 6

RESULTS OF DYNAMIC ANALYSIS

6.1 Introduction

In this chapter, the dynamic response behaviour of the designed frames subjected to the earthquake records described in Chapter 2 are studied. The dynamic responses of the frames are analyzed statistically for the three separate groups of earthquake accelerograms having low, intermediate, and high A/V ratios. The mean and mean plus one standard deviation (mean+σ) values of the various response parameters are obtained for each A/V group of 15 earthquake records. The mean+σ level is considered to be appropriate for design purposes. A comparison between the mean and mean+σ values provides an indication of the dispersion characteristics of the various response parameters within each A/V group of ground motions.

Four different parts are involved in this chapter. First, the statistical results of the various response parameters are obtained for the designed frames subjected to the three A/V groups of earthquake records scaled to the design level peak ground velocity of 0.4 m/s. The statistical results are used to investigate the effect of ground motion A/V ratio on the seismic responses of reinforced concrete frame structures and to evaluate the seismic performance of the reinforced concrete frame structures designed in compliance with NBCC 1985 and CAN3-

A23.3-M84. Secondly, the effect of peak ground velocity level on the inelastic responses of the designed frames is investigated. Thirdly, the statistical results of the inelastic responses of the frames are compared with those of their corresponding elastic responses. Finally, the distributions of overall response parameters are compared for four different analyses, namely: (a) elastic static ; (b) elastic dynamic; (c) inelastic static; and (d) inelastic dynamic analyses.

6.2 Characteristics of Dynamic Response Parameters

Before the presentation of the statistical results, the characteristics of some of the dynamic response parameters observed from the dynamic analysis are described in this section.

6.2.1 Energy Time History Response

The various energy terms have been defined in Chapter 4 for MDOF systems based on the equation of motion. In this section, the energy time history responses of the 10S frame subjected to three earthquake records are presented. These three records are taken from the three A/V groups of ground motions described in Chapter 2. The three records are (a) the 1933 Long Beach, N39E component; (b) the 1940 El Centro, S00E component; and (c) the 1985 Nahanni, longitudinal component. As shown in Tables 2.2 to 2.4, the Long Beach, El Centro, and Nahanni records have an A/V ratio of 0.37, 1.04, and 2.38 g/m/s, respectively. Shown in Fig.6.1 are the comparisons between E_I' and $E_K'+E_D'+E_H'+E_S'$ for the 10S frame subjected to the three records scaled to a peak velocity of 0.4 m/s. Ideally, E_I' should be

equal to $E'_K+E'_D+E'_H+E'_S$. However, because of the approximations involved in the numerical integration as described in Chapter 4, some differences are to be expected. It can be seen that the two curves associated with E'_I and $E'_K+E'_D+E'_H+E'_S$ are nearly identical at the beginning of the response, and they deviate towards the end of the response. In the beginning, the frame remains elastic, and the errors involved in the numerical integration are very small. As the frame is excited well into the inelastic range, the errors become relatively significant. It is also clear from Fig. 6.1 that the accuracy of the numerical integration is markedly affected by the frequency characteristics of the input ground motion. When subjected to the Long Beach record which has a low frequency content, the difference between the two curves is negligible at the end of the response. However, the difference is relatively large when subjected to the Nahanni record which has a very high frequency content. Ground motion having a high frequency content tends to excite higher vibrational modes of a frame, whereas the response of a frame tends to be dominated by its fundamental mode when subjected to ground motion with a low frequency content. Therefore, for the same time increment used in the numerical integration, the errors would be generally higher for high frequency excitation than for low frequency excitation. It has also been observed in this study that the errors in the displacement time history response are generally much lower than those in the energy time history response.

Plotted in Fig.6.2 are the time history responses of the different energy indices for the 10S frame subjected to the three earthquake records. It can be seen that the kinetic and elastic strain energy stored temporarily in the frame becomes very small at the end of the responses,

and the energy imparted to the frame is almost equal to energy dissipated by damping and inelastic deformation. In this chapter, the statistical results of the input energy (E_I^*), the damping energy (E_D^*), and the hysteretic energy (E_H^*) at the end of the inelastic responses are obtained for the frames subjected to the three A/V groups of earthquake records.

6.2.2 Relationship among Different Definitions of Member Ductility Factors

The relationships among the different definitions of member ductility factors for the inelastic dynamic analysis are very similar to those for the inelastic static analysis discussed in Chapter 5. For the beams, the rotation ductility is similar to the curvature ductility. In the case of the columns in the lower storeys, the rotation ductility is generally higher than the curvature ductility, particularly for the 10S and 18S frames. For the exterior columns in the lower storeys, the ductility factors defined on the basis of the current column axial forces under combined gravity loading and earthquake excitation tend to be higher than those defined on the basis of initial column axial forces under gravity loading. This is particularly true for the 10S and 18S frames. In this chapter, only curvature ductility factors are presented for the beams and columns. The curvature ductility factor for the columns is based on the current column axial forces under combined gravity loading and earthquake excitation.

6.2.3 Overall vs. Local Ductility Demands

A comparison between the overall displacement ductility and the localized member curvature ductility for the inelastic dynamic responses

reveals that even though the overall displacement ductility is a conservative estimate based on the first yielding point, it is generally lower than the maximum curvature ductility for the structural members. The ratio of the maximum member curvature ductility to the overall displacement ductility ranges from about 1.4 to 2.7 for all the analysis cases. This ratio is generally higher for the 18S and 10S frames than for the 4S1 and 4S2 frames. The higher localized member ductility as compared to the overall displacement ductility has been demonstrated by the experimental results of structural subassemblages (68,71).

6.3 Effect of Ground Motion A/V Ratio on Short Period Frames

In order to accommodate the effect of ground motion A/V ratio on short period structures, NBCC 1985 suggests the use of three different seismic response factors for three different zonal combinations in the short period range (up to 0.5 sec), as shown in Fig. 3.4. In this section, the effectiveness of this scheme is evaluated based on the following two different analyses performed for the 4S1 frames:

Analysis I: The 4S11 frame is subjected to each of the three groups of earthquake ground motions having low, intermediate, and high A/V ratios. The inelastic responses resulting from each of the three groups of earthquake records are analyzed statistically, and the statistical results for the three groups of ground motions are compared. This analysis is intended to examine the consequences on the inelastic responses of a frame structure with a very short fundamental period if the frame is designed based on the seismic response factor for $Z_a=Z_v$ only, irrespective of the A/V ratios of the input ground motions to which

it is subjected.

Analysis II: The 4S1L, 4S1I, and 4S1H frames are subjected to the low, intermediate, and high A/V groups of ground motions, respectively. For each of the three frames, its inelastic responses to the corresponding A/V group of ground motions are analyzed statistically. In this analysis, the NBCC 1985 base shear provisions are exactly followed.

A comparison of the statistical results of the various response parameters between these two analyses will permit an assessment of the effectiveness of the NBCC 1985 base shear provisions to account for the effect of ground motion A/V ratio on short period frame structures.

Shown in Fig. 6.3 are the mean and mean+σ values of the various response parameters for Analysis I. It can be seen that the statistical results of the response parameters are substantially different among the three A/V groups of ground motions. The statistical results for the high A/V group of ground motions are higher than those for the intermediate A/V group, whereas the statistical results for the low A/V group are lower. With the exception of the cumulative plastic rotation, the mean curve of a response parameter for one group of ground motions does not cross over with the mean+σ curve for another group. Therefore, the differences in the response parameters among the three A/V groups of ground motions are much more significant than those within each individual group. The smaller difference in the cumulative plastic rotation as compared to the other response parameters can be attributed to the fact that the cumulative plastic rotation is affected by both the peak level and the sustained duration of inelastic response, and the strong-motion durations of the high A/V ground motions are shorter than

those of the intermediate and low A/V ground motions (Table 2.5 and Fig.2.7).

The statistical results of the overall displacement ductility and the three energy indices for Analysis I are included in Table 6.1. It can be seen that the mean+σ overall ductility demand for the high A/V group of ground motions is about three times that for the low A/V group. Also, the input energy for the high A/V group is much higher than that for the low A/V group. For the high A/V group of ground motions, 70% of the input energy is dissipated by hysteretic action, whereas it is 51% for the low A/V group.

Plotted in Fig. 6.4 are the statistical results of the various response parameters for Analysis II. A comparison between Figs. 6.4 and 6.3 reveals that the use of three different seismic response factors for the three different A/V ranges results in only slight improvement in the consistency of the maximum storey displacement and interstorey drift among the three A/V groups of ground motions. However, the consistency in the curvature ductility demand for the structural members is significantly improved. This is particularly true for the curvature ductility demands at the base of the first storey columns. For the beam curvature ductility in the first storey, the mean+σ value for the high A/V group of records is about 242% higher than that for the low A/V group for Analysis I, whereas the difference reduces to 84% for Analysis II. For the curvature ductility at the base of the first storey exterior columns, the mean+σ value for the high A/V group is about 208% higher than that for the low A/V group for Analysis I, whereas the difference decreases to 25% for Analysis II.

The curvature ductility depends on both the maximum and yield curvature. The use of three different seismic design forces for the three zonal combinations results in different member strengths for the 4S1L, 4S1I, and 4S1H frames. Since the three frames have the same initial elastic member stiffnesses, the differences in their member strengths lead to differences in their member yield deformations. Even though the maximum deformations of the 4S1H frame are still higher than those for the 4S1I frame in Analysis II (Fig.6.4(a)), the higher member yield deformations for the 4S1H frame bring down the member curvature ductility demands. Likewise, the lower member yield deformations for the 4S1L frame increase the member curvature ductility demands. As a result, the consistency in the member curvature ductility demands among the three A/V groups of ground motic ; is improved. The more significant improvement in the consistency of the curvature ductility demands at the base of the first storey columns results from the fact that the design moments at the base of the first storey columns are more sensitive to a change in the magnitude of the lateral seismic design force than the beam design moments or the column design moments in the upper storeys.

The statistical results of the overall displacement ductility and the three energy indices for Analysis II are included in Table 6.1. Although the maximum roof displacements for the three A/V groups of ground motions are still very different for Analysis II (Fig.6.4(a)), the consistency in the overall displacement ductility is significantly improved, as can be seen from a comparison of the second and first rows of Table 6.1(a). This is again because the roof displacement at first yielding on which the definition of the overall displacement ductility is

based, is different for the 4S1L, 4S1I, and 4S1H frames (Fig. 5.4(a)). It is of interest to note that while the use of three different seismic response factors for the three different A/V ranges results in a 32% decrease in the mean overall ductility demand for the high A/V group and a 50% increase for the low A/V group (Table 6.1(a)), the corresponding changes in the mean input energy are only 2% and 8% (Table 6.1(b)). Therefore, a change in the strength of a short period frame has very little effect on the energy imparted to the frame. This observation is consistent with that for SDOF systems reported by Zahrah and Hall (97). However, a change in the strength results in some internal redistribution between damping and hysteretic energy. As can be seen in Tables 6.1(c) and (d), the decrease in the strength for the 4S1L frame leads to an increase in its hysteretic energy and a decrease in its damping energy. On the other hand, the increase in the strength for the 4S1H frame reduces its hysteretic energy and increases its damping energy.

6.4 Seismic Performance of Frames Designed Based on NBCC 1985 and CAN3-A23.3-M84

The purpose of this section is to evaluate the seismic performance of reinforced concrete frames having different fundamental periods designed in compliance with NBCC 1985 and CAN3-A23.3-M84 when subjected to earthquake ground motions having different A/V ratios. The evaluation focuses on the magnitude and distribution of the various response parameters for each frame as well as their consistency among frames having different fundamental periods. The statistical results for the 4S1L, 4S1I, and 4S1H frames subjected to the low, intermediate, and high A/V groups of earthquake records have already been presented in the

previous section for Analysis II (Fig.6.4; Table 6.1). The statistical results of the various response parameters for the 4S2 (4S2L, 4S2I, and 4S2H), 10S, and 18S frames are also obtained, and they are shown in Figs. 6.5 to 6.7 and included in Table 6.1.

6.4.1 Comparison of Response Parameters among Three A/V Groups of Ground Motions

It can be seen in Figs. 6.4 and 6.5 that for the 4S1 and 4S2 frames subjected to all three A/V groups of ground motions, a concentration of large inelastic deformations is produced in the beams located at the bottom two storeys. For the columns, large inelastic deformations are developed at the base of the first storey columns. These large member inelastic deformations lead to very large interstorey drifts in the bottom two storeys. This distribution of inelastic deformations for earthquake excitation is similar to that for monotonically increased lateral loading observed in Chapter 5.

In contrast with the 4S1 and 4S2 frames, the distribution of inelastic deformations for the 10S and 18S frames are strongly affected by the A/V ratio of the input ground motions. It can be seen in Figs.6.6 and 6.7 that for the low A/V group of ground motions, beam inelastic deformations tend to be concentrated in the lower storeys. For the high A/V group of ground motions, however, beam inelastic deformations in the upper storeys can be significantly higher than those in the lower storeys. While the low A/V group of ground motions results in larger inelastic deformations at the base of the first storey columns, the high A/V group of ground motions tends to produce more inelastic deformations in the upper storey columns. The distributions of the interstorey drifts

over height for the three A/V groups of ground motions are similar to those of the beam inelastic deformations. The "whiplash" effect observed for the high A/V group of ground motions can be ascribed to more significant effect of higher mode participation for the high A/V group of earthquake ground motions. The spectral analysis of the three A/V groups of earthquake accelerograms performed in Chapter 2 has indicated that the frequency content of the high A/V ground motions is much higher than that of the low A/V ground motions. As a result, the high A/V group of earthquake records tends to excite the higher vibrational modes of the 10S and 18S frames.

To gain some insight into the effect of ground motion frequency characteristics on the inelastic response, the sequences of plastic hinge formation for the 10S frame subjected to three earthquake records from the three A/V groups of ground motions are shown in Fig.6.8. These three records are (a) the 1985 Mexico, Mesa Vibradora, N90W component; (b) the 1952 Kern County, Taft, S69E component; and (c) the 1935 Helena, Carroll College, N00E component. As shown in Tables 2.2 to 2.4, the Mesa Vibradora, Taft, and Carroll College records have an A/V ratio of 0.36, 1.01, and 2.03 g/m/s, respectively. It can be seen in Fig. 6.8 that when subjected to the Mesa Vibradora record which has a very low frequency content, plastic hinges develop in the lower storey beams first and then migrate from the bottom to the top of the frame. Column plastic hinges are located only at the base of the first storey columns. When subjected to the Carroll College record which has a very high frequency content, beam plastic hinges develop in the upper storey first, and column hinges are developed only in the upper storeys. The Taft record has a broad

range of significant frequency content, and consequently, it produces column plastic hinges both at the base of the first storey columns and in the upper storeys. It should be noted that the sequences of plastic hinge formation shown in Fig.6.8 are for the total durations of the inelastic responses, and therefore, these plastic hinges do not occur simultaneously.

It can be seen in Figs.6.6 and 6.7 that while the beam inelastic deformations for the low A/V group of ground motions are slightly lower than those for the high A/V group in the upper storeys of the 10S and 18S frames, they are considerably higher in the lower storeys. In the lower storeys, the difference in the cumulative plastic rotation between the low and high A/V groups of ground motions is generally more significant than that of the maximum plastic rotation because the strong-motion durations of the low A/V ground motions are longer than those of the high A/V ground motions. The low A/V ground motions also produce higher inelastic deformations at the base of the first storey columns than the high A/V ground motions. The lower storeys of a high rise frame are more critical than the upper storeys due to the high axial forces carried by the lower storey columns. Therefore, low A/V ground motions are more damaging to high rise frames than high A/V ground motions even when the frames are designed based on peak ground velocity.

6.4.2 Comparison of Response Parameters among Different Frames

A comparison of the curvature ductility demands for the structural members among the frames indicates that the member curvature ductility demands for short period frames tend to be higher than those for long

period frames. This is particularly true for the column curvature ductility demand. For the intermediate A/V group of ground motions, the maximum mean+σ curvature ductility demand for the beams is about 11, 6.5, 5, and 5 for the 4S11, 4S21, 10S, and 18S frames, respectively; the mean+σ curvature ductility demand at the base of the first storey columns is about 12, 8, 3.5, and 2 for the 4S11, 4S21, 10S, and 18S frames, respectively. Because the roof deflection of a frame is highly sensitive to column yielding, the significant difference in the column curvature ductility among the frames leads to different overall displacement ductility demands for the frames. For the intermediate A/V group of earthquake records, the mean+σ overall displacement ductility demand is 7.48, 5.12, 3.22, and 2.41 for the 4S11, 4S21, 10S, and 18S frames, respectively.

The nonuniform ductility demands for frames having different fundamental periods may be attributed to the following two reasons. As noted in Chapter 3, the structural behaviour coefficient, K, in the NBCC 1985 base shear formula is independent of structural period. The use of a constant K factor in the specification of total lateral seismic design forces would lead to uneven ductility demands over period with very high ductility demands for short period structural systems. This can be best demonstrated by the inelastic responses of SDOF systems. Plotted in Fig. 6.9 are the mean and mean+σ values of the maximum displacement ductility demand for bilinear hysteretic SDOF systems with periods ranging from 0.1 to 3.0 sec when subjected to the three A/V groups of earthquake ground motions scaled to a common peak velocity of 0.4 m/s. The yield strengths of the SDOF systems are specified from the NBCC 1985 base shear formula

multiplied by a load factor of 1.5. The values for the v, K, I, and F factors in the base shear formula are taken to be the same as those used in the design of the frames. Note that the ductility demand of a SDOF system only depends on the seismic resistance coefficient which is defined as the ratio of the yield strength of the system to its weight. It can be seen clearly in Fig. 6.9 that the use of a constant K factor results in very high displacement ductility demands in the short period range. The displacement ductility demand drops very rapidly with an increase in period. Another factor which causes lower column ductility demands for the 18S and 10S frames as compared to the 4S1 and 4S2 frames is the column design moment amplification due to slenderness effect. As shown in Table 3.7, the amplification factors for column design moments due to slenderness effect for the 18S and 10S frames are higher than those for the 4S1 and 4S2 frames, particularly in the lower storeys.

A comparison of the cumulative and maximum plastic rotations at the base of the first storey columns for the 4S1 and 4S2 frames indicates that the column sections at the foundation undergo about four to five major inelastic excursions. A similar comparison for the 10S and 18S frames indicates that the column sections at the foundation experience only one major yield excursion. Therefore, the column sections at the foundation for the 4S1 and 4S2 frames sustain not only higher curvature ductility but also larger number of inelastic deformation excursions.

6.4.3 Magnitude of Response Parameters

It is instructive to compare the ductility demands of the frames with those of the correponding SDOF systems. Presented in Table 6.2 are

the statistical results of the maximum displacement ductility for the SDOF systems whose periods are the same as the fundamental periods of the frames and whose yield strengths are specified from the NBCC 1985 base shear formula multiplied by a load factor of 1.5, when subjected to the three A/V groups of ground motions scaled to a common peak velocity of 0.4 m/s. It can be seen from a comparison of Table 6.2 with Tables 6.1(a) that the ductility demands of the SDOF systems are significantly higher than the global ductility demands of the frames for all three A/V groups of earthquake records. This difference becomes particularly pronounced for the 4S1 and 4S2 frames. For the intermediate A/V group of ground motions, the mean+σ ductility demand for the SDOF systems is about 102%, 82%, 64%, and 43% higher than the mean+σ overall ductility demand of the 4S11, 4S21, 10S, and 18S frames, respectively. Furthermore, it can be noted from a comparison of Table 6.2 with Figs.6.4 to 6.6 that for the 4S1, 4S2, and 10S frames, even the maximum curvature ductility demands of the structural members are below or around the maximum displacement ductility demands of the corresponding SDOF systems. For the SDOF systems, their yield strengths are exactly equal to the factored seismic design forces obtained from the NBCC 1985 base shear formula. However, as noted in Chapter 5, the actual overall strengths of the frames are higher than their factored design base shears. Therefore, the overstrength of the frames as compared to their factored seismic design forces leads to lower overall displacement ductility demands for the frames than the corresponding SDOF systems. The 4S1 and 4S2 frames have more significant overstrength than the 10S and 18S frames. Consequently, the overall displacement ductility demands of the 4S1 and 4S2 frames are considerably

lower than the displacement ductility demands of their corresponding SDOF systems in comparison with the 18S and 10S frames.

Previous studies (33,72,86) have suggested that the structural behaviour coefficient K in NBCC 1985 be related to a force reduction factor R. Because the force reduction factor R is directly applied to the elastic base shear design spectrum, its value can be explicitly related to the expected overall inelastic behaviour of different structural systems. In fact, the value of R assigned to a structural system can be interpreted as the "system ductility" that is expected to be developed during the seismic response of the structural system to the design level earthquake excitation. For a SDOF system, the value of R can be directly related to the maximum displacement ductility of the system. For a multistorey building, the "system ductility" cannot be easily defined. However, the R factor may be related to the global displacement ductility as defined in Chapter 4. A study by Rainer (72) indicates that the product of the K and R factors is approximately 4.53. Therefore, structural systems designed with K=0.7 would be expected to develop a system ductility of 6.5. It can be seen in Tables 6.1(a) that although the overall displacement ductility is a conservative estimate based on the first yielding point, the mean+σ overall displacement ductility demands for the 4S2, 10S, and 18S frames are well below the expected value of 6.5 for all three A/V groups of ground motions. For the 10S and 18S frames, even the mean+σ curvature ductility demands of the structural members are lower than 6.5. In the case of the 4S1 frames, the mean+σ overall displacement ductility for the low A/V group of ground motions is slightly lower than 6.5, whereas the overall ductility demands for the

intermediate and high A/V groups of ground motions exceed the expected value of 6.5 by 15% and 23%, respectively.

Comparison of the computed beam inelastic deformation demands with the observed beam inelastic deformation capacities from previous experimental studies (16,47,51,67) indicates that the beams in the designed frames should be capable of safely resisting the design level earthquake excitations if sufficient transverse reinforcement is provided to prevent premature shear failure.

For all the frames subjected to the three A/V groups of ground motions, large inelastic deformations are generally developed at the base of the first storey columns. For the 4S1 and 4S2 frames, the curvature ductility demands at the base of the first story columns are similar to or slightly higher than the maximum beam curvature ductility demands. In the case of the 10S and 18S frames, the curvature ductility demands at the base of the first storey columns are lower than the maximum beam curvature ductility demands. The large inelastic deformations at the base of the first storey columns are attributable to the large axial forces and overturning moments at the frame base and to the assumption that the frames are perfectly fixed at their base. In reality, foundation rocking may occur during seismic response, thereby alleviating some of the inelastic deformation demand. As noted previously, the column sections at the foundation for the 4S1 and 4S2 frames experience higher curvature ductility demands and larger number of yield excursions as compared to the 10S and 18S frames. However, for the 4S1 and 4S2 frames, the maximum axial forces in the first storey columns are well below their balanced axial forces, as shown in Figs. 6.10(a) and (b). The lower axial forces

in the columns enable them to develop large curvature ductility before the buckling of the compressive reinforcing steel. For the 10S and 18S frames, however, the maximum axial forces in the first storey columns during the dynamic response exceed their balanced axial forces, as shown in Figs. 6.10(c) and (d). Because of the excessive compressive axial forces in these columns, their ability to develop ductility is limited, and a large amount of confining reinforcement is required to prevent the compressive steel bars from buckling. Therefore, for these columns, a lower curvature ductility demand is desirable.

An examination of the curvature ductility demands for the columns reveals that the use of a column overstrength factor of 1.2 in the design of the columns does not prevent column yielding in the upper or middle storeys. Column yielding in the upper or middle storeys during dynamic response to the earthquake excitations can be attributed to the following factors. First, the distribution of the beam moments at a joint between the column sections immediately above or below the joint during dynamic response can be considerably different from that assumed in the design. In the design, the beam moment strengths at a beam-column joint are distributed to the columns below and above the joint based on the relative elastic stiffnesses of the columns as described in Chapter 3. However, the formation of beam and column plastic hinges and the higher mode effect can alter the moment distribution at the joint to such an extent that the sum of the beam moments is resisted only by one of the columns framing into the joint. Second, strain-hardening effect has been considered for the beams. The strain-hardening effect increases the beam moments over their yield strengths. Previous studies by Paulay et al

(69,70) have indicated that in order to prevent upper or middle storey columns from yielding, the summation of column moment strengths should be 1.8 to 2.5 times that of beam moment strengths at a joint. However, the computed column inelastic deformation demands in the upper storeys are generally small, and in most cases, these upper storey columns experience only one yield excursion. These inelastic deformation demands are within the observed deformation capacities of ductile reinforced concrete columns (9,96).

6.4.4 Dynamic vs. Static Overstrength

The mean values of the maximum storey shears associated with the inelastic responses of the frames to the three A/V groups of ground motions are compared with the factored design storey shears of the frames in Fig.6.11. Table 6.3 presents the percentages by which the mean values of the maximum inelastic dynamic base shears are higher than their corresponding factored design base shears. The corresponding mean overall drifts are also shown in the table. It can be seen in Fig.6.11 that the inelastic dynamic storey shears are higher than the factored design storey shears. The overstrength of the frames has been observed for the case of monotonically increased lateral loading in Chapter 5, and some of the factors causing this overstrength have been discussed there. However, as indicated in Table 6.3, the dynamic overstrength is generally higher than the static overstrength for the comparable level of overall drift. This is particularly true for the 10S and 18S frames. In the static analysis, the lateral loading for a frame is increased monotonically, and plastic hinges spread over the frame with increasing the lateral loading.

During the dynamic response, however, the reversal of excitation may cause some of the plastic hinges developed earlier to close. Therefore, at a particular time instant, the plastic hinge pattern would not be the same as in the case of static loading. This is particularly true for taller frames. As a result, the dynamic overstrength is usually higher than the static overstrength.

6.5 Effect of Peak Ground Velocity Level on Inelastic Response

In the previous analysis, all the input ground motions have been scaled to a common peak velocity of 0.4 m/s. This peak ground velocity level has been used for the specification of lateral seismic design forces, corresponding to an exceedance probability of 10% in 50 years. However, because of the random nature of earthquake ground excitations, the peak velocity level of earthquake ground motions that will strike a building in the future may exceed the level assumed in the design of the building. Therefore, it is desirable to examine the consequences on the inelastic responses of building frames if the intensity of the input ground motions for the frames is increased over that assumed for their seismic design.

In this section, the peak ground velocity level used for scaling the earthquake records is increased by 50%, and the inelastic responses of the 4S2, 10S, and 18S frames to the three A/V groups of ground motions scaled to a common peak velocity of 0.6 m/s are computed. A comparison of the statistical results of the various response parameters between the two peak ground velocity levels of 0.6 and 0.4 m/s will permit an assessment of the sensitivity of the inelastic responses of the frames to

an increase in the intensity of earthquake excitations.

6.5.1 Deformation Response Parameters

The mean+σ values of the various response parameters for the two levels of peak ground velocity are compared in Figs. 6.12 to 6.14 for the 4S2, 10S, and 18S frames, respectively. It can be seen that when the intensity of the input ground motions is increased by 50%, the beam inelastic deformations in the lower storeys are increased by about 100%, whereas those in the upper storeys remain relatively unchanged. For the columns, an about 100% increase in the curvature ductility demand occurs at the base of the first storey columns. This significant increase in the member inelastic deformations in the lower storeys leads to an about 100% increase in the interstorey drifts in the lower storeys. Therefore, as the intensity of the input ground motions increases, inelastic deformations tend to be concentrated at the bottom of the frames for all three A/V groups of ground motions. This observation for earthquake excitation is consistent with that for monotonically increased lateral loading. In Chapter 5, it has been shown that inelastic deformations tend to be concentrated in the lower storeys as the magnitude of the distributed lateral loading is increased.

Presented in Table 6.4(a) are the statistical results of the overall displacement ductility demands for the 4S2, 10S, and 18S frames subjected to the three A/V groups of ground motions scaled to a common peak velocity of 0.6 m/s. To facilitate comparison with the statistical results for the design level peak ground velocity of 0.4 m/s, the ratios of the mean overall displacement ductilities between V = 0.6 and 0.4 m/s

are shown in Table 6.5(a). It can be seen that the increase in the overall displacement ductility resulting from an increase in the intensity of the input ground motions is generally lower than that in the maximum member curvature ductility. Again, it is instructive to compare the increases in the ductility demands of the frames with those of the corresponding SDOF systems. Shown in Table 6.6 are the statistical results of the maximum displacement ductility demand of the bilinear SDOF systems subjected to the three A/V groups of ground motions scaled to a common peak velocity of 0.6 m/s. To facilitate comparison, the ratios of the mean displacement ductilities for the SDOF systems between V = 0.6 and 0.4 m/s are shown in Table 6.7. A comparison between Tables 6.7 and 6.5(a) reveals that the increase in the overall displacement ductility demand of the frames is similar to that in the displacement ductility demand of the corresponding SDOF systems.

Comparison of Table 6.4(a) with Table 6.6 indicates again that the overstrength of the frames as compared to their factored seismic design forces leads to much lower overall ductility demands than the ductility demands of the corresponding SDOF systems for the increased peak ground velocity level of 0.6 m/s. For the intermediate A/V group of ground motions, the mean+σ ductility demands for the SDOF systems are 73%, 85%, and 40% higher than the mean+σ overall ductility demands for the 4S2I, 10S, and 18S frames, respectively. These differences in the ductility demands between the frames and the corresponding SDOF systems are similar to those for the design level peak ground velocity of 0.4 m/s. Under the increased peak ground velocity of 0.6 m/s, the mean+σ overall ductility demands of the 4S2 frames have exceeded the expected "system ductility"

of 6.5, whereas the mean+σ overall ductility demands of the 10S and 18S frames are still below 6.5. However, the mean+σ member curvature ductility demands for the 10S and 18S frames have exceeded 6.5 for the low and intermediate A/V groups of ground motions.

6.5.2 Energy Indices

The statistical results of the three energy indices are shown in Tables 6.4(b), (c), and (d) for the 4S2, 10S, and 18S frames subjected to the three A/V groups of ground motions scaled to a common peak velocity of 0.6 m/s. To facilitate comparison with the results associated with the design level peak ground velocity of 0.4 m/s, the ratios of the mean values of the three energy indices between V=0.6 and 0.4 m/s are presented in Tables 6.5(b), (c), and (d). A comparison between Tables 6.5(a) and (b) indicates that the increase in the input energy resulting from a 50% increase in the ground motion intensity is more significant than that in the overall displacement ductility demand.

It can be seen from Eq. (4.9a) in Chapter 4 that for the elastic response of a frame, an increase in the intensity of its input ground motion by a factor of λ will result in a corresponding increase in the energy imparted to the frame by a factor of λ^2. For the inelastic response of a frame, the relationship between its response and the intensity of its input ground motion becomes nonlinear, and simple scaling factors for input energy cannot be easily obtained. However, based on studies of SDOF yielding systems, Jennings (44) indicated that the scaling factor for the energy input to elastic systems may also be used for yielding systems. It can be seen in Table 6.5(b) that the ratio

of the input energy between V=0.6 and 0.4 m/s ranges from 2.02 to 2.46, depending upon the frame and the A/V group of ground motions in question. These ratios are very close to the scaling factor of $(0.6/0.4)^2 = 2.25$. Therefore, it appears that the scaling factor for elastic input energy may also be used for inelastic input energy in the case of MDOF systems.

A comparison between Tables 6.5(c) and (d) reveals that the increase in the hysteretic energy is more significant than that of the damping energy. Therefore, most of the increased input energy resulting from an increase in the intensity of the input ground motions has to be dissipated through hysteretic action. This is consistent with the observed substantial increase in the beam and column curvature ductility demands in the lower storeys.

6.6 Comparison between Inelastic and Elastic Responses

In this section, the inelastic and elastic responses are compared for the frames when subjected to the three A/V groups of earthquake records. The comparison is made for the design peak ground velocity level of 0.4 m/s. The relationships between the inelastic and elastic responses for V = 0.6 m/s are similar to those for V = 0.4 m/s, and therefore, they are not presented herein. This comparison is useful for the following two reasons. First, the elastic response of a building structure can be used as a reference against which the effect of allowing inelastic deformations in the building can be evaluated. Second, the information regarding the relationship between the inelastic and elastic responses would enable a rational design to be obtained from the results of an elastic dynamic analysis which is less expensive than an inelastic

dynamic analysis.

6.6.1 Deformation Response Parameters

Fig. 6.15 compares the mean values of the maximum storey displacement and interstorey drift between the inelastic and elastic responses for the 4S1, 4S2, 10S, and 18S frames, respectively. The use of the mean+σ values instead of the mean values will not affect the comparison because the coefficients of variation for the inelastic and elastic responses are similar. It can be seen in Fig. 6.15 that the maximum storey displacements of the inelastic response are generally higher than those of the elastic response for the 4S1 frames for all three A/V groups of ground motions. In the case of the 10S and 18S frames, the maximum storey displacements for the inelastic response are generally lower than those for the elastic response. Therefore, for frames with very short fundamental periods, the maximum storey displacements of their inelastic responses tend to be higher than those of their corresponding elastic responses, whereas the reverse tends to be true for frames with moderate or long fundamental periods. This conclusion based on statistical analysis for realistic frame structures is consistent with that obtained in the previous studies for SDOF systems, shear beam models, and simple moment-resisting frames subjected to individual earthquake ground motions (41,90,91).

For the 4S1 frames, the interstorey drifts of the inelastic response are higher than those of the elastic response in the bottom two storeys and lower in the top two storeys. The higher interstorey drifts for the inelastic response in the bottom two storeys result from fact

that large inelastic deformations are concentrated at the bottom two storeys during the inelastic responses of the frames. The lower interstorey drifts for the inelastic response in the upper two storeys are presumably because the concentration of inelastic deformations at the bottom of the frames tends to relieve the interstorey deflections of the top two storeys. The relationship of interstorey drifts between the inelastic and elastic responses for the 4S2 frames is similar to that for the 4S1 frames. For the 10S and 18S frames, the interstorey drifts for the inelastic response are lower than those for the elastic response in the upper and middle storeys. In the lower storeys, the interstorey drifts of the inelastic response are similar to or higher than those of the elastic response, depending on the A/V group of ground motions. This is again due to the effect of the concentration of inelastic deformations in the lower storeys for the inelastic response.

6.6.2 Force Response Parameters

The mean maximum storey shears are compared in Fig.6.11 between the inelastic and elastic responses for the 4S1, 4S2, 10S, and 18S frames, respectively. It can be seen that the difference in the storey shears among the three A/V groups of ground motions for the inelastic response is considerably smaller than that for the elastic response. This is not surprising since the maximum storey shears in the inelastic response are limited by the yield strengths of the structural members, and the variations resulting from the strain-hardening effect beyond the member yield strengths are relatively small. Furthermore, it can be observed that the storey shears for the elastic response are substantially higher

than those for the inelastic response. This clearly demonstrates the economic advantage of relying on inelastic deformations in the seismic design of building structures. By allowing limited amount of inelastic deformation, the forces resisted by the frames are considerably lower than those that would be required if the frames were to remain elastic.

Table 6.8 compares the mean overall displacement ductility demands with the ratios of the mean elastic to inelastic base shears for the 4S1, 4S2, 10S, and 18S frames, respectively. The ratio of elastic to inelastic base shears can be interpreted as a force reduction factor through which the elastic strength demand is reduced to obtain the actual base shear resisted in the inelastic response. It can be seen that for the 10S and 18S frames, the overall ductility demands are close to the force reduction factors. However, for the 4S1 frames, the overall ductility demands are significantly higher than the corresponding force reduction factors. This observation is consistent with that for SDOF systems (90).

6.6.3 Energy Indices

Table 6.9 presents the statistical results of the input energy per unit mass for the elastic responses of the 4S1, 4S2, 10S, and 18S frames subjected to the three A/V groups of earthquake ground motions scaled to a common peak velocity of 0.4 m/s. To facilitate comparison with the input energy per unit mass for the inelastic responses, the ratios of the mean inelastic to elastic input energy are shown in Table 6.10. It can be seen that the input energy for the inelastic response is similar to that for the elastic response. To examine the detailed correlation of the input energy between the inelastic and elastic responses, the inelastic

input energy is plotted against the elastic input energy in Fig. 6.16 for the individual earthquake records for the 4S1, 4S2, 10S, and 18S frames, respectively. It can be seen that the correlation of input energy between the inelastic and elastic responses for long period frames appears to be better than that for short period frames. The similarity in the input energy between elastic and inelastic responses has been observed for SDOF systems in previous studies by Jennings (44) and Zahrah and Hall (97). Based on this study, it may be concluded that this similarity between inelastic and elastic input energy is also true for multistorey building frames.

6.7 Distribution of Response Parameters for Different Analyses

In current practice, the elastic static analysis is used for the design of regular building structures. It has also been suggested (5,88) that the interstorey deflections of the designed buildings under design level earthquake excitation may be estimated from the elastic static analysis of the buildings under the design lateral seismic loading coupled with a deflection amplification factor. Therefore, it is implicitly assumed that the distribution of the inelastic interstorey deflections resulting from earthquake ground shaking would be similar to that of the elastic interstorey deflections resulting from the design lateral seismic loading. However, the use of the conventional elastic static analysis for estimating the distribution of the actual inelastic deflections for a building may be inappropriate for the following two reasons. First, the presence of local inelastic deformations in the beams and columns during the dynamic response may significantly alter the

characteristics of the building. Second, the effect of higher mode contributions may change the distributions of the inelastic deflections.

In this section, the distributions of the overall response parameters over the height of the 4S2, 10S, and 18S frames are compared for four different analyses. These four analyses are (a) elastic static; (b) elastic dynamic; (c) inelastic static; and (d) inelastic dynamic analyses. This comparison is made for each of the three A/V groups of ground motions. Furthermore, for each A/V group of ground motions, two different levels of peak ground velocity are considered, namely V = 0.4 and 0.6 m/s. These comparisons serve two purposes. The first purpose is to evaluate the capability of the three relatively simple analyses (elastic static, inelastic static, and elastic dynamic analyses) to estimate the distributions of the overall response parameters associated with the inelastic dynamic responses of the frames to earthquake ground excitations. The second purpose is to examine the effect of ground motion characteristics on the relationships among the four different analyses for moment-resisting frames with different numbers of storeys.

The overall response parameters considered are the interstorey drift and storey shear. For the inelastic and elastic dynamic analyses, the distribution shapes are associated with the mean values of the response parameters. While the distributions for the elastic dynamic analysis are independent of the intensity of the input ground motions, those for the inelastic dynamic analysis depend on the ground motion intensity. The distributions for the inelastic dynamic analysis are considered for the two peak ground velocity levels (0.4 and 0.6 m/s) used to scale the input ground motions. In determining the response parameter

distributions for the inelastic and elastic static analyses, the lateral loading is distributed over the height of each frame according to the NBCC 1985 distribution formula. The distributions for the elastic static analysis do not depend on the level of roof displacement. The distributions for the inelastic static analysis are associated with two roof displacement levels. The two roof displacements are set equal to the two mean values obtained from the inelastic dynamic analysis for the two levels of peak ground velocity.

To eliminate the difference attributable to the magnitude of roof displacement, the interstorey drifts obtained from each analysis are normalized with respect to the correponding roof displacement obtained from the same analysis. The storey shears computed from each analysis are normalized to the corresponding base shear obtained from the same analysis to eliminate the difference attributable to the magnitude of base shear.

6.7.1 Interstorey Deflection

Figs. 6.17 to 6.19 compare the variations of interstorey drift over height among the four analyses for the 4S2, 10S and 18S frames, respectively. For the distributions of the 4S2 frames, the relationships among the four analyses are similar for the three A/V groups of ground motions. The distributions obtained from the inelastic static analysis are close to those of the inelastic dynamic analysis. The distributions computed from the elastic static analysis are similar to those from the elastic dynamic analysis. Therefore, for the 4S2 frames, the contributions of higher modes are insignificant. Both elastic static and

dynamic analyses underestimate the interstorey drift in the bottom two storeys and overestimate the interstorey drift in the top two storeys. This is particularly true for high inelastic response level corresponding to the peak ground velocity of 0.6 m/s. The underestimation in the bottom two storeys results from the fact that the inelastic deformations of the 4S2 frames subjected to the three A/V groups of ground motions are concentrated at the bottom of the frames, whereas the elastic static and dynamic analyses cannot account for this concentration.

In contrast with the 4S2 frames, the relationships among the distributions associated with the four analyses for the 10S and 18S frames are strongly affected by the A/V ratio of the input ground motions. For the high A/V group of ground motions, the interstorey drifts obtained from the inelastic and elastic dynamic analyses are substantially higher than those computed by the inelastic and elastic static analyses in the upper storeys. In the case of the low A/V group of ground motions, the differences in the interstorey drift between the dynamic and static analyses are relatively small. Therefore, the effect of higher mode contributions on the interstorey deflection for high A/V ground motions is much more significant than that for low A/V ground motions. The use of both inelastic and elastic static analyses will grossly underestimate the interstorey drift in the upper storeys for high A/V ground motions. The more significant contribution of higher modes for the high A/V ground motions results from the fact that the high A/V ground motions have higher frequency content, and therefore, they tend to excite the higher modes of the 10S and 18S frames. While the elastic dynamic analysis provides interstorey drift distributions similar to

those of the inelastic dynamic analysis in the upper storeys, it underestimates the interstorey drift in the lower storeys. This underestimation becomes particularly pronounced for the low A/V ground motions. This is because for the low A/V ground motions, inelastic deformations are concentrated in the lower storeys, and both the elastic dynamic and static analyses cannot account for this concentration.

The relationships of the interstorey deflection distributions among the four analyses for the 10S and 18S frames are also markedly affected by the level of inelastic response associated with the peak ground velocity level of the input ground motions. A comparison of the distributions between V=0.4 and 0.6 m/s indicates that the contributions of higher modes to the interstorey drift in the upper storeys tend to decrease with an increase in the inelastic response level. The less significant effect of higher mode contribution for higher level inelastic response may be attributable to the following two factors. First, the significant period elongation due to high level inelastic response reduces the intensity of higher mode responses because the response intensity associated with the three groups of ground motions decreases rapidly with an increase in period for periods longer than about 0.3 sec, as can be seen in Fig. 2.5. This decrease is particularly pronounced for the high A/V group of ground motions. Second, yielding of the 10S and 18S frames also modifies their apparent mode of vibration so as to increase the participation factor for the "fundamental mode". In the lower storeys, an increase in the inelastic response level tends to increase the differences in the interstorey drift between the inelastic and elastic analyses. This is because the concentration of inelastic

deformations in the lower storeys becomes more significant for high level inelastic response.

6.7.2 Storey Shear

Figs.6.20 to 6.22 compares the variations of storey shears over height among the four analyses for the 4S2, 10S, and 18S frames, respectively. It can be seen that for the 10S and 18S frames, the contribution of higher modes to storey shear for the high A/V group of ground motions is more significant than that for the low A/V group. In comparison with interstorey drift, the contribution of higher modes to storey shear is generally less significant.

6.8 Summary

In this chapter, the inelastic dynamic responses of the designed frames subjected to the three groups of earthquake records having low, intermediate, and high A/V ratios are analyzed statistically. The statistical results are used to investigate the effect of ground motion A/V ratio on the inelastic dynamic responses of frame structures and to evaluate the seismic performance of frame structures having different fundamental periods designed in accordance with NBCC 1985 and CAN3-A23.3-M84. In addition, the effect of peak ground velocity level on the inelastic response is investigated. The statistical results of the inelastic dynamic responses are compared with those of the corresponding elastic dynamic analysis. Finally, the distributions of overall response parameters over frame height are compared for four different analyses, namely: (a) elastic static; (b) elastic dynamic; (c) inelastic static;

and (d) inelastic dynamic analyses. Based on this statistical study, the following conclusions can be drawn:

(1) If the specification of seismic design forces is directly tied to peak ground velocity, the use of a single seismic response factor results in different values for the various overall and localized response parameters for frames with short fundamental periods, when subjected to earthquake ground motions having different A/V ratios. The response parameters for high A/V ground motions are considerably higher than those for low A/V ground motions. The use of three different seismic response factors for three different A/V ranges, as suggested in NBCC 1985, provides slight improvement in the consistency of maximum storey displacement and interstorey drift. However, the consistency in member curvature ductility demands and overall displacement ductility demands is significantly improved. This improvement is particularly pronounced for the curvature ductility demand at the base of the first storey columns. The improvement results from the fact that the use of three different seismic design forces for the three A/V ranges leads to three frames having different member yield curvatures and overall yield displacements on which the computation of ductility factors is based.

(2) For low rise frames, inelastic deformations tend to be concentrated at the bottom of the frames, irrespective of the A/V ratio of the input ground motions. This distribution of inelastic deformations over height for earthquake excitation is similar to that for monotonically increased lateral loading. For high rise frames, the distributions of inelastic deformations over height are strongly affected by the A/V ratio of the input ground motions. For low A/V ground motions

which have lower frequency content, inelastic deformations tend to be concentrated in lower storeys. For high A/V ground motions which have higher frequency content, the "whiplash" effect is very significant due to significant contribution of higher modes, and inelastic deformation in the upper storeys can be significantly higher than those in the lower storeys.

(3) While low A/V ground motions produce slightly lower inelastic deformations than high A/V ground motions in the upper storeys of high rise frames, they develop considerably higher inelastic deformations in the lower storeys. Because the lower storeys are more critical than the upper storeys due to the high axial loads carried by the columns, low A/V ground motions tend to be more damaging to high rise frames than high A/V ground motions even when the frames are designed based on peak ground velocity.

(4) Seismic design based on NBCC 1985 and CAN3-A23.3-M84 leads to nonuniform ductility demands for frames having different fundamental periods. The member curvature ductility demands and the overall displacement ductility demands for short period frames tend to be higher than those for long period frames. This is particularly true for the curvature ductility demands at the base of the first storey columns. The nonuniform ductility demands for frames with different fundamental periods are attributable to the use of a period-independent structural behaviour coefficient K and different amplifications of column design moments due to slenderness effect for frames having different numbers of storeys.

(5) Because of the overstrength of the frames as compared to their factored seismic design forces, the global displacement ductility demands of the frames are generally lower than the displacement ductility demands of the corresponding SDOF systems whose periods are the same as the fundamental periods of the frames and whose yield strengths are specified as factored seismic design forces from the NBCC 1985 base shear formula. This difference is particularly pronounced for short period frames, because short period frames have more significant overstrength than long period frames.

(6) The mean+σ global displacement ductility demands for frames with moderate and long fundamental periods subjected to design level earthquake excitations are generally lower than the expected "system ductility" as implied by the value of the K factor used in the design. For frames with very short fundamental periods, the mean+σ overall displacement ductility demands would exceed the expected value.

(7) For a comparable level of overall drift, the dynamic overstrength of the frames as compared to their factored seismic design forces tends to be more significant than the static overstrength. This is particularly true for high rise frames.

(8) The inelastic deformations in the lower storeys are highly sensitive to the peak ground velocity level of the input ground motions for both low and high rise frames. A 50% increase in the peak ground velocity of the input ground motions results in nearly 100% increase in the curvature ductility demands for the structural members in the lower storeys. As a result, the interstorey drifts in the lower storeys are also significantly increased. In addition, the input energy is more than

doubled. Most of the increased input energy has to be dissipated through hysteretic action. This clearly points out the need for accurate evaluation of the peak ground velocity expected at a building site as well as appropriate assessment of the uncertainties associated with this evaluation.

(9) For frames having very short fundamental periods, the maximum storey displacements for inelastic response tend to be higher than those for elastic response. The reverse tends to be true for frames having moderate or long fundamental periods. The global displacement ductility demands are close to the ratios of elastic to inelastic dynamic base shears for moderate or long period frames, whereas the overall ductility demands are significantly higher than the force ratios for short period frames. The input energy for inelastic response is similar to that for elastic response. This correlation appears to be better for long period frames than for short period frames.

(10) For low rise frames, the inelastic static analysis provides very similar distributions of interstorey deflections to those of the inelastic dynamic analysis. Both elastic static and dynamic analyses tend to underestimate the interstorey deflections at the bottom of the frames. For high rise frames, the distribution of interstorey deflections for the elastic dynamic analysis is similar to that for the inelastic dynamic analysis in the upper storeys. The use of both inelastic and elastic static analyses grossly underestimates the interstorey drift in the upper storeys. This underestimation is particularly pronounced for high A/V ground motions. In the lower storeys, the distribution of interstorey drift for the inelastic static analysis is close to that for the

inelastic dynamic analysis. The use of elastic dynamic or static analyses tends to underestimate interstorey drift in the lower storeys. This is particularly true for low A/V ground motions.

(11) For high rise frames, the contribution of higher modes to interstorey drift in the upper storeys tends to decrease with an increase in the level of inelastic response.

(12) For high rise frames, the higher modes of vibration make a more significant contribution to interstorey deflection than to storey shear.

Table 6.1 Statistical Results of Overall Displacement Ductility and Energy Indices for 4S1, 4S2, 10S, and 18S Frames Subjected to Low, Intermediate, and High A/V Ground Motions Scaled to a Common Peak Velocity of 0.4 m/s

Frame	Low A/V			Intermediate A/V			High A/V		
	Mean	Mean+σ	COV	Mean	Mean+σ	COV	Mean	Mean+σ	COV
(a) Overall Displacement Ductility μ_δ									
4S1I*	2.87	4.04	0.41	6.08	7.48	0.23	9.40	12.19	0.30
4S1+	4.31	6.15	0.43	6.08	7.48	0.23	6.36	7.97	0.25
4S2	3.37	4.26	0.26	4.13	5.12	0.24	3.89	4.97	0.28
10S	2.55	3.21	0.26	2.72	3.22	0.19	1.89	2.35	0.24
18S	1.91	2.46	0.29	2.02	2.41	0.19	1.26	1.70	0.35
(b) Input Energy E_I^* $(cm/sec)^2$									
4S1I	1462	2607	0.78	4537	6226	0.37	5494	7204	0.31
4S1	1581	2795	0.77	4537	6226	0.37	5416	7057	0.30
4S2	3144	5251	0.67	7486	10123	0.35	6231	9538	0.53
10S	5875	8911	0.52	7693	10533	0.37	4329	6441	0.49
18S	4816	7108	0.48	5649	7620	0.35	2827	4087	0.45
(c) Damping Energy E_D^* $(cm/sec)^2$									
4S1I	695	1193	0.72	1530	2129	0.39	1514	1960	0.29
4S1	630	1081	0.72	1530	2129	0.39	1604	2078	0.29
4S2	1609	2634	0.64	3073	4227	0.37	2358	3296	0.40
10S	2999	4165	0.39	3689	4841	0.31	2089	2973	0.42
18S	2501	3463	0.38	3138	4261	0.36	1634	2243	0.37
(d) Hysteretic Energy E_H^* $(cm/sec)^2$									
4S1I	724	1365	0.89	2845	3946	0.39	3617	4886	0.35
4S1	899	1641	0.83	2845	3946	0.39	3406	4602	0.35
4S2	1422	2492	0.75	4074	5585	0.37	3300	5651	0.71
10S	2680	4568	0.70	3544	5371	0.52	1655	2820	0.70
18S	2121	3595	0.70	2076	2865	0.38	636	1209	0.90

* Analysis I
+ Analysis II

Table 6.2 Statistical Results of Maximum Displacement Ductility for SDOF Systems Subjected to Low, Intermediate, and High A/V Ground Motions Scaled to a Common Peak Velocity of 0.4 m/s

Period	Low A/V			Intermediate A/V			High A/V		
	Mean	Mean+σ	COV	Mean	Mean+σ	COV	Mean	Mean+σ	COV
0.23	9.36	13.28	0.42	11.63	15.08	0.30	8.89	11.67	0.31
0.47	5.57	7.34	0.32	7.08	9.31	0.31	6.04	7.59	0.26
1.20	4.14	5.15	0.24	4.29	5.27	0.23	2.56	3.54	0.38
2.01	2.87	3.86	0.34	2.63	3.45	0.31	1.50	2.04	0.35

Table 6.3 Dynamic Overstrength

Frame	Low A/V		Intermediate A/V		High A/V	
	Overall Drift	Overstrength	Overall Drift	Overstrength	Overall Drift	Overstrength
4S1	0.08%	86%	0.16%	71%	0.23%	55%
4S2	0.25%	80%	0.36%	78%	0.41%	63%
10S	0.40%	43%	0.42%	52%	0.29%	56%
18S	0.35%	27%	0.37%	41%	0.23%	46%

Table 6.4 Statistical Results of Overall Displacement Ductility and Energy Indices for 4S2, 10S and 18S Frames Subjected to Low, Intermediate, and High A/V Ground Motions Scaled to a Common Peak Velocity of 0.6 m/s

Frame	Low A/V			Intermediate A/V			High A/V		
	Mean	Mean+σ	COV	Mean	Mean+σ	COV	Mean	Mean+σ	COV
(a) Overall Displacement Ductility μ_δ									
4S2	5.73	7.88	0.38	6.80	9.02	0.33	5.80	7.22	0.24
10S	4.01	4.92	0.23	4.08	4.97	0.22	2.71	3.35	0.24
18S	3.18	4.30	0.35	2.94	3.73	0.27	1.65	2.20	0.34
(b) Input Energy E_I^* $(cm/sec)^2$									
4S2	7727	12443	0.61	16716	22048	0.32	12582	18972	0.51
10S	12397	18075	0.46	15880	21296	0.34	8778	12795	0.46
18S	11018	15205	0.38	12517	16357	0.31	6040	8675	0.44
(c) Damping Energy E_D^* $(cm/sec)^2$									
4S2	2822	4481	0.59	5449	7336	0.35	4039	5693	0.41
10S	4808	6645	0.38	6029	7942	0.32	3455	4740	0.37
18S	4404	5802	0.32	5462	7210	0.32	2898	3968	0.37
(d) Hysteretic Energy E_H^* $(cm/sec)^2$									
4S2	4650	7746	0.67	10541	13864	0.31	7312	11920	0.63
10S	7167	11156	0.56	8869	12341	0.39	4050	6584	0.63
18S	6182	9271	0.50	6097	8110	0.33	1917	3307	0.72

Table 6.5 Ratios of Mean Overall Displacement Ductilities and Energy Indices for 4S2, 10S, and 18S Frames between Two Peak Ground Velocity Levels of 0.6 and 0.4 m/s

Frame	Low A/V	Intermediate A/V	High A/V
(a) Overall Displacement Ductility μ_δ			
4S2	1.70	1.65	1.49
10S	1.57	1.50	1.43
18S	1.66	1.46	1.31
(b) Input Energy E_I^*			
4S2	2.46	2.23	2.02
10S	2.11	2.06	2.03
18S	2.29	2.22	2.14
(c) Damping Energy E_D^*			
4S2	1.75	1.77	1.71
10S	1.60	1.63	1.65
18S	1.76	1.74	1.77
(d) Hysteretic Energy E_H^*			
4S2	3.27	2.59	2.22
10S	2.67	2.50	2.45
18S	2.91	2.94	3.01

Table 6.6 Statistical Results of Maximum Displacement Ductility for SDOF Systems Subjected to Low, Intermediate, and High A/V Ground Motions Scaled to a Common Peak Velocity of 0.6 m/s

Period	Low A/V			Intermediate A/V			High A/V		
	Mean	Mean+σ	COV	Mean	Mean+σ	COV	Mean	Mean+σ	COV
0.47	10.35	13.75	0.33	12.25	15.58	0.27	9.03	11.15	0.23
1.20	6.96	8.73	0.25	7.00	9.19	0.31	3.64	4.97	0.37
2.01	4.47	6.03	0.35	4.00	5.24	0.31	2.07	2.92	0.41

Table 6.7 Ratios of Mean Maximum Displacement Ductilities for SDOF Systems between Two Peak Ground Velocity Levels of 0.6 and 0.4 m/s

Period	Low A/V	Intermediate A/V	High A/V
0.47	1.86	1.73	1.50
1.20	1.68	1.63	1.42
2.01	1.56	1.52	1.38

Table 6.8 Comparison of Mean Overall Displacement Ductility with Ratio of Mean Elastic to Inelastic Base Shears for V = 0.4 m/s

Frame	Low A/V		Intermediate A/V		High A/V	
	μ_δ	R_S	μ_δ	R_S	μ_δ	R_S
4S1	4.31	2.13	6.08	2.77	6.36	3.89
4S2	3.37	1.73	4.13	2.67	3.89	3.01
10S	2.55	2.18	2.72	2.25	1.89	1.79
18S	1.91	1.86	2.02	1.74	1.26	1.33

μ_δ = Global Displacement Ductility
R_S = Ratio of Elastic to Inelastic Base Shears

Table 6.9 Statistical Results of Elastic Input Energy for 4S1, 4S2, 10S and 18S Frames Subjected to Low, Intermediate, and High A/V Ground Motions Scaled to a Common Peak Velocity of 0.4 m/s

Frame	Input Energy E_I' $(cm/sec)^2$								
	Low A/V			Intermediate A/V			High A/V		
	Mean	Mean+σ	COV	Mean	Mean+σ	COV	Mean	Mean+σ	COV
4S1	1177	2192	0.86	3299	5334	0.62	5547	8760	0.58
4S2	2772	5065	0.83	7444	10709	0.44	7613	11756	0.54
10S	6933	12080	0.74	8253	11522	0.40	4899	7849	0.60
18S	5131	8799	0.71	5527	7954	0.44	2943	4353	0.48

Table 6.10 Ratios of Mean Inelastic to Elastic Input Energy for V=0.4 m/s

Frame	Low A/V	Intermediate A/V	High A/V
4S1	1.34	1.38	0.98
4S2	1.13	1.01	0.82
10S	0.85	0.93	0.88
18S	0.94	1.02	0.96

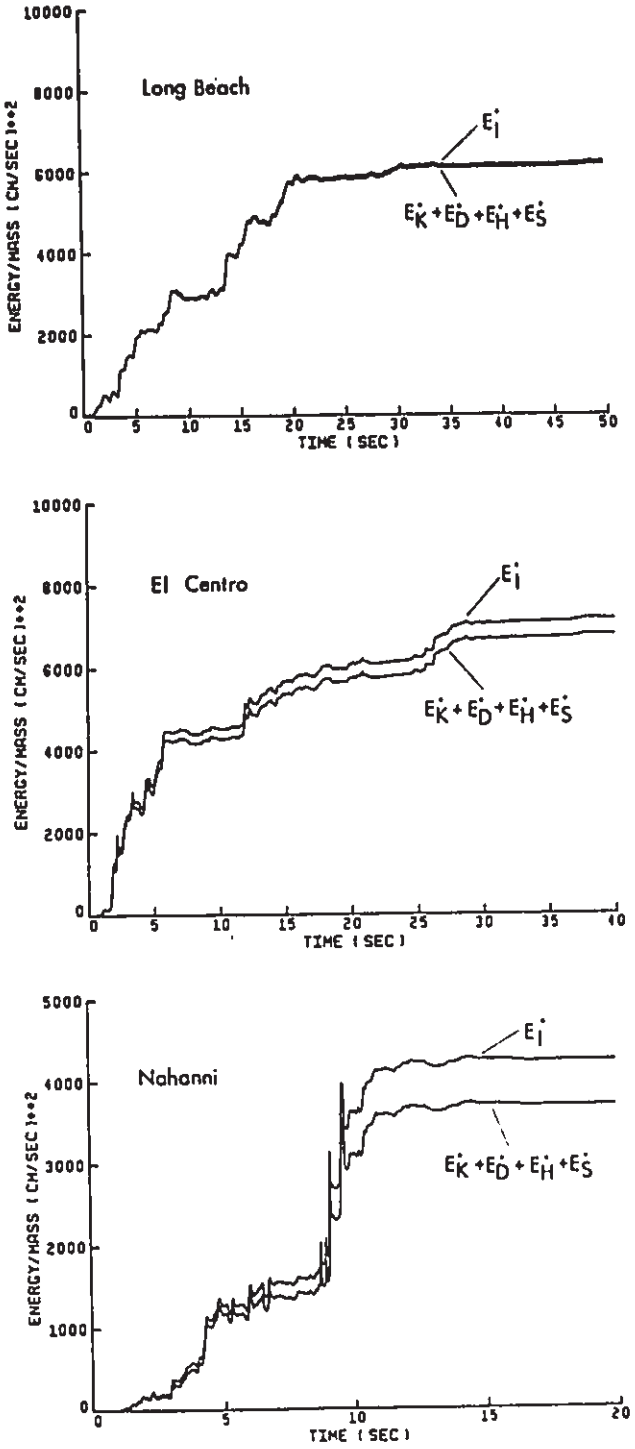

Fig. 6.1 Comparison between $E_I^{\cdot}$ and $E_K^{\cdot}+E_D^{\cdot}+E_H^{\cdot}+E_S^{\cdot}$ for 10S Frame Subjected to (a) Long Beach; (b) El Centro; and (c) Nahanni Records Scaled to a Peak Velocity of 0.4 m/s

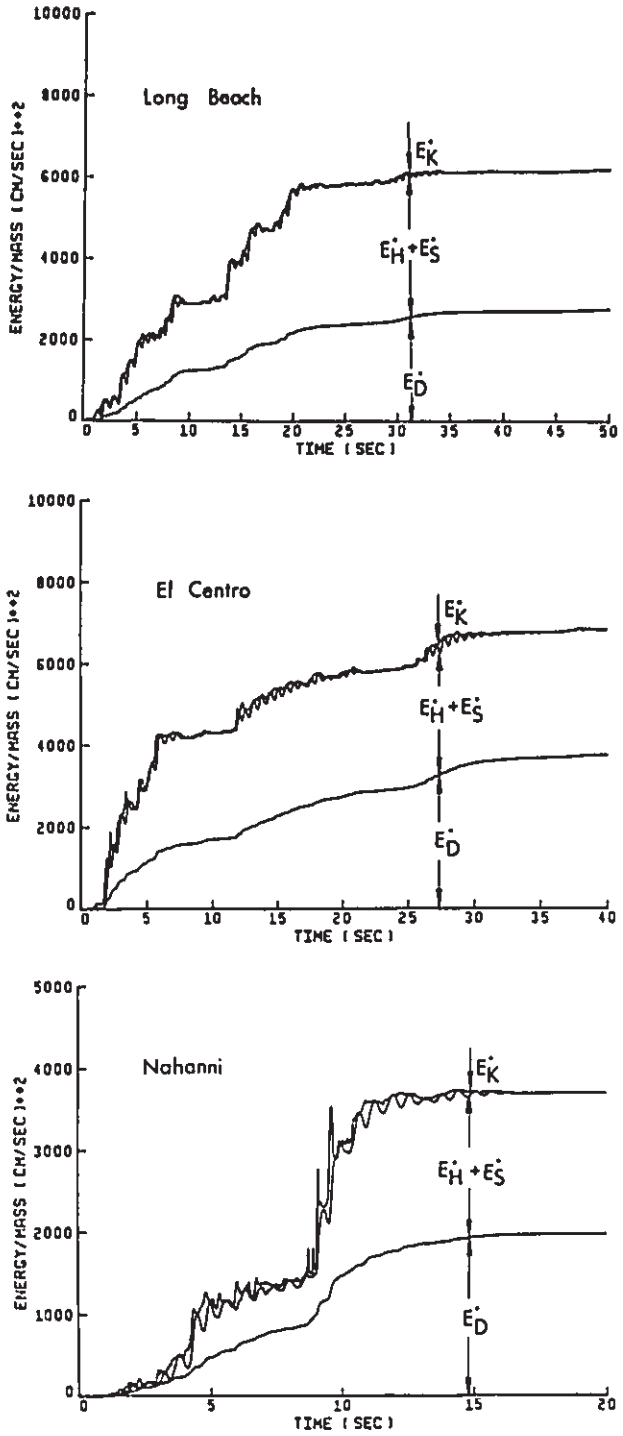

Fig. 6.2 Time History Response of Energy Indices for 10S Frame Subjected to (a) Long Beach; (b) El Centro; and (c) Nahanni Records Scaled to a Peak Velocity of 0.4 m/s

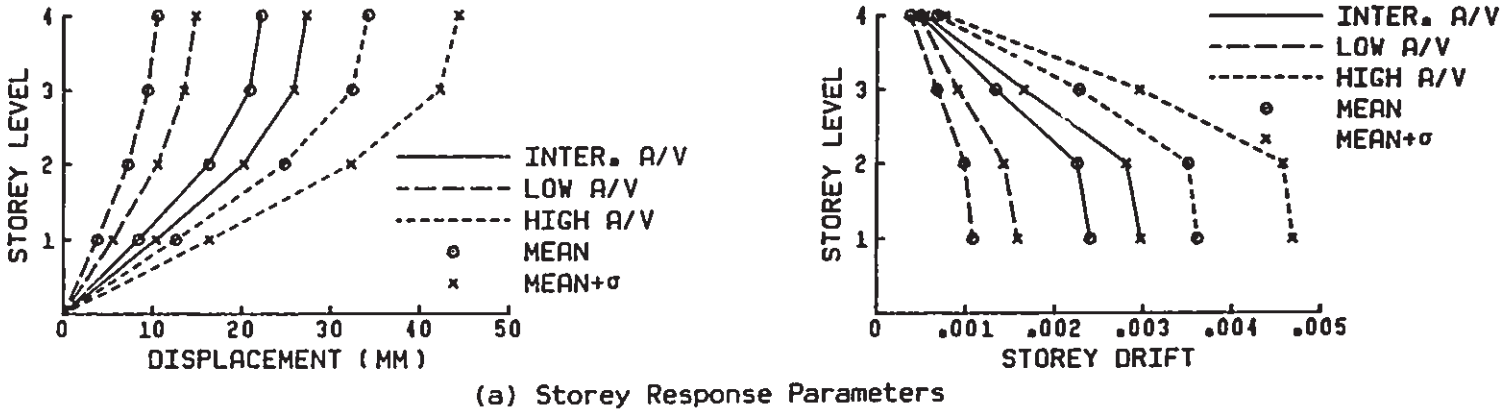

(a) Storey Response Parameters

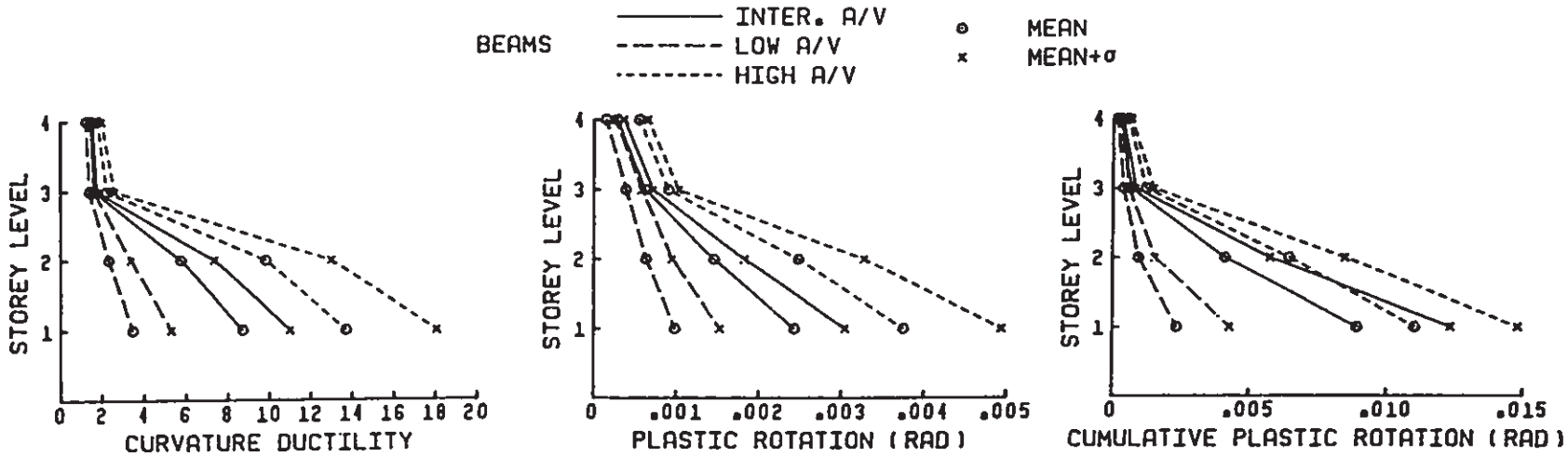

(b) Beam Response Parameters

Fig. 6.3 Mean and Mean+σ Values of Response Parameters for 4S11 Frame Subjected to Low, Intermediate, and High A/V Groups of Ground Motions Scaled to a Common Peak Velocity of 0.4 m/s - Analysis I

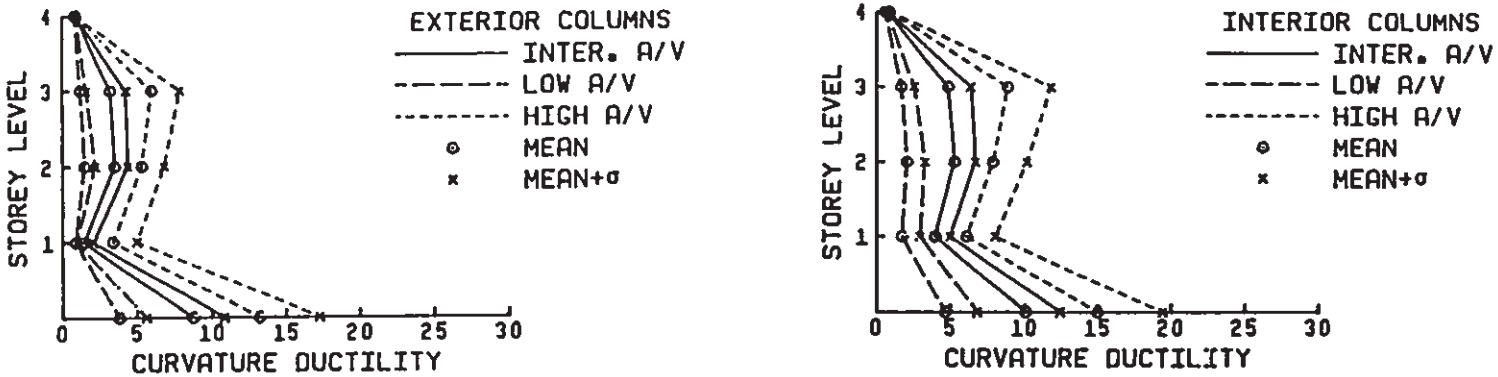

(c) Column Response Parameters

Fig. 6.3 (cont'd) Mean and Mean+σ Values of Response Parameters for 4S11 Frame Subjected to Low, Intermediate, and High A/V Groups of Ground Motions Scaled to a Common Peak Velocity of 0.4 m/s - Analysis I

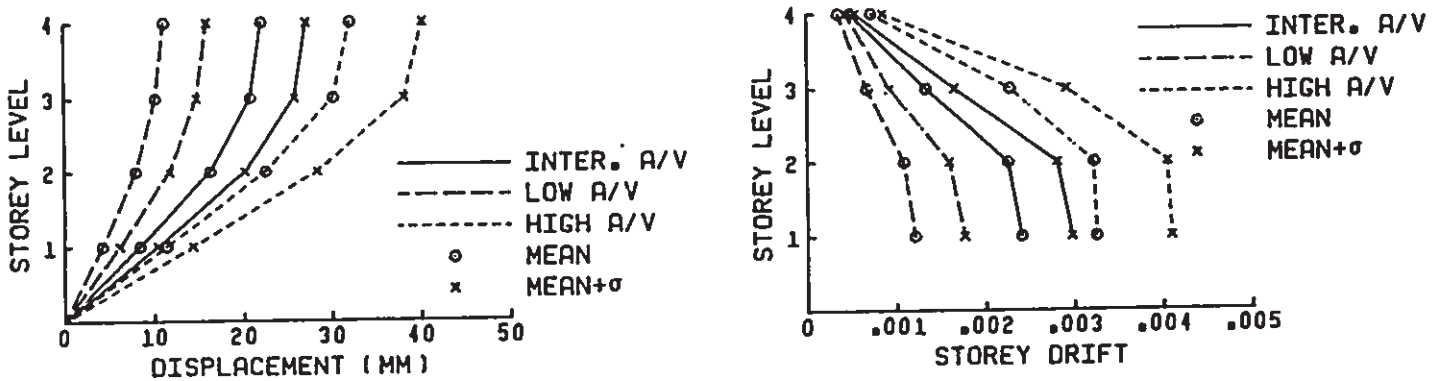

(a) Storey Response Parameters

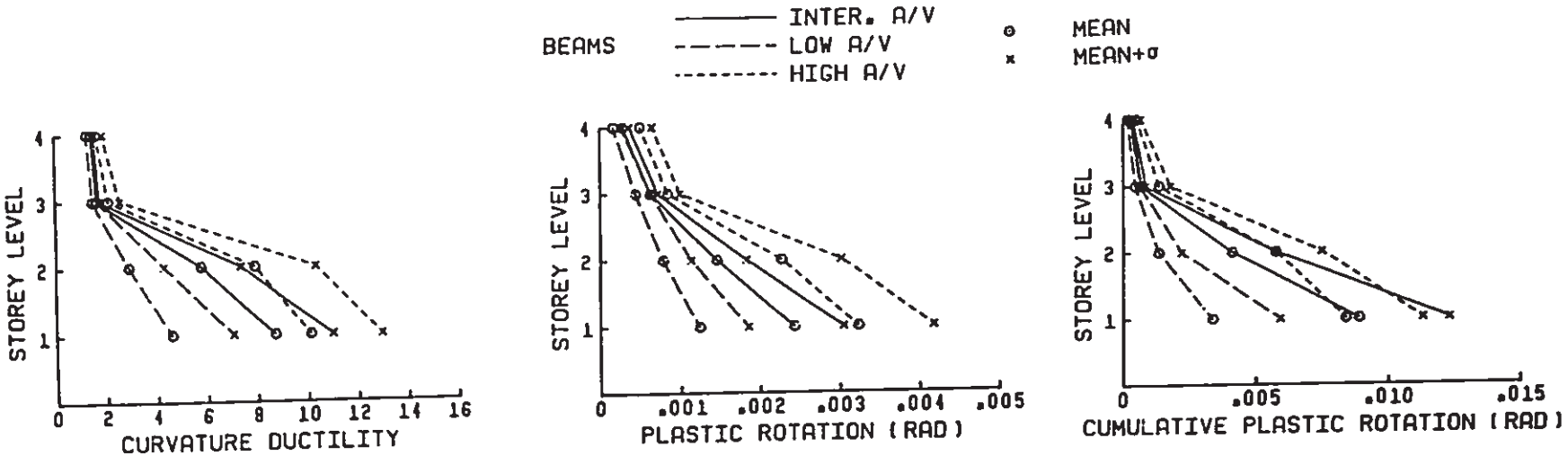

(b) Beam Response Parameters

Fig. 6.4 Mean and Mean+σ Values of Response Parameters for 4S1 Frames Subjected to Low, Intermediate, and High A/V Groups of Ground Motions Scaled to a Common Peak Velocity of 0.4 m/s - Analysis II

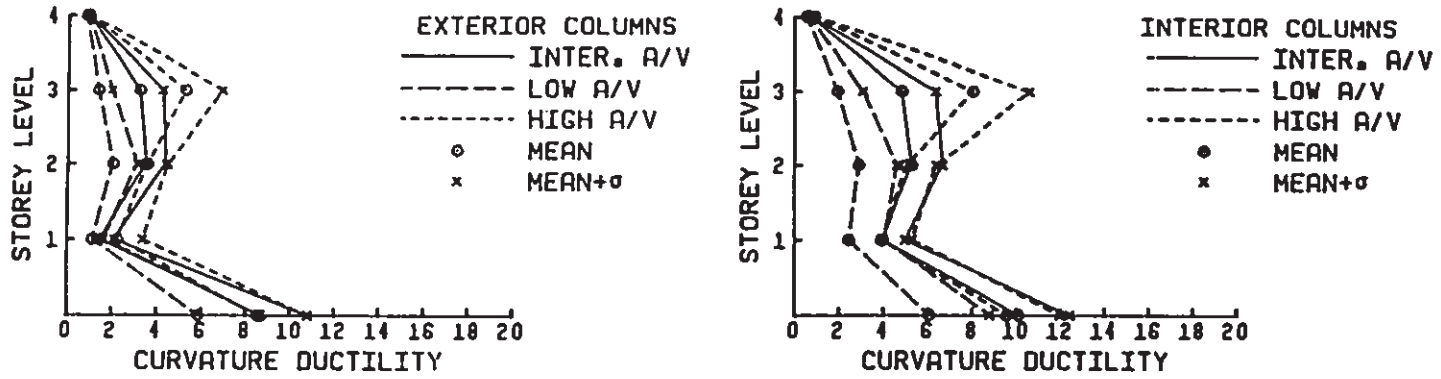

(c) Column Response Parameters

Fig. 6.4 (cont'd) Mean and Mean+σ Values of Response Parameters for 4S1 Frames Subjected to Low, Intermediate, and High A/V Groups of Ground Motions Scaled to a Common Peak Velocity of 0.4 m/s - Analysis II

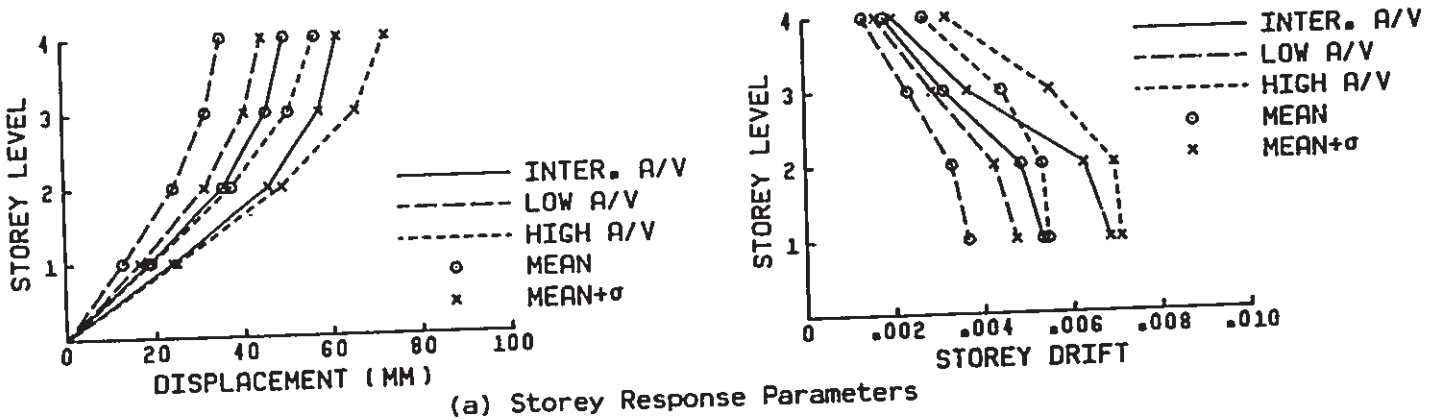

(a) Storey Response Parameters

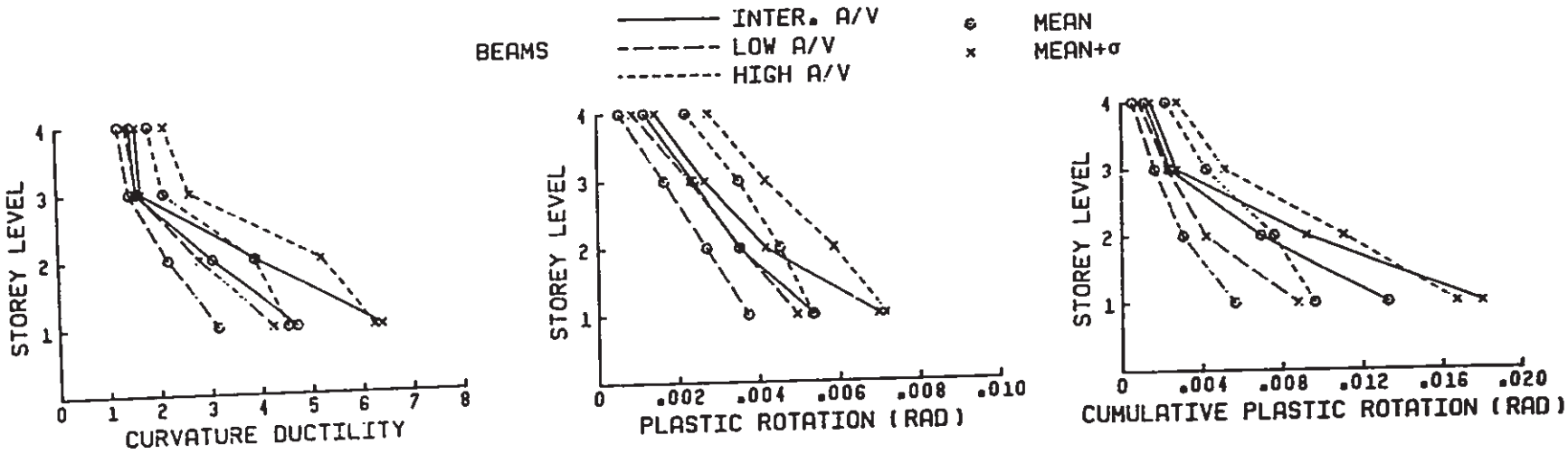

(b) Beam Response Parameters

Fig. 6.5 Mean and Mean+σ Values of Response Parameters for 4S2 Frames Subjected to Low, Intermediate, and High A/V Groups of Ground Motions Scaled to a Common Peak Velocity of 0.4 m/s

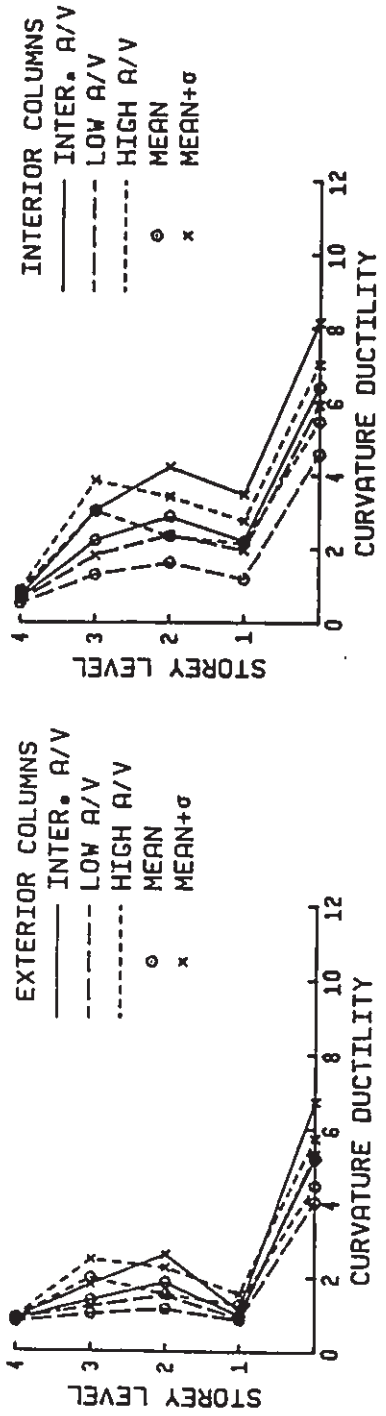

(c) Column Response Parameters

Fig. 6.5 (cont'd) Mean and Mean+σ Values of Response Parameters for 452 Frames Subjected to Low, Intermediate, and High A/V Groups of Ground Motions Scaled to a Common Peak Velocity of 0.4 m/s

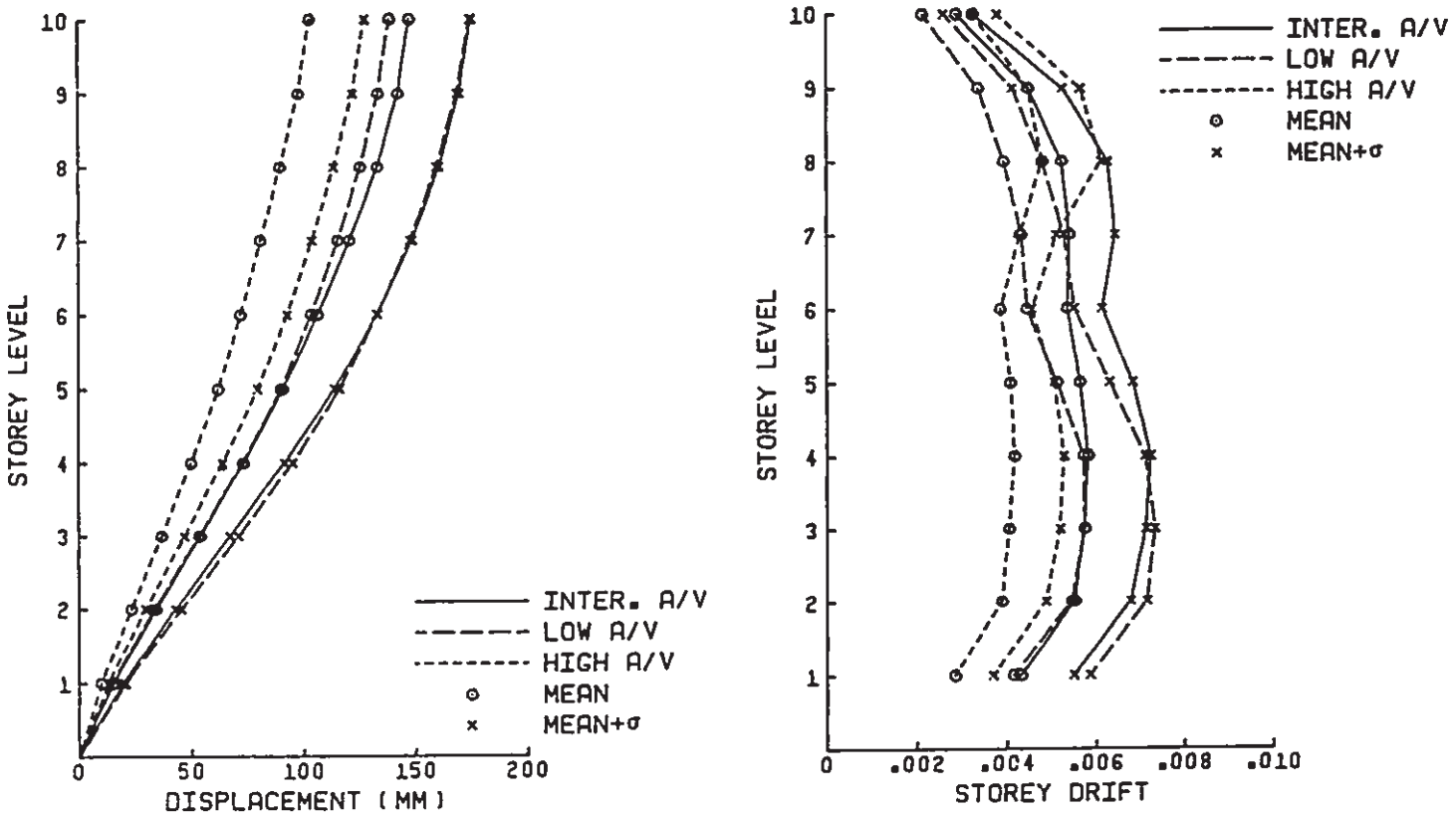

(a) Storey Response Parameters

Fig. 6.6 Mean and Mean+σ Values of Response Parameters for 10S Frame Subjected to Low, Intermediate, and High A/V Groups of Ground Motions Scaled to a Common Peak Velocity of 0.4 m/s

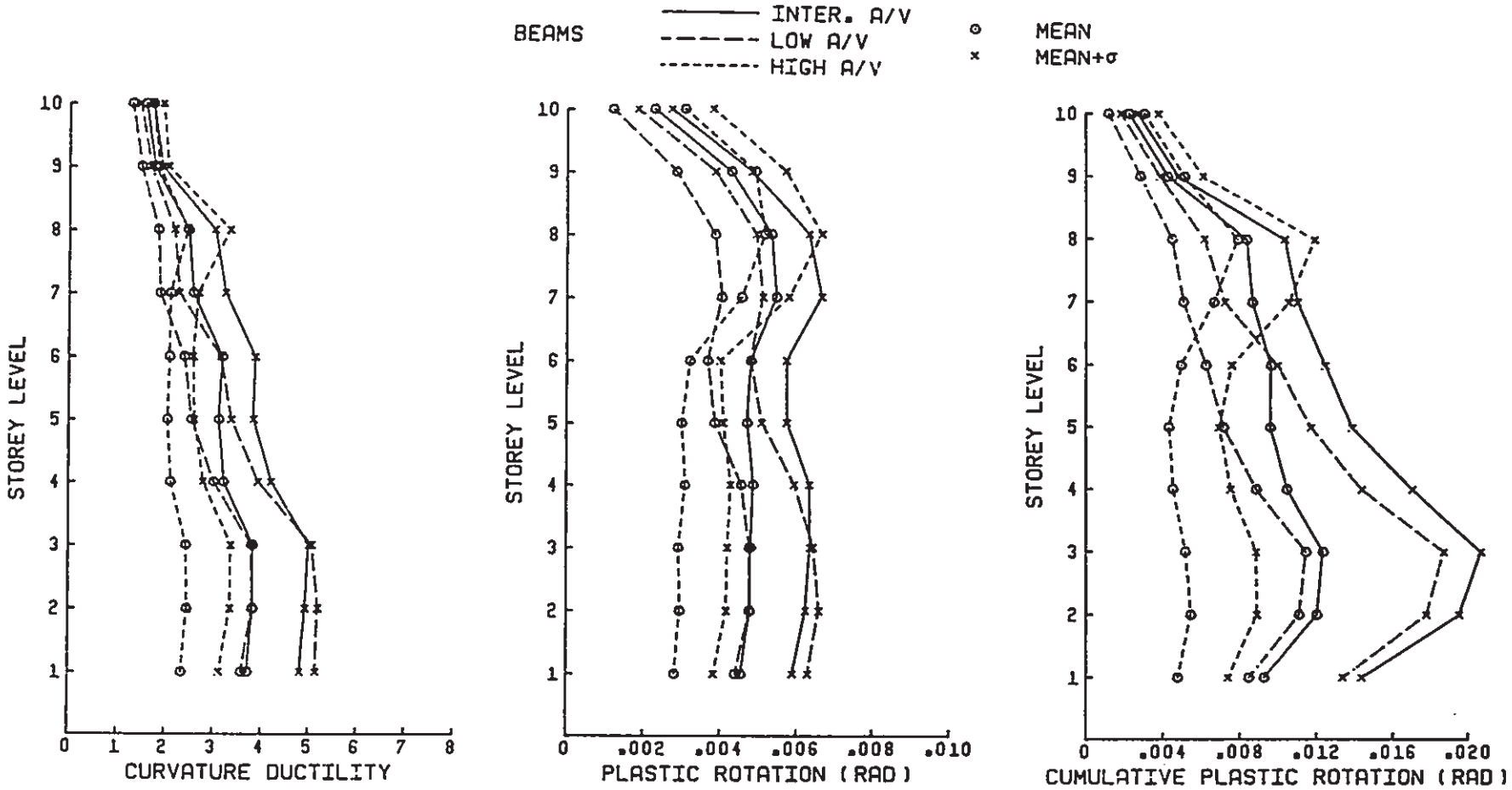

(b) Beam Response Parameters

Fig. 6.6 (cont'd) Mean and Mean+σ Values of Response Parameters for 10S Frame Subjected to Low, Intermediate, and High A/V Groups of Ground Motions Scaled to a Common Peak Velocity of 0.4 m/s

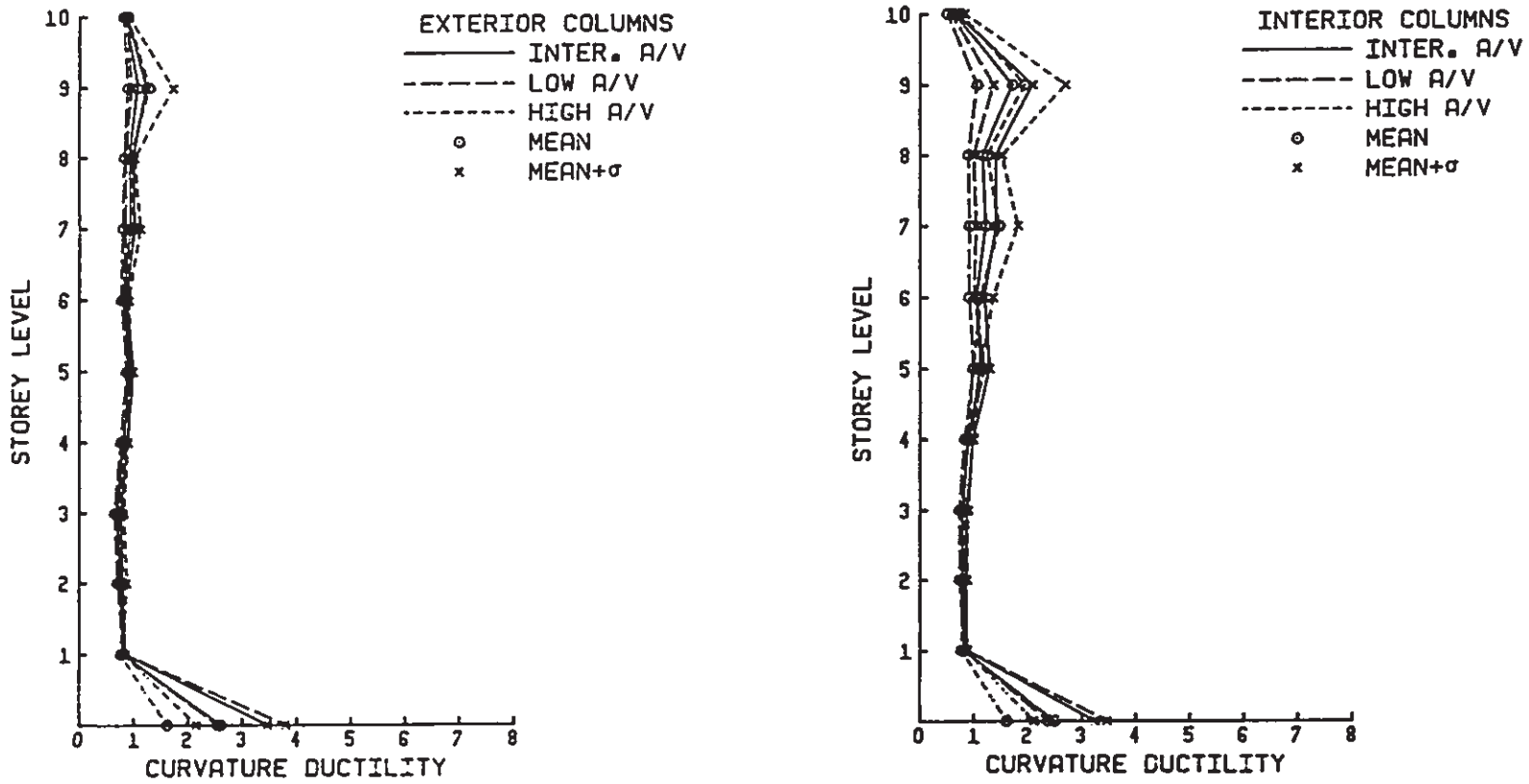

(c) Column Response Parameters

Fig. 6.6 (cont'd) Mean and Mean+σ Values of Response Parameters for 10S Frame Subjected to Low, Intermediate, and High A/V Groups of Ground Motions Scaled to a Common Peak Velocity of 0.4 m/s

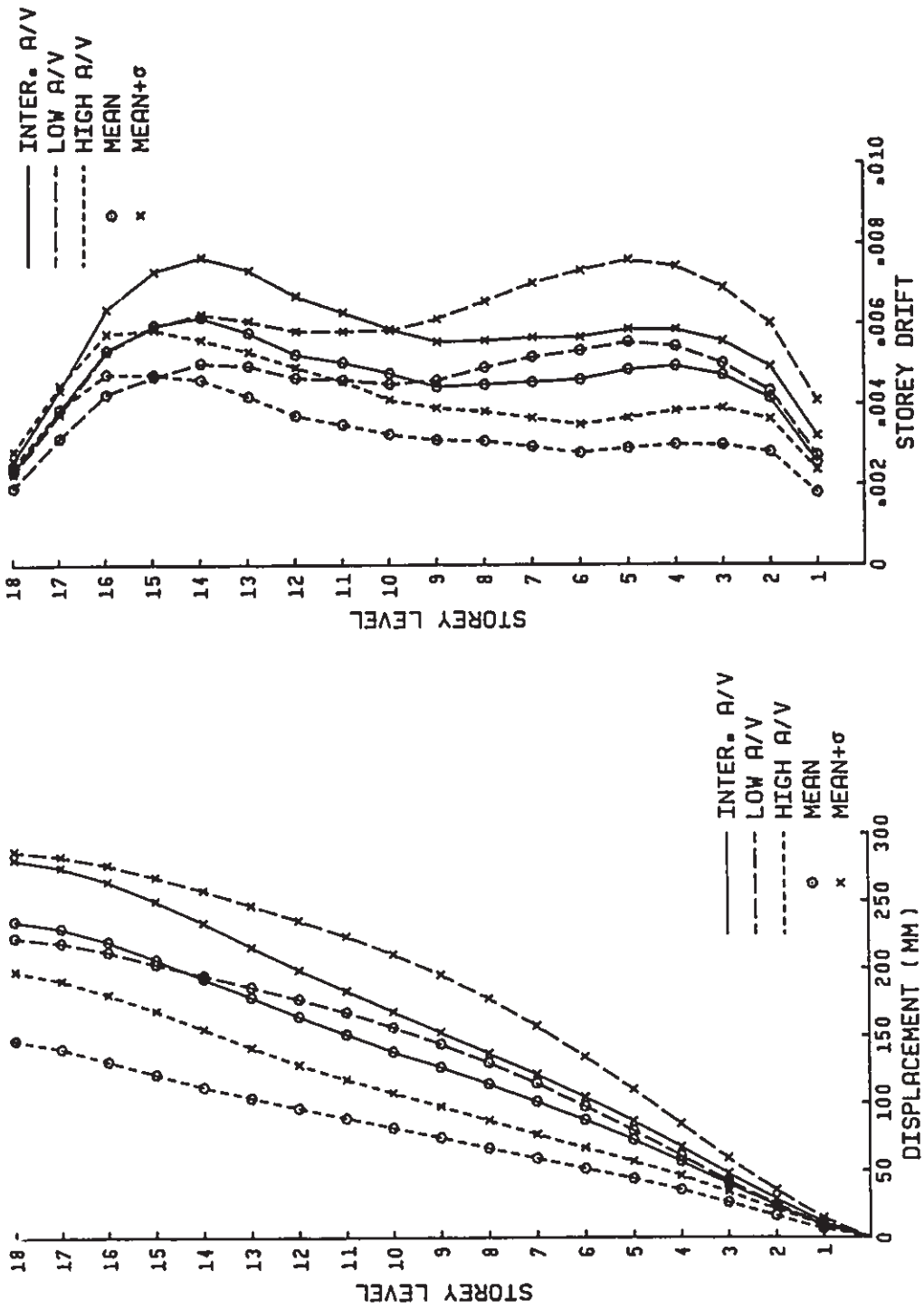

(a) Storey Response Parameters

Fig. 6.7 Mean and Mean+σ Values of Response Parameters for 18S Frame Subjected to Low, Intermediate, and High A/V Groups of Ground Motions Scaled to a Common Peak Velocity of 0.4 m/s

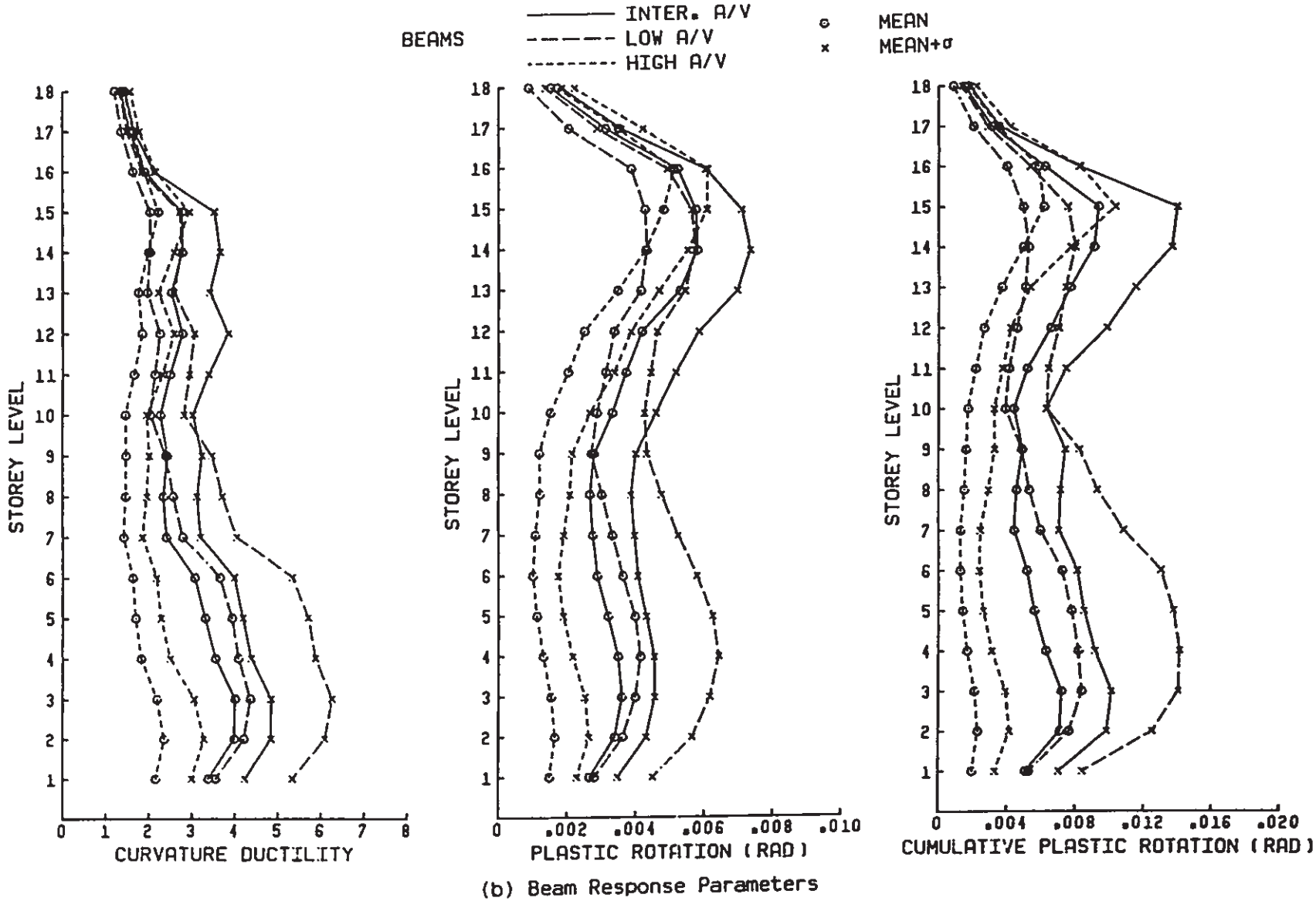

(b) Beam Response Parameters

Fig. 6.7 (cont'd) Mean and Mean+σ Values of Response Parameters for 18S Frame Subjected to Low, Intermediate, and High A/V Groups of Ground Motions Scaled to a Common Peak Velocity of 0.4 m/s

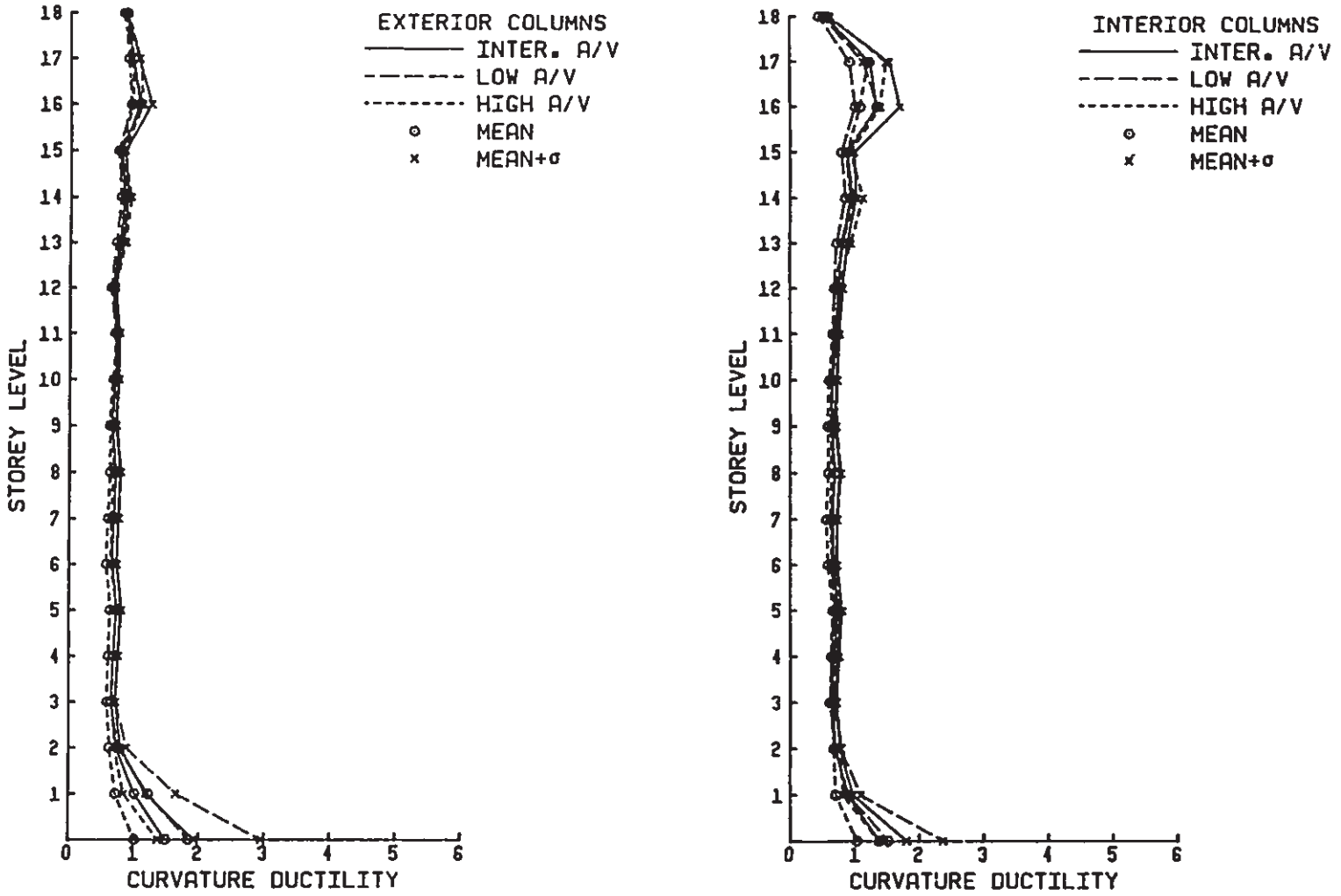

(c) Column Response Parameters

Fig. 6.7 (cont'd) Mean and Mean+σ Values of Response Parameters for 18S Frame Subjected to Low, Intermediate, and High A/V Groups of Ground Motions Scaled to a Common Peak Velocity of 0.4 m/s

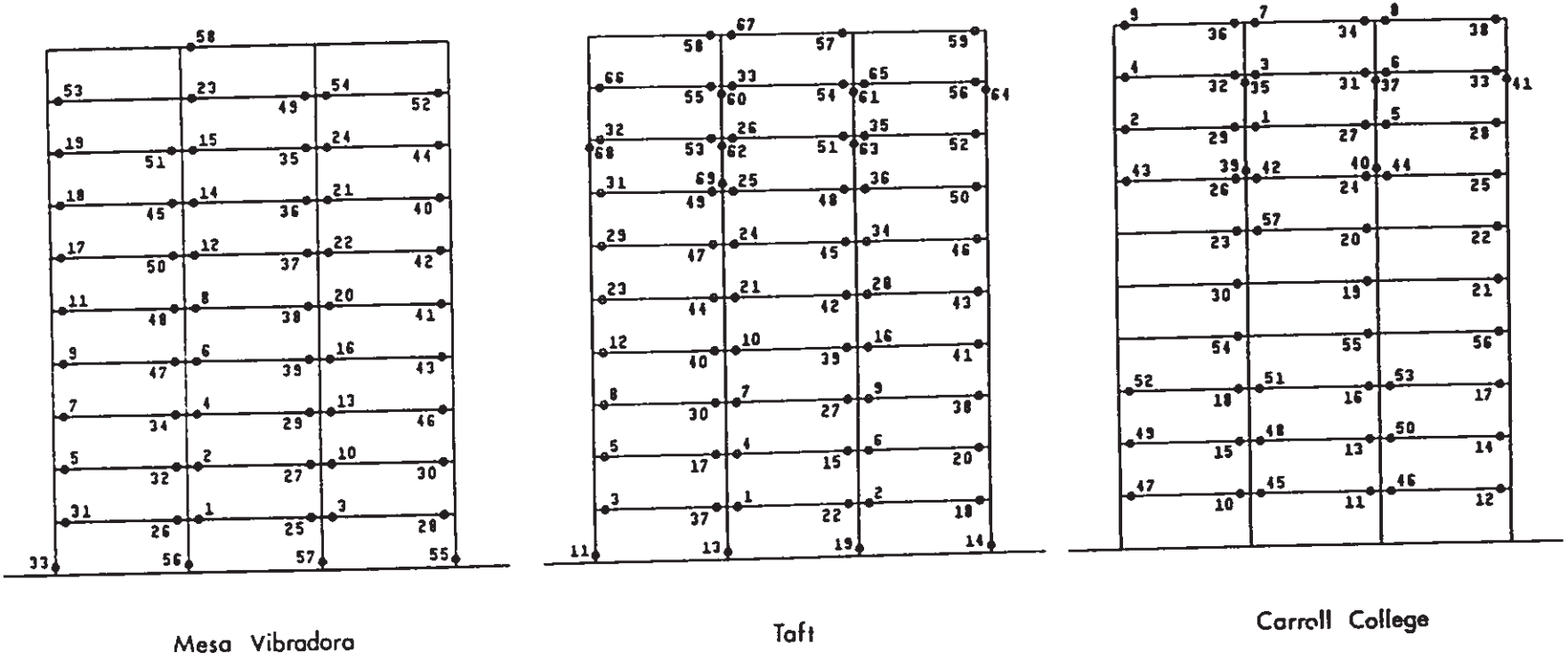

Fig. 6.8 Sequence of Plastic Hinge Formation for 10S Frame Resulting from (a) Mesa Vibradora; (b) Taft; and (c) Carroll College Records Scaled to a Peak Velocity of 0.4 m/s

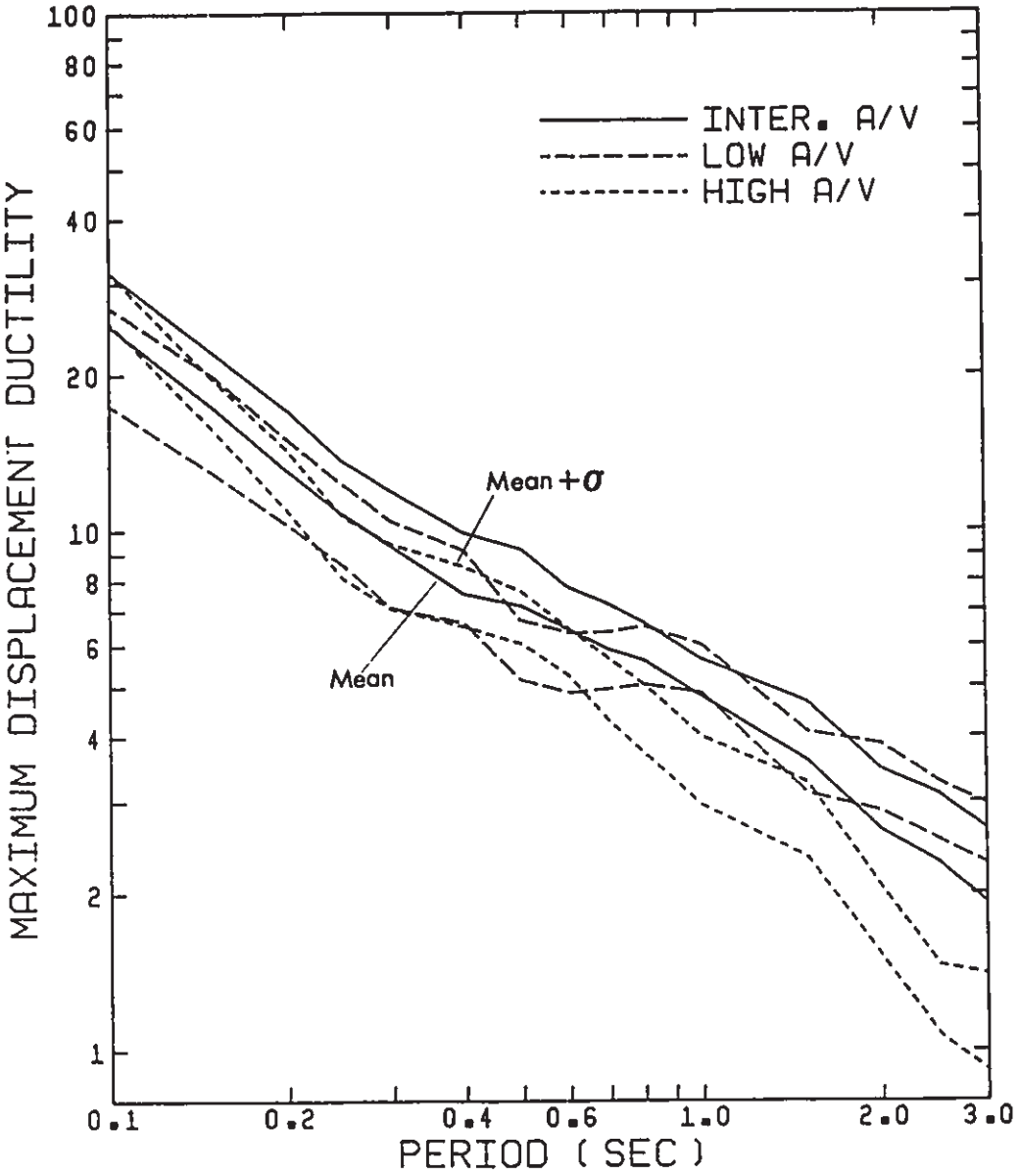

Fig. 6.9 Mean and Mean+σ Values of Maximum Displacement Ductility Demand for SDOF Systems Designed Based on NBCC 1985

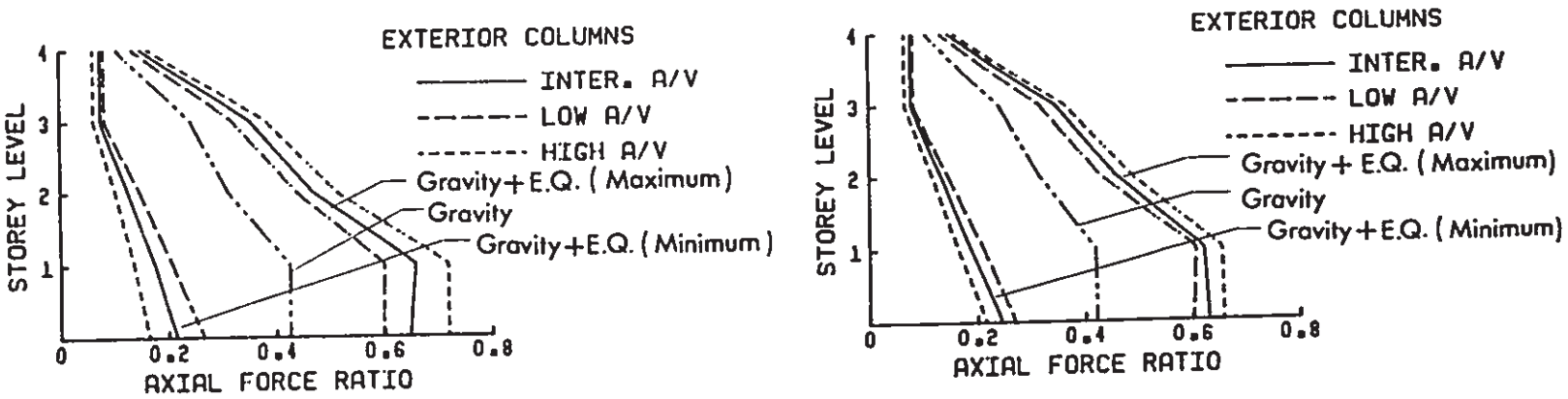

(a) 4S1 Frames

(b) 4S2 Frames

Fig. 6.10 Ratios of Mean Column Axial Forces Resulting from Gravity and Seismic Loading to Balanced Axial Forces for 4S1, 4S2, 10S, and 18S Frames

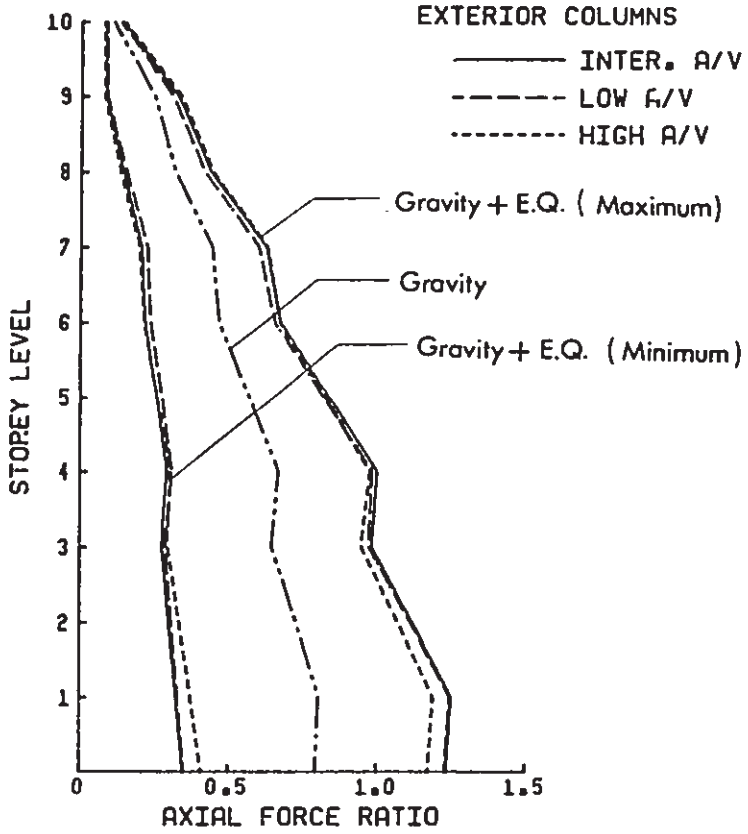

(c) 10S Frame

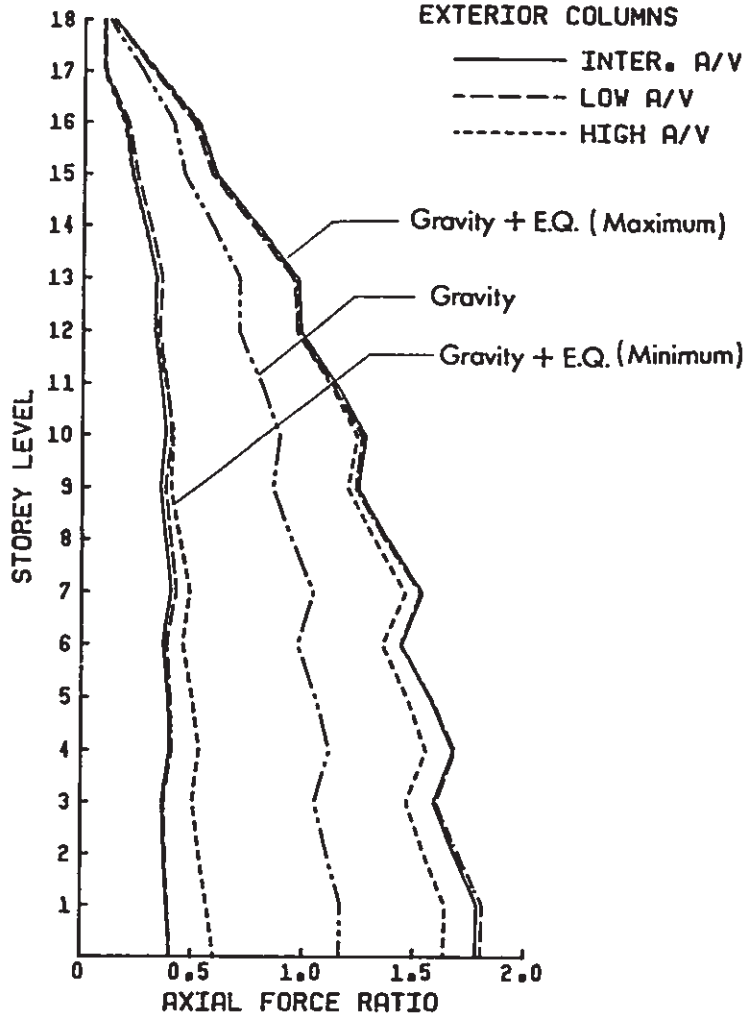

(d) 18S Frame

Fig. 6.10 (cont'd) Ratios of Mean Column Axial Forces Resulting from Gravity and Seismic Loading to Balanced Axial Forces for 4S1, 4S2, 10S, and 18S Frames

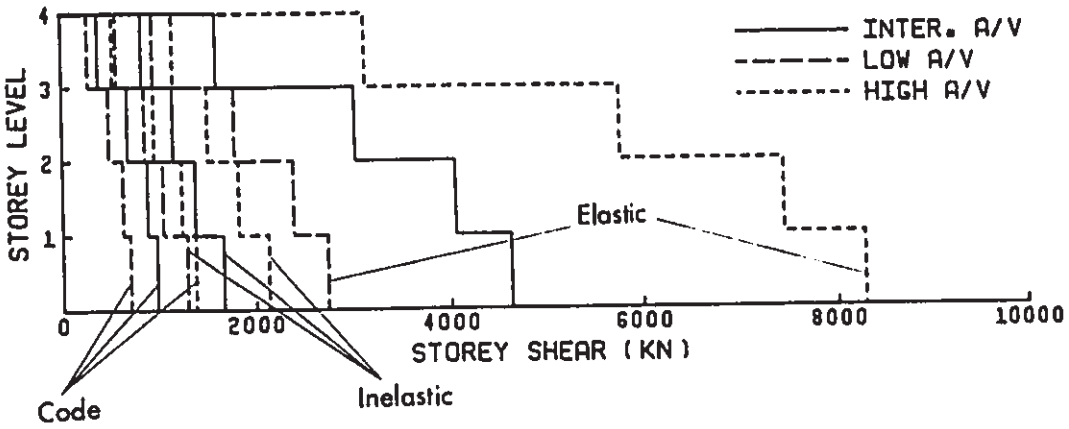

(a) 4S1 Frames

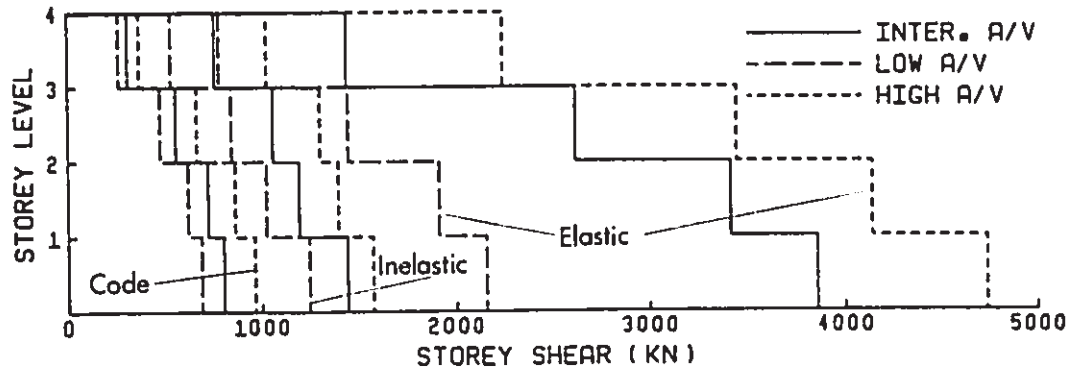

(b) 4S2 Frames

Fig. 6.11 Comparison of Design Storey Shears with Mean Values of Maximum Inelastic and Elastic Dynamic Storey Shears for 4S1, 4S2, 10S, and 18S Frames

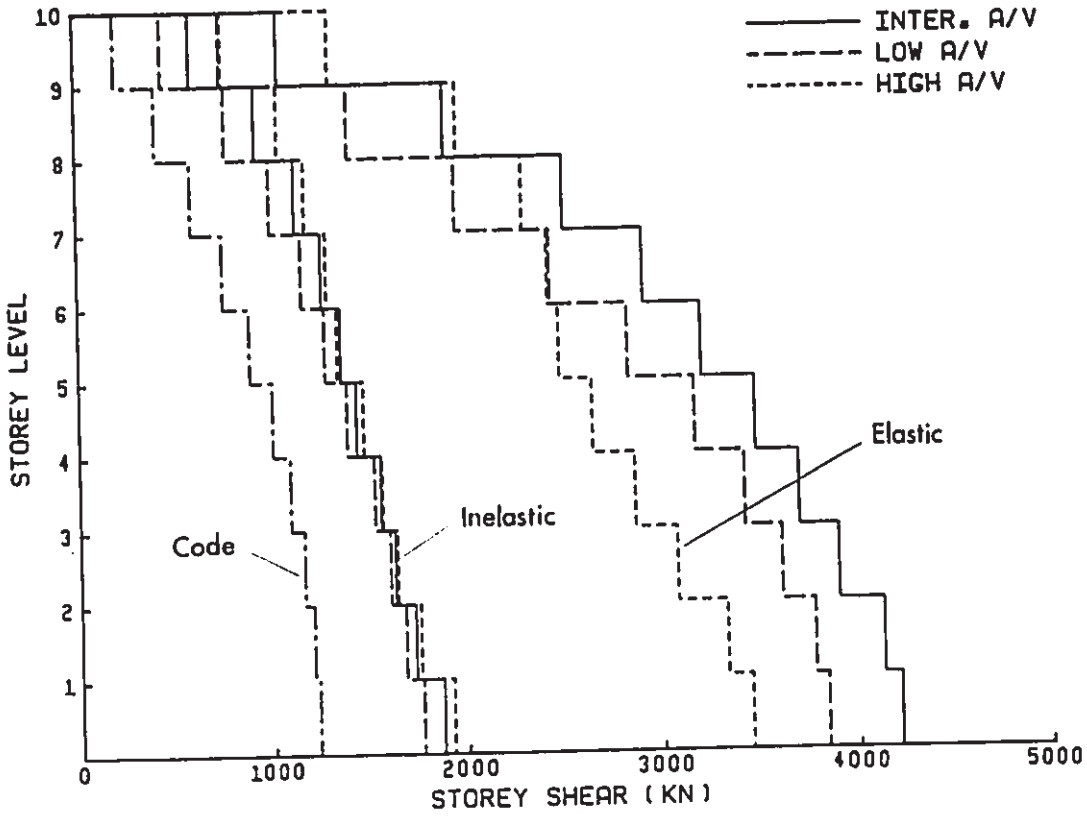

(c) 10S Frame

Fig. 6.11 (cont'd) Comparison of Design Storey Shears with Mean Values of Maximum Inelastic and Elastic Dynamic Storey Shears for 4S1, 4S2, 10S, and 18S Frames

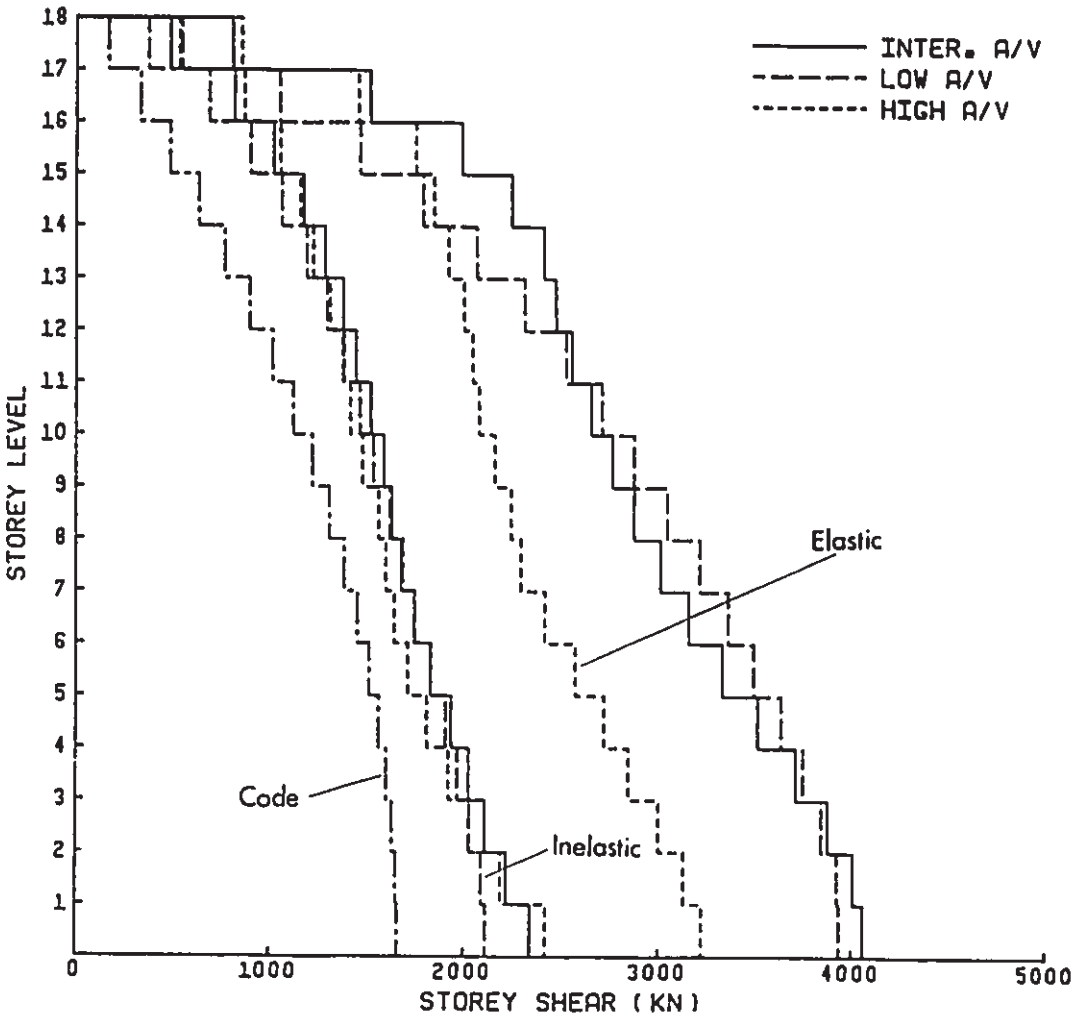

(d) 18S Frame

Fig. 6.11 (cont'd) Comparison of Design Storey Shears with Mean Values of Maximum Inelastic and Elastic Dynamic Storey Shears for 4S1, 4S2, 10S, and 18S Frames

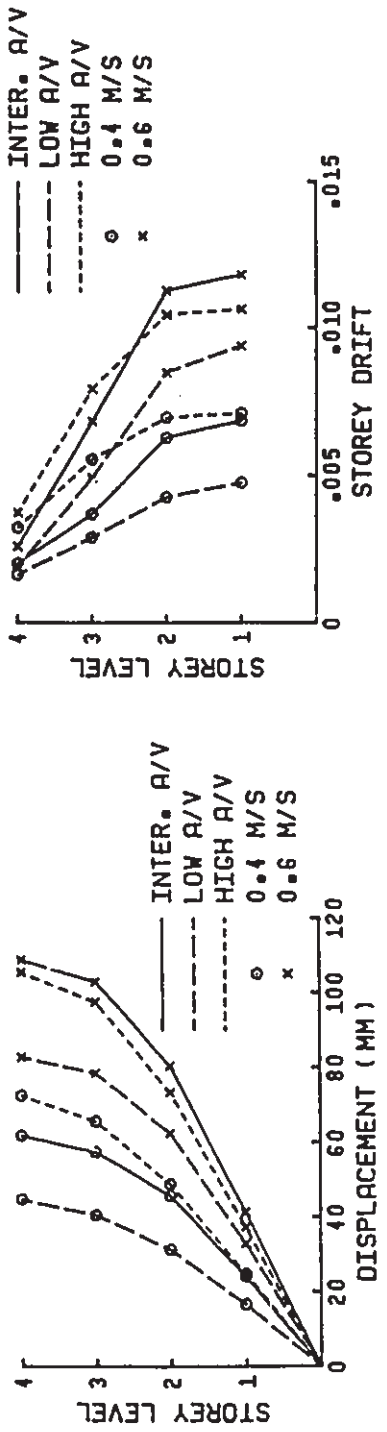

(a) Storey Response Parameters

Fig. 6.12 Comparison of Mean±σ Values of Response Parameters between Two Peak Ground Velocity Levels of 0.4 and 0.6 m/s for 452 Frames

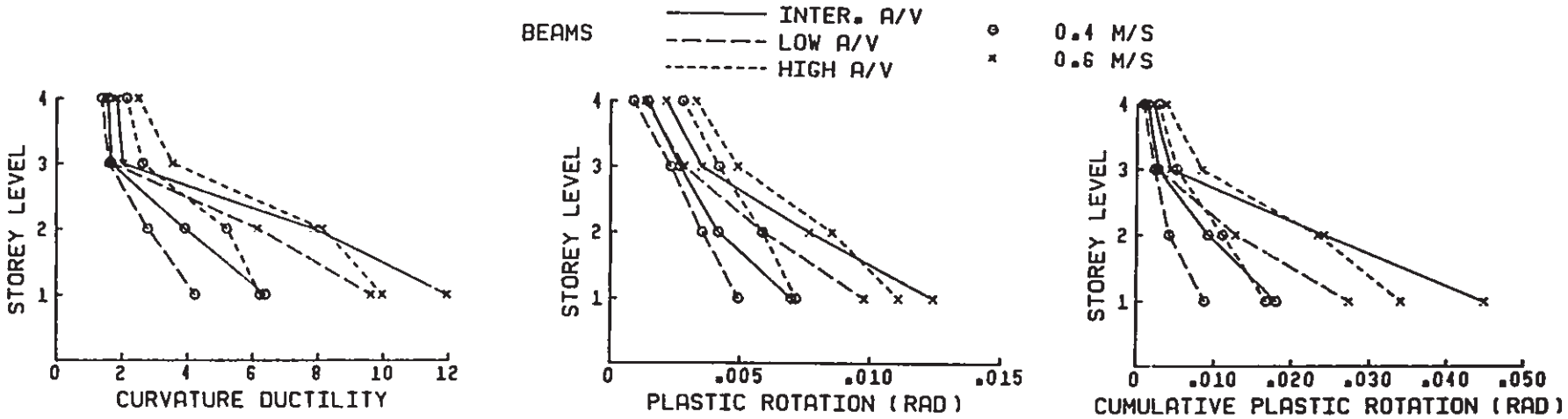

(b) Beam Response Parameters

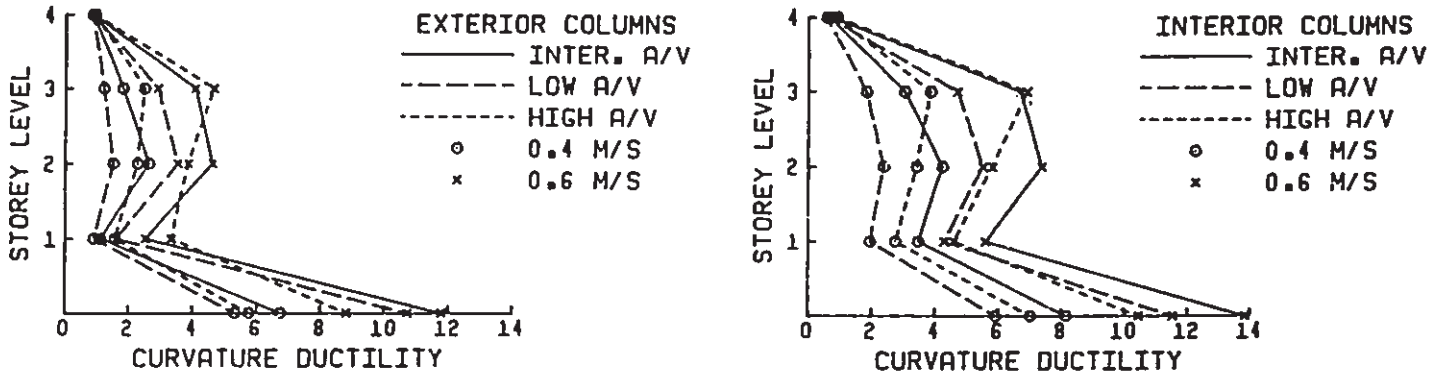

(c) Column Response Parameters

Fig. 6.12 (cont'd) Comparison of Mean+σ Values of Response Parameters between Two Peak Ground Velocity Levels of 0.4 and 0.6 m/s for 4S2 Frames

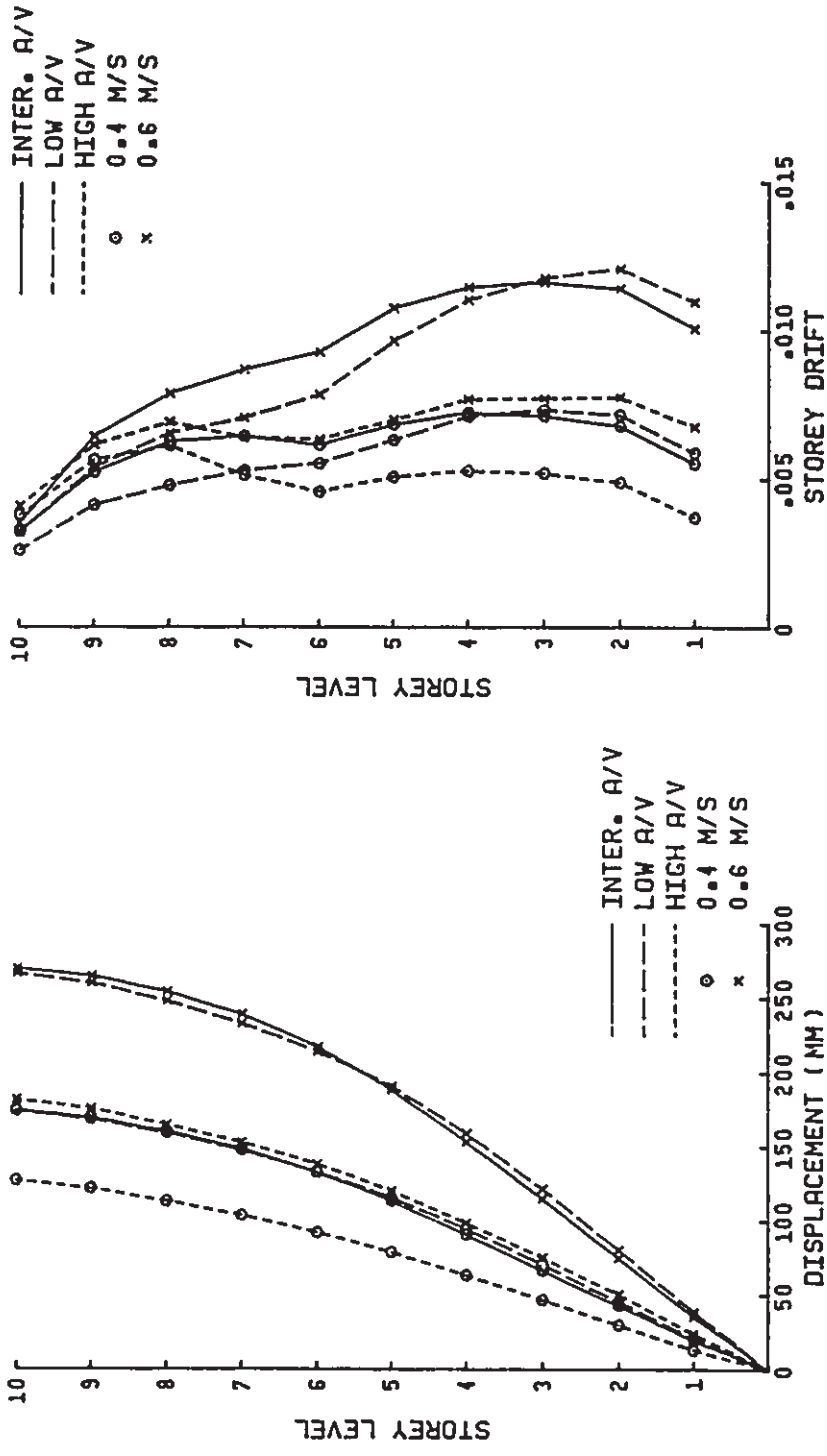

(a) Storey Response Parameters

Fig. 6.13 Comparison of Meanσ Values of Response Parameters between Two Peak Ground Velocity Levels of 0.4 and 0.6 m/s for 10S Frame

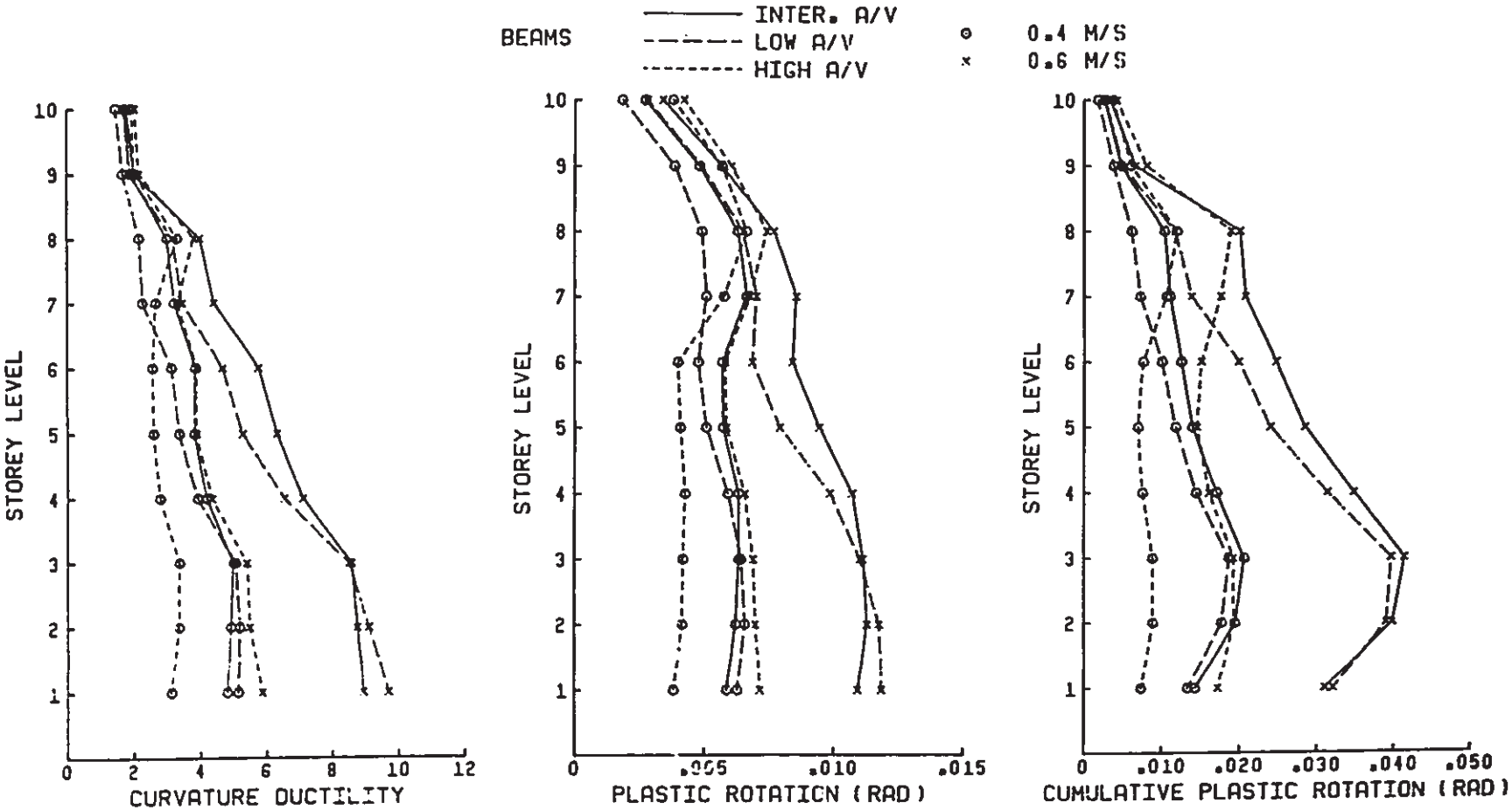

(b) Beam Response Parameters

Fig. 6.13 (cont'd) Comparison of Mean±σ Values of Response Parameters between Two Peak Ground Velocity Levels of 0.4 and 0.6 m/s for 10S Frame

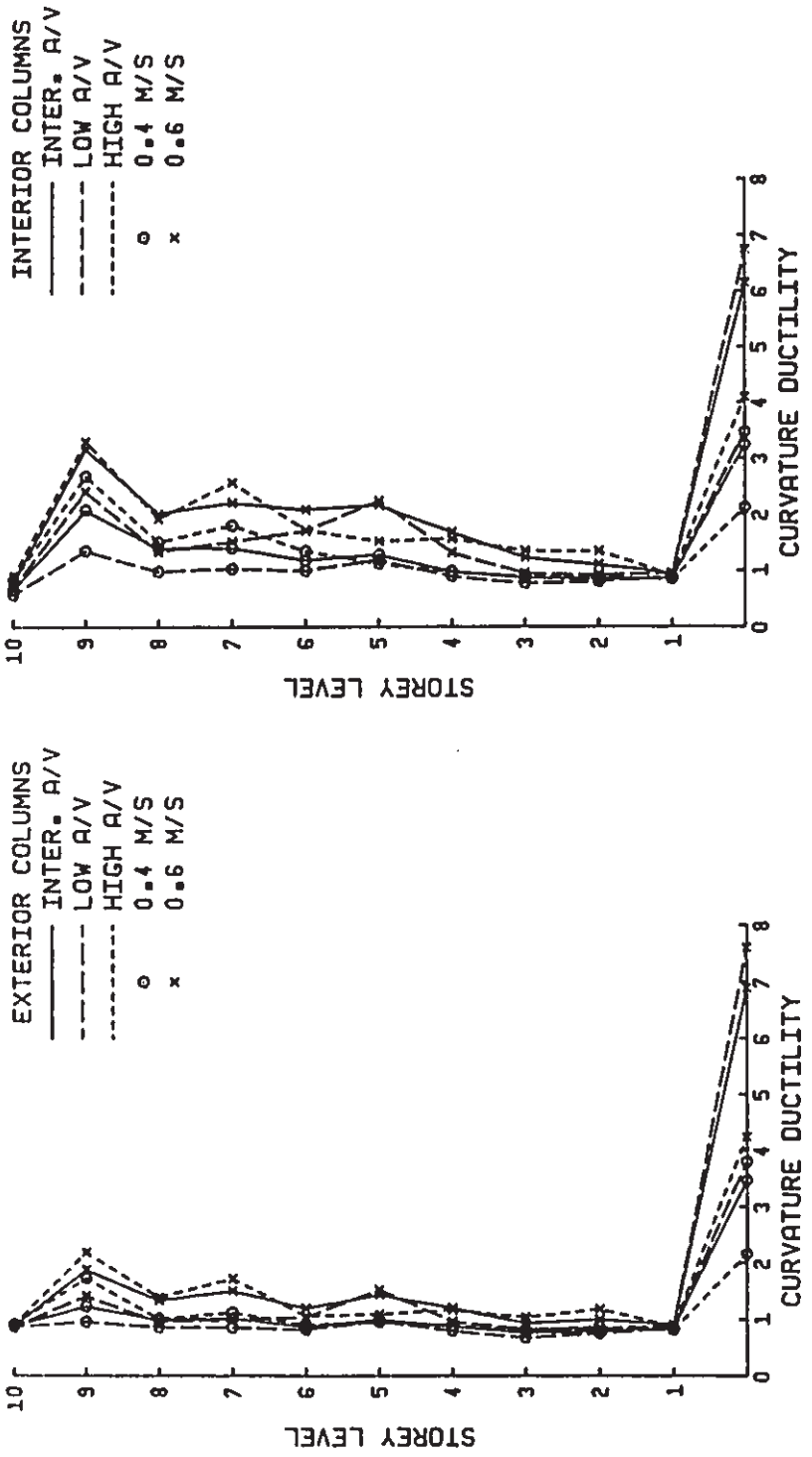

(c) Column Response Parameters

Fig. 6.13 (cont'd) Comparison of Mean+σ Values of Response Parameters between Two Peak Ground Velocity Levels of 0.4 and 0.6 m/s for 10S Frame

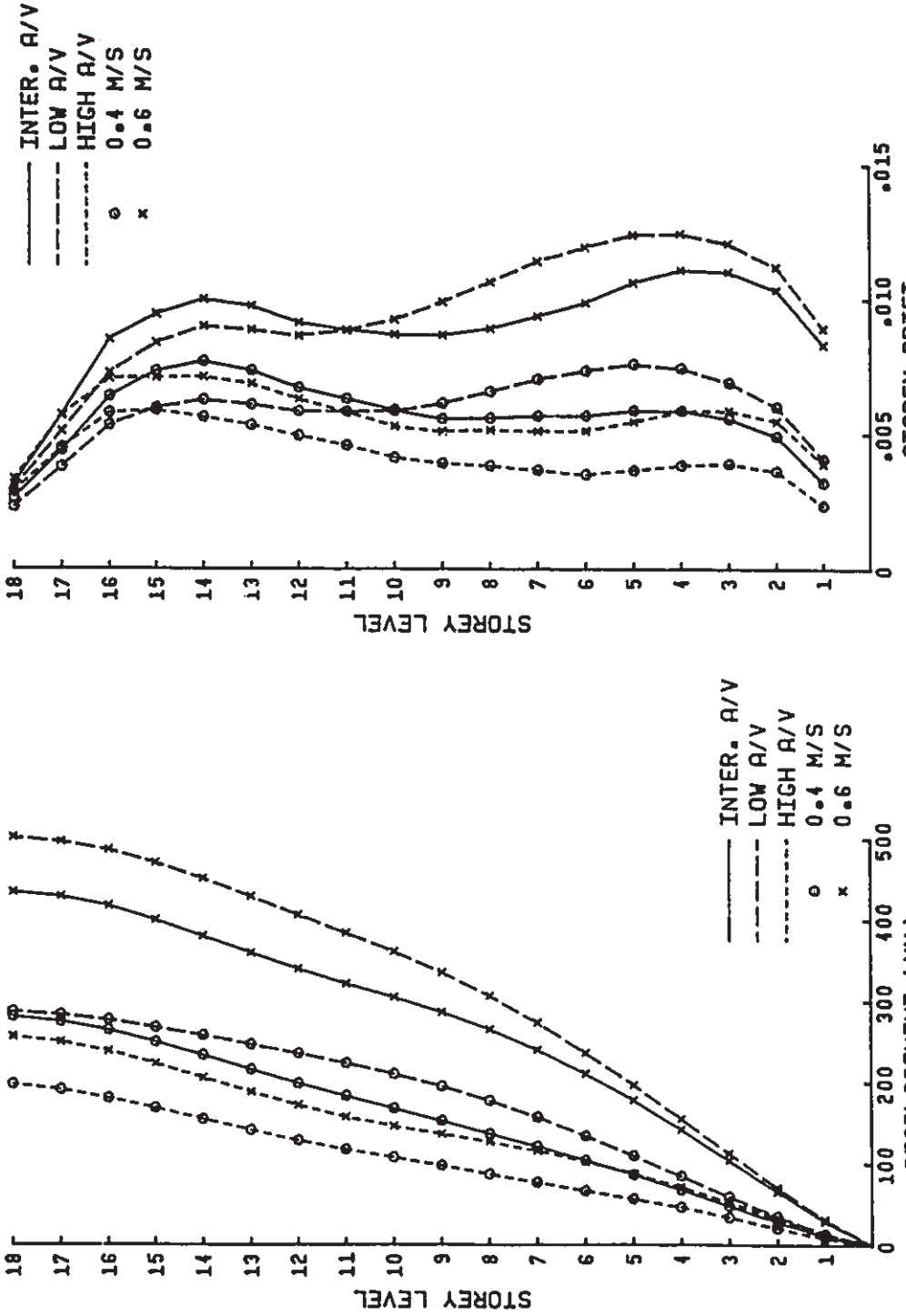

(a) Storey Response Parameters

Fig. 6.14 Comparison of Mean+σ Values of Response Parameters between Two Peak Ground Velocity Levels of 0.4 and 0.6 m/s for 18S Frame

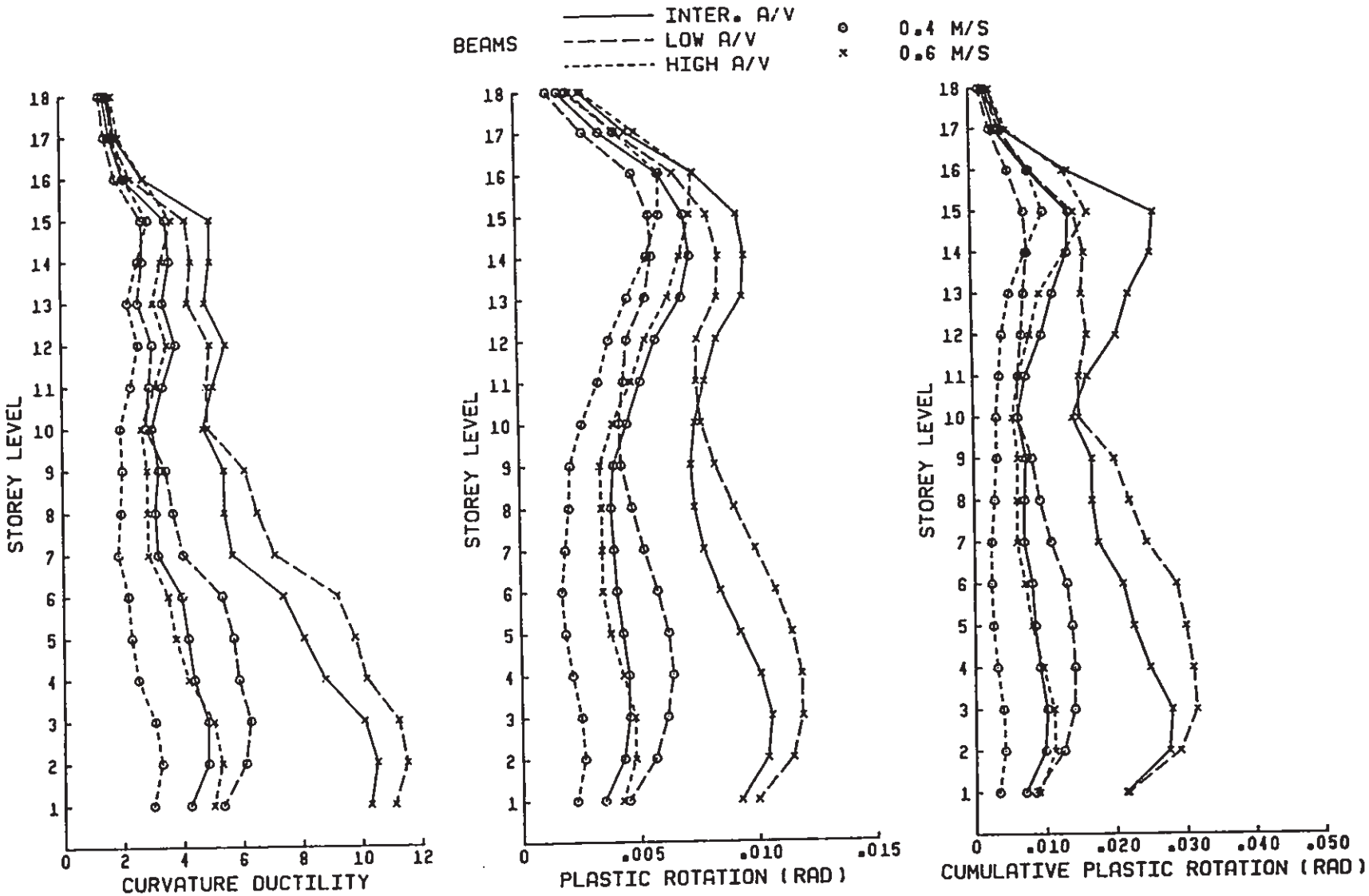

(b) Beam Response Parameters

Fig. 6.14 (cont'd) Comparison of Mean+σ Values of Response Parameters between Two Peak Ground Velocity Levels of 0.4 and 0.6 m/s for 18S Frame

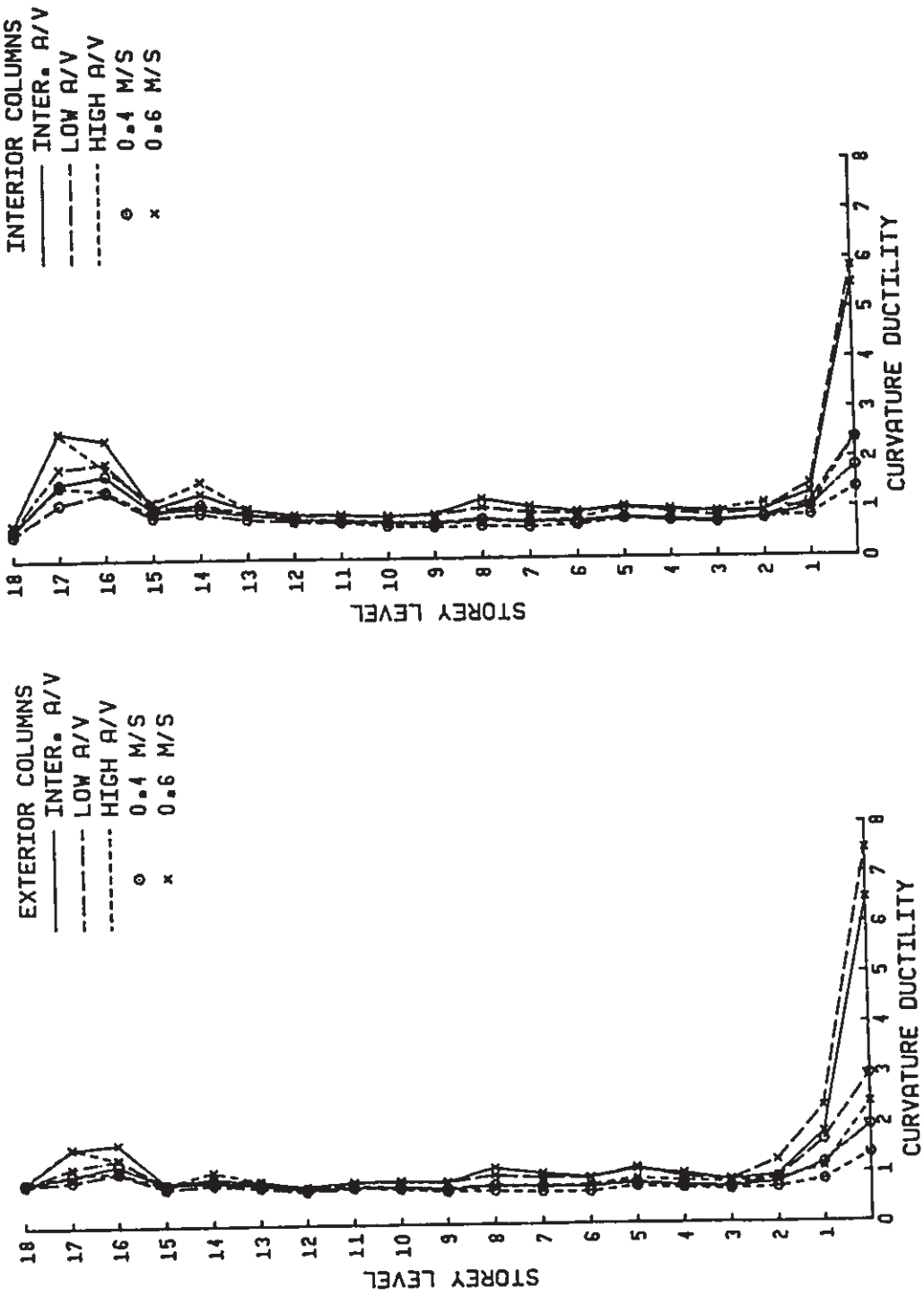

(c) Column Response Parameters

Fig. 6.14 (cont'd) Comparison of Mean+σ Values of Response Parameters between Two Peak Ground Velocity Levels of 0.4 and 0.6 m/s for 18S Frame

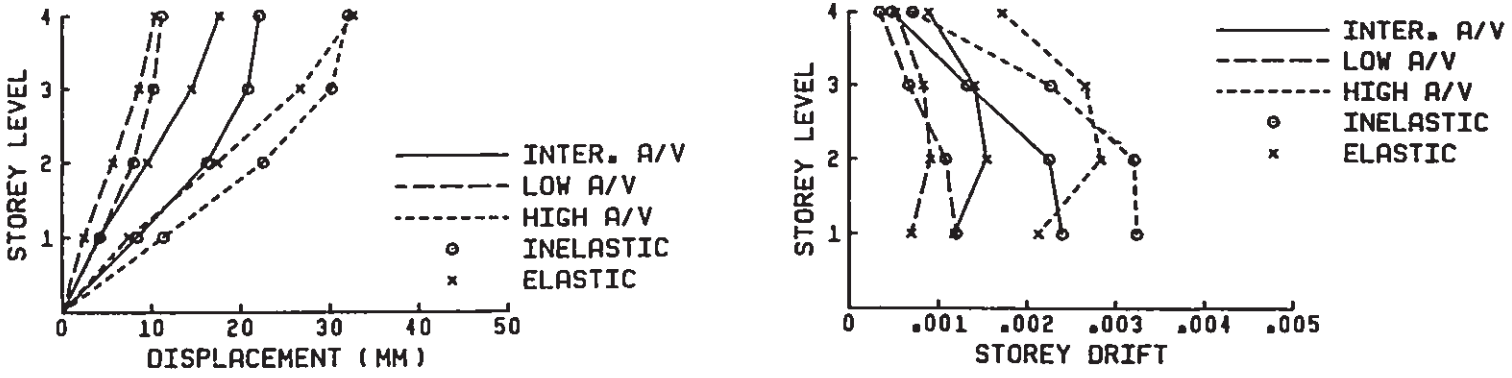

(a) 4S1 Frames

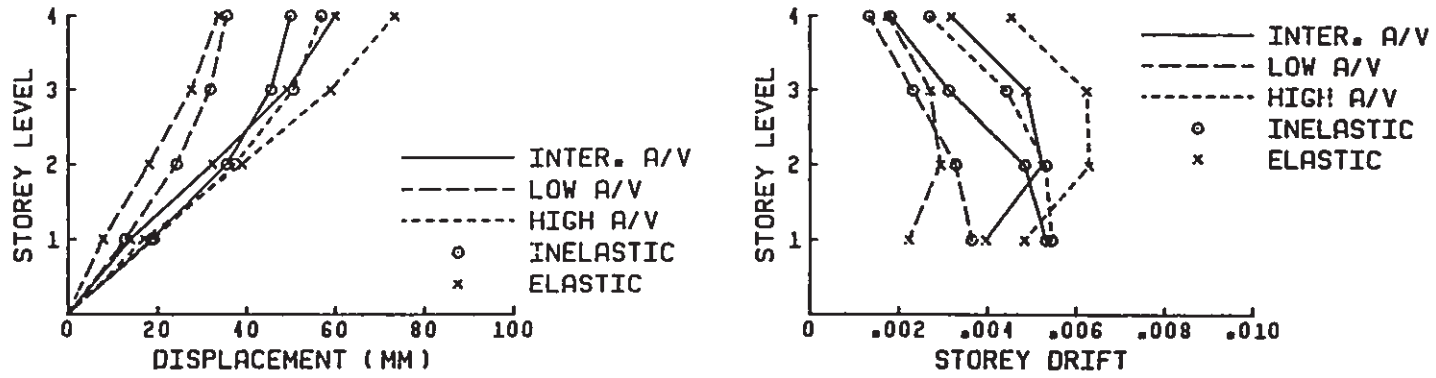

(b) 4S2 Frames

Fig. 6.15 Comparison of Mean Storey Displacements and Interstorey Drifts between Inelastic and Elastic Responses for 4S1, 4S2, 10S, and 18S Frames

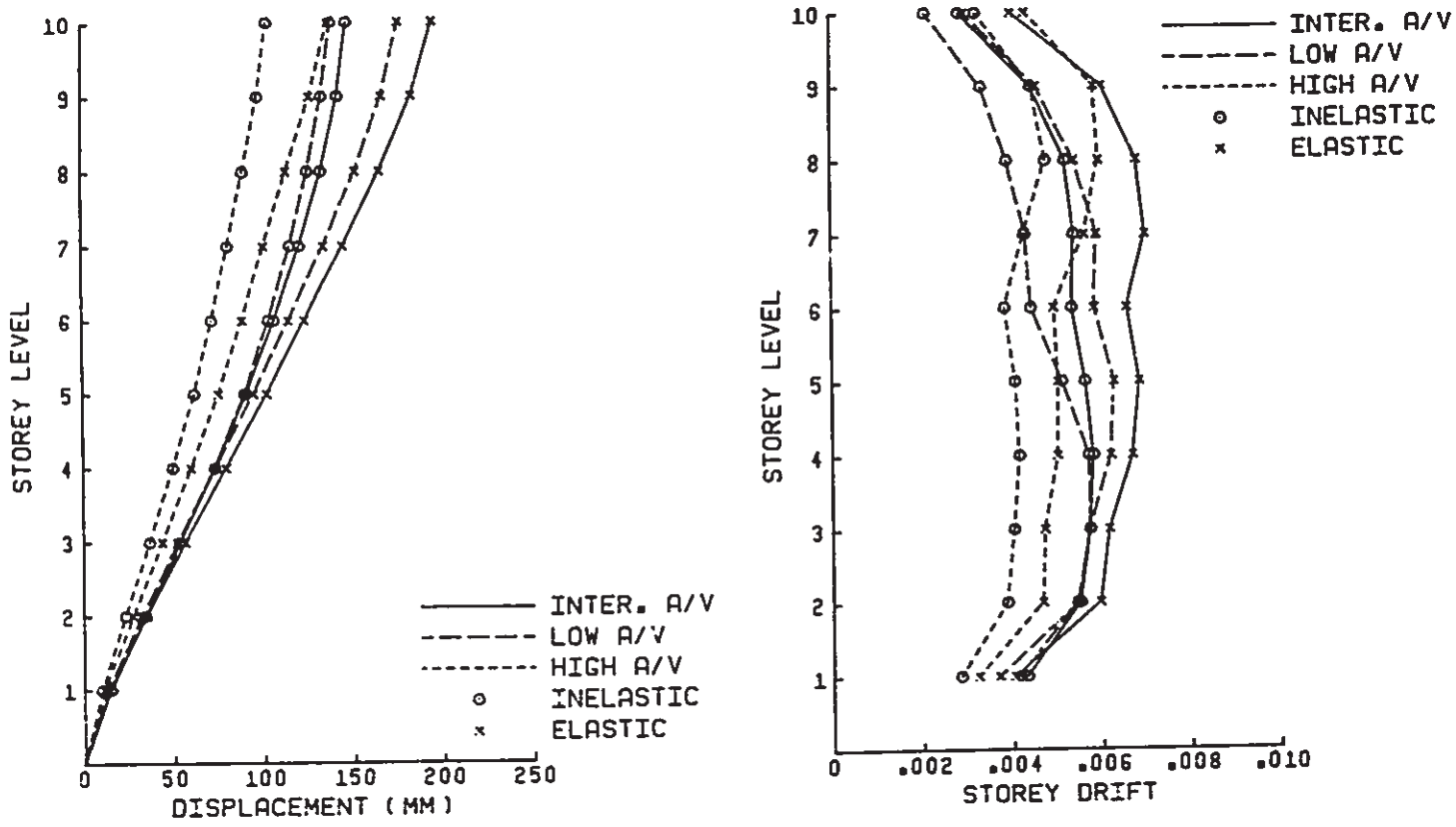

(c) 10S Frame

Fig. 6.15 (cont'd) Comparison of Mean Storey Displacements and Interstorey Drifts between Inelastic and Elastic Responses for 4S1, 4S2, 10S, and 18S Frames

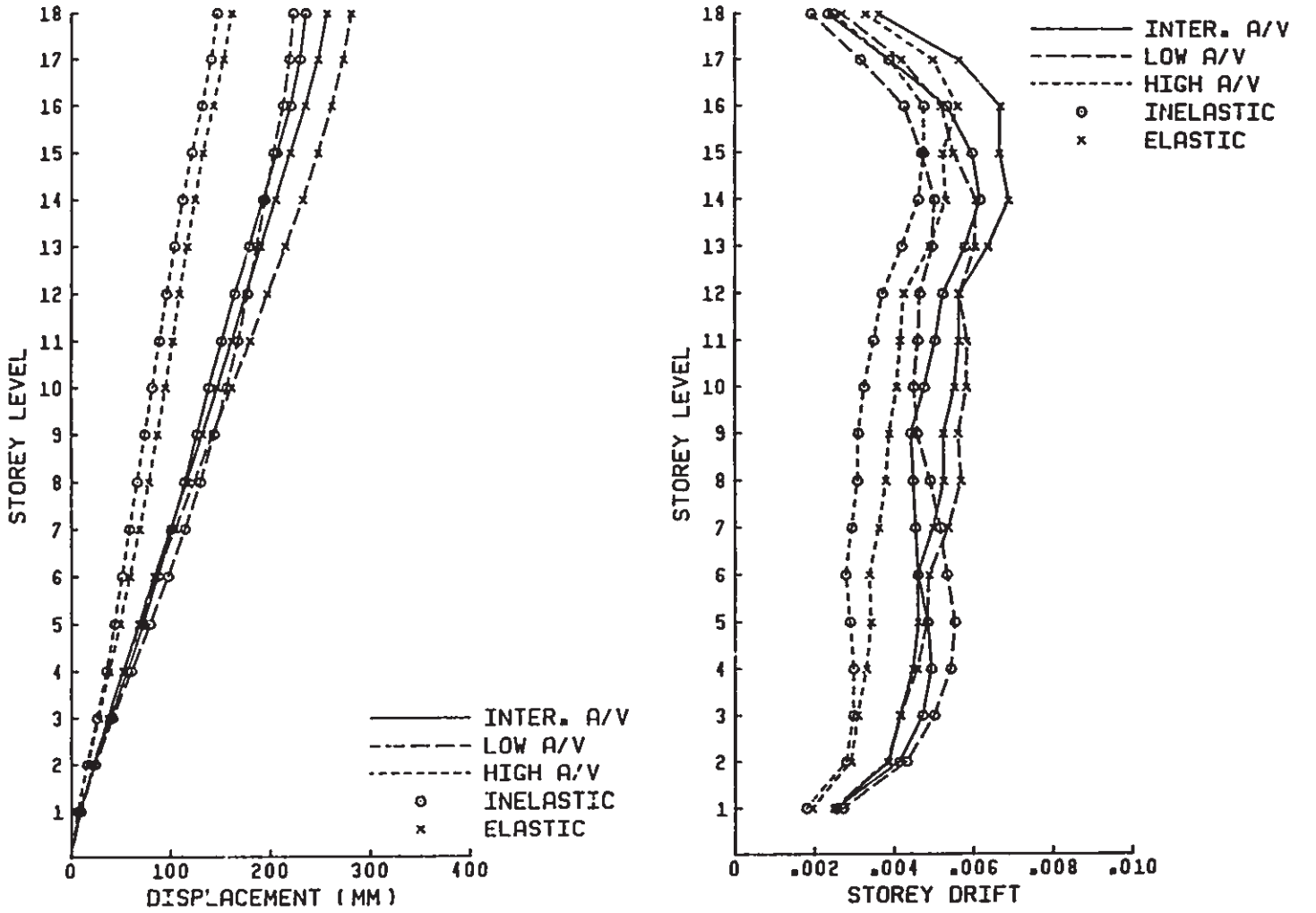

(d) 18S Frame

Fig. 6.15 (cont'd) Comparison of Mean Storey Displacements and Interstorey Drifts between Inelastic and Elastic Responses for 4S1, 4S2, 10S, and 18S Frames

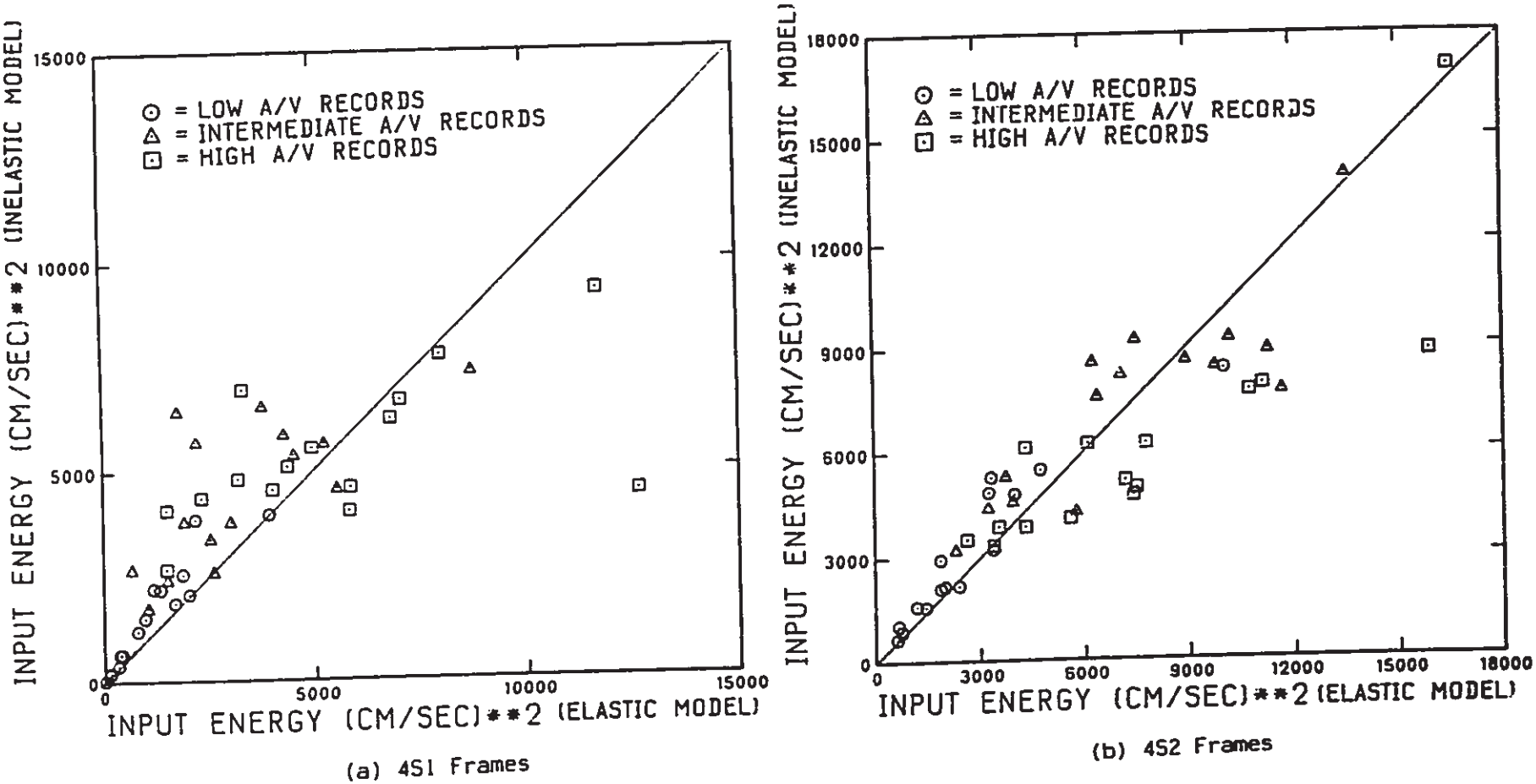

(a) 4S1 Frames

(b) 4S2 Frames

Fig. 6.16 Comparison of Input Energy between Inelastic and Elastic Responses for 4S1, 4S2, 10S, and 18S Frames

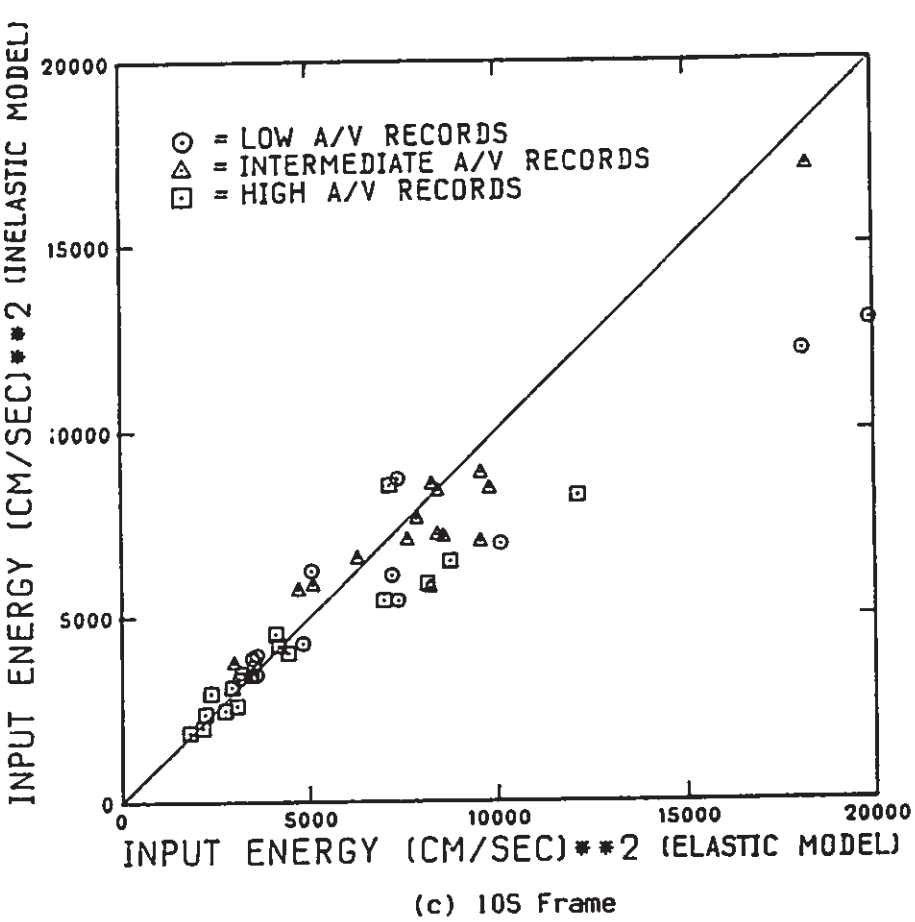

(c) 10S Frame

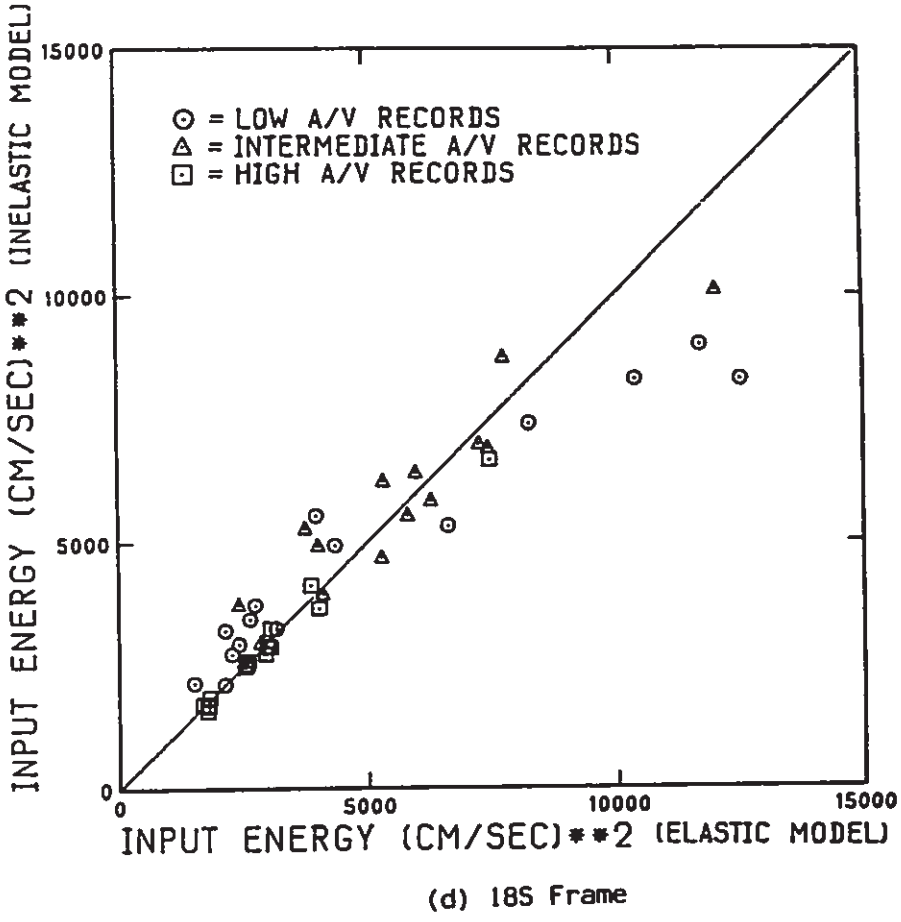

(d) 18S Frame

Fig. 6.16 (cont'd) Comparison of Input Energy between Inelastic and Elastic Responses for 4S1, 4S2, 10S, and 18S Frames

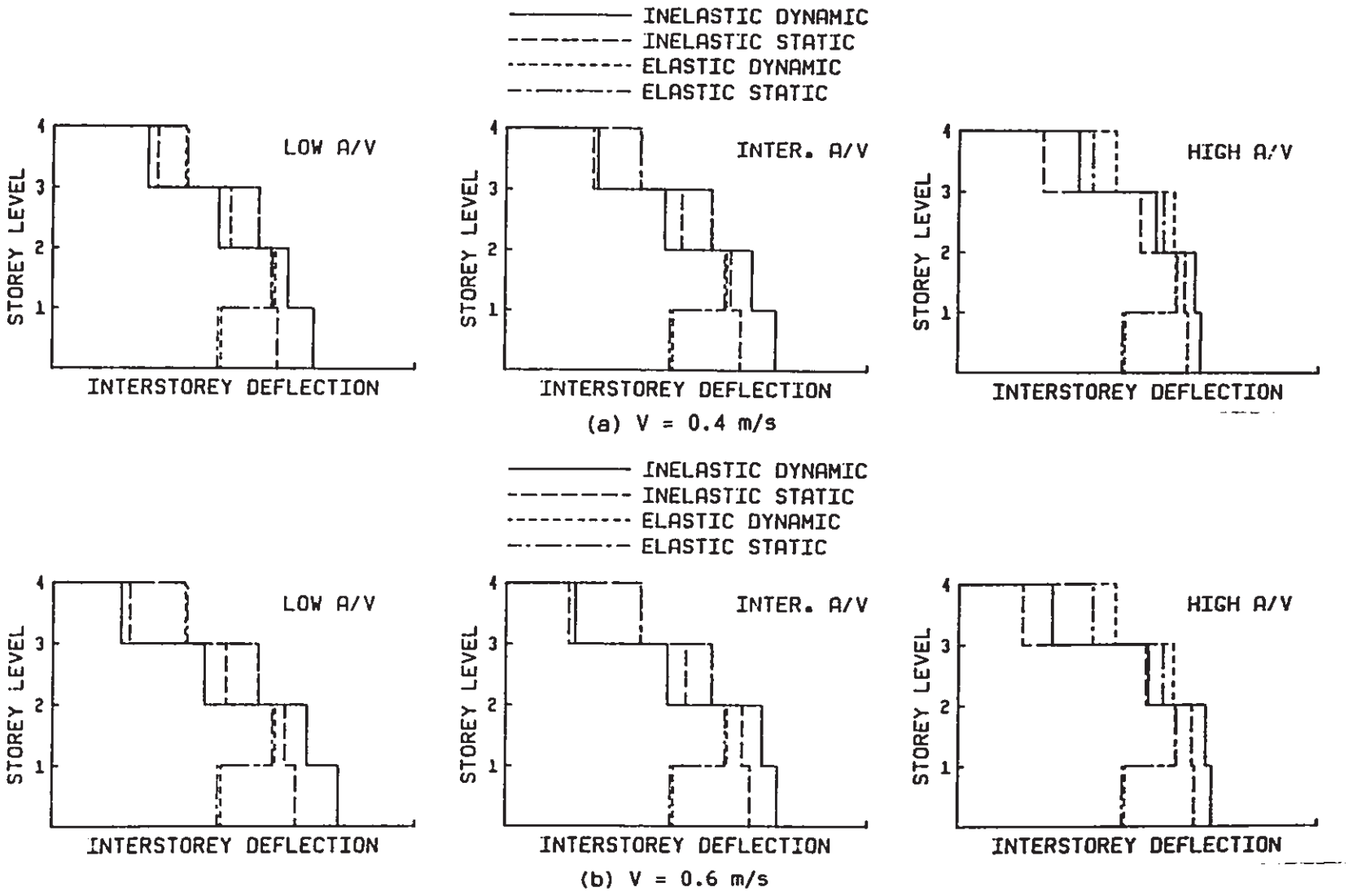

Fig. 6.17 Comparison of Interstorey Deflection Distributions among Four Different Analyses for 4S2 Frames

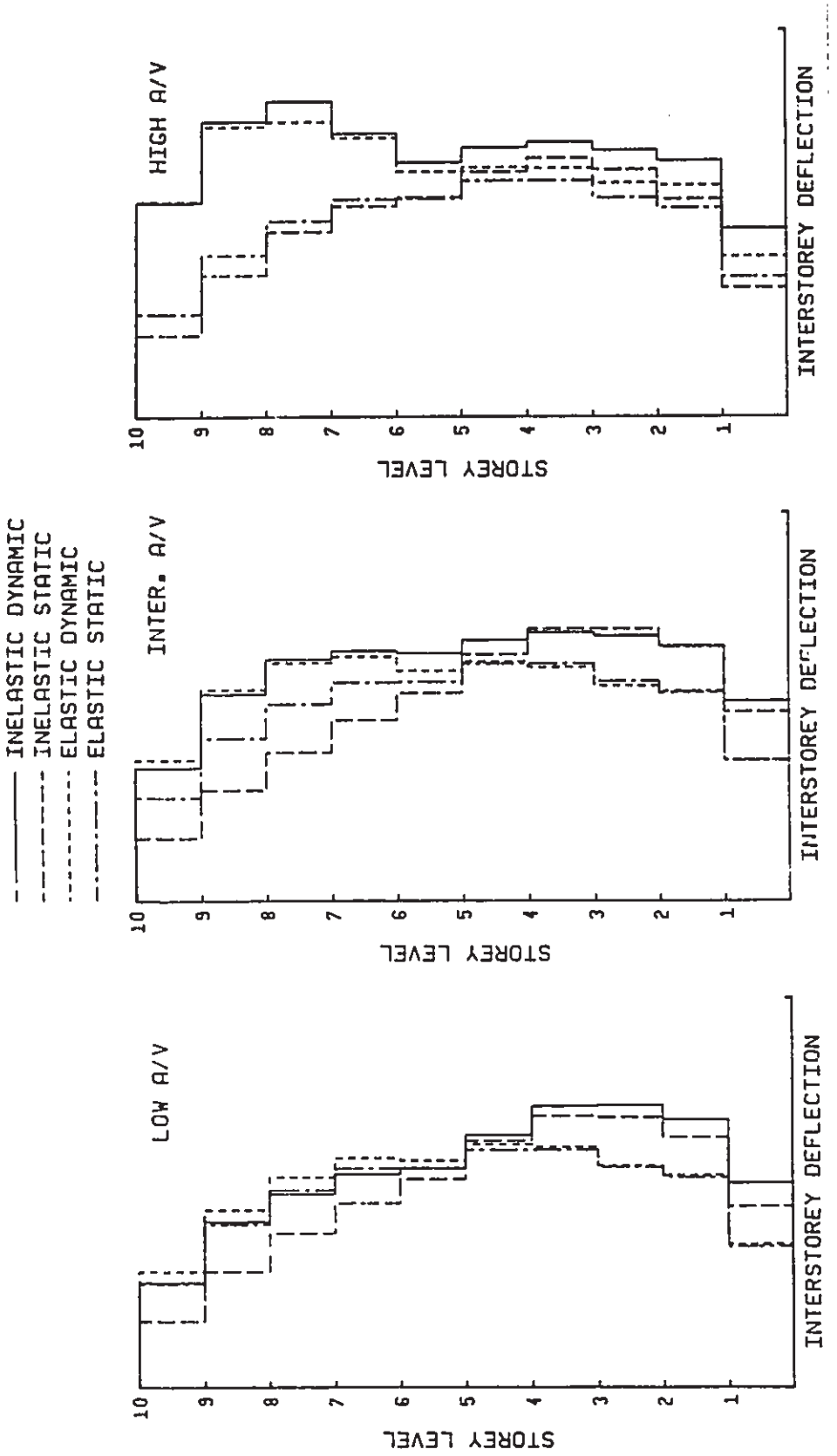

(a) V = 0.4 m/s

Fig. 6.18 Comparison of Interstorey Deflection Distributions among Four Different Analyses for 10S Frame

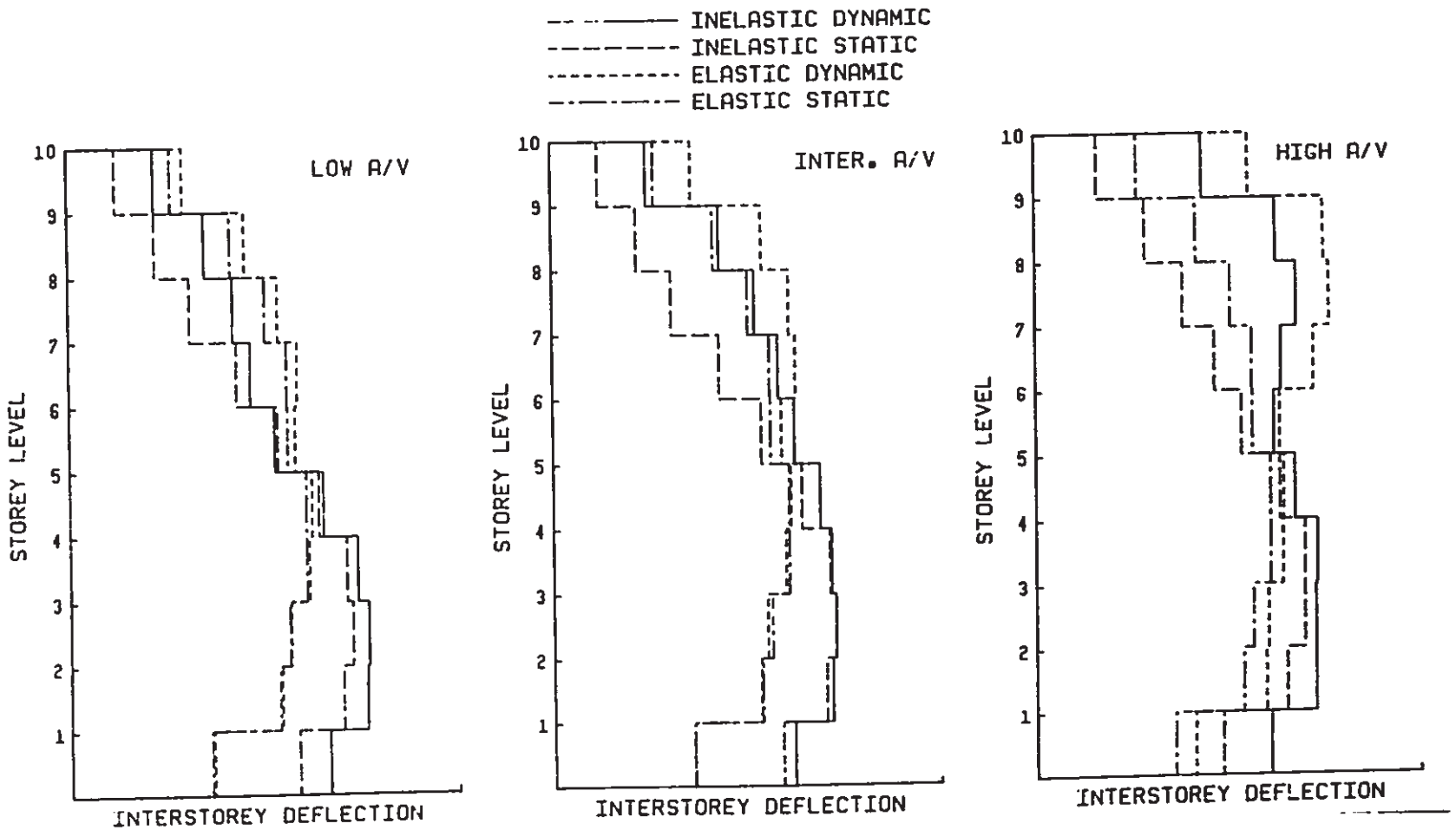

(b) V = 0.6 m/s

Fig. 6.18 (cont'd) Comparison of Interstorey Deflection Distributions among Four Different Analyses for IOS Frame

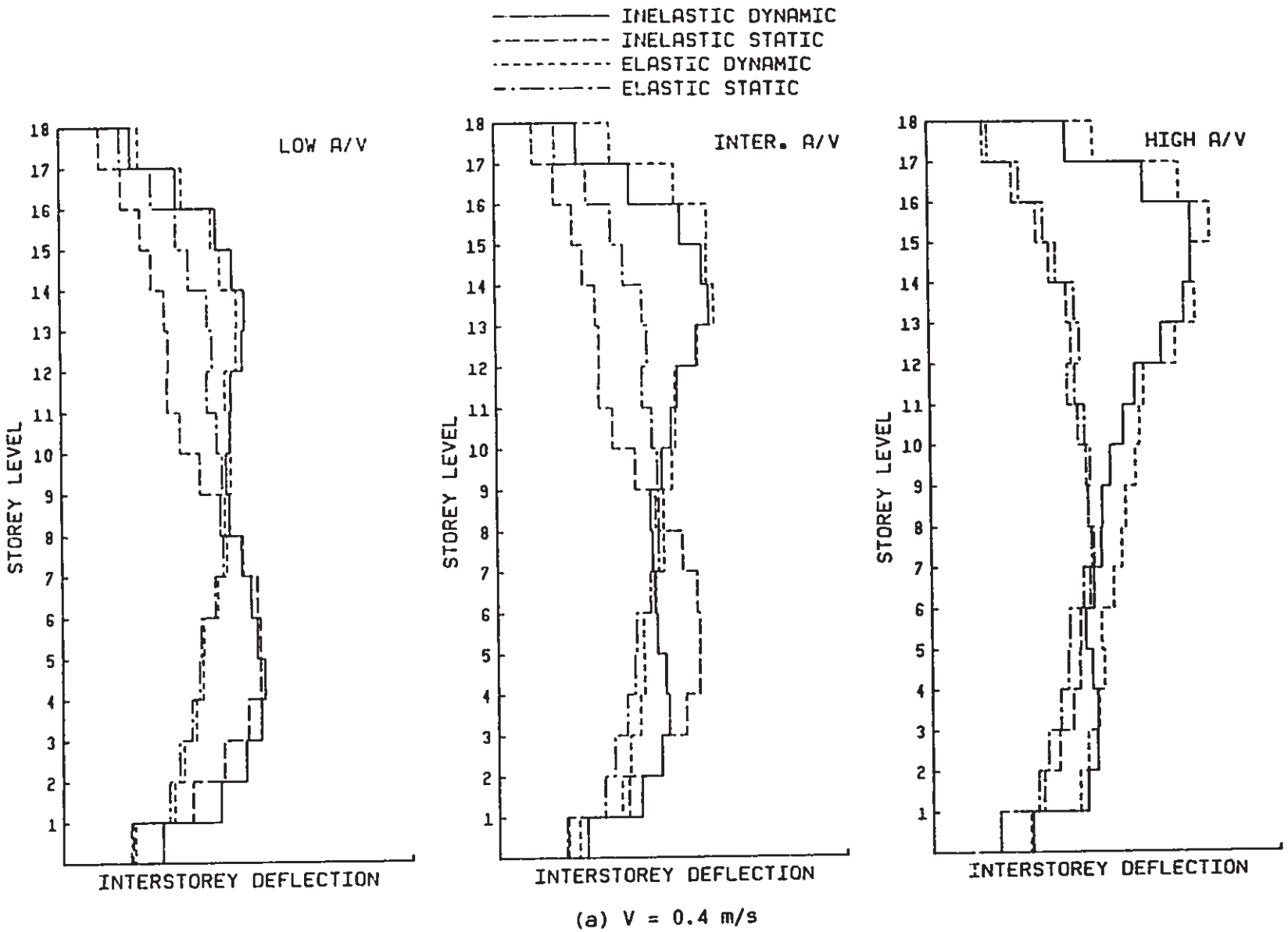

(a) V = 0.4 m/s

Fig. 6.19 Comparison of Interstorey Deflection Distributions among Four Different Analyses for 18S Frame

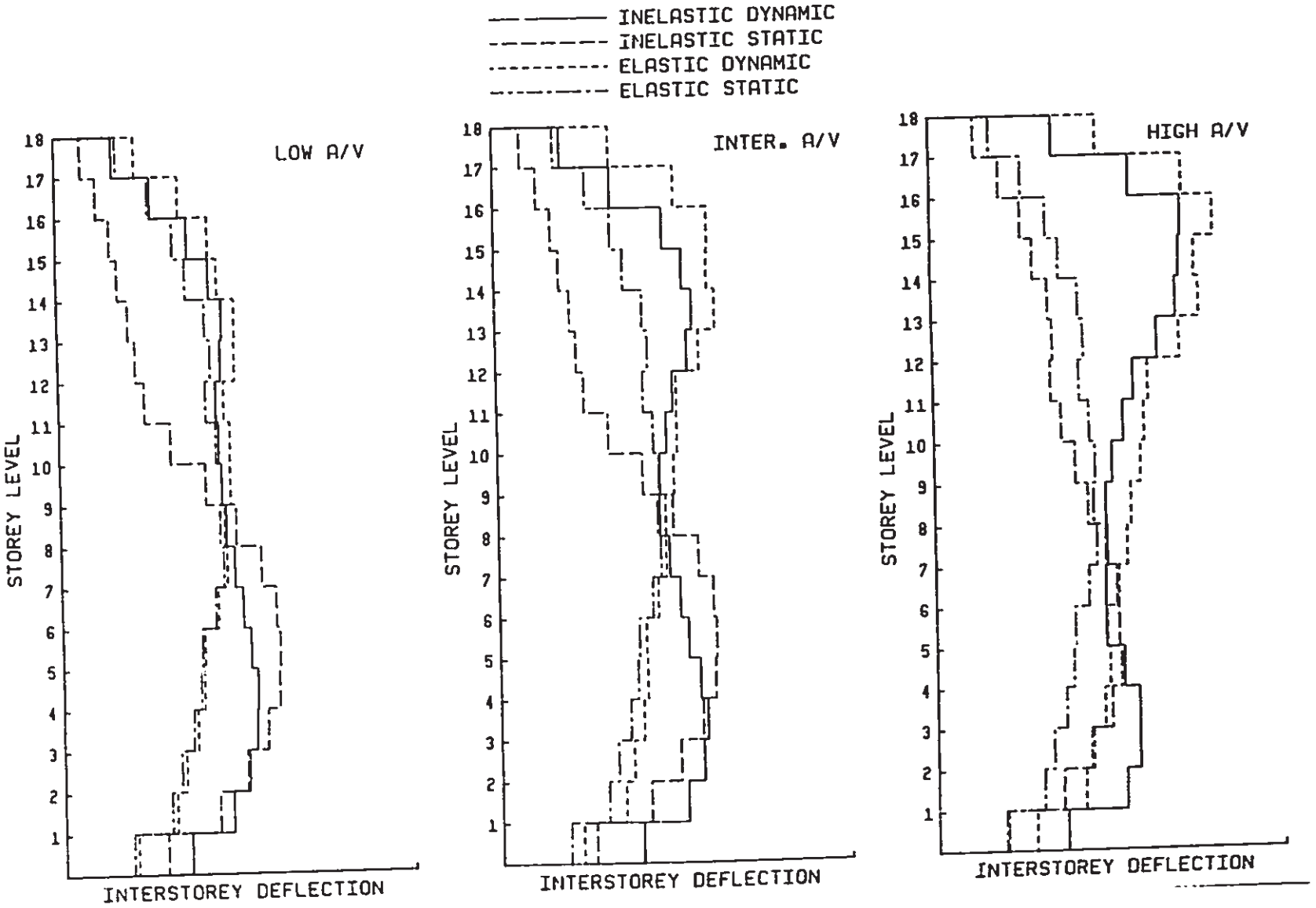

(b) V = 0.6 m/s

Fig. 6.19 (cont'd) Comparison of Interstorey Deflection Distributions among Four Different Analyses for 18S Frame

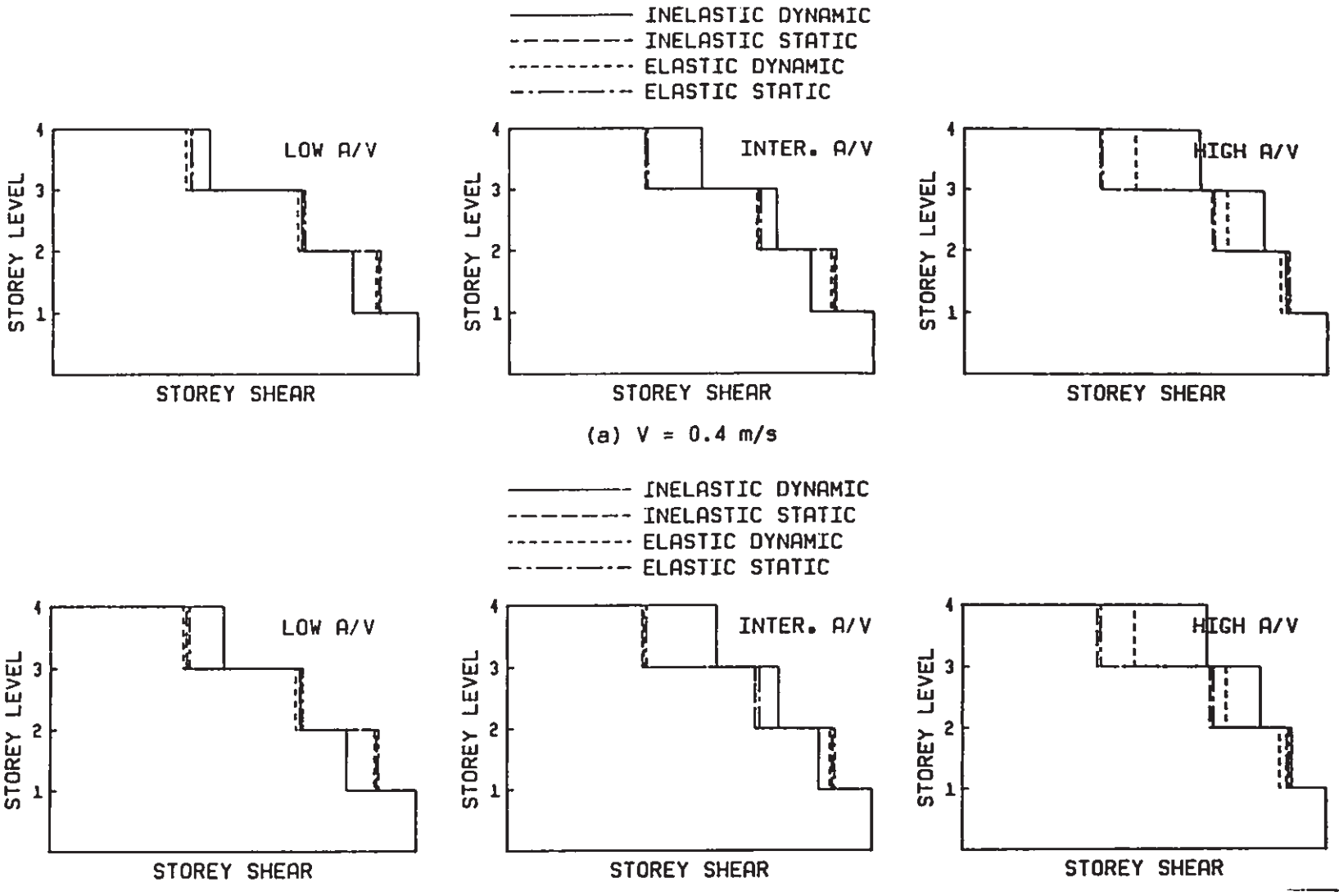

(a) V = 0.4 m/s

(b) V = 0.6 m/s

Fig. 6.20 Comparison of Storey Shear Distributions among Four Different Analyses for 4S2 Frame

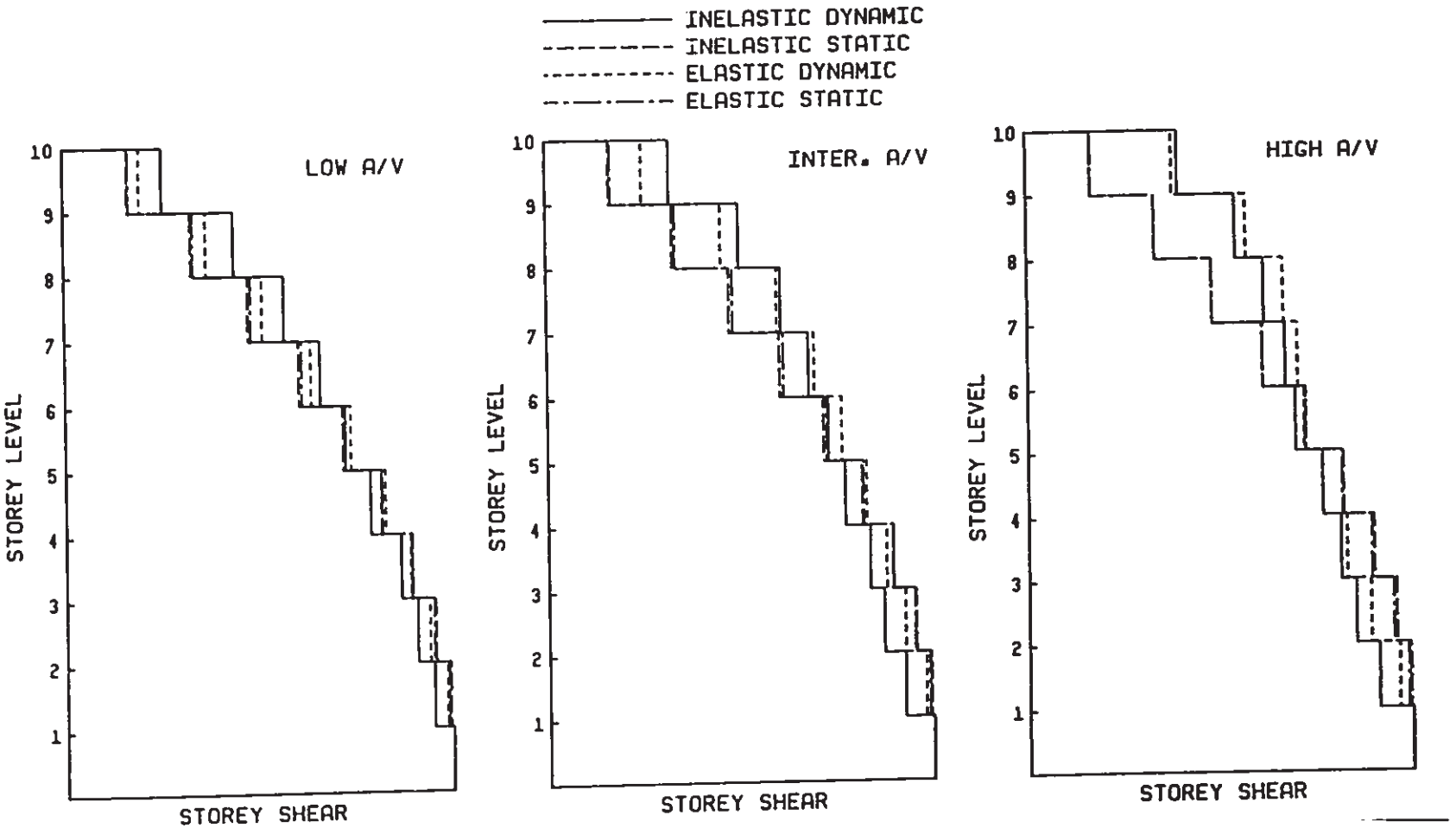

(a) V = 0.4 m/s

Fig. 6.21 Comparison of Storey Shear Distributions among Four Different Analyses for 10S Frame

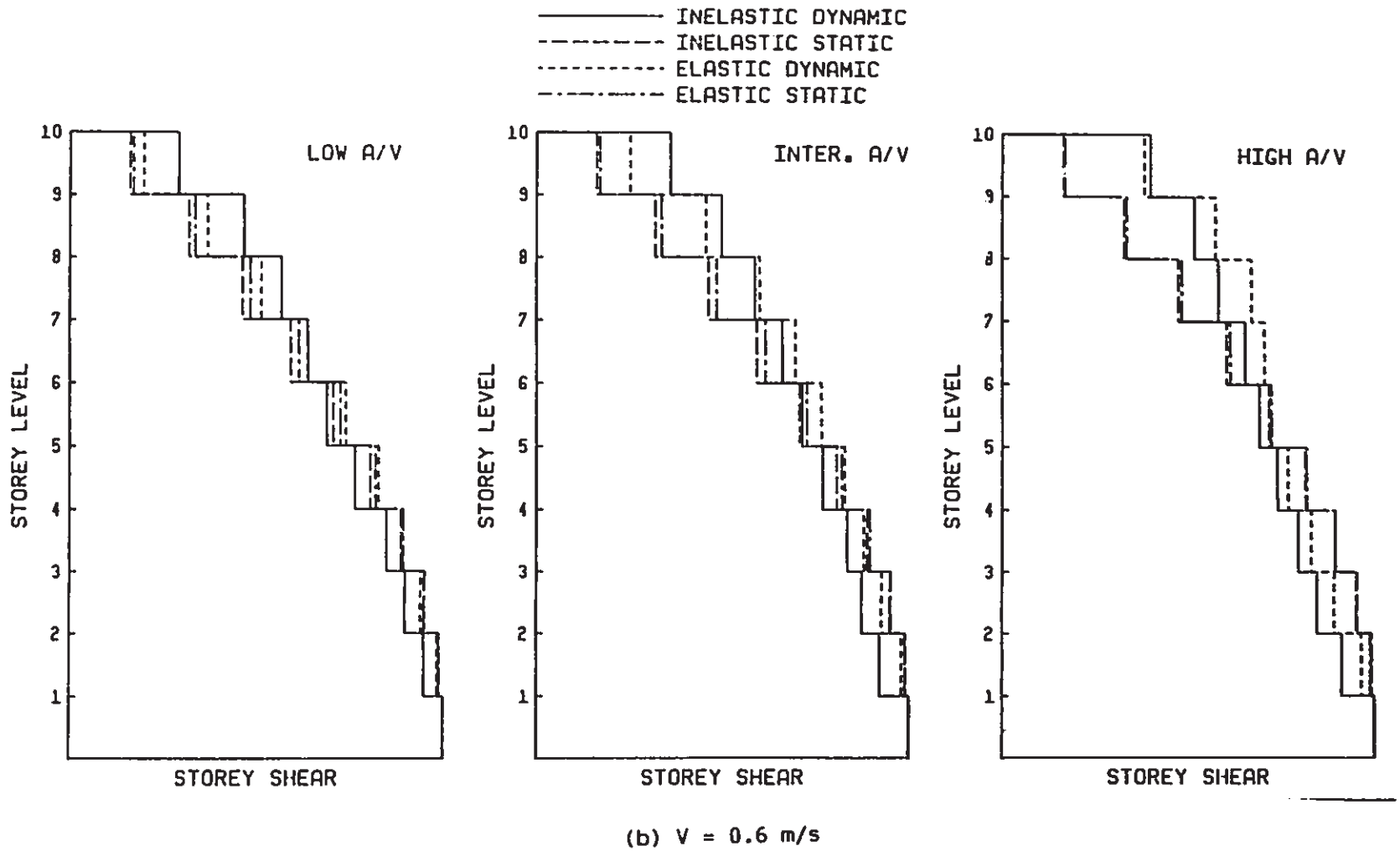

(b) V = 0.6 m/s

Fig. 6.21 (cont'd) Comparison of Storey Shear Distributions among Four Different Analyses for 10S Frame

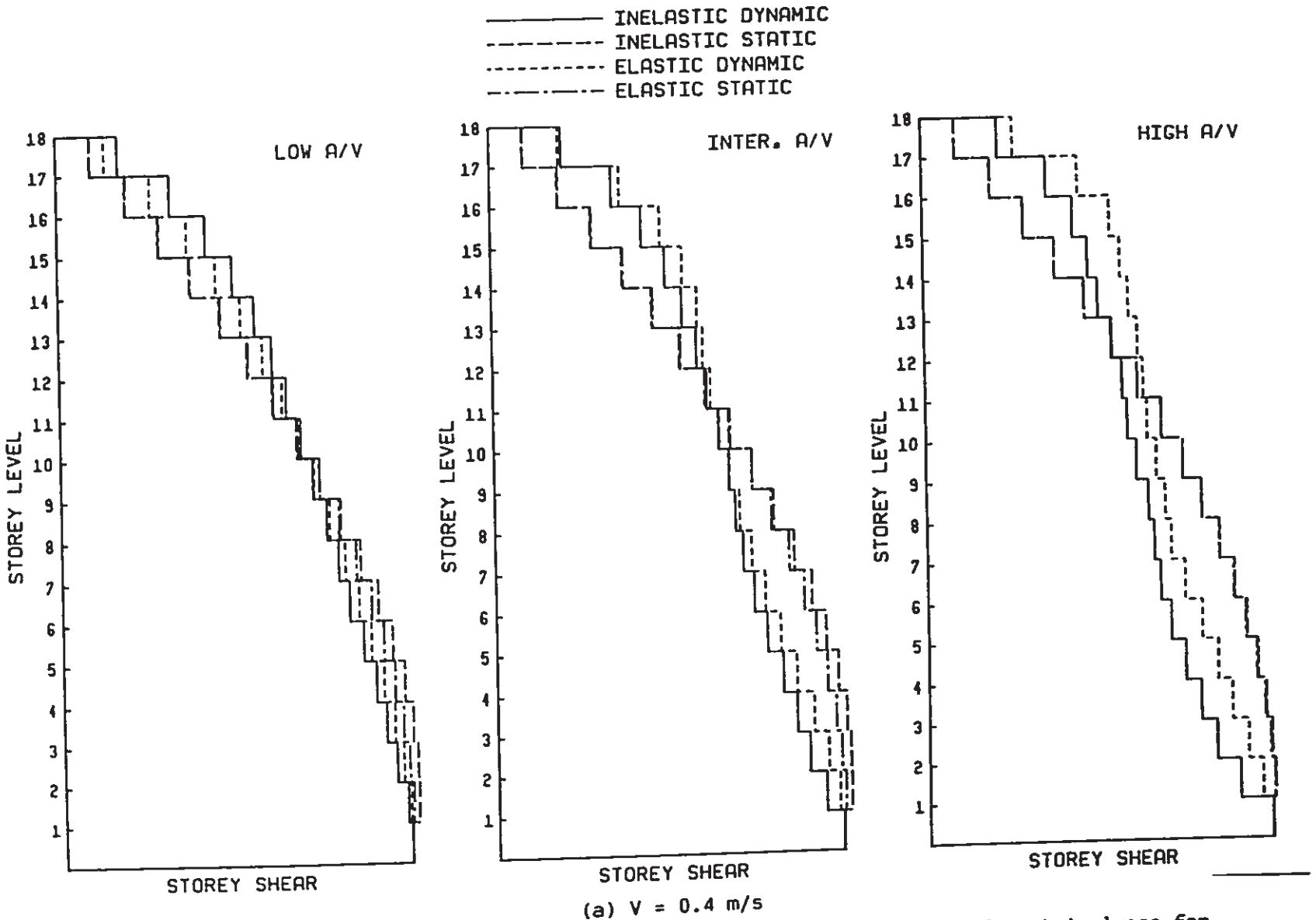

(a) V = 0.4 m/s

Fig. 6.22 Comparison of Storey Shear Distributions among Four Different Analyses for 18S Frame

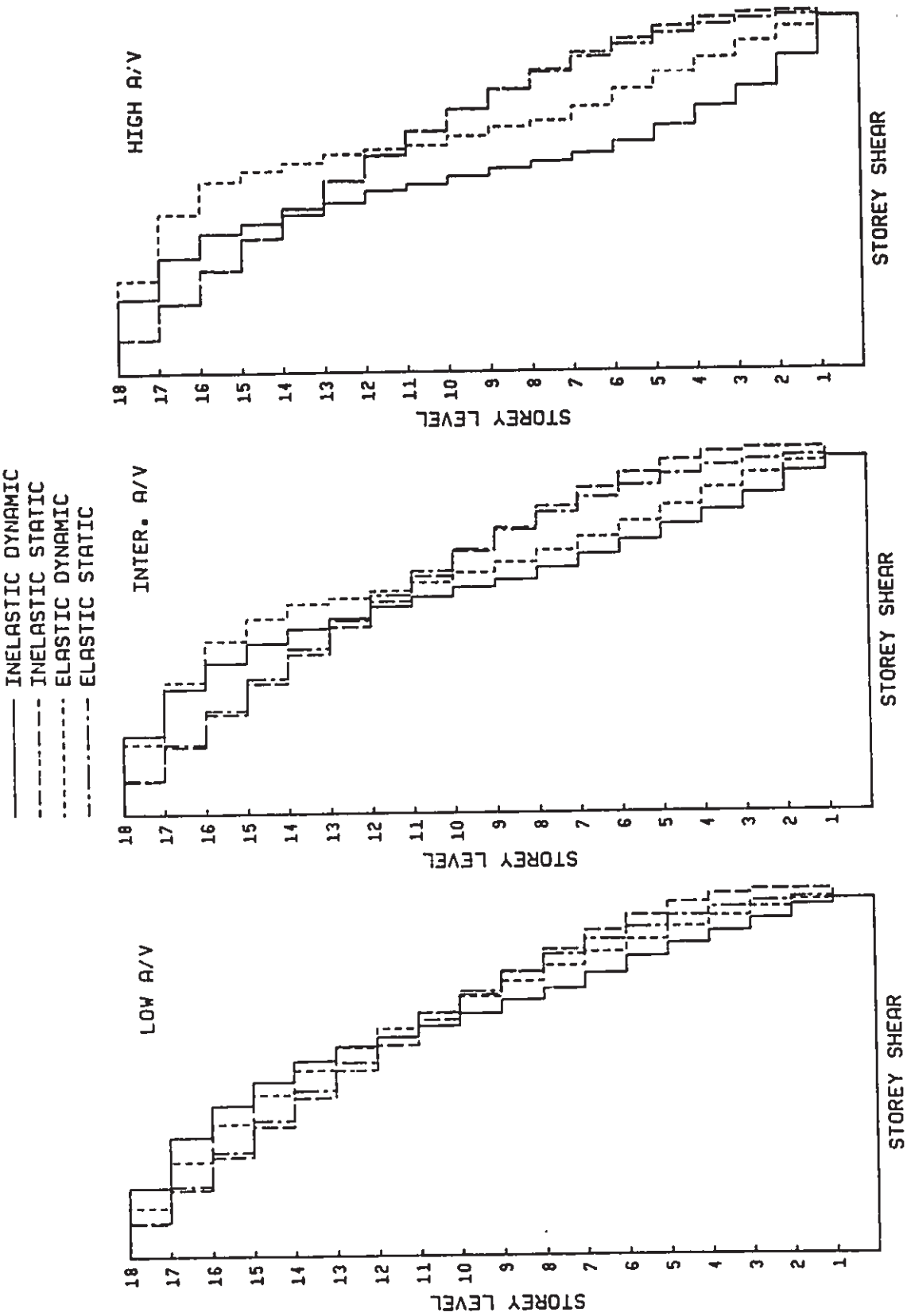

(b) V = 0.6 m/s

Fig. 6.22 (cont'd) Comparison of Storey Shear Distributions among Four Different Analyses for 18S Frame

CHAPTER 7

SIMPLIFIED ANALYSIS PROCEDURE

7.1 Introduction

In the preliminary stages of design, it is desirable to evaluate the relative merits of various design alternatives and the relative effects of different earthquake excitations. The use of sophisticated nonlinear dynamic analysis computer programs for such an evaluation may be economically infeasible because of the high costs involved. Therefore, it is desirable to use simplified analytical models that will result in reliable estimates of inelastic deformational demands for building structures. Two simplified analytical models have been used in the previous studies for the inelastic dynamic analysis of building structures. One is the inelastic shear beam idealization of a building structure (2), and the other is the representation of a building structure by an equivalent inelastic SDOF system (76). Both simplified models only provide information regarding the overall inelastic response of a building structure.

In this chapter, a simplified analysis procedure is proposed to estimate both overall and localized inelastic deformational demands for building frames. The applicability of this simplified analysis procedure is evaluated for frame structures having different number of storeys and for earthquake ground motions having different frequency characteristics. The evaluation is based on a comparison of the inelastic deformational demands estimated from the simplified analysis procedure with the

statistical results of the inelastic dynamic analysis performed in Chapter 6.

7.2 Simplified Analysis Procedure

Fig.7.1 shows a schematic illustration of the simplified analysis procedure proposed in this study. This procedure involves two inelastic static analyses of the original frame structure and one inelastic dynamic analysis of the transformed equivalent inelastic SDOF system. First, the frame structure is transformed into an equivalent inelastic SDOF system based on an assumed deflection shape and the force-deformation behaviour of the frame subjected to monotonically increased lateral loading. In this transformation, it is implicitly assumed that the deflected shape of the frame remains relatively constant during large amplitude inelastic response. Secondly, the maximum inelastic responses of the derived SDOF system subjected to different earthquake excitations are obtained from inelastic dynamic analysis. The statistical result of the maximum inelastic responses of the equivalent SDOF system combined with the assumed deflection shape provides an estimate of the roof displacement of the original frame resulting from the same earthquake excitations. Finally, the overall inelastic deformations at storey levels and the localized inelastic deformations in the structural members are estimated for the frame based on an inelastic static analysis in which the lateral loading is increased monotonically until the roof displacement of the frame reaches the value obtained from the SDOF analysis.

7.3 Equivalent Inelastic SDOF System

The first step in the proposed simplified analysis procedure is to convert an actual multistorey frame structure into an equivalent inelastic SDOF system. Two approaches for modelling a multistorey frame as an equivalent SDOF oscillator are investigated in this study. The first model is based on the first Ritz vector taken as the deflected shape of the frame subjected to distributed lateral loading. This model is referred to as SDOF-1. The second model is based on the first mode shape of the frame and denoted as SDOF-2. The detailed derivation of the two SDOF models is given below.

7.3.1 SDOF-1 Model

In this model, a MDOF system is transformed into an equivalent SDOF system using the first Ritz vector. The first Ritz vector is taken as the displaced shape of a multistorey frame resulting from the application of lateral loading which is distributed over height in accordance with the NBCC 1985 distribution formula. The properties of the equivalent SDOF oscillator are related to those of the original MDOF system based on the derivation by Biggs (17). This model was modified and extensively used for the analysis of reinforced concrete structures by Saiidi (76).

Based on the derivation by Biggs (17), the equation of motion for the equivalent SDOF system representing a frame is given by

$$M_e\ddot{X} + C\dot{X} + F_e(X) = - M_t\ddot{U}_g \qquad (7.1)$$

where $M_e = \left(\sum_{i=1}^{n} m_i\psi_i^2 \Big/ \sum_{i=1}^{n} m_i\psi_i \right) M_t$ = equivalent mass;

m_i = mass at level i;

ψ_i = ordinate of the first Ritz vector at level i;

n = total number of levels;

M_t = total mass of the frame;

C = damping coefficient;

$\ddot{u}_g$ = ground acceleration;

$F_e(X)$ = equivalent restoring force;

X = relative displacement of equivalent mass.

The equivalent mass is located at an equivalent height L_e above the base. The equivalent height L_e is given by

$$L_e = \frac{\sum_{i=1}^{n} m_i \psi_i h_i}{\sum_{i=1}^{n} m_i \psi_i} \qquad (7.2)$$

where h_i = height of level i above the base. The equivalent SDOF model is shown in Fig.7.2.

The storey displacements of the frame resulting from the NBCC 1985 lateral loading are normalized with respect to the top-level displacement. The normalized storey displacements form the first Ritz vector (ψ). The computed first Ritz vectors for the 4S2, 10S, and 18S frames are shown in Table 7.1.

The skeleton curve for the bilinear force-deformation relationship of the nonlinear spring in the equivalent SDOF system is determined from the inelastic static analysis of the frame subjected to monotonically increased lateral loading. The lateral loading is distributed over height based on the NBCC 1985 distribution formula. In the inelastic static analysis of the frame, X is taken as the lateral displacement at the

equivalent height of L_e above the base, and F_e is taken as the base overturning moment divided by L_e. The computed F_e vs. X curve resulting from the monotonically increased lateral loading is shown in Fig.7.3 for the 10S frame. This curve is idealized as a bilinear curve as indicated by the dashed line. The resulting yield displacement and force corresponding to the breakpoint are denoted as X_y and $(F_e)_y$. The ratio of the post-yielding slope to the initial slope of the idealized bilinear primary curve is designated as p.

The M_e, L_e, $(F_e)_y$, X_y, and p values obtained for the 4S2, 10S, and 18S frames are shown in Table 7.2. The damping coefficient for the equivalent SDOF system is taken as 5% of critical. This damping ratio is the same as the assumed first modal damping ratio of the original MDOF system. The roof displacement of the MDOF system is related to the displacement of the equivalent SDOF system by

$$\delta = (\psi_n/\psi_e) X \tag{7.3}$$

where δ = roof displacement;

ψ_e = ordinate of the $\{\psi\}$ vector at equivalent height L_e;

ψ_n = ordinate of the $\{\psi\}$ vector at top level.

7.3.2 SDOF-2 Model

In this model, a MDOF system is converted into an equivalent SDOF oscillator using the first mode shape. The equation of motion for the original MDOF system is given by

$$[M]\{\ddot{u}\} + [C]\{\dot{u}\} + \{R\} = - [M]\{r\}\ddot{u}_g \tag{7.4}$$

where $\{u\}$ = relative displacement vector;

$[M]$ = mass matrix;

[C] = damping matrix;

{R} = restoring force vector;

{r} = a vector relating structural degrees of freedom to ground motion;

$\ddot{u}_g$ = ground acceleration.

Assuming that the displacement response is dominated by the first mode ($\{u\}=\{\phi\}Y_1$), Eq.(7.4) can be transformed to the first modal coordinate Y_1 as follows:

$$M_1\ddot{Y}_1(t) + C_1\dot{Y}_1(t) + \{\phi\}^T\{R\} = - \Gamma_1\ddot{u}_g \qquad (7.5)$$

where $\{\phi\}$ = the first mode shape vector;

$M_1 = \{\phi\}^T[M]\{\phi\}$ = the generalized mass for the first mode;

$C_1 = \{\phi\}^T[C]\{\phi\}$ = the generalized damping for the first mode;

$\Gamma_1 = \{\phi\}^T[M]\{r\}$.

Eq.(7.5) can be written as

$$M_1\ddot{Y}_1(t) + C_1\dot{Y}_1(t) + R_1(Y_1(t)) = - \Gamma_1\ddot{u}_g \qquad (7.6)$$

where $R_1(Y_1(t)) = \{\phi\}^T\{R\}$ = the generalized restoring force for the first mode.

The first mode shapes obtained for the 4S2, 10S, and 18S frames are normalized with respect to the top-level displacement. The normalized mode shape vectors for the 4S2, 10S, and 18S frames are shown in Table 7.3.

The relationship between R_1 and Y_1 are assumed to be bilinear in the inelastic dynamic analysis of the equivalent SDOF system. The primary curve is determined from an inelastic static analysis of the original frame subjected to monotonically increased lateral loading. The lateral loading is distributed over the height in accordance with the NBCC 1985 distribution formula. The lateral storey displacement vector {u} and the

restoring force vector {R} resulting from the monotonically increased lateral loading are converted to the first modal displacement Y_1 and restoring force R_1 as follows:

$$Y_1 = \{\phi\}^T\{u\} \tag{7.7a}$$

$$R_1 = \{\phi\}^T\{R\} = \{\phi\}^T\{P\} \tag{7.7b}$$

where {P} = the applied lateral load vector in the inelastic static analysis. The relationship between R_1 and Y_1 resulting from the monotonically increased lateral loading for the 10S frame is shown in Fig.7.4. This calculated curve is idealized as a bilinear curve as indicated by the dashed line. The resulting R_1 and Y_1 values corresponding to the breakpoint are referred to as the first modal yield force and displacement, and they are denoted as $(R_1)_y$ and $(Y_1)_y$. The ratio of the post-yielding slope to the initial slope of the idealized bilinear curve is designated as p.

The values of M_1, Γ_1, $(R_1)_y$, $(Y_1)_y$, and p obtained for the 4S2, 10S, and 18S frames are shown in Table 7.4. In the inelastic dynamic analysis of the equivalent SDOF system, the damping coefficient is taken as 5% of critical. Since {ϕ} has been normalized to have unity at the top level, the Y_1 value computed from the inelastic dynamic analysis is numerically equal to the estimated roof displacement.

7.4 Evaluation of Simplified Analysis Procedure

The mean values of the maximum roof displacement estimated from the two SDOF models are shown in Tables 7.5 and 7.6 for the two peak ground velocity levels of 0.4 and 0.6 m/s, respectively. Included in the same tables are the mean values of the maximum roof displacement obtained from

the inelastic dynamic analysis of the MDOF models of the frames. It can be seen that both SDOF models provide reasonably good estimates of the maximum roof displacement for the frames. The errors resulting from the use of the SDOF models are within 20%. Furthermore, it can be observed that the maximum roof displacements estimated from the SDOF-2 model are higher than those from the SDOF-1 model in a consistent manner. The maximum roof displacements estimated from the SDOF-1 model are generally closer to those obtained from the MDOF model than the SDOF-2 model. Therefore, the SDOF-1 model provides a better estimate for the maximum roof displacement. However, considering the approximate nature of the SDOF idealization, either model may be considered satisfactory.

For the maximum roof displacement estimated from each of the two SDOF models, an inelastic static analysis is performed for the frame to estimate the overall inelastic deformations at storey levels and the localized inelastic deformations in the structural members. For the roof displacement estimated from the SDOF-1 model, the lateral loading in the inelastic static analysis is distributed over height in accordance with $\{\psi\}$. The distribution of the lateral loading is based on $\{\phi\}$ for the roof displacement estimated from the SDOF-2 model. In the inelastic static analysis, the lateral loading is increased monotonically until the roof displacement of the frame reaches the value obtained from the SDOF analysis.

The overall and local inelastic deformations obtained from the two inelastic static analyses associated with the two SDOF models are compared with those obtained from the inelastic dynamic analyses of the MDOF models in Figs.7.5 to 7.7 for the 4S2, 10S, and 18S frames,

respectively. This comparison is made for the three separate A/V groups of earthquake ground motions scaled to the two peak ground velocity levels of 0.4 and 0.6 m/s. On the basis of the comparison shown in Figs.7.5 to 7.7, the following observations can be made:

(1) For the maximum storey displacements, the simplified analysis procedure provides adequate estimates for all the frames considered and for all three A/V groups of earthquake records.

(2) For the interstorey drifts, the use of the simplified analysis procedure results in good estimates for the 4S2 frames subjected to all three A/V groups of earthquake records. However, the simplified analysis procedure becomes less adequate with an increase in the number of storeys. For the 18S frame, the simplified analysis procedure gives reasonable estimates of the interstorey drift in the lower storeys, but it grossly underestimates the interstorey drifts in the upper storeys. This underestimation becomes particularly pronounced for the high and intermediate A/V groups of ground motions. The interstorey drifts obtained from the inelastic dynamic analysis can be more than twice as large as those estimated from the simplified analysis procedure.

(3) The beam curvature ductility demands estimated using the simplified analysis procedure compare favourably with those obtained from the inelastic dynamic analysis for the 4S2 frames. For the 10S and 18S frames, the simplified analysis procedure produces reasonable estimates of beam curvature ductility demand in the lower storeys, but it tends to underestimate the beam curvature ductility demands in the upper storeys.

(4) For the columns in the 4S2 frames, the simplified analysis procedure provides reasonably good estimates of the curvature ductility

demand except at the first and second storeys where the simplified analysis procedure tends to underestimate the curvature ductility demands particularly for the increased peak ground velocity level of 0.6 m/s. In the case of the 10S and 18S frames, the use of the simplified analysis procedure results in reasonable estimates of the curvature ductility demand in the lower storeys, but it tends to underestimate the curvature ductility demands in the upper storeys. This is particularly true for the interior columns. The underestimation is particularly pronounced for the high and intermediate A/V groups of earthquake ground motions.

It is clear from the above evaluation that the reduction of a regular multistorey frame to an equivalent SDOF system is capable of estimating the maximum roof displacement of the frame. The simplified analysis procedure produces good estimates of both overall and local inelastic deformations for low rise frames (say lower than 10 storeys) subjected to earthquake ground motions having different A/V ratios. The success of the simplified analysis procedure for low-rise frames results from the fact that the contributions of higher modes to their inelastic dynamic responses are insignificant. For high rise frames, the maximum storey displacements can be estimated reasonably well by the simplified analysis procedure. However, the simplified analysis procedure grossly underestimates the interstorey drifts in the upper storeys. The simplified analysis procedure also underestimates the beam and column inelastic deformations in the upper storeys. The relative success of the simplified analysis procedure to estimate the maximum storey displacements for high-rise frames is attributable to the fact that higher modes have relatively insignificant contributions to the maximum

storey displacement response even for high-rise frames. By contrast, higher modes have very significant contribution to interstorey drift and member inelastic deformations which are directly related to member bending moments, as discussed in Chapter 6. The simplified analysis procedure clearly fails to account for this higher mode contribution because it is based on an inelastic static analysis for estimating the distributions of interstorey drift and member inelastic deformations.

It is of interest to compare the energy per unit mass imparted to the MDOF models of the frames with that imparted to the equivalent SDOF systems. Since the SDOF-1 model is a physical idealization of the MDOF model, a direct comparison is made between the input energy for the MDOF model and that for the SDOF-1 model. Figs. 7.8 to 7.10 show such comparisons for individual earthquake records for the 4S2, 10S, and 18S frames, respectively. For each frame, two peak ground velocity levels of 0.4 and 0.6 m/s are considered. It can be seen that for the 4S2 frames (Fig.7.8), the input energy per unit mass estimated from the SDOF-1 model is very close to that obtained from the MDOF model for both levels of peak ground velocity. However, this correlation becomes weak with an increase in the number of storeys. For the 18S frame (Fig.7.10), most of the data points corresponding to the individual earthquake records scatter away from the 45 degree line. The weaker correlation of the input energy between the MDOF and the SDOF-1 models for the 18S frame is clearly due to the effect of higher modes, and this is consistent with the relatively poor performance of the simplified analysis procedure for the 18S frame.

The hysteretic energy per unit mass for the MDOF model is also

compared with that for the SDOF-1 model in Figs. 7.11 to 7.13 for the 4S2, 10S, and 18S frames, respectively. Again, the hysteretic energy for the SDOF-1 model is very similar to that of the MDOF model for the 4S2 frames. However, the correlation becomes poorer for the 18S frame.

7.5 Summary

A simplified analysis procedure is proposed to estimate both overall and localized inelastic deformations for regular building frames. The procedure consists of two inelastic static analyses of a frame and one inelastic dynamic analysis of an equivalent inelastic SDOF system. First, a frame is converted into an equivalent SDOF system based on an inelastic static analysis of the frame. Secondly, an inelastic dynamic analysis is performed for the equivalent SDOF system subjected to earthquake excitation. The computed maximum displacement of the equivalent SDOF system provides an estimate of the maximum roof displacement of the original frame. Finally, the overall and localized inelastic deformations of the frame are estimated from an inelastic static analysis in which the lateral loading is increased monotonically until the roof displacement of the frame reaches the value obtained from the SDOF analysis. Two approaches of modelling a multistorey frame as an equivalent SDOF system are considered. One is based on the first Ritz vector, and the other is based on the first mode shape.

The accuracy of the simplified analysis procedure is evaluated based on the statistical results obtained from the inelastic dynamic analysis of the MDOF models of the frames. On the basis of this evaluation, the following conclusions can be drawn:

(1) The two equivalent SDOF models examined in this study provide satisfactory estimates of the maximum roof displacement for frames having different number of storeys and for earthquake ground motions having different A/V ratios.

(2) For low-rise frames, the simplified analysis procedure produces good estimates of both overall and localized inelastic deformations for earthquake ground motions having different A/V ratios.

(3) For high-rise frames, the simplified analysis procedure results in reasonable estimates of the maximum storey displacement. However, the simplified analysis procedure grossly underestimates the interstorey drifts in the upper storeys. This underestimation is particularly pronounced for high and intermediate A/V ground motions. The beam and column inelastic deformations in the upper storeys are also underestimated by the simplified analysis procedure.

(4) There is a close correlation of the input and hysteretic energy per unit mass between the SDOF-1 and MDOF models for low-rise frames. Therefore, the SDOF-1 model may be used to estimate the energy per unit mass imparted to and the hysteretic energy per unit mass dissipated in a low-rise frame. For high-rise frames, there is no consistent correlation of the input and hysteretic energy between the SDOF-1 and MDOF models.

It is suggested that the simplified analysis procedure be used for regular building frames having number of storeys lower than 10. For high-rise frames, the simplified analysis procedure may be used to estimate maximum storey displacements. The interstorey drifts and member inelastic deformation in the lower storeys may also be estimated by the simplified analysis procedure.

Table 7.1 Normalized Deflected Shape Vectors Used in SDOF-1 Model

Storey Level	4S2	10S	18S
18			1.000
17			0.980
16			0.949
15			0.909
14			0.863
13			0.811
12			0.758
11			0.705
10		1.000	0.649
9		0.957	0.588
8		0.883	0.522
7		0.786	0.450
6		0.677	0.375
5		0.563	0.299
4	1.000	0.437	0.222
3	0.844	0.304	0.148
2	0.580	0.178	0.083
1	0.275	0.066	0.030

Table 7.2 Properties of Equivalent SDOF Systems Based on SDOF-1 Model

Frame	M_e ($\times 10^3$ kg)	L_e (m)	$(F_e)_y$ (kN)	$(u_e)_y$ (mm)	p (%)
4S2L	420	10.39	1090	14.3	3.21
4S2I	420	10.39	1167	15.5	3.15
4S2H	420	10.39	1278	16.2	3.11
10S	1020	24.36	1491	54.4	2.42
18S	1827	43.01	1788	103.6	1.84

Table 7.3 Normalized First Mode Shape Vectors Used in SDOF-2 Model

Storey Level	4S2	10S	18S
18			1.000
17			0.974
16			0.933
15			0.882
14			0.826
13			0.761
12			0.693
11			0.629
10		1.000	0.560
9		0.948	0.490
8		0.865	0.422
7		0.765	0.354
6		0.652	0.289
5		0.538	0.231
4	1.000	0.416	0.173
3	0.817	0.293	0.120
2	0.533	0.180	0.072
1	0.228	0.072	0.028

Table 7.4 Properties of Equivalent SDOF Systems Based on SDOF-2 Model

Frame	M_1 ($\times 10^3$ kg)	Γ_1 ($\times 10^3$ kg)	$(F_1)_y$ (kN)	$(Y_1)_y$ (mm)	p (%)
4S2L	264	343	845	17.2	3.19
4S2I	264	343	900	18.8	3.26
4S2H	264	343	991	20.3	3.25
10S	571	775	1100	71.9	2.60
18S	919	1283	1255	143.8	1.94

Table 7.5 Comparison of Maximum Roof Displacements (mm) Between MDOF Model and SDOF Models for V = 0.4 m/s

Frame	MDOF	SDOF-1	SDOF-2
		Low A/V	
4S2L	35.5	34.3	37.7
10S	138.5	145.5	154.3
18S	223.0	243.5	261.1
		Intermediate A/V	
4S2I	49.8	53.3	56.9
10S	147.4	157.9	166.9
18S	235.2	232.6	249.8
		High A/V	
4S2H	56.8	58.8	63.5
10S	102.7	103.8	109.6
18S	146.6	131.0	141.2

Table 7.6 Comparison of Maximum Roof Displacements (mm) Between MDOF Model and SDOF Models for V = 0.6 m/s

Frame	MDOF	SDOF-1	SDOF-2
		Low A/V	
4S2L	60.2	66.1	72.2
10S	217.5	235.4	249.8
18S	370.3	381.8	409.7
		Intermediate A/V	
4S2I	82.1	83.7	91.1
10S	221.7	243.7	260.0
18S	342.7	345.6	371.6
		High A/V	
4S2H	84.7	92.1	98.5
10S	147.1	153.0	162.0
18S	191.8	193.5	208.5

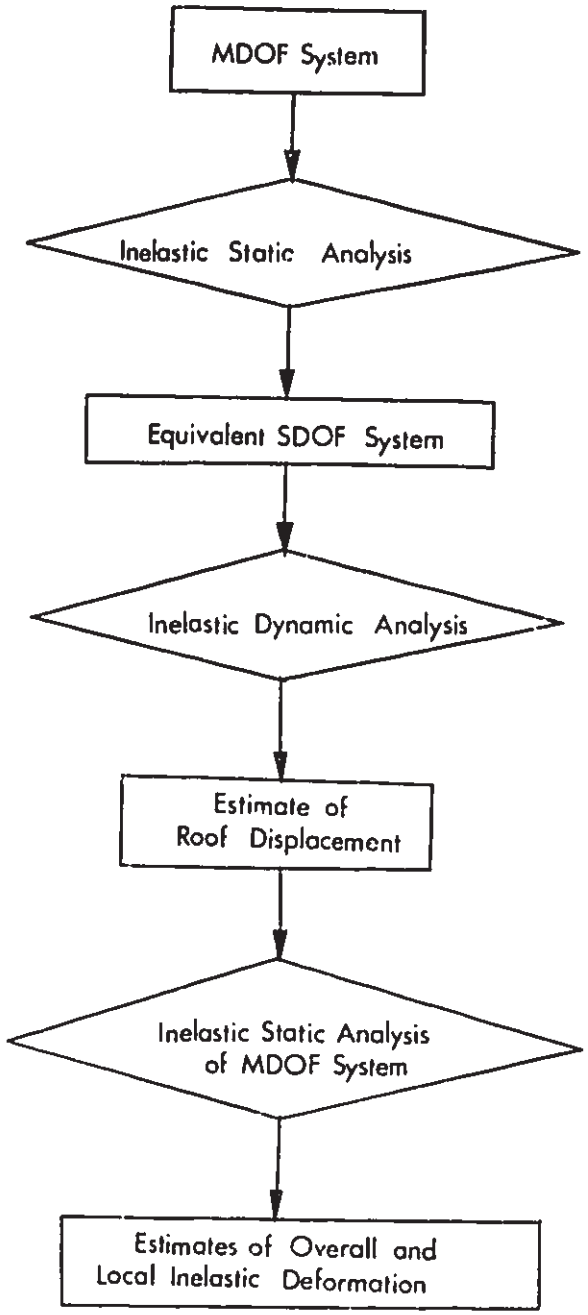

Fig. 7.1 Schematic Illustration of Simplified Analysis Procedure

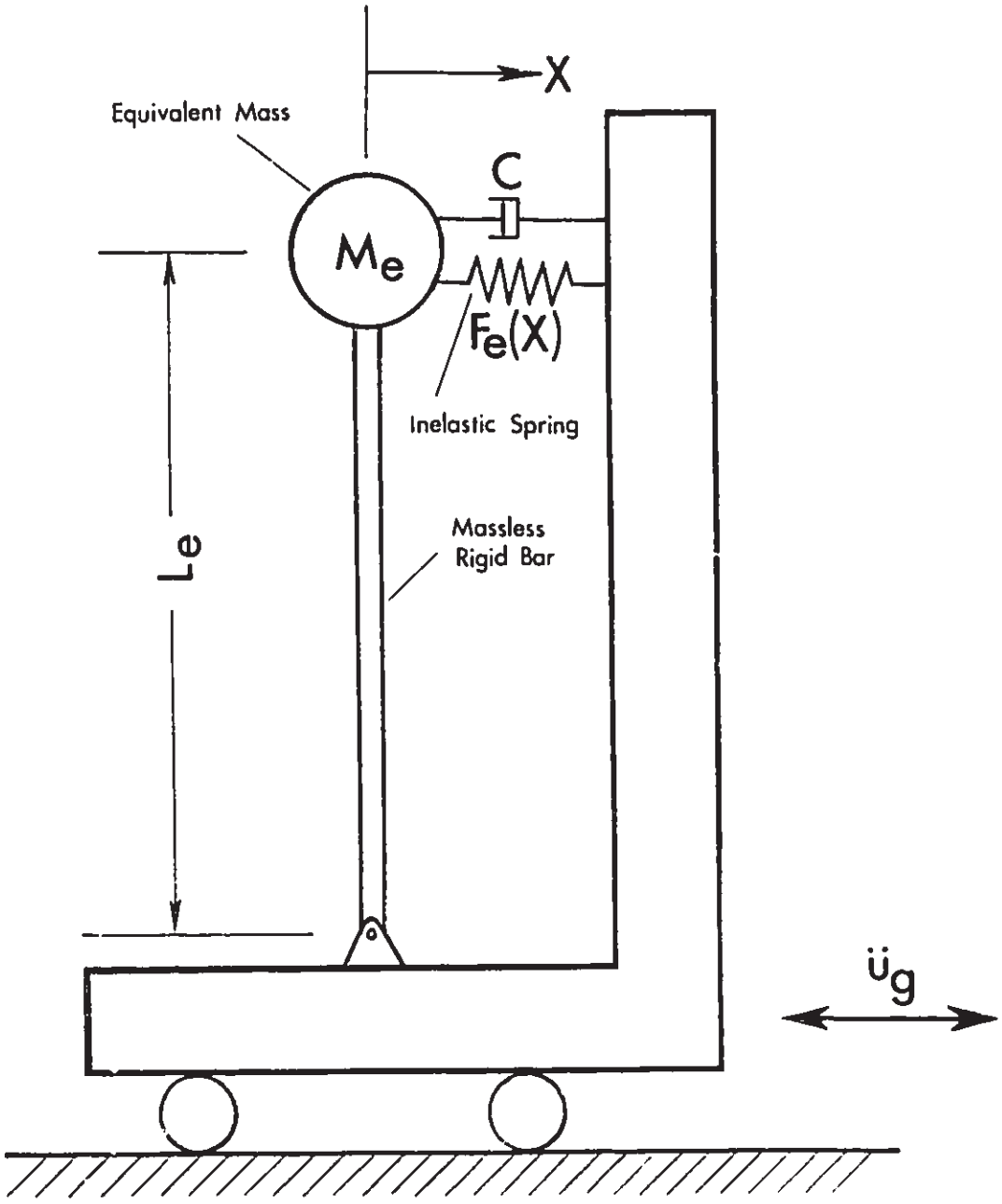

Fig. 7.2 SDOF-1 Model

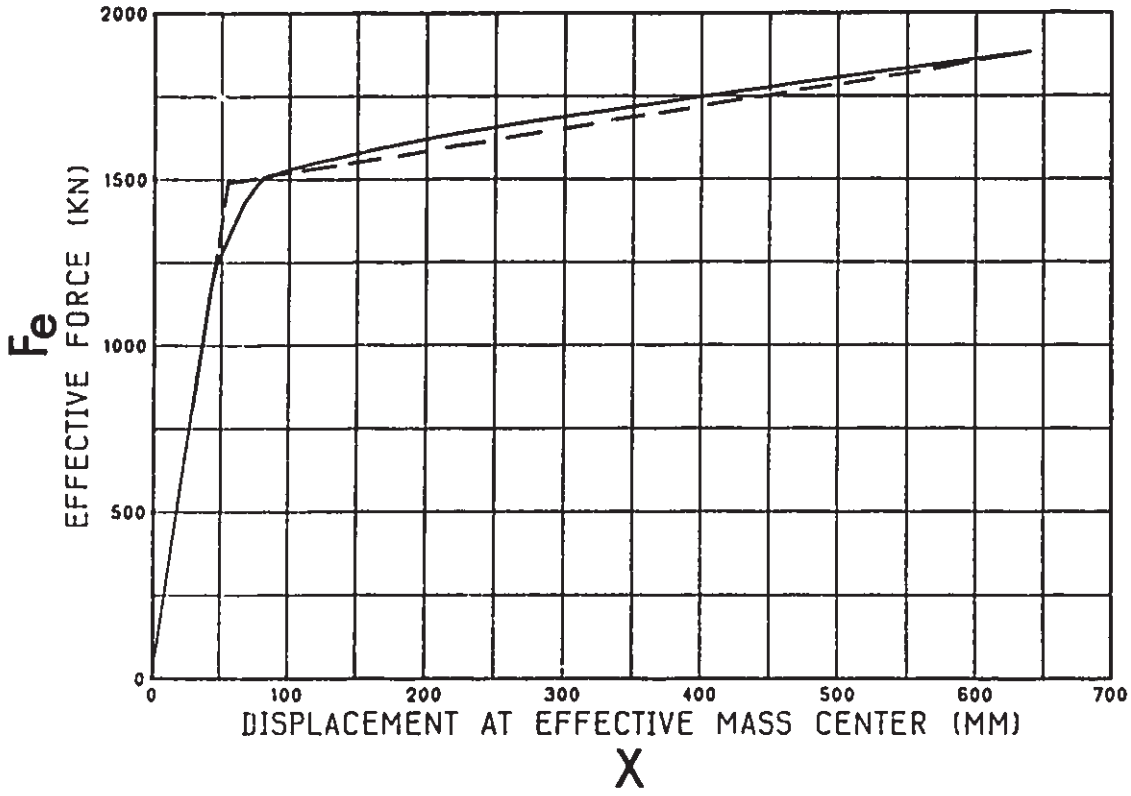

Fig. 7.3 F_e vs. X Primary Curve Resulting from Monotonically Increased Lateral Loading and Idealized Bilinear Curve for SDOF-1 Model (10S Frame)

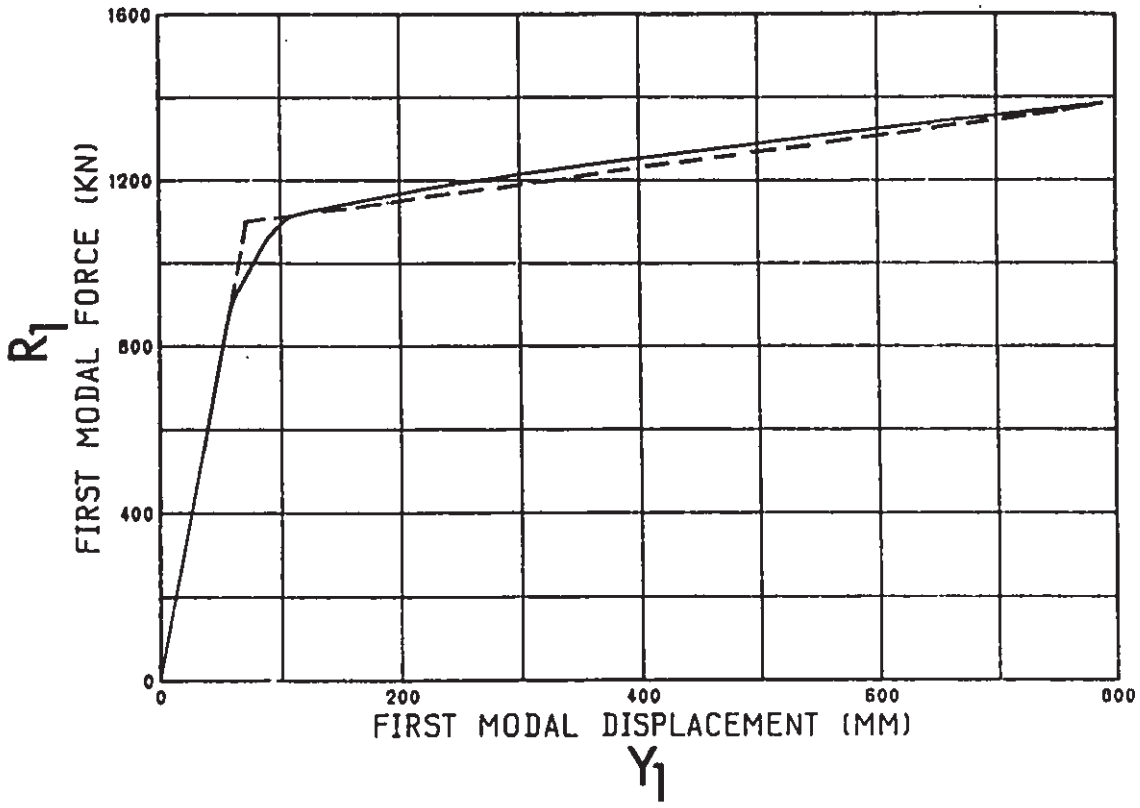

Fig. 7.4 R_1 vs. Y_1 Primary Curve Resulting from Monotonically Increased Lateral Loading and Idealized Bilinear Curve for SDOF-2 Model (IOS Frame)

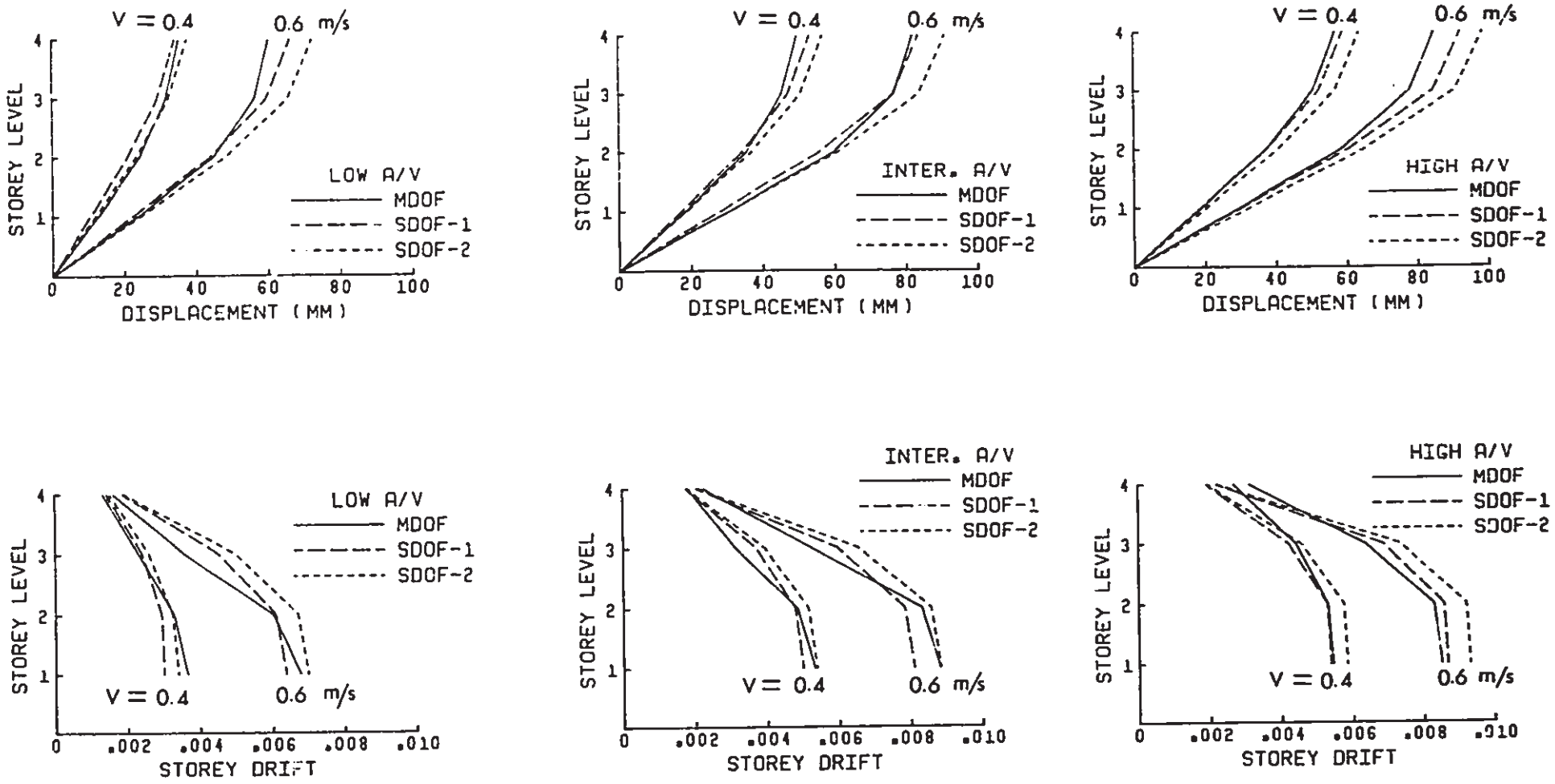

(a) Storey Response Parameters

Fig. 7.5 Comparison of Response Parameters between Simplified Analysis Procedure and MDOF Inelastic Dynamic Analysis for 4S2 Frames

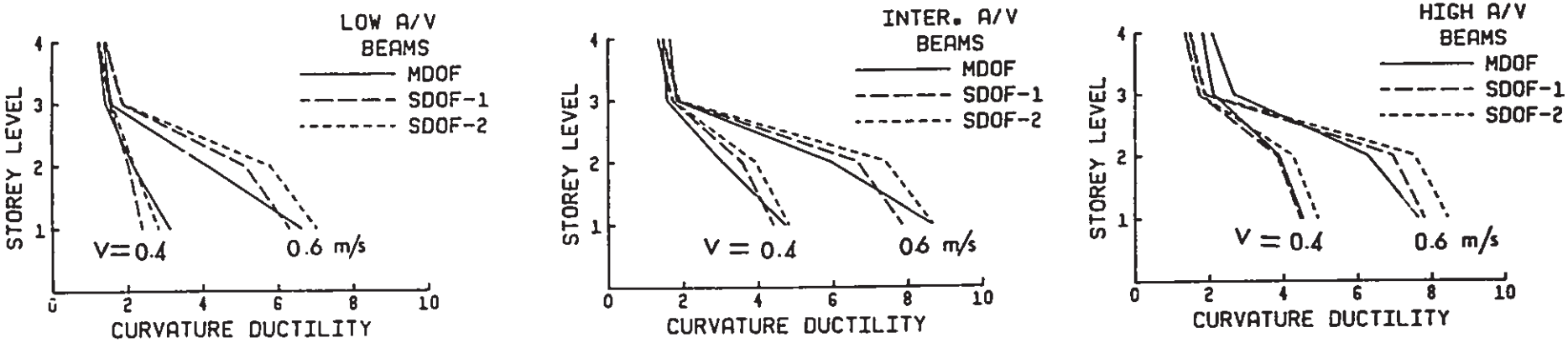

(b) Beam Response Parameters

Fig. 7.5 (cont'd) Comparison of Response Parameters between Simplified Analysis Procedure and MDOF Inelastic Dynamic Analysis for 4S2 Frames

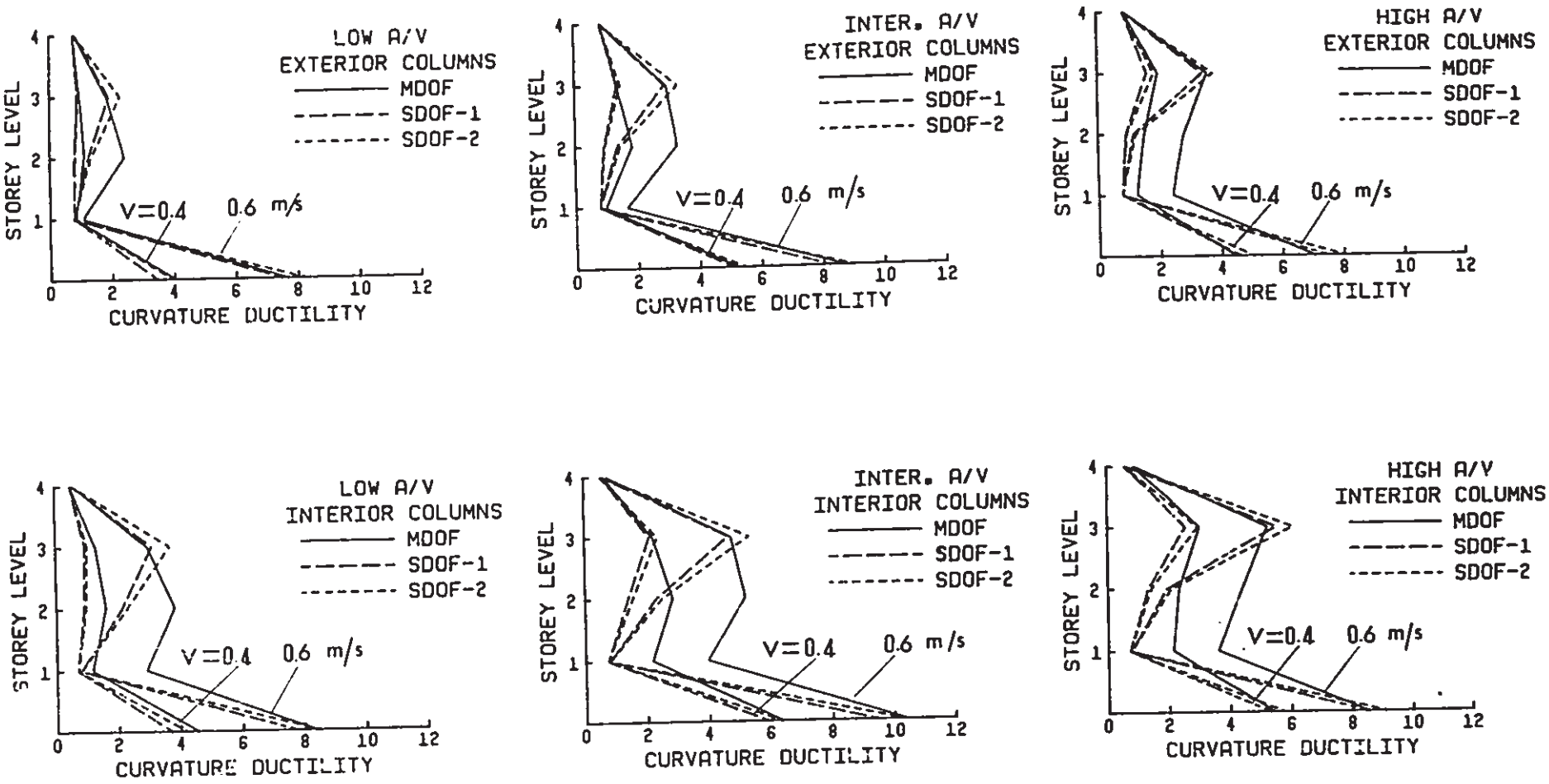

(c) Column Response Parameters

Fig. 7.5 (cont'd) Comparison of Response Parameters between Simplified Analysis Procedure and MDOF Inelastic Dynamic Analysis for 4S2 Frames

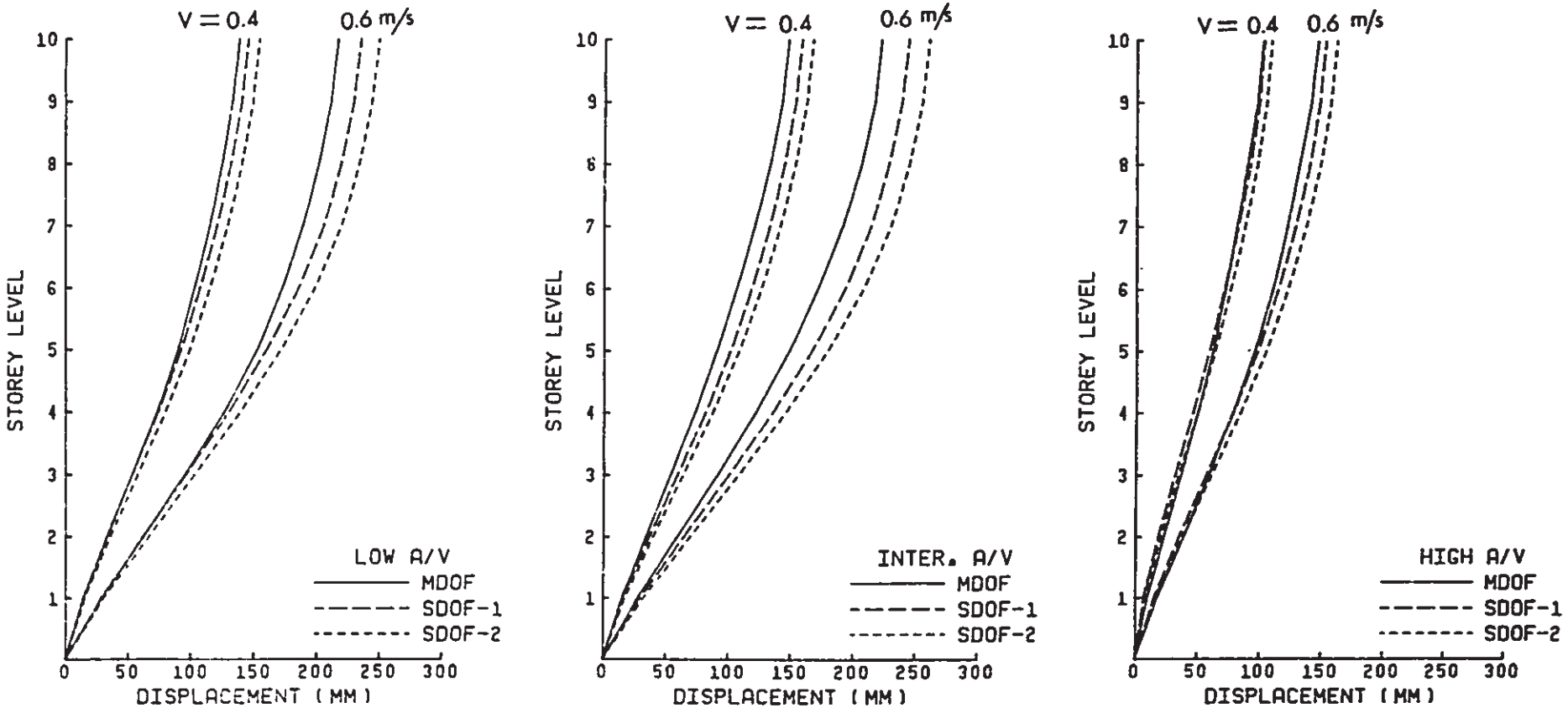

(a) Storey Response Parameters

Fig. 7.6 Comparison of Response Parameters between Simplified Analysis Procedure and MDOF Inelastic Dynamic Analysis for 10S Frame

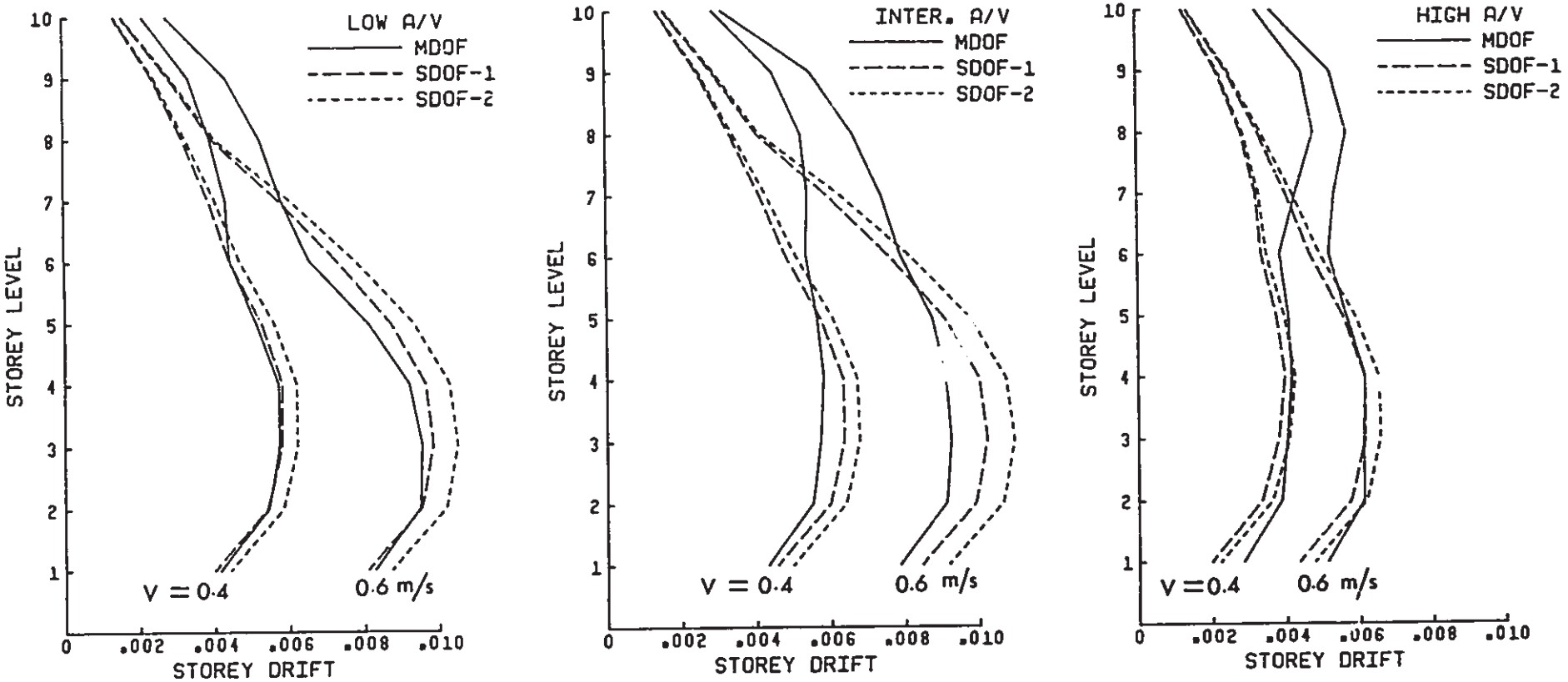

(a) Storey Response Parameters

Fig. 7.6 (cont'd) Comparison of Response Parameters between Simplified Analysis Procedure and MDOF Inelastic Dynamic Analysis for IOS Frame

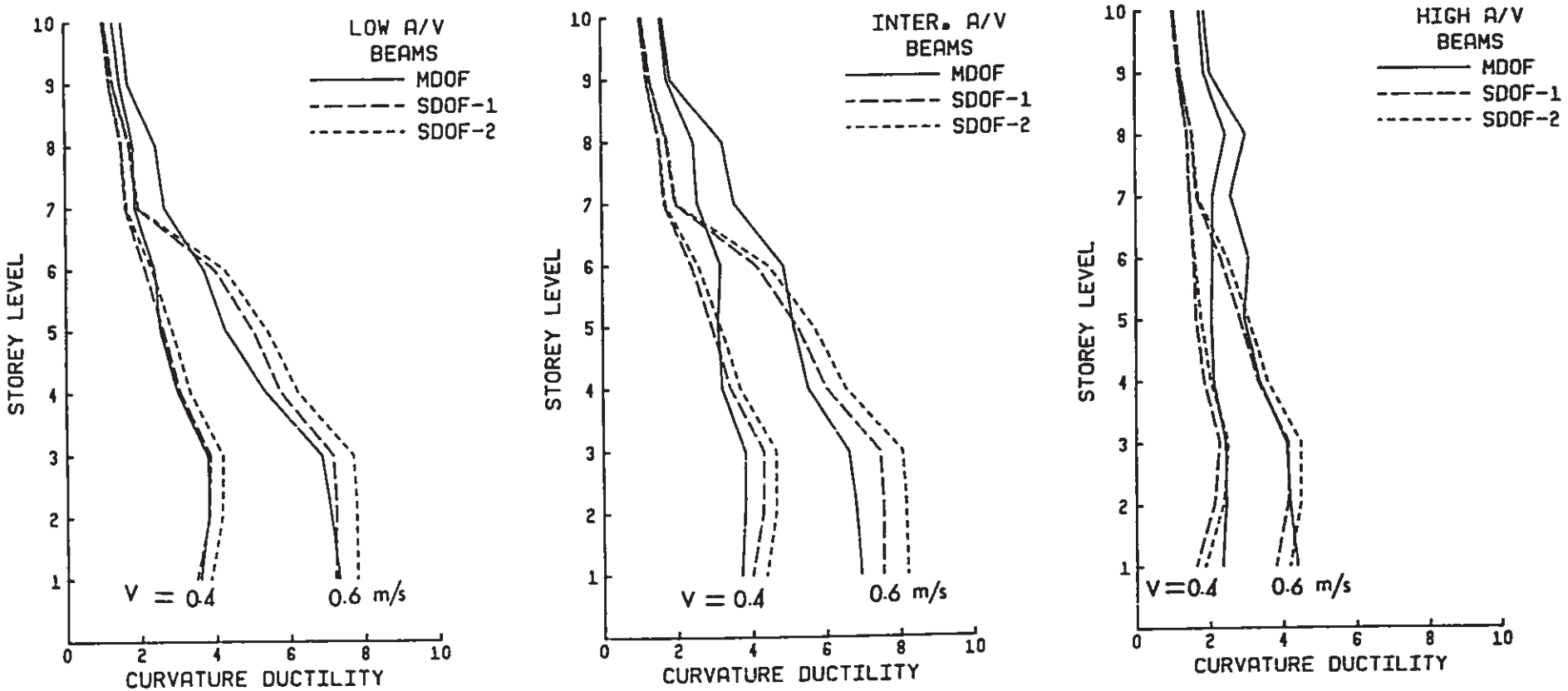

(b) Beam Response Parameters

Fig. 7.6 (cont'd) Comparison of Response Parameters between Simplified Analysis Procedure and MDOF Inelastic Dynamic Analysis for 10S Frame

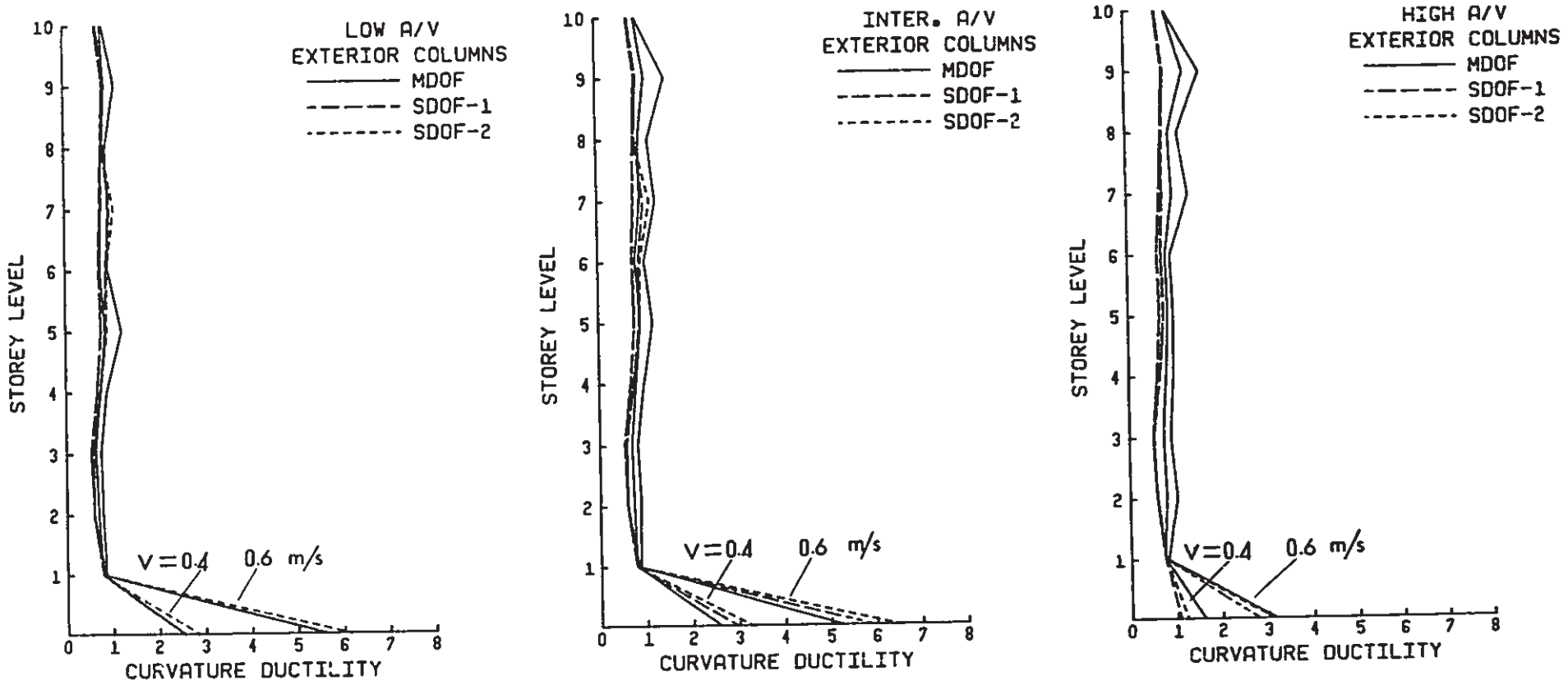

(c) Column Response Parameters

Fig. 7.6 (cont'd) Comparison of Response Parameters between Simplified Analysis Procedure and MDOF Inelastic Dynamic Analysis for 10S Frame

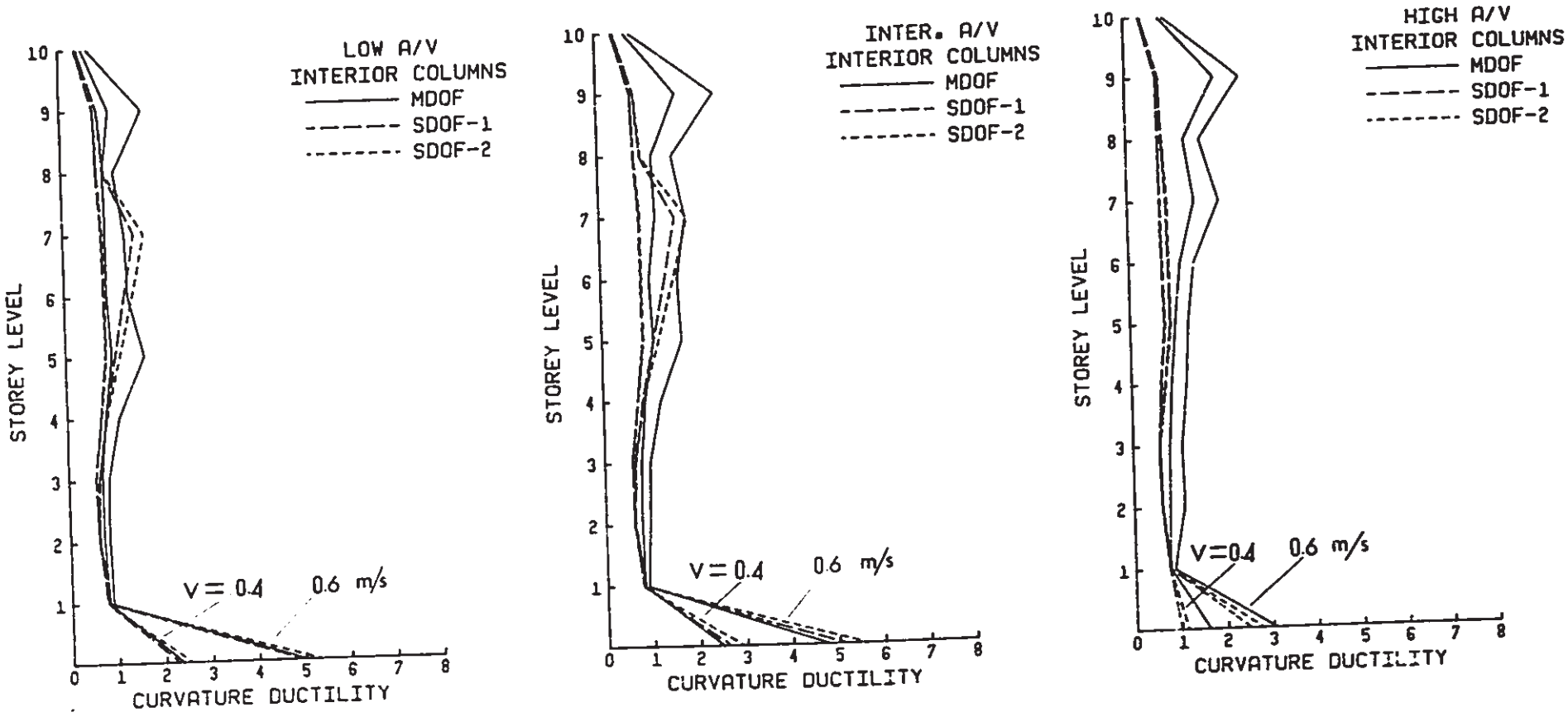

(c) Column Response Parameters

Fig. 7.6 (cont'd) Comparison of Response Parameters between Simplified Analysis Procedure and MDOF Inelastic Dynamic Analysis for 10S Frame

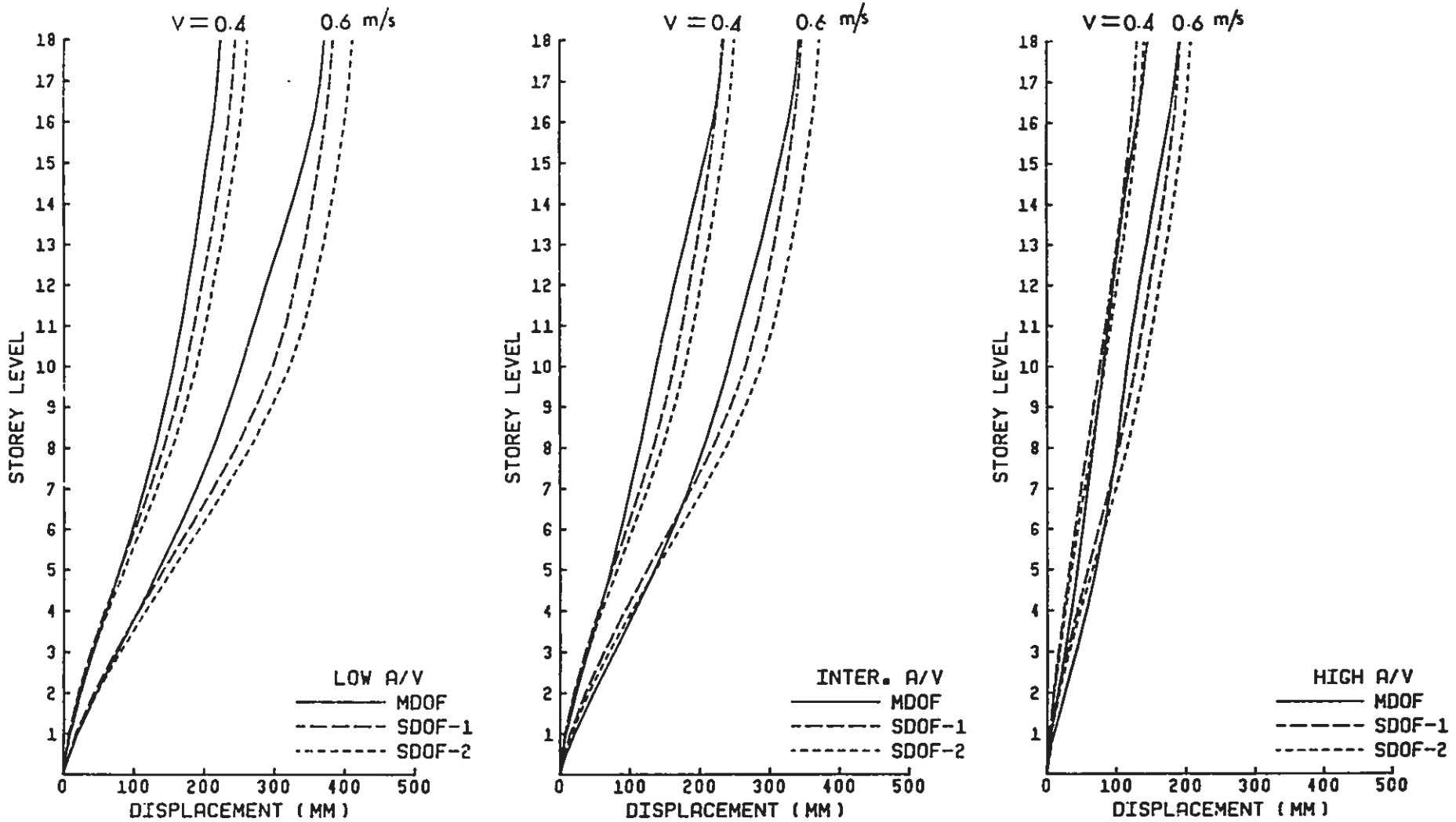

(a) Storey Response Parameters

Fig. 7.7 Comparison of Response Parameters between Simplified Analysis Procedure and MDOF Inelastic Dynamic Analysis for 18S Frame

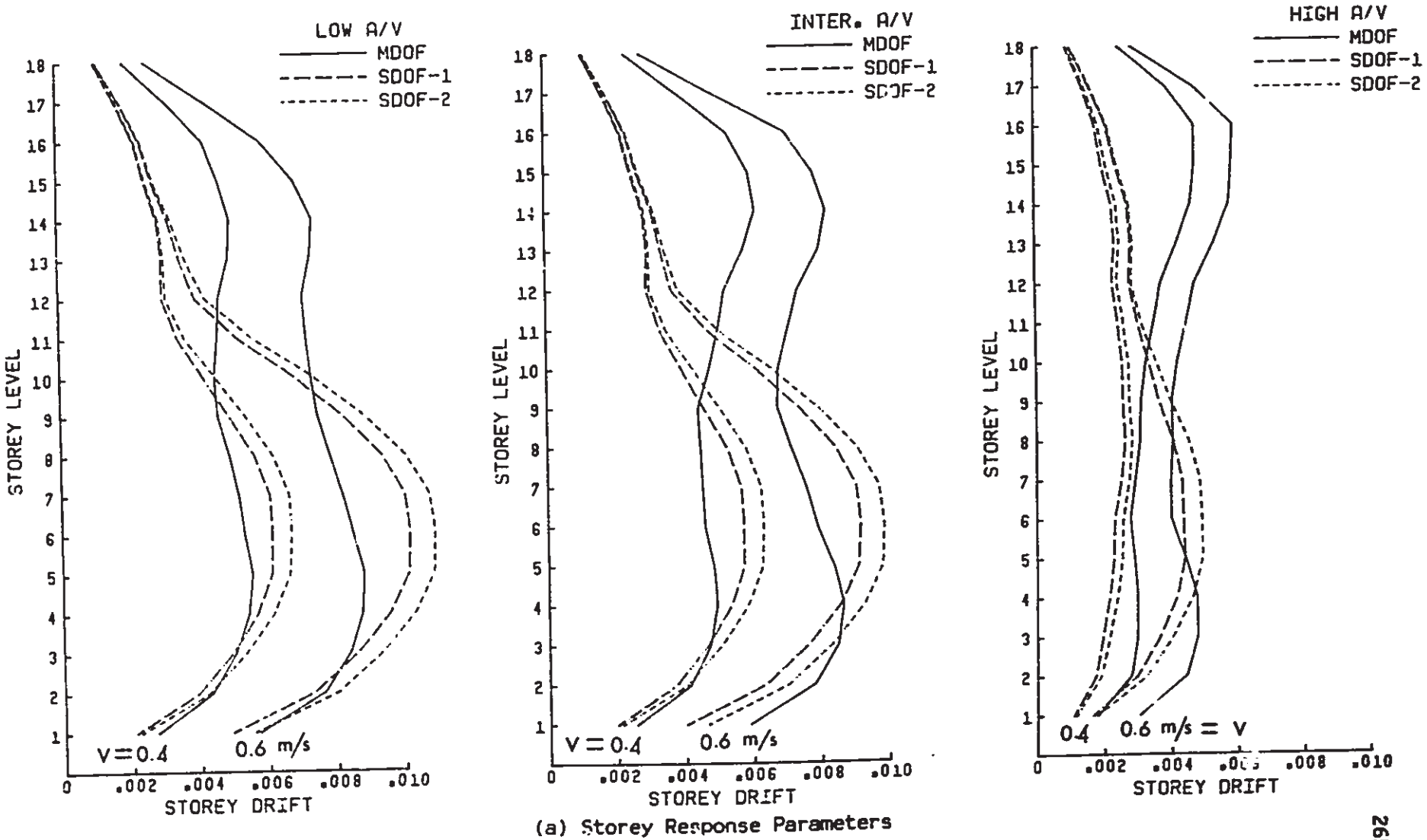

(a) Storey Response Parameters

Fig. 7.7 (cont'd) Comparison of Response Parameters between Simplified Analysis Procedure and MDOF Inelastic Dynamic Analysis for 18S Frame

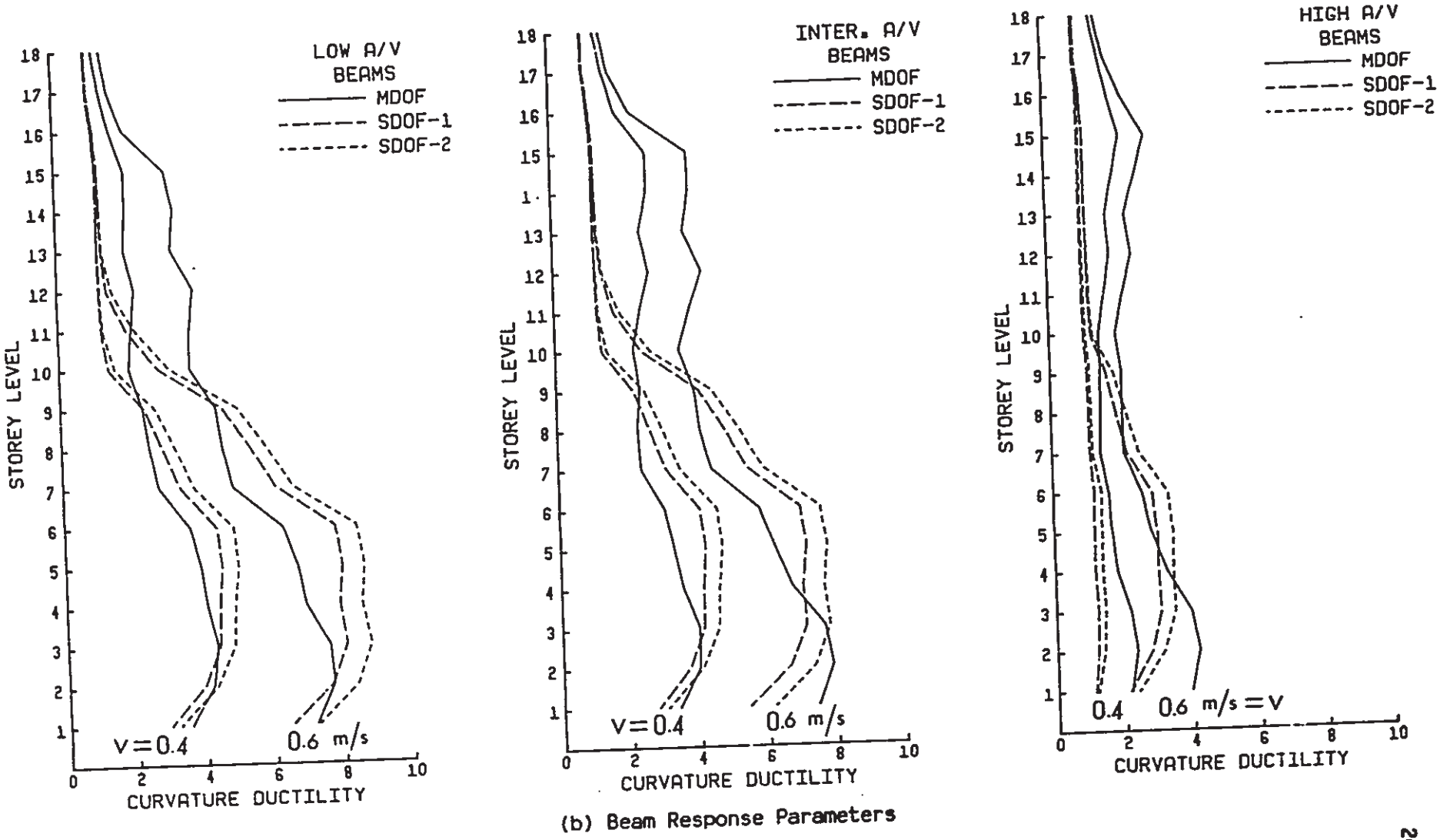

(b) Beam Response Parameters

Fig. 7.7 (cont'd) Comparison of Response Parameters between Simplified Analysis Procedure and MDOF Inelastic Dynamic Analysis for 18S Frame

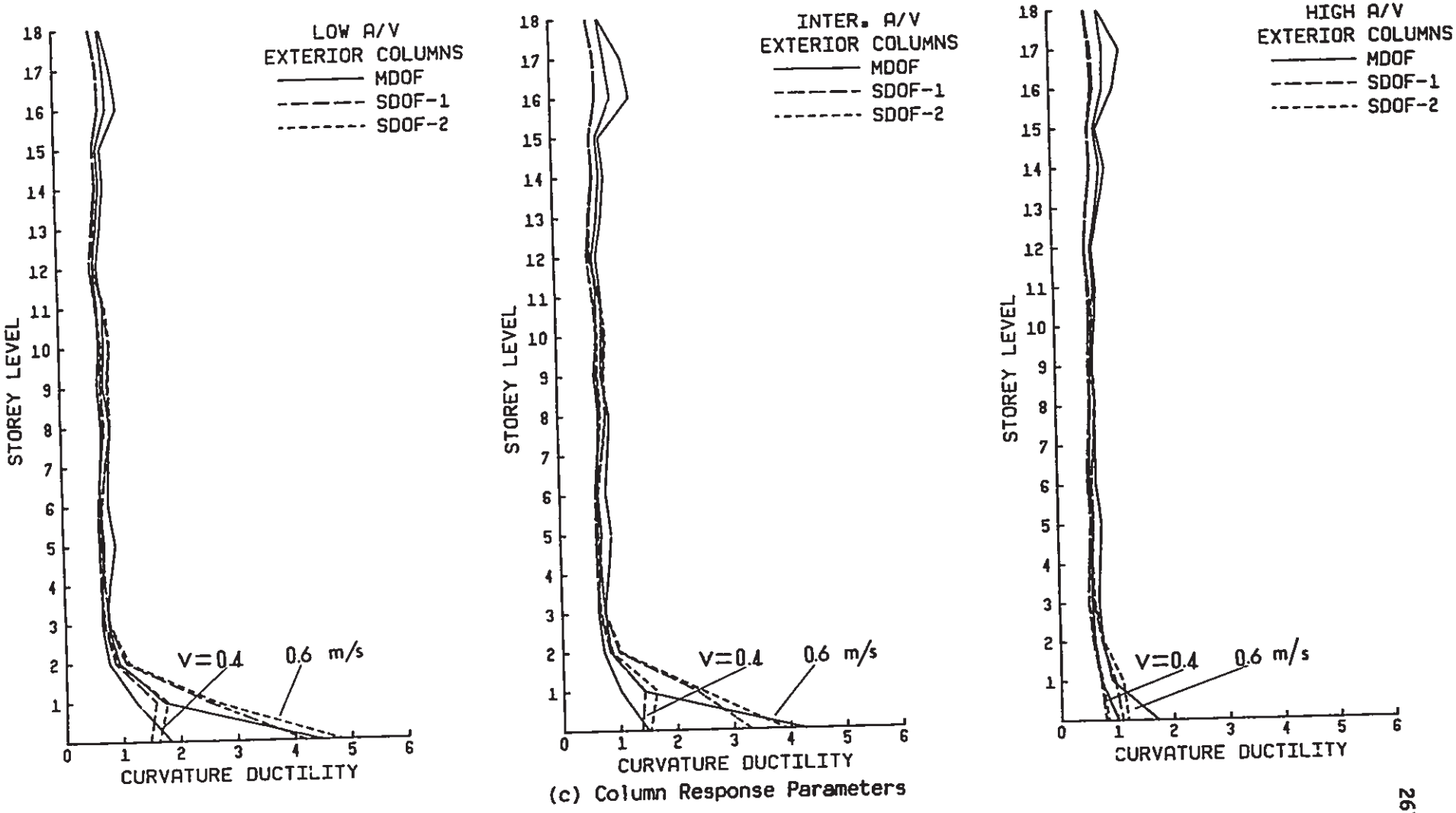

(c) Column Response Parameters

Fig. 7.7 (cont'd) Comparison of Response Parameters between Simplified Analysis Procedure and MDOF Inelastic Dynamic Analysis for 18S Frame

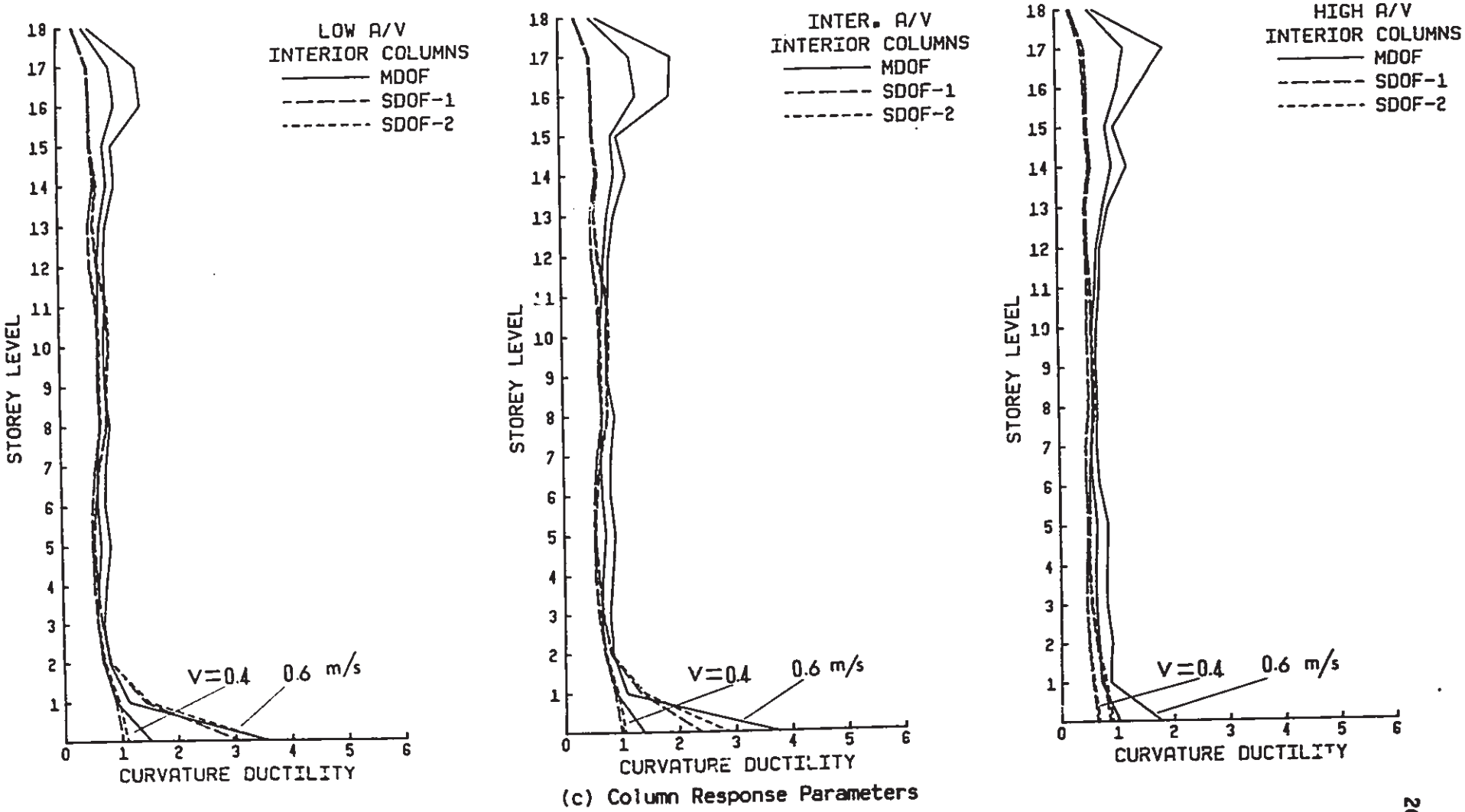

(c) Column Response Parameters

Fig. 7.7 (cont'd) Comparison of Response Parameters between Simplified Analysis Procedure and MDOF Inelastic Dynamic Analysis for 18S Frame

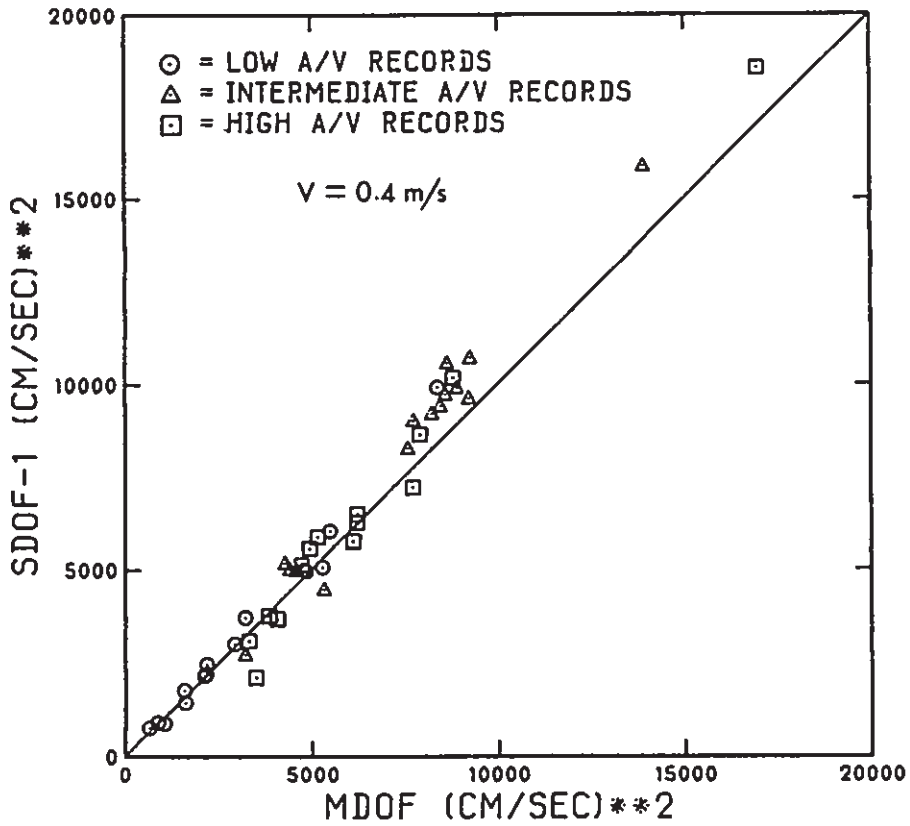

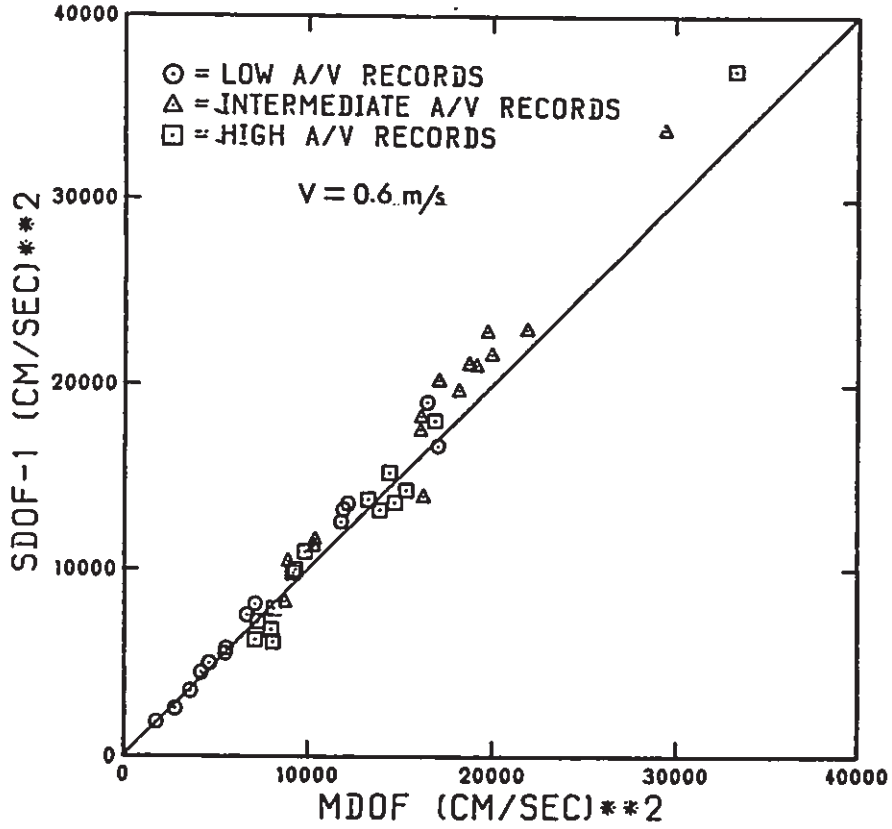

Fig. 7.8 Comparison of Input Energy between SDOF-1 and MDOF Models for 4S2 Frames

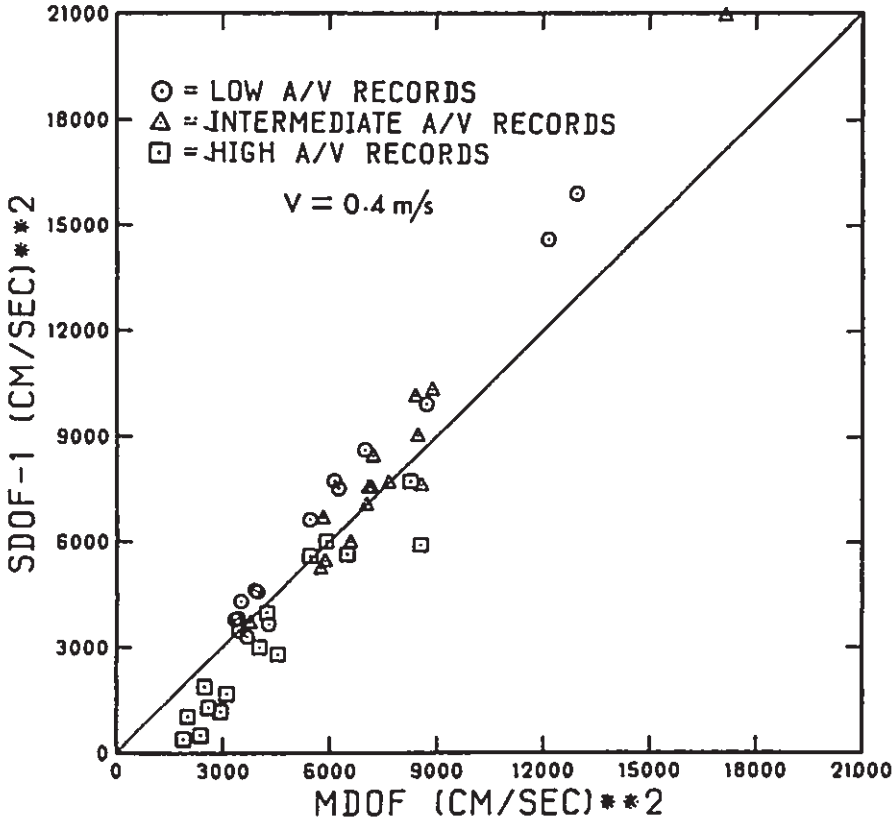

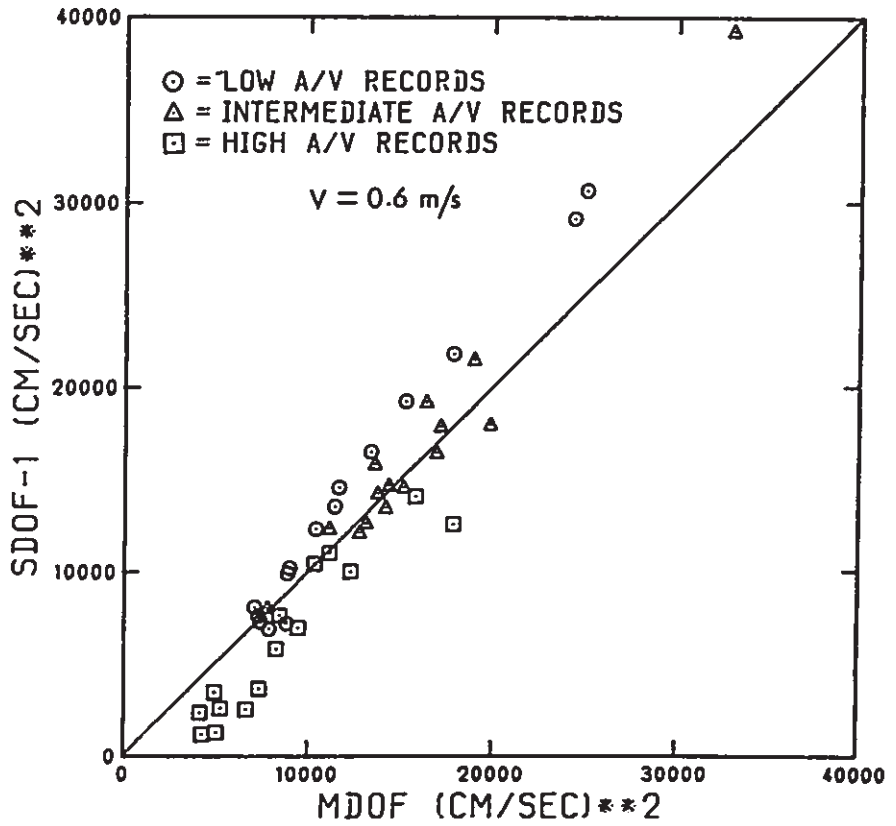

Fig. 7.9 Comparison of Input Energy between SDOF-1 and MDOF Models for 10S Frame

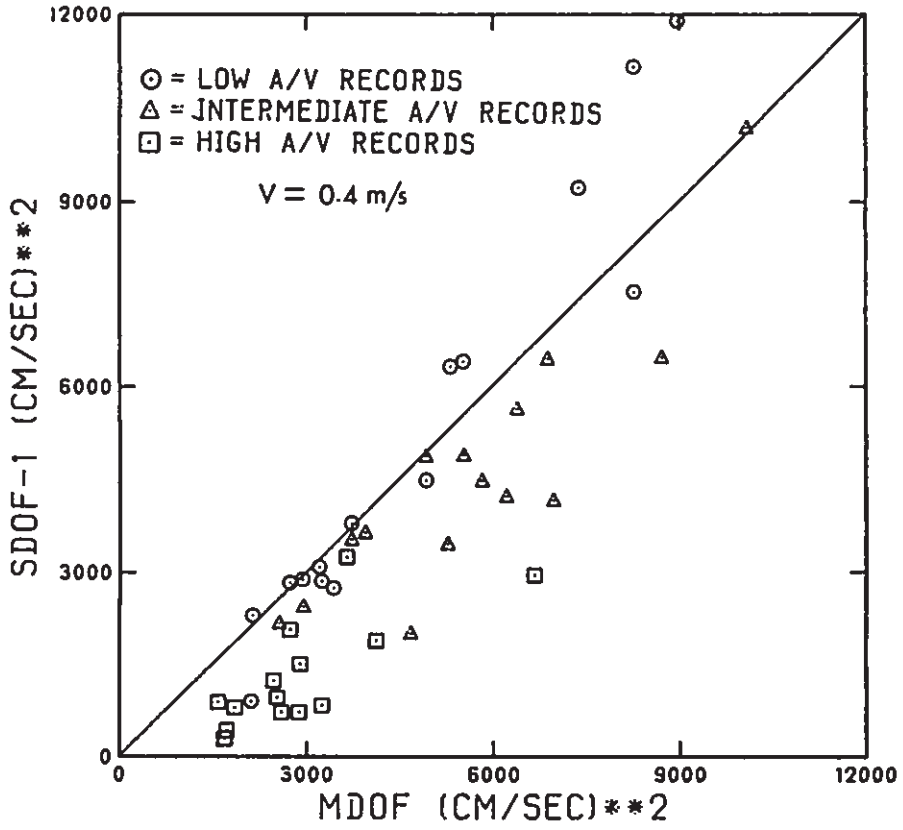

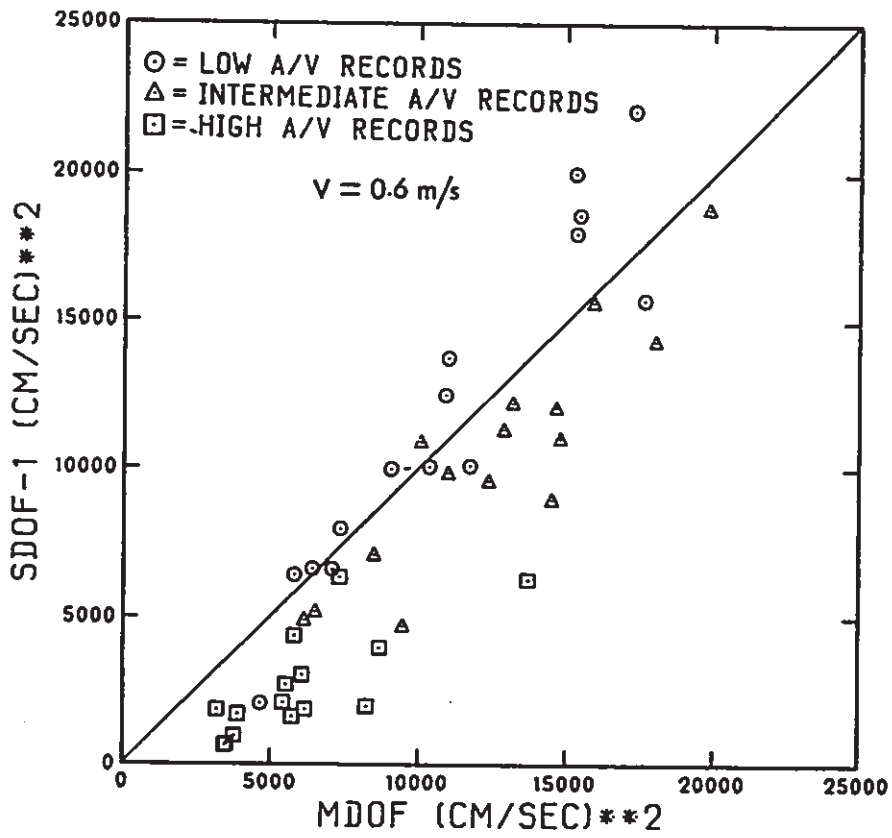

Fig. 7.10 Comparison of Input Energy between SDOF-1 and MDOF Models for 18S Frame

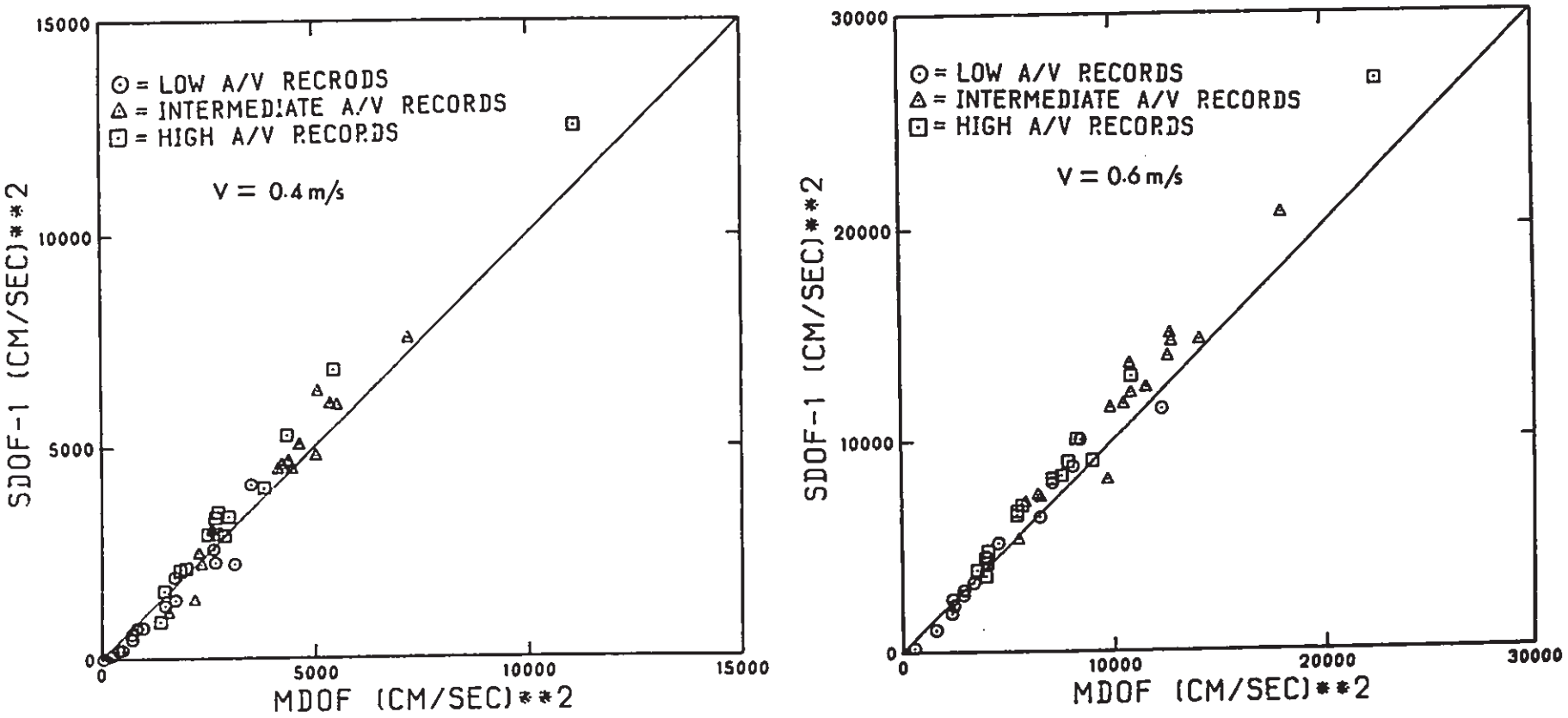

Fig. 7.11 Comparison of Hysteretic Energy between SDOF-1 and MDOF Models for 4S2 Frames

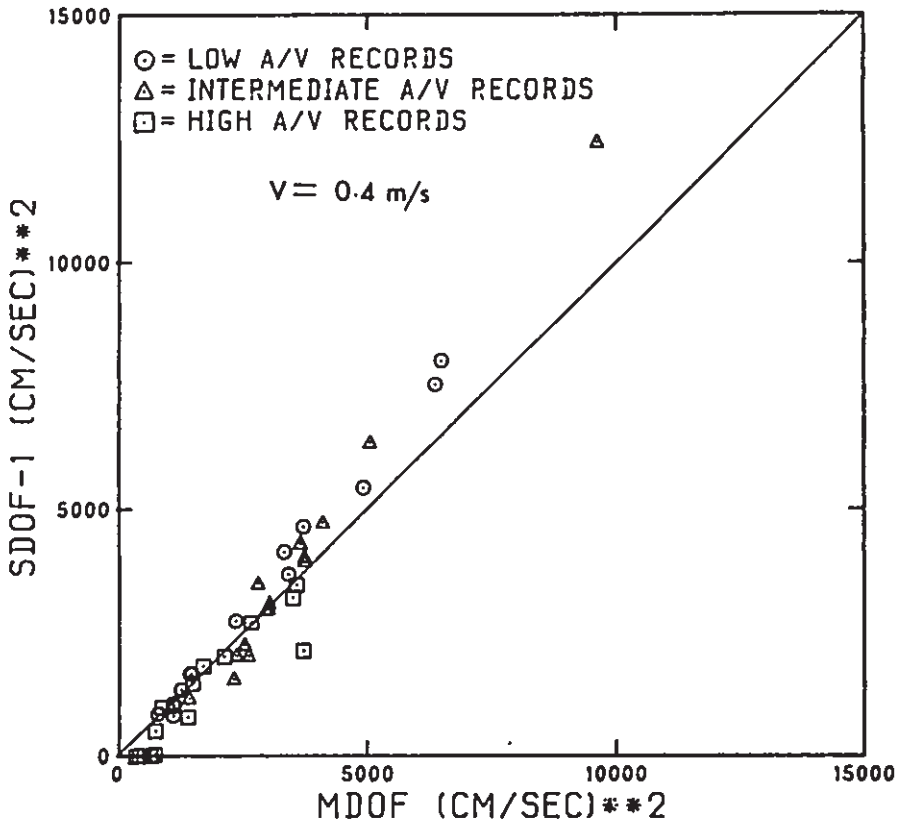

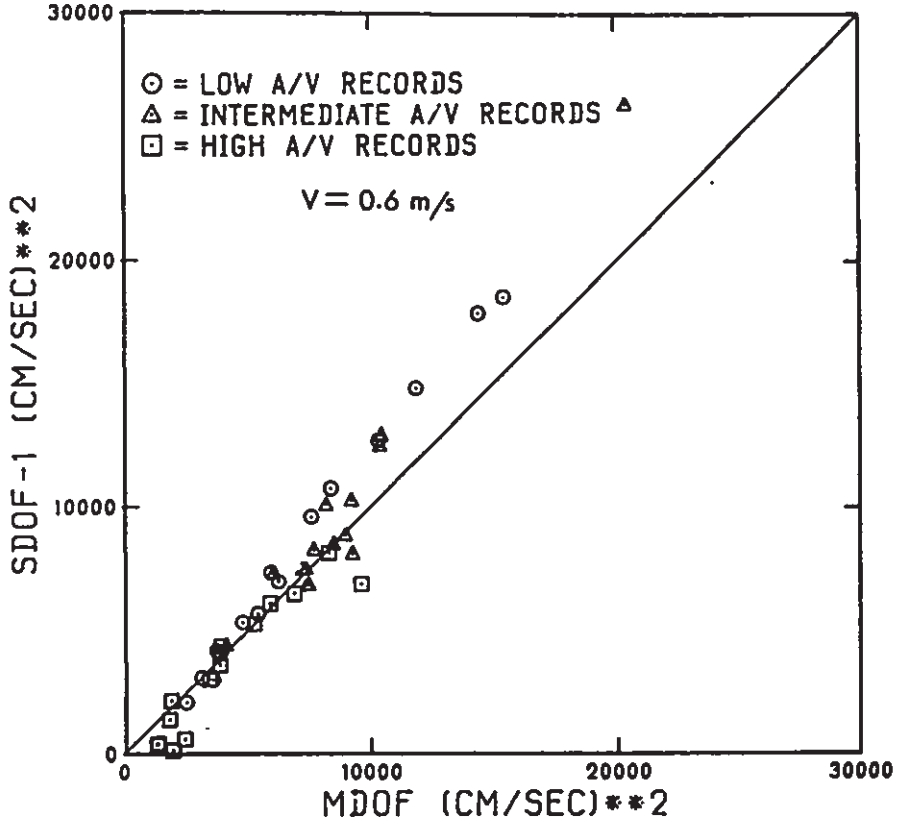

Fig. 7.12 Comparison of Hysteretic Energy between SDOF-1 and MDOF Models for 10S Frame

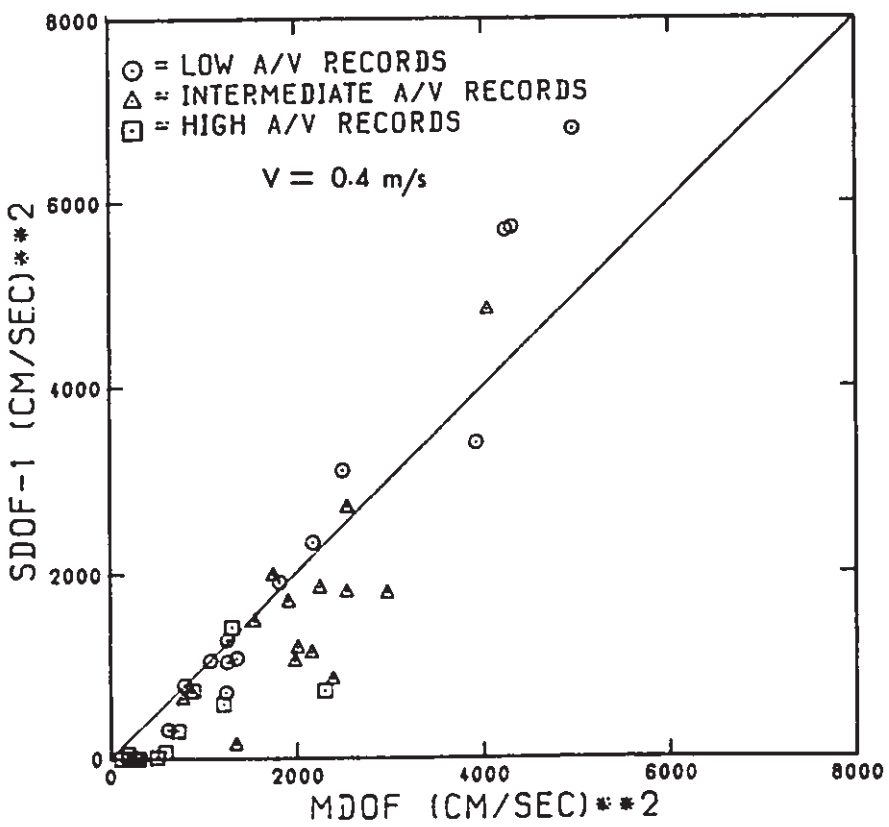

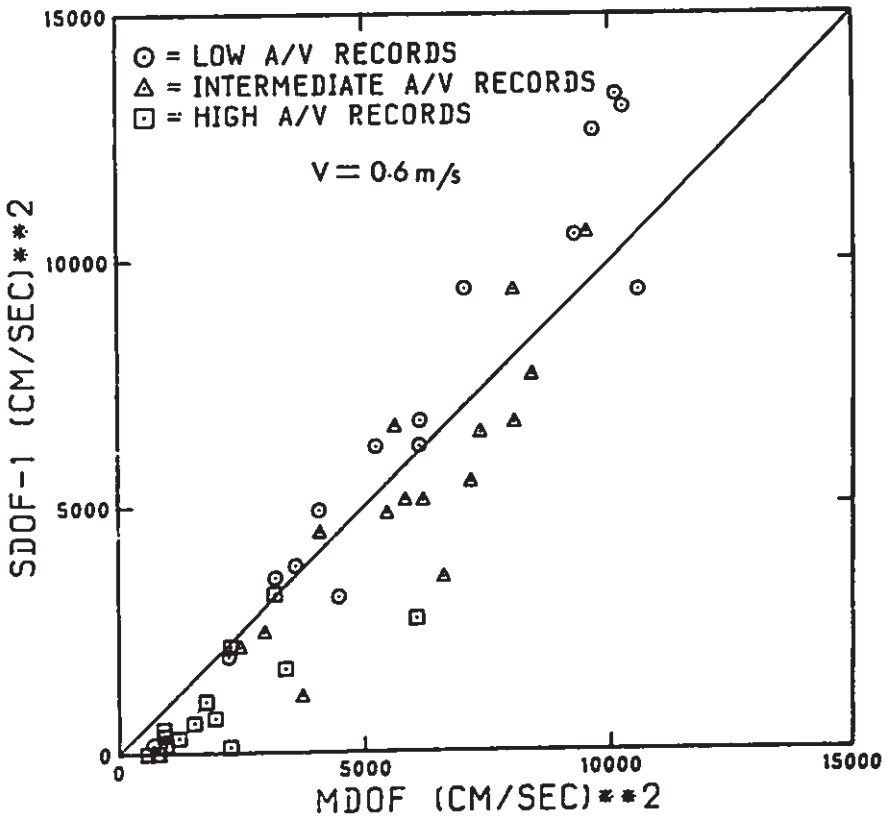

Fig. 7.13 Comparison of Hysteretic Energy between SDOF-1 and MDOF Models for 18S Frame

CHAPTER 8

SUMMARY AND CONCLUSIONS

8.1 Summary

The objectives of the present study were (a) to investigate the effect of ground motion A/V ratio on the inelastic response of multistorey reinforced concrete frame structures; (b) to evaluate the seismic performance of reinforced concrete frame structures designed in conformance with current Canadian seismic provisions; and (c) to study the possibility of using simplified analysis procedure to estimate both overall and localized inelastic deformations for regular building frames. To achieve these objectives, five different phases were involved in this study. They were (a) selection and analysis of an earthquake data set; (b) design of typical reinforced concrete building frames; (c) static analysis of the designed frames subjected to monotonically increased lateral loading; (d) dynamic analysis of the designed frames subjected to earthquake ground motions; and (e) development and evaluation of a simplified analysis procedure. A brief summary of these five phases is given below.

A total of 45 horizontal components of strong motion records were selected to form an earthquake data set for this study. This data set encompasses a wide range of earthquake magnitude and epicentral distance. The data set was subdivided into three groups representing earthquake ground motions having low, intermediate, and high A/V ratios. The three groups of earthquake accelerograms were analyzed to investigate the

significance of the A/V ratio as a parameter to indicate the dynamic characteristics of earthquake ground motions. First, the correlation between the A/V ratio and the M-R relationship was examined. In light of this examination, the usefulness of the A/V ratio to reflect information regarding the relative frequency content and duration of strong shaking for earthquake ground motions resulting from different seismic environments was investigated. Finally, the correlation of the A/V ratio with the more refined ground motion parameter of spectrum intensity was studied.

Regular moment-resisting reinforced concrete building frames were considered as structural models in this study. Three basic frames (4S2, 10S, and 18S) with four, ten, and eighteen storeys, respectively, were designed based on typical material properties. These three frames modeled regular buildings having short, moderate, and long fundamental periods. A special frame (4S1) was created from the 4S2 frame by increasing its member stiffness. This special frame modeled a regular building having a very short fundamental period. The frames were designed for combined gravity and seismic effects, determined in accordance with NBCC 1985. The structural members were proportioned and detailed to satisfy the requirements of CAN3-A23.3-M84. For the 4S1 or 4S2 frame, three different seismic design forces were used for the three different combinations of acceleration and velocity seismic zones, whereas the seismic design force for the 10S or 18S frame was independent of zonal combinations. Therefore, the seismic design resulted in a total of eight frames (4S1L, 4S1I, 4S1H, 4S2L, 4S2I, 4S2H, 10S, and 18S) having different amounts of flexural reinforcement for beams and columns.

In order to provide background information for the evaluation of the inelastic dynamic response of the designed frames to earthquake ground shaking, the inelastic behaviour of the designed frames subjected to monotonically increased lateral loading was studied first. The lateral loading was distributed over the height of the frames in accordance with the NBCC 1985 distribution formula. The inelastic behaviour of the frames under monotonically increased lateral loading was investigated from three different aspects. First, the sequence of plastic hinge formation in the beams and columns was traced. Secondly, the base shear versus roof displacement response of the frames was examined. Finally, the distributions of the various response parameters along the height of the frames for two different levels of overall drift was examined. In addition, the P-delta effect on the inelastic behaviour of the frames was studied, and the relationships among the different definitions of member ductility factors were examined.

The inelastic dynamic responses of the designed frames subjected to the three A/V groups of earthquake records were analyzed statistically. This inelastic dynamic analysis involved five different parts. First, the effectiveness of the NBCC 1985 base shear provisions to account for the effect of ground motion A/V ratio on short-period frames was investigated. This investigation was based on a comparison of two different analyses performed for the 4S1 frames. Second, the seismic performance of reinforced concrete building frames designed in conformance with NBCC 1985 and CAN3-A23.3-M84 was evaluated based on the statistical results of the various response parameters obtained for the 4S1, 4S2, 10S, and 18S frames. Third, the effect of peak ground velocity

level on the inelastic responses of frame structures was investigated. Fourth, the statistical results of the inelastic responses of the frames were compared with those of their corresponding elastic responses. Finally, the distributions of overall response parameters over height were compared for four different analyses, namely: (a) elastic static; (b) elastic dynamic; (c) inelastic static; and (d) inelastic dynamic analyses. In the course of the dynamic analyses, overall energy indices were defined for multistorey building frames, and their numerical computation was implemented in the DRAIN-2D program. This definition for multistorey frames is an extension of the definition for SDOF systems.

A simplified analysis procedure was proposed to estimate both overall and localized inelastic deformations for regular moment-resisting building frames. The procedure consists of three steps. These three steps are (a) transformation of a multistorey frame into an equivalent SDOF system based on an inelastic static analysis of the frame; (b) inelastic dynamic analysis of the equivalent SDOF system to provide an estimate of the roof displacement of the original frame; and (c) inelastic static analysis of the frame associated with the estimated roof displacement to provide estimates of overall and localized inelastic deformations. The simplified analysis procedure was evaluated for frames having different number of storeys and for earthquake ground motions having different A/V ratios. The evaluation was based on a comparison of the inelastic deformational demands estimated from the simplified analysis procedure with the statistical results obtained from the inelastic dynamic analysis of the frames.

8.2 Conclusions

The significant conclusions obtained from this study are summarized as follows:

(1) Ground Motion A/V Ratio

(a) The A/V ratio of earthquake ground motions is a viable parameter to indicate the M-R relationship associated with the motions. Ground motions in the proximity of small or moderate earthquakes usually have high A/V ratios whereas those at long distances from large earthquakes usually have low A/V ratios.

(b) Due to its tacit correlation with the M-R relationship, the A/V ratio is a useful, yet simple, parameter to indicate the relative frequency content and duration of strong shaking for earthquake ground motions resulting from different seismic environments. Ground motions having high A/V ratios are usually of short duration with seismic energy in the high frequency range whereas those with low A/V ratios usually have long duration with energy in the low frequency range.

(c) Peak ground velocity correlates well with the spectrum intensity, irrespective of the A/V ratio of earthquake records, whereas the relationship between peak ground acceleration and the spectrum intensity strongly depends on the A/V ratio. Therefore, peak ground velocity is a superior descriptor of the intensity of earthquake ground shaking at a site for building design, as compared to peak ground acceleration.

(2) Inelastic Static Analysis

(a) The sway mechanisms of the frames designed in conformance with NBCC 1985 and CAN3-A23.3-M84 are somewhat between the beam sidesway mechanism and the column sidesway mechanism, when they are subjected to monotonically increased lateral loading which is distributed over height in accordance with the NBCC 1985 distribution formula. In order to attain the desired complete beam sidesway mechanism, the column strengths need to be increased over those suggested by CAN3-A23.3-M84.

(b) The actual overall strengths of the frames are higher than their factored design base shears. Therefore, there is seismic overstrength for the frames designed in conformance with NBCC 1985 and CAN3-A23.3-M84. This overstrength for low rise frames is more significant than that for high rise frames.

(c) The overall stiffnesses of the frames are reduced substantially after the formation of the first column hinge. This reduction in the overall stiffness is particularly pronounced for high rise frames because the softening effect due to the P-Delta phenomenon for high rise frames is more significant than that for low rise frames in the inelastic range.

(d) As the frames are loaded well into the inelastic range, inelastic deformations tend to be concentrated in the lower storey beams and at the base of the first storey columns. This concentration of inelastic deformations leads to very large interstorey displacements in the lower storeys, and the maximum interstorey drift in the lower storeys can be substantially higher than the corresponding overall drift.

(3) Inelastic Dynamic Analysis

(a) If the specification of seismic design forces is directly tied to peak ground velocity, ground motion A/V ratio has a very significant effect on the inelastic response of building frames having short fundamental periods. The use of a single seismic response factor results in different values for the various overall and localized response parameters for short period frames, when subjected to earthquake ground motions having different A/V ratios. The response parameters for high A/V ground motions are considerably higher than those for low A/V ground motions. The use of three different seismic response factors for the three different ranges of A/V ratio, as suggested in NBCC 1985, provides slight improvement in the consistency of maximum storey displacement and interstorey drift. However, the consistency in member curvature ductility demands and overall displacement ductility demands is significantly improved. This improvement in ductility demands results from the fact that the use of three different seismic design forces for the three different A/V ranges leads to three frames having different member yield curvatures and overall yield displacements on which the computation of ductility factors is based.

(b) For low rise frames, inelastic deformations tend to be concentrated at the bottom of the frames, irrespective of the A/V ratio of the input ground motions. This distribution of inelastic deformations over height for earthquake excitation is similar to that for monotonically increased lateral loading. For high rise frames, the distributions of inelastic deformations over height are strongly affected by the A/V ratio of the input ground motions. For low A/V ground motions

which have lower frequency content, inelastic deformations tend to be concentrated in lower storeys. For high A/V ground motions which have higher frequency content, the "whiplash" effect is very significant due to significant contribution of higher modes, and inelastic deformation in the upper storeys can be significantly higher than those in the lower storeys.

(c) While low A/V ground motions produce slightly lower inelastic deformations than high A/V ground motions in the upper storeys of high rise frames, they develop considerably higher inelastic deformations in the lower storeys. Because the lower storeys are more critical than the upper storeys due to the high axial loads carried by the columns, low A/V ground motions tend to be more damaging to high rise frames than high A/V ground motions even when the frames are designed based on peak ground velocity.

(d) Seismic design based on NBCC 1985 and CAN3-A23.3-M84 leads to nonuniform ductility demands for frames having different fundamental periods. The member curvature ductility demands and the overall displacement ductility demands for short period frames tend to be higher than those for long period frames. This is particularly true for the curvature ductility demands at the base of the first storey columns. The nonuniform ductility demands for frames with different fundamental periods are attributable to the use of a period-independent structural behaviour coefficient K and different amplifications of column design moments due to slenderness effect for frames having different numbers of storeys.

(e) Because of the seismic overstrength of the frames as compared to their factored seismic design forces, the global displacement ductility demands of the frames are generally lower than the displacement ductility demands of the corresponding SDOF systems whose periods are the same as the fundamental periods of the frames and whose yield strengths are specified as factored seismic design forces from the NBCC 1985 base shear formula. This difference is particularly pronounced for short period frames, because short period frames have more significant overstrength than long period frames.

(f) The mean+σ global displacement ductility demands for frames with moderate and long fundamental periods subjected to design level earthquake excitations are generally lower than the expected "system ductility" as implied by the value of the K factor used in the design. For frames with very short fundamental periods, the mean+σ overall displacement ductility demands would exceed the expected value.

(g) For a comparable level of overall drift, the dynamic overstrength of the frames as compared to their factored seismic design forces tends to be more significant than the static overstrength. This is particularly true for high rise frames.

(h) The inelastic deformations in the lower storeys are highly sensitive to the peak ground velocity level of the input ground motions for both low and high rise frames. A 50% increase in the peak ground velocity of the input ground motions results in nearly 100% increase in the curvature ductility demands for the structural members in the lower storeys. As a result, the interstorey drifts in the lower storeys are also significantly increased. In addition, the input energy is more than

doubled. Most of the increased input energy has to be dissipated through hysteretic action. This clearly points out the need for accurate evaluation of the peak ground velocity expected at a building site as well as appropriate assessment of the uncertainties associated with this evaluation.

(i) For frames having very short fundamental periods, the maximum storey displacements for inelastic response tend to be higher than those for elastic response. The reverse tends to be true for frames having moderate or long fundamental periods. The global displacement ductility demands are close to the ratios of elastic to inelastic dynamic base shears for moderate or long period frames, whereas the overall ductility demands are significantly higher than the force ratios for short period frames. The input energy for inelastic response is similar to that for elastic response. This correlation appears to be better for long period frames than for short period frames.

(j) For low rise frames, the inelastic static analysis provides very similar distributions of interstorey deflections to those of the inelastic dynamic analysis. Both elastic static and dynamic analyses tend to underestimate the interstorey deflections at the bottom of the frames. For high rise frames, the distribution of interstorey deflections for the elastic dynamic analysis is similar to that for the inelastic dynamic analysis in the upper storeys. The use of both inelastic and elastic static analyses grossly underestimates the interstorey drift in the upper storeys. This underestimation is particularly pronounced for high A/V ground motions. In the lower storeys, the distribution of interstorey drift for the inelastic static analysis is close to that for the

inelastic dynamic analysis. The use of elastic dynamic or static analysis tends to underestimate interstorey drift in the lower storeys. This is particularly true for low A/V ground motions.

(k) For high rise frames, the contribution of higher modes to interstorey drift in the upper storeys tends to decrease with an increase in the level of inelastic response.

(4) Simplified Analysis Procedure

(a) The two equivalent SDOF models examined in this study provide satisfactory estimates of the maximum roof displacement for frames having different number of storeys and for earthquake ground motions having different A/V ratios.

(b) For low-rise frames, the simplified analysis procedure produces good estimates of both overall and localized inelastic deformations for earthquake ground motions having different A/V ratios.

(c) For high-rise frames, the simplified analysis procedure results in reasonable estimates of the maximum storey displacement. However, the simplified analysis procedure grossly underestimates the interstorey drifts in the upper storeys. This underestimation is particularly pronounced for high and intermediate A/V ground motions. The beam and column inelastic deformations in the upper storeys are also underestimated by the simplified analysis procedure.

(d) There is a close correlation of the input and hysteretic energy per unit mass between the SDOF-1 and MDOF models for low rise frames. Therefore, the SDOF-1 model may be used to estimate the energy per unit mass imparted to and the hysteretic energy per unit mass dissipated in a

low rise frame. For high rise frames, there is no consistent correlation of the input and hysteretic energy between the SDOF-I and MDOF models.

It is suggested that the simplified analysis procedure be used for regular building frames having number of storeys lower than 10. For high-rise frames, the simplified analysis procedure may be used to estimate maximum storey displacements. The interstorey drifts and member inelastic deformations in the lower storeys may also be estimated by the simplified analysis procedure.

8.3 Design Implications and Recommendations for Future Research

In this study, the nonlinear dynamic response of reinforced concrete building frames to earthquake ground motions having different A/V ratios has been investigated. The analytical results have permitted an evaluation of the current Canadian seismic design practice. In this section, the significant design implications of this evaluation are reviewed, and recommendations for future research are provided.

The ductility demands for low rise building frames are generally much higher than those for high rise building frames despite the fact that low rise building frames have more significant seismic overstrength than high rise building frames with respect to their nominal code design strengths. The higher ductility demand for low rise buildings is mainly due to the use of a period-independent structural behaviour coefficient, K, in the specification of total lateral seismic design forces in NBCC 1985. This issue needs to be addressed in the future development of the base shear provisions in the National Building Code of Canada. To avoid excessive ductility demand, the design strengths for low rise buildings

should not be significantly reduced from their elastic strength demands. In addition, inelastic deformation tends to be concentrated at the bottom of low rise building frames, irrespective of the A/V ratio of the input ground motions. Therefore, special attention should be given to the design and detailing of columns and beams at the bottom of low rise buildings.

For high rise building frames located in high A/V seismic zones, inelastic deformation tends to be concentrated in the upper storeys. In particular, plastic hinges would be developed in the upper storey columns. Therefore, careful detailing should be given to the upper storey columns. For high rise buildings situated in low A/V seismic regions, inelastic deformation tends to be concentrated in the lower storeys. To avoid excessive P-delta effect, the interstorey drift needs to be controlled.

The use of elastic static analysis coupled with a displacement amplification factor for estimating interstorey drift, as currently suggested in many building codes, is inadequate for both low and high rise buildings. For low rise buildings, the elastic static analysis seriously underestimates interstorey drift at the bottom of the buildings. For high rise buildings, the elastic static analysis grossly underestimates interstorey drift in the upper storeys. Therefore, improved methods for estimating interstorey drift need to be developed for building codes.

REFERENCES

1. Adeli, H., Gere, J. M., and Weaver, W., "Algorithms for Nonlinear Structural Dynamics", Journal of Structural Division, ASCE, Vol. 104, No. ST2, Feb. 1978, pp. 263-280.

2. Anagnostopoulos, S. A., "Nonlinear Dynamic Response and Ductility Requirements of Building Structures Subjected to Earthquakes", Report No. R72-54, Department of Civil Engineering, Massachusetts Institute of Technology, Cambridge, Mass., Sept. 1972.

3. Anagnostopoulos, S. A., Haviland, R. W., and Biggs, J. M., "Use of Inelastic Spectra in Aseismic Design", Journal of the Structural Division, ASCE, Vol.104, No.ST1, Jan. 1978, pp. 95-109.

4. Applied Technology Council, An Evaluation of a Response Spectrum Approach to Seismic Design of Buildings, San Francisco, Calif., Sept. 1974.

5. Applied Technology Council, Tentative Provisions for the Development of Seismic Regulations for Buildings, Special Publication 510, National Bureau of Standards, Washington, D.C., 1978.

6. Arias, A., "A Measure of Earthquake Intensity", in Seismic Design for Nuclear Power Plants, R. J. Hansen, Editor, Massachusetts Institute of Technology Press, Cambridge, Mass., 1970, pp. 438-483.

7. Associate Committee on National Building Code, National Building Code of Canada 1980, NRCC No. 17303; The Supplement to the National Building Code of Canada 1980, NRCC No. 17724, National Research Council, Ottawa, 1980.

8. Associate Committee on National Building Code, National Building Code of Canada 1985, NRCC No. 23174; The Supplement to the National Building Code of Canada 1985, NRCC No. 23178, National Research Council, Ottawa, 1985.

9. Atalay, M. B. and Penzien, J., "The Seismic Behavior of Critical Regions of Reinforced Concrete Components as Influenced by Moment, Shear and Axial Force", Report No. EERC 75-19, Earthquake Engineering Research Center, University of California, Berkeley, Calif., Dec. 1975.

10. Basham, P. W., Weichert, D. H., Anglin, F. M., and Berry, M. J., "New Probabilistic Strong Seismic Ground Motion Maps of Canada", Bulletin of the Seismological Society of America, Vol.75, 1985, pp. 563-595.

11. Bathe, K. J. and Wilson, E. L., "Stability and Accuracy Analysis of Direct Integration Methods", Earthquake Engineering and Structural Dynamics, Vol. 1, No. 3, Jan.-Mar. 1973, pp. 283-291.

12. Bertero, V. V., Herrera, R. A., and Mahin, S. A., "Establishment of Design Earthquakes - Evaluation of Present Methods", Proceedings of the International Symposium on Earthquake Structural Engineering, St. Louis, Mo., Aug. 1976, Vol. I, pp. 551-580.

13. Bertero, V. V. and Kamil, H., "Nonlinear Seismic Design of Multistory Frames", Canadian Journal of Civil Engineering, Vol.2, No.4, Dec. 1975, pp. 494-516.

14. Bertero, V. V. and Mahin S. A., "Need for a Comprehensive Approach in Establishing Design Earthquakes", Proceedings of the Second International Conference on Microzonation for Safer Construction, Research and Application, San Francisco, Calif., Nov.-Dec. 1978, pp. 1145-1156.

15. Bertero, V. V., Mahin, S. A., and Herrera, R. A., "Aseismic Design Implications of Near-Fault San Fernando Earthquake Records", Earthquake Engineering and Structural Dynamics, Vol. 6, No. 1, Jan.-Feb. 1978, pp. 1304-1313.

16. Bertero, V. V., Popov, E. P., and Wang, T. Y., "Hysteretic Behavior of Reinforced Concrete Members with Special Web Reinforcement", Report No. EERC 74-9, Earthquake Engineering Research Center, University of California, Berkeley, Calif., 1974.

17. Biggs, J. M., Introduction to Structural Dynamics, McGraw-Hill Book Co., 1964.

18. Bolt, B. A., "Duration of Strong Ground Motion", Proceedings of the Fifth World Conference on Earthquake Engineering, Rome, Italy, 1973, Vol. I, pp. 1304-1313.

19. Canadian Portland Cement Association, Metric Design Handbook for Reinforced Concrete Elements in Accordance with the Strength Design Method of CSA A23.3-M1977, 1978.

20. Canadian Standards Association, Design of Concrete Structures for Buildings, CAN3-A23.3-M84, Ottawa, 1984.

21. Chopra, A. K. and Kan, C. L., "Effect of Stiffness Degradation on Earthquake Ductility Requirements for Multistorey Buildings", Earthquake Engineering and Structural Dynamics, Vol.2, No.1, 1973, pp. 35-45.

22. Cloud, W. K., "Intensity Map and Structural Damage, Parkfield, California, Earthquake of June 27, 1966", Bulletin of the Seismological Society of America, Vol. 57, No. 6, Dec. 1967, pp. 1161-1178.

23. Clough, R. W. and Benuska, K. L., "Nonlinear Earthquake Behavior of Tall Buildings", Journal of the Engineering Mechanics Division, ASCE, Vol.93, No. EM3, June 1967, pp. 129-146.

24. Clough, R. W. and Johnston, S. B., "Effect of Stiffness Degradation on Earthquake Ductility Requirement", Proceedings of Japan Earthquake Engineering Symposium, Tokyo, Japan, Oct. 1966, pp. 227-232.

25. Esteva, L. and Rosenblueth, E., "Espectros de Temblores a Distancias Moderadas y Granades", Bol. Soc. Mex. Ing. Sism. Vol.2, No.1, 1964, pp. 1-18.

26. Furlong, R. W., "Column Slenderness and Charts for Design", Journal of the American Concrete Institute, Vol.68, No.1, Jan. 1971, pp. 9-17.

27. Giberson, M. F., "Two Nonlinear Beams with Definitions of Ductility", Journal of the Structural Division, ASCE, Vol.95, No.ST2, Feb. 1969, pp. 137-157.

28. Gulkan, P. and Sozen, M. A., "Inelastic Response of Reinforced Concrete Structures to Earthquake Motions", Journal of the American Concrete Institute, Vol. 71, No. 12, Dec. 1974, pp. 604-610.

29. Hall, W. J., "Observations on Some Current Issues Pertaining to Nuclear Power Plant Seismic Design", Nuclear Engineering and Design, Vol.69, 1982, pp. 365-378.

30. Hall, W. J. and McCabe, S. L., "Observations on Spectra and Design", Proceedings of the Third U.S. National Conference on Earthquake Engineering, Charleston, South Carolina, 1986, pp. 1117-1127.

31. Heidebrecht, A. C., Basham, P. W., Rainer, J. H., and Berry, M. J., "Engineering Applications of New Probabilistic Seismic Ground-Motion Maps of Canada", Canadian Journal of Civil Engineering, Vol. 10, No. 4, 1983, pp. 670-680.

32. Heidebrecht, A. C. and Tso, W. K., "Seismic Loading Provision Changes in National Building Code of Canada 1985", Canadian Journal of Civil Engineering, Vol.12, 1985, pp. 653-660.

33. Heidebrecht, A. C., Tso, W. K., and Cherry, S., "Future Directions of Canadian Seismic Code Provisions", Proceedings of Annual Conference of Canadian Society of Civil Engineering, Edmonton, Alberta, June 1983, pp. 381-394.

34. Hidalgo, P. and Clough, R. W., "Earthquake Simulation Study of a Reinforced Concrete Frame", Report No. EERC 74-13, Earthquake Engineering Research Center, University of California, Berkeley, Calif., 1974.

35. Housner, G. W., "Spectrum Intensities of Strong-Motion Earthquakes", Proceedings of the Symposium on Earthquakes and Blast Effects on Structures, Los Angeles, Calif., 1952, pp. 20-36.

36. Housner, G. W., "Intensity of Ground Shaking near the Causative Fault", Proceedings of the Third World Conference on Earthquake Engineering, Wellington, New Zealand, Vol.I, 1965, pp. 94-115.

37. Housner, G. W., "Strong Ground Motion", Chapter IV in Earthquake Engineering, R. L. Wiegle, Prentice-Hall, Englewood Cliffs, N.J., 1970.

38. Housner, G. W., "Earthquake Research Needs for Nuclear Power Plants", Journal of the Power Division, ASCE, Vol. 97, No. PO1, Jan. 1971, pp. 77-91.

39. Housner, G. W., "Measures of Severity of Earthquake Ground Shaking", Proceedings of the First U.S. National Conference on Earthquake Engineering, An Arbor, Mich., June 1975, pp. 25-33.

40. Humar, J. L., "Seismic Design of Multistorey Steel-Frame Buildings Using Dynamic Analysis", Canadian Journal of Civil Engineering, Vol.6, No.2, June 1979, pp. 173-185.

41. Humar, J. L., "Seismic Response of Reinforced Concrete Frames", Journal of the Structural Division, ASCE, Vol.107, No.ST7, July 1981, pp. 1215-1232.

42. Iwan, W. D., "Estimating Inelastic Response Spectra from Elastic Spectra", Earthquake Engineering and Structural Dynamics, Vol. 8, No. 4, July-Aug. 1980, pp. 375-388.

43. Iwan, W. D. and Gates, N. C., "The Effective Period and Damping of a Class of Hysteretic Structures", Earthquake Engineering and Structural Dynamics, Vol. 7, No. 3, May-June 1979, pp. 199-211.

44. Jennings, P. C., "Earthquake Response of a Yielding Structure", Journal of the Engineering Mechanics Division, ASCE, Vol.91, No.EM4, Aug. 1965, pp. 41-68.

45. Kaba, S. and Mahin, S., "Refined Modelling of Reinforced Columns for Seismic Analysis", Report No. EERC 84-03, Earthquake Engineering Research Center, University of California, Berkeley, Calif., 1984.

46. Kanaan, A. and Powell, G. H., "General Purpose Computer Program for Inelastic Dynamic Response of Plane Structures", Report No. EERC 73-6, Earthquake Engineering Research Center, University of California, Berkeley, Calif., 1973.

47. Kent, D. C. and Park, R., "Flexural Members with Confined Concrete", Journal of the Structural Division, ASCE, Vol.97, No.ST7, July 1971, pp. 1969-1990.

48. Keshavarzian, M. and Schnobrich, W. C., "Inelastic Analysis of R/C Coupled Shear Walls", Earthquake Engineering and Structural Dynamics, Vol.13, 1985, pp. 427-448.

49. Lai, S. A. and MacGregor, J. G., "Geometric Nonlinearities in Unbraced Multistory Frames", Journal of Structural Engineering, ASCE, Vol.109, No.11, Nov. 1983, pp. 2528-2545.

50. Lai, S. P. and Biggs, J. M., "Inelastic Response Spectra for Aseismic Building Design", Journal of the Structural Division, ASCE, Vol.106, No.ST6, June 1980, pp. 1295-1310.

51. Ma, S. M., Bertero, V. V., and Popov, E. P., "Experimental and Analytical Studies on the Hysteretic Behavior of Reinforced Concrete Rectangular and T-Beams", Report No. EERC 76-2, Earthquake Engineering Research Center, University of California, Berkeley, Calif., May 1976.

52. Mahin, S. A. and Bertero, V. V., "Prediction of Nonlinear Seismic Building Behavior", Journal of the Technical Councils, ASCE, Vol.104, No.TC1, Nov. 1978, pp. 21-37.

53. Mahin, S. A. and Bertero, V. V., "An Evaluation of Inelastic Seismic Design Spectra", Journal of the Structural Division, ASCE, Vol. 107, No. ST9, Sept. 1981, pp. 1777-1795.

54. McCann, N. W. and Shah, H. C., "Determining Strong-Motion Duration of Earthquakes", Bulletin of the Seismological Society of America, Vol. 69, No. 4, Aug. 1979, pp. 1253-1265.

55. Muto, K., Seismic Analysis of Reinforced Concrete Buildings, Skokoku-Sha, Japan, 1965.

56. Nau, J. M. and Hall, W. J., "Scaling Methods for Earthquake Response Spectra", Journal of Structural Engineering, ASCE, Vol. 110, No. 7, July 1984, pp. 1533-1548.

57. Newmark, N. M., "A Method of Computation for Structural Dynamics", Transactions, ASCE, Vol. 127, 1962, pp. 1406-1435.

58. Newmark, N. M., "Seismic Design Criteria for Structures and Facilities, Trans-Alaska Pipeline Systems", Proceedings of the First U.S. National Conference on Earthquake Engineering, Earthquake Engineering Research Institute, Ann Arbor, Mich., June 1975, pp. 94-103.

59. Newmark, N. M., "A Rationale for Development of Design Spectra for Diablo Canyon Reactor Facility", Report for the U.S. Nuclear Regulatory Commission, N. M. Newmark Consulting Engineering Services, Urbana, Ill., 1976

60. Newmark, N. M. and Hall, W. J., "Procedures and Criteria for Earthquake Resistant Design", Building Practices for Disaster Mitigation, Building Science Series No. 46, National Bureau of Standards, Washington, D.C., Feb. 1973, pp. 209-236.

61. Newmark, N. M. and Hall, W. J., "Development of Criteria for Review of Selected Nuclear Power Plants, Report for the U. S. Nuclear Regulatory Commission, NUREG/CR-0098, N. M. Newmark Consulting Engineering Services, Urbana, Ill., 1978.

62. Newmark, N. M. and Hall, W. J., Earthquake Spectra and Design, Earthquake Engineering Research Institute, Berkeley, Calif., 1982.

63. Otani, S., "Nonlinear Dynamic Analysis of Reinforced Concrete Building Structures", Canadian Journal of Civil Engineering, Vol. 7, 1980, pp. 334-344.

64. Otani, S., "Hysteretic Models of Reinforced Concrete for Earthquake Response Analysis", Journal of the Faculty of Engineering, University of Tokyo, Vol.36, No.2, 1981.

65. Otani, S. and Sozen, M. A., "Behavior of Multistory Reinforced Concrete Frames during Earthquakes", Structural Research Series No. 392, Civil Engineering Studies, University of Illinois, Urbana, Ill., Nov. 1972.

66. Page, R. A., Boore, D. M., Joyner, W. B., and Coulter, H. W., "Ground Motion Values for Use in the Seismic Design of the Trans-Alaska Pipeline System", Circular 672, U. S. Geological Survey, Washington, D.C., 1972.

67. Park, R., Kent, D. C., and Sampson, R. A., "Reinforced Concrete Members with Cyclic Loading", Journal of the Structural Division, ASCE, Vol.98, No.ST7, July 1972, pp. 1341-1360.

68. Park, R. and Paulay, T., Reinforced Concrete Structures, John Wiley and Sons, Inc., 1975.

69. Paulay, T., "Deterministic Design Procedure for Ductile Frames in Seismic Areas", American Concrete Institute, Publication SP63, Detroit, Mich., 1980, pp. 357-381.

70. Paulay, T., "Developments in the Seismic Design of Reinforced Concrete Frames in New Zealand", Canadian Journal of Civil Engineering, Vol.8, 1981, pp. 91-113.

71. Popov, E. P., "Seismic Behavior of Structural Subassemblages", Journal of the Structural Division, ASCE, Vol. 106, No. ST7, July 1980, pp. 1451-1474.

72. Rainer, J. H., "Force Reduction Factors for the Seismic Provisions of the National Building Code of Canada", Canadian Journal of Civil Engineering, Vol.14, 1987, pp. 447-454.

73. Riddle, R. and Newmark, N. M., "Statistical Analysis of the Response of Nonlinear Systems Subjected to Earthquakes", Civil Engineering Studies, Structural Research Series No. 468, University of Illinois, Urbana, Ill., Aug. 1979.

74. Rutenberg, A., "Simplified P-Delta Analysis for Asymmetric Structures", Journal of Structural Division, ASCE, Vol.108, No.9, Sept. 1982.

75. Saatcioglu, M., Derecho, A. T., and Corley, W. G., "Modelling Hysteretic Behavior of Coupled Walls for Dynamic Analysis", Earthquake Engineering and Structural Dynamics, Vol. 2, No. , 1983, pp. 711-726.

76. Saiidi, M. and Sozen, M. A., "Simple Nonlinear Seismic Analysis of R/C Structures", Journal of the Structural Division, ASCE, Vol. 107, No. ST5, May 1981, pp. 937-952.

77. Seed, H. B., Murarka, R., Lysmer, J., and Idriss, I. M., "Relationships of Maximum Acceleration, Maximum Velocity, Distance from Source, and Local Site Conditions for Moderately Strong Earthquakes", Bulletin of the Seismological Society of America, Vol. 66, No. 4, Aug. 1976, pp. 1323-1342.

78. Seed, H. B., Ugas, C., and Lysmer, J., "Site-Dependent Spectra for Earthquake-Resistant Design", Bulletin of the Seismological Society of America, Vol. 66, No. 1, Feb. 1976, pp. 221-243.

79. Sehayek, S., "Effect of Ductility on Response Spectra for Elasto-Plastic Systems", Publication No. R76-42, Dept. of Civil Engineering, Massachusetts Institute of Technology, Cambridge, Mass., Sept. 1976.

80. Shibata, A. and Sozen, M. A., "Substitute-Structure Method for Seismic Design in R/C", Journal of the Structural Division, ASCE,Vol. 102, No. ST1, Jan. 1976, pp. 1-18.

81. Takayangi, T. and Schnobrich, W. C., "Non-linear Analysis of Coupled Wall Systems", Earthquake Engineering and Structural Dynamics, Vol. 7, No. 1, Jan.-Feb. 1979, pp. 1-22.

82. Takeda, T., Sozen, M. A., and Nielson, N. M., "Reinforced Concrete Response to Simulated Earthquakes", Journal of the Structural Division, ASCE, Vol. 96, No. ST12, Dec. 1970, pp. 2557-2573.

83. Trifunac, M. D., "Low Frequency Digitization Errors and a New Method for Zero Baseline Correction of Strong-Motion Accelerograms", EERL 70-07, Earthquake Engineering Research Laboratory, California Institute of Technology, Pasadena, Calif., Sept. 1970.

84. Trifunac, M. D. and Brady, A. G., "A Study on the Duration of Strong Earthquake Ground Motion", Bulletin of the Seismological Society of America, Vol. 65, No. 3, June 1975, pp. 581-626.

85. Trifunac, M. D., Udwadia, F. E., and Brady, A. G., "High Frequency Errors and Instrument Corrections of Strong-Motion Accelerograms", EERL 71-05, Earthquake Engineering Research Laboratory, California Institute of Technology, Pasadena, Calif., July 1971.

86. Tso, W. K., Heidebrecht, A. C., and Cherry, S., "Canadian Seismic Code Provisions beyond 1985", Proceedings of the Fourth Canadian Conference on Earthquake Engineering, Vancouver, B. C., pp. K34-K45.

87. Tso, W. K. and Naumoski, N., "Velocity Based Inelastic Design Spectra for Ductility Control", EERG Report 88-02, Earthquake Engineering Research Group, McMaster University, Hamilton, Ont., 1988.

88. Uniform Building Code, International Conference of Building Officials, Whittier, Calif., 1979.

89. Vanmarcke, E. M. and Lai, S. P., "Strong-Motion Duration and RMS Amplitude of Earthquake Records", Bulletin of the Seismological Society of America, Vol. 70, No. 4, Aug. 1980, pp. 1293-1307.

90. Veletsos, A. S. and Newmark, N. M., "Effect of Inelastic Behavior on the Response of Simple Systems to Earthquake Motions", Proceedings of the Second World Conference on Earthquake Engineering, Tokyo and Kyoto, Japan, July 1960, Vol. 2, pp. 895-912.

91. Veletsos, A. S. and Vann, W. P., "Response of Ground-Excited Elastoplastic Systems", Journal of the Structural Division, ASCE, Vol.97, No.ST4, April 1971, pp. 1257-1281.

92. Werner, S. D., "Engineering Characteristics of Earthquake Ground Motions", Nuclear Engineering and Design, Vol. 36, 1976, pp. 367-395.

93. Wilson, E. L. and Habibullah, A., "Static and Dynamic Analysis of Multi-Story Buildings, Including P-Delta Effects", Earthquake Spectra, Vol.3, No.2, 1987, pp. 289-298.

94. Wilson, E. L., Hollings, J. P., and Dovey, H. H., "Three Dimensional Analysis of Building Systems (Extended Version)", Report No. EERC 75-13, Earthquake Engineering Research Center, University of California, Berkeley, Calif., April 1975.

95. Zagajeski, S. W. and Bertero, V. V., "Optimum Seismic-Resistant Design of R/C Frames", Journal of the Structural Division, ASCE, Vol.105, No.ST5, May 1979, pp. 829-845.

96. Zagajeski, S. W., Bertero, V. V., and Bouwkamp, J. G., "Hysteretic Behavior of Reinforced Concrete Columns Subjected to High Axial and Cyclic Shear Forces", Report No. EERC 78-05, Earthquake Engineering Research Center, University of California, Berkeley, Calif., Apr. 1978.

97. Zahrah, T. F. and Hall, W. J., "Earthquake Energy Absorption in SDOF Structures", Journal of Structural Engineering, ASCE, Vol. 110, No.8, Aug. 1984, pp. 1757-1772.

98. Zhu, T. J., Heidebrecht, A. C., and Tso, W. K., "Effect of Peak Ground Acceleration to Velocity Ratio on Ductility Demand of Inelastic Systems", Earthquake Engineering and Structural Dynamics, Vol.16, 1988, pp. 63-79.

99. Zhu, T. J., Tso, W. K., and Heidebrecht, A. C., "Ductility Demand on Structures Designed Based on NBCC 1985 Base Shear Specification", Proceedings of the Fifth Canadian Conference on Earthquake Engineering, Ottawa, July 1987, pp. 275-283.

100. Zhu, T. J., Tso, W. K., and Heidebrecht, A. C., "Effect of Peak Ground a/v Ratio on Structural Damage", Journal of Structural Engineering, ASCE, Vol.114, 1988, pp. 1019-1037.

101. Zhu, T. J., Tso, W. K., and Heidebrecht, A. C., "Evaluation of Base Shear Provisions in the 1985 edition of the National Building Code of Canada", Canadian Journal of Civil Engineering, Vol. 16, Feb. 1989, pp. 22-35.